OPCML and the IgLON Family: Expression, Function and Links with Ovarian Cancer

Evangelos Ntougkos

A thesis submitted for the degree of Doctor of Philosophy
in the College of Medicine and Veterinary Medicine

The University of Edinburgh

October 2005

Declaration

It is hereby declared that this thesis has been composed by the author in its entirety.

The work presented herein is either the author's own, or whenever there had been a contribution by a colleague, this has been duly acknowledged.

This work has not been submitted for any other degree or professional qualification.

Evaṅgelos Ntougkos

October 2005

Acknowledgments

I am greatly indebted to the following coleagues that directly contributed to the work presented in this thesis:
Frank Cheung, who generated the HeLa Tet-On clones;
Eric Miller, who was involved in the generation of the SKOV-3 Tet-On system and in FACS studies;
Morwenna Muir and everyone else in the Biomedical Research Facility, who were responsible for animal work and helped me with mouse embryo collections;
Diane Scott, who made cell line and tissue RNA samples;
Tobias Frankenberg, who helped me in the EOC study;
and Robert Rush, who provided the statistical expertise.

I would like to thank Laura Lettice and Mel Jackson for technical advice and help on in situ studies and Helen Newbery for providing mouse tissue and sections.

This work would have not been possible or enjoyable, without the support of, and interaction with, Genevieve Rabiasz, the rest of my group and everyone in the CR UK Cancer Research Centre. Thank you so much.

Finally, I am deeply grateful for the advice, stimulation and support from my supervisor Grant Sellar, my second supervisor Cathy Abbott and my initial supervisor Hani Gabra. Thank you for guiding me in science and making the way fruitful and satisfying.

Abstract

The IgLONs are an immunoglobulin subfamily of glycosylphosphatidylinositol-anchored cell adhesion molecules, comprising four members: OPCML, HNT, LSAMP and NEGR1. They have been mainly studied in the brain of rat and chick, where they affect cell adhesion and cell-cell recognition. Both homophilic and heterophilic interactions are thought to be important in facilitating IgLON functions.

Human *OPCML* has been proposed as a novel tumour suppressor gene (TSG) in sporadic epithelial ovarian cancer (EOC). EOC, the leading cause of death from gynaecological malignancy, arises in the monolayer of cells overlying the ovary called the ovarian surface epithelium. *OPCML* is normally expressed in these cells, but is epigenetically silenced in EOC. Moreover, it has functional features typical of a TSG: suppression of cell growth *in vitro* and suppression of tumourigenicity *in vivo*.

The deficiency in our knowledge of the functions of OPCML beyond the locality of the brain renders the understanding of its connexion to ovarian cancer insufficient. The relevance of the other IgLON family members in this type of cancer has not been investigated, even though there is much speculation about their interactions. Addressing these two key issues has been the main objective in the work that is presented in this thesis.

In order to study the functions of OPCML, two transfected cell line resources were used: an over-expression system based on SKOV-3 ovarian cancer cells and an inducible expression system based on HeLa cervical cancer cells. Upon induction with doxycycline, selected HeLa inducible clones were shown to demonstrate regulated expression of *OPCML*, both at the RNA and protein levels; however, low-level uninduced expression was also detected, a feature commonly associated with this type of system.

Expression studies of *OPCML* and the other IgLON family members were undertaken in cancer cell lines, as well as normal mouse and human tissues. Expression analysis of the IgLONs in the two *OPCML*-transfected cell line systems identified a transcriptional effect of *OPCML* on two other IgLONs in SKOV-3 cells only: expression of *OPCML* reduces the expression of both *LSAMP* and *NEGR1* at the RNA level. In the mouse and human, the expression profile of the family was established in panels of multiple-tissue cDNAs, where similarities but also differences among different IgLONs were highlighted. Immunohistochemical studies of OPCML were used to profile expression developmentally and in adult tissues. A comparison between IgLON RNA levels in human normal ovaries and a panel of ovarian tumours has pointed to significantly reduced levels of *OPCML*, *LSAMP* and *NEGR1* in specific histological subtypes of ovarian cancer; *HNT* expression, on the other hand, was significantly elevated. This study has revealed the importance of the IgLON family as a whole in EOC.

Various assays were undertaken in the two transfected cell line systems in order to suggest potential functions of OPCML. In SKOV-3 cells, OPCML was shown to significantly decrease chemotactic migration and increase adhesion to fibronectin and vitronectin. Moreover, OPCML was found to promote cell-to-cell adhesion. The growth suppression effect of OPCML *in vitro* was reproduced, and the underlying mechanism was investigated. This effect is not accounted for by a difference in proliferation; on the contrary, OPCML was shown to significantly increase apoptosis. Expression of *OPCML* in the non-ovarian HeLa inducible cells did not recapitulate the phenotypic features identified in the ovarian SKOV-3 cells, indicating the importance of context specificity.

In summary, IgLON expression profiling has yielded valuable observations; most significantly, it demonstrated a link between the family as a whole and EOC. One of the family's members, *OPCML*, has functional features that fit the role of a TSG in SKOV-3 cells, in particular a pro-apoptotic role. In the future, a SKOV-3 inducible system will offer a refined method to further study its functions and connexion to ovarian cancer.

Table of contents

List of abbreviations

aa	amino acid(s)
ACTB	beta actin
ACTG1	gamma actin
AMPS	ammonium persulphate
AMV	avian myeloblastosis virus
bp	base pair(s)
BSA	bovine serum albumin
BRCA1	breast cancer 1, early onset
BRCA2	breast cancer 2, early onset
X-gal	5-bromo-4-chloro-3-indolyl-βD-galactoside
BrdUrd	bromodeoxyuridine
CPT	camptothecin
CA125	cancer antigen 125
CMV	Cytomegalovirus
CNS	central nervous system
CHO	Chinese hamster ovary
CHAPS	3-[(3-chloamidopropyl)dimethylammonio]-1-1propanesulfonic acid
CCRCC	clear cell renal cell carcinoma
cDNA	complementary DNA
DNase	deoxynuclease
dNTP	deoxynucleoside triphosphate
DNA	deoxyribonucleic acid
DAB	diaminobenzidine
DEPC	diethylpyrocarbonate
DIG	digoxygenin
MTT	3-(4,5-dimethyldiazol-2-yl)-2,5 diphenyl tetrazolium bromide
DMSO	dimethyl sulphoxide
DRG	dorsal root ganglion(-a)
Dox	doxycycline
DMEM	Dulbecco's modified Eagle medium
EGFP	enhanced green fluorescent protein
EGF(R)	epidermal growth factor (receptor)
EOC	epithelial ovarian cancer
EMC	epithelial to mesenchymal conversion
EtBr	ethidium bromide
EDTA	ethyl diamine tetetric acid
ECM	extracellular matrix
FIGO	Fédération Internationale de Gynécologie et d'Obstétrique
FITC	fluorescein isothyocianate
FACS	fluorescence-activated cell sorter
FCS	foetal calf serum
FSH	follicle stimulating hormone
FSC	forward scatter
G	gauge

GPI	glycosylphosphatidylinositol
GnRH	gonadotrophin releasing hormone
GPI-AP	GPI-anchored protein
g	gram(s)
(G)M-CSF	(granulocyte) macrophage colony stimulating factor
HSV	Herpes Simplex virus
h	hour(s)
HUGO	Human Genome Organisation
HNPCC	human non-polyposis colorectal carcinoma
Ig	immunoglobulin
IgLON	immunoglobulin LAMP OBCAM Neurotrimin
IgCAM	immunoglobulin-like cell adhesion molecule
IHC	immunohistochemistry
IOD	integrated optical density
IL	interleukin
IPTG	isopropyl-βD-thiogalactopyranoside
kb	kilobase(s)
kDa	kilodalton(s)
KILON	kindred of IgLON
L(S)AMP	limbic (system)-associated membrane protein
l	litre(s)
LoH	loss of heterozygosity
LMP	low malignant potential
LB	Luria-Bertani
LH	luteinising hormone
mRNA	messenger RNA
µg	microgram(s)
µl	microlitre(s)
µM	micromolar
mg	milligram(s)
ml	millilitre(s)
mM	millimolar
min	minute(s)
MMR	mismatch repair
MAPK	mitogen-activated protein kinase
M	molar
Mut	mutant
TEMED	N,N,N',N'-tetramethylethylenediamine
ng	nanogram(s)
NCBI	National Centre for Biotechnology Information
NHS	National Health Service
NEGR1	neuronal growth factor regulator 1
HNT	neurotrimin
ORF	open reading frame
OBCAM	opioid binding cell adhesion molecule
OPCML	opioid binding protein / cell adhesion molecule-like
OD	optical density
OSE	ovarian surface epithelium

PTEN	phosphatase and tensin homologue
PBS	phosphate-buffered saline
PI-PLC	phosphatidylinositolphospholipase C
PS	phosphatidylserine
PI3K	phosphoinositide 3-kinase
PNGase F	peptide N-glycosidase F
pg	picogram(s)
PCR	polymerase chain reaction
pH	power of hydrogen
qRT-PCR	quantitative RT-PCR
RLU	relative luminescence unit(s)
RE	restriction endonuclease
RT-PCR	reverse-transcription PCR
rpm	revolutions per minute
RNase	ribonuclease
RNA	ribonucleic acid
RPMI	Roswell Park Memorial Institute
s	second(s)
SCID	severe combined immunodeficiency
SSC	side scatter
SV40	Simian virus 40
SSC	sodium citrate buffer
SDS	sodium dodecyl sulphate
SD	standard deviation
SEM	standard error of the mean
TdT	terminal deoxynucleotidyl transferase
Tet	tetracycline
TRE	tetracycline response element
TGF	transforming growth factor
TBS	Tris-buffered saline
TNF	tumour necrosis factor
TP53	tumour protein 53
TSG	tumour suppressor gene
UV	ultraviolet
ERBB2	v-erb-b2 erythroblastic leukaemia viral oncogene homologue 2
KRAS	v-Ki-ras2 Kirsten rat sarcoma viral oncogene homologue
V	volt(s)
vol	volume
v/v	volume per volume
W	watt(s)
w/v	weight per volume
WISH	whole-mount in situ hybridisation
WT	wild type

Chapter 1

General introduction

1.1 The IgLON family

The term "IgLON" was coined in 1995 by Levitt and colleagues to describe a group of three neural glycoproteins that had features characteristic of the cell adhesion molecules of the immunoglobulin superfamily[1]. These three proteins, namely LAMP, OBCAM and Neurotrimin, have three immunoglobulin domains and a glycosylphosphaditylinositol (GPI) anchor. To date, the family has expanded and now includes a fourth member, originally known as KILON. The nomenclature of the family is shown in Table 1.1. The following sections will provide an in-depth introduction to the biology of the IgLON family, firstly focusing on individual members and then on their interactions, as well as their potential roles in cancer.

Official human symbol	*Official name*	*Alternative designations*
OPCML	Opioid binding protein/cell adhesion molecule-like	OBCAM
HNT	Neurotrimin	NTM, CEPU-1 (chick)
LSAMP	Limbic system-associated membrane protein	LAMP, AvGp50 (chick)
NEGR1	Neuronal growth regulator 1	KILON, Neurotractin (chick)

Table 1.1 IgLON nomenclature
Official nomenclature and aliases of the IgLON family according to the HUGO Gene Nomenclature Committee.

1.1.1 *OPCML*

The protein known as OPCML or OBCAM was originally purified from rat brain as a μ opioid-specific receptor by Cho and colleagues[2]. The majority of the initial work on OPCML centred on its characterisation as an opioid receptor, although it had been hinted from the beginning that such a function would be unusual, as most opioid receptors are seven-transmembrane domain receptors[3] a feature not met in OPCML. Thus, early papers reported that antibodies against OPCML, as well as antisense transfection of the gene, inhibit opioid binding[4,5]. When *OPCML*-transfected NG108-15 cells (a neuroblastoma/glioma hybrid cell line) were treated with opioid agonists, which reduce levels of opioid receptors, OPCML immunoreactivity was decreased[6]; conversely, when CHO (Chinese hamster ovary) cells were transfected with an opioid receptor they exhibited high surface OPCML immunoreactivity[7]. Eventually, it was realised that OPCML did not fit the criteria of an opioid receptor; for example, PI-PLC treatment of brain membranes, which should result in the cleavage of GPI anchors, did not have an effect on opioid binding[8].

The *OPCML* coding sequence was firstly cloned in the rat and was found to encode a protein of 345 amino acids, with evidence for a GPI linkage[9]. *OPCML* was subsequently cloned in the human: it was positioned on chromosome 11 and contained a putative open reading frame of 1038 bp[10]. The human *OPCML* sequence was found to be 93% identical to the rat sequence at the nucleotide level and 98% at the amino acid level. In the chick, two *OPCML* cDNAs have been cloned, both encoding the same mature protein, but differing in the coding of the N-terminal signal peptide with respect to its length[11].

Although the predicted molecular weight of the OPCML protein is 36 kDa, its apparent weight is approximately 58 kDa and it is commonly detected as a doublet by immunoblotting[8]. The increase in the molecular weight, as well as the presence of two bands, has been accounted for by N-linked glycosylation. In addition, the protein is entirely extracellular and is tethered to the cell membrane by a GPI anchor. This has been demonstrated with the use of the enzyme PI-PLC, which cleaves GPI anchors[8,12,13]. Moreover, the OPCML protein is detected in the Triton-insoluble fraction of cell membrane preparations[14], a fraction that is

associated with lipid rafts. Lipid rafts can be described as membrane subdomains, enriched in cholesterol and glycosphingolipids, which exist in a liquid-ordered phase[15,16]. They are thought to facilitate signal transduction, by bringing in close proximity signalling components and favouring specificity and sensitivity in their interactions[17].

As an IgLON, *OPCML* is typically expressed in the brain, and its expression patterns have been widely studied in this locality. In bovine brain, OPCML is strongly detected in the striatum and cerebral cortex[8]. In the rat brain, OPCML is detected in almost all of the grey matter, with very restricted expression in the white matter, only found in the corpus callosum and the deep part of the dorsal funiculus[18]. Its expression is at its peak in the cerebral cortex and the hippocampus, moderate in the olfactory bulb and the diencephalon and weaker in the cerebellum, medulla oblongata and spinal cord[14]. OPCML has been described as a dendrite-specific cell adhesion molecule, as it has been reported to localise in the dendrites of fully polarised cortical and hippocampal neurones[19,20]. More specifically, *Opcml* is mainly expressed at post-synaptic sites of cortical and hippocampal synapses[14]. Within dendrites, OPCML localises in vasopressin-positive neurosecretory granules. In the chick, *OPCML* is widely expressed in the CNS, where studies have particularly focused on its expression in the retina, and neurones of the dorsal root and sympathetic ganglia[11]. Outside the CNS, *OPCML* expression has been reported in the spleen, heart, placenta, liver, kidney, pancreas, testis, colon and the epithelial component of the ovary[8,18,21].

In all the aforementioned species, *OPCML* expression in the brain is known to rise in development. In the rat, its expression starts being detectable at E16 and has been reported to peak either around the second post-natal week or between P28 and P56[14,22]. Early in development, *Opcml* is expressed on all post-mitotic neurones and strongly in fibre tracts containing expanding neurones, whilst in the adult it is principally expressed in the grey matter. In the developing chick retina, the expression of *OPCML* rises from E7 to E20[11].

After the opioid receptor notion was disproved, a number of studies tried to identify the functions of OPCML in the brain. One concept that emerged is that OPCML can bind homophilically, but also heterophilically with other members of

the IgLON fanily[11,14]. Although originally thought to influence axon guidance by modulating neurite growth, there is more recent evidence that it might be primarily involved in cell-cell adhesion and cell recognition[23]. DRG (dorsal root ganglia) neurones and sympathetic neurones to a lesser extent adhered to a substrate of OPCML-Fc chimaeras presented on protein A, but did not extend neurites. In addition, OPCML has been implicated in visual cortex plasticity due to the finding that it is highly expressed in the visual cortex of kittens but only mininally of older cats[24,25]. Further support for this hypothesis comes from the observation that the number of *OPCML*-expressing neurones is higher in the visual cortex of older cats that have been dark-reared in comparison to normal-reared ones. Finally, there is indirect evidence of a potential role in the inflammatory response, as in a model of rheumatoid arthritis, *OPCML* was found to be four times down-regulated following IL-1β stimulation of chondrocytes[26].

Additional information on the human *OPCML* gene and the protein it encodes is shown in Figure 1.1; this is not based on published data, but on analysis undertaken for this thesis specifically.

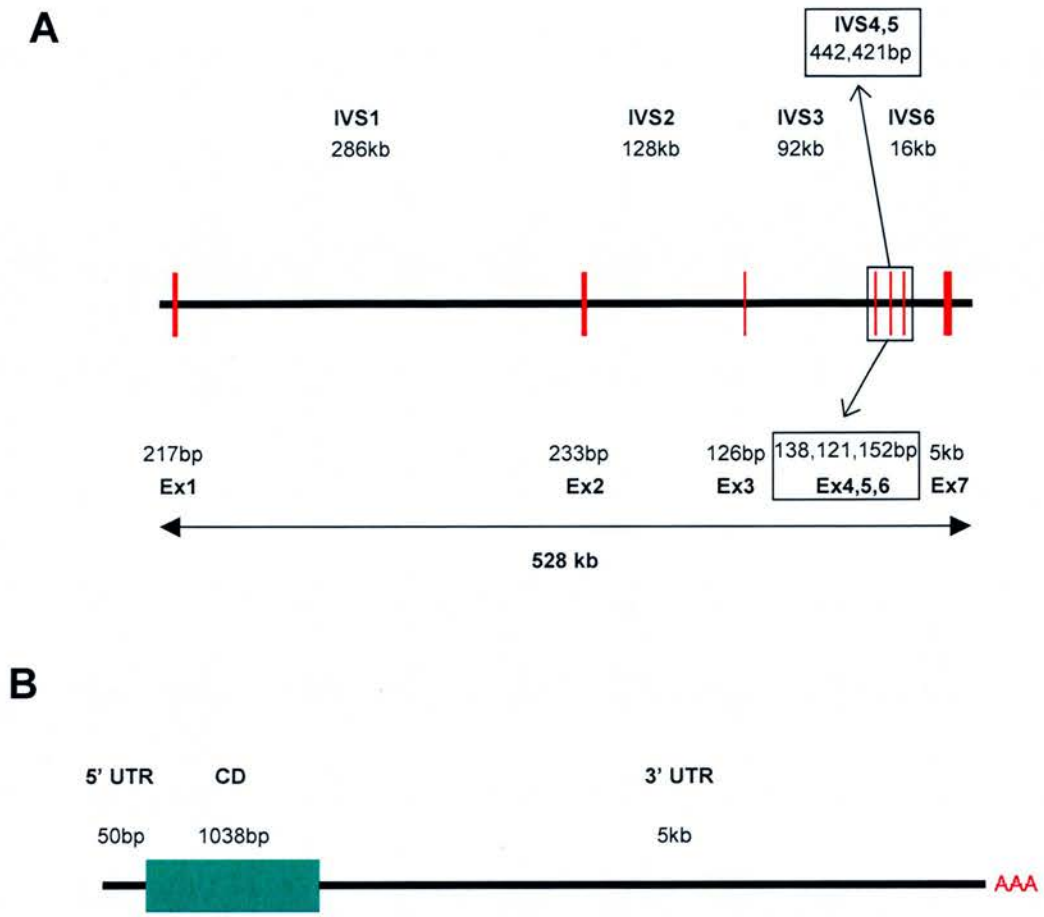

Figure 1.1i *OPCML* at a glance
Gene structure (A) and mature mRNA structure (B) of human *OPCML* based on NCBI 11q25 sequence and NM_002545 (not to scale). IVS = intron; Ex = exon; UTR = untranslated region; CD = coding region; AAA = poly(A) track.

C

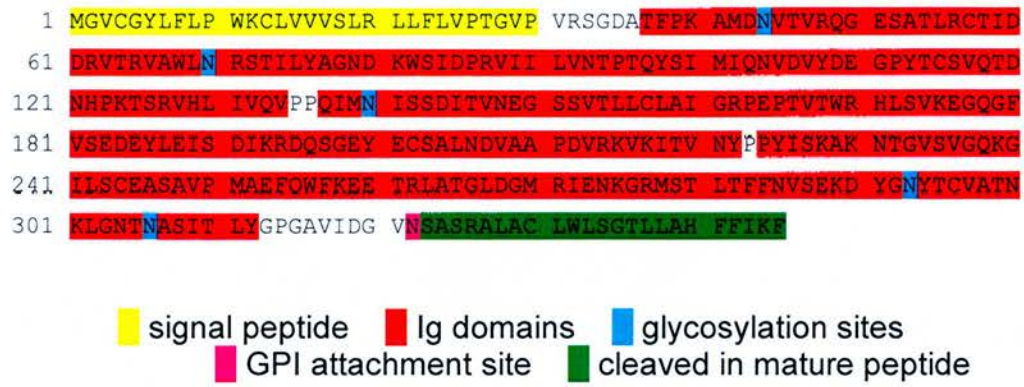

D

Species	*Accession number*	*% identity*
M.musculus	AAH76581	97
G.gallus	CAB41420	85
X.laevis	AAH74283	67
D.rerio	AAH81685	57
D.melanogaster	AAY55132	32

Figure 1.1ii OPCML at a glance
Human OPCML proprotein sequence (NCBI NP_002536) annotated with features (C) and its percentage identity with orthologues and homologous sequences across species (D). Note that for homologous sequences there is not always a one-to-one match for a specific IgLON between species.

1.1.2 *HNT*

Neurotrimin (HNT) was originally isolated from rat brain as a GPI-anchored protein, together with OPCML[27]. The cDNA was cloned and positioned on the proximal end of mouse chromosome 9. The chick orthologue, usually termed CEPU-1, was identified subsequently[28]. In the chick, neurotrimin alternative isoforms have been well documented[11,29]. The prototype CEPU-1 protein can be described as α CEPU-1. There is also β CEPU-1, which has an additional C-terminal insert. Both these can have a longer (1) or a shorter signal peptide (2); for example, α1 and α2 CEPU-1. Finally, there is another form, termed CEPU-Se, which differs to CEPU-1 at the C terminus, missing the GPI attachment sequence, and hence is thought to be secreted. In the human, *HNT* has been recently cloned[30]. The gene is reported to contain an open reading frame of 1032 bp, encoding a protein of 344 amino acids with a predicted molecular weight of 37 kDa. The *HNT* gene is located on chromosome 11q25, approximately 80 kb away from the *OPCML* gene, but it is transcribed at the opposite orientation. Some evidence of alternative isoforms exists in the human, with multiple transcripts detected by northern blotting. Human *HNT* is 87% identical to the rat nucleotide sequence and 97% to the rat peptide sequence.

In the rat nervous system, *Hnt* has a wide expression pattern, being expressed in neurones of the thalamus, subplate, lower cortical laminae, pontine nucleus, cerebellar granule cells, Purkinje cells, olfactory bulb, retina, dorsal root ganglia, spinal cord, basal ganglia and hippocampus[27]. In the chick cerebellum, *HNT* expression has been described in granule cells, but there are conflicting reports on its expression in Purkinje cells[28,29]. In the human, its highest expression was found in the cerebellum; it is also the only species where expression outside the CNS has been documented, namely in the heart and lung[30].

Developmentally, like *OPCML*, *HNT* expression rises with age. In the developing chick brain, the timing of *HNT* expression has been linked with the growth of the dendritic tree[28]. Moreover, there is evidence of alternative isoforms being expressed differentially in development[11]. This is not true for the secreted isoform, though, which is co-expressed with CEPU-1 at all stages examined[29]. More detailed neurodevelopmental studies in the chick have indicated that early in development, *HNT* has a broad expression pattern, which is subsequently restricted

to a ring-shaped domain in the midbrain-hindbrain boundary, co-localising with *WNT1* expression in the isthmus, as well as migrating neural crest cells[31]. Later still, *HNT* expression is switched on in other parts of the brain, for example sensory ganglia and ventral aspects. In the human brain, adult expression has been shown to be higher than foetal expression[30].

What are the functions of HNT? Cross-linking studies of transfected CHO cells have demonstrated that HNT forms dimers and multimers *in cis* and mediates homophilic adhesion[32]. HNT can bind to and promote neurite outgrowth in neurones that express it (e.g. from DRG) but not those that do not (e.g. sympathetic neurones). Interestingly, the secreted form of HNT does not have this effect, although it can act as a soluble ligand when it is dimerised[29]. HNT has been also shown to bind heterophilically with OPCML and LSAMP[11]. As with OPCML, a subsequent report raised concerns on the ability of HNT to modulate neurite growth and highlighted a more favourable role in cell-cell adhesion and cell recognition[23]. This hypothesis is supported by the finding that HNT promotes cell-cell aggregation[30].

Additional information on the human *HNT* gene and the protein it encodes is shown in Figure 1.2; this is not based on published data, but on analysis undertaken for this thesis specifically.

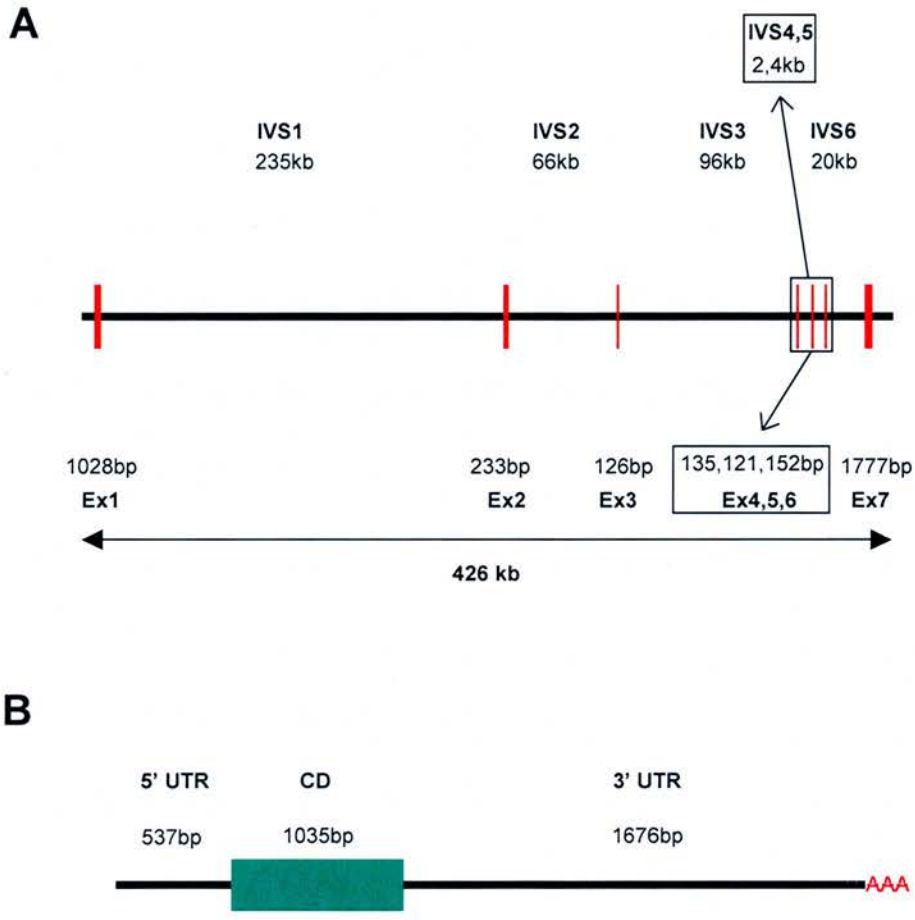

Figure 1.2i *HNT* at a glance
Gene structure (A) and mature mRNA structure (B) of human *HNT* based on NCBI 11q25 sequence and NM_016522 (not to scale). IVS = intron; Ex = exon; UTR = untranslated region; CD = coding region; AAA = poly(A) track.

C

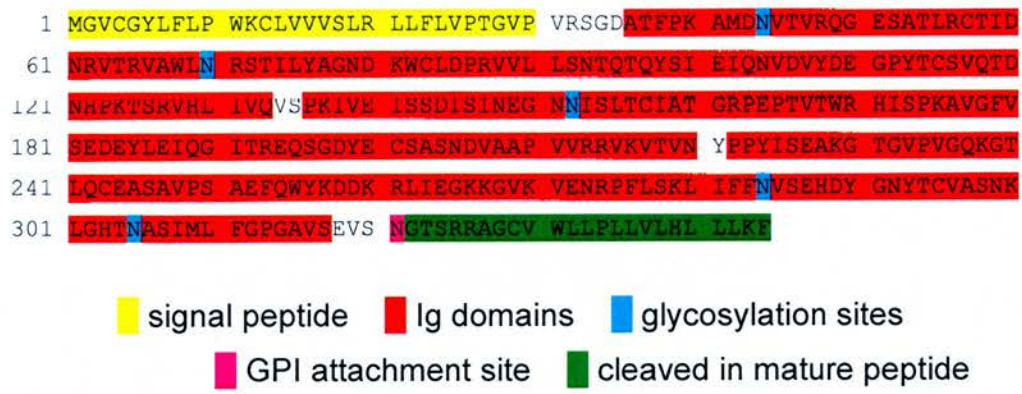

D

Species	*Accession number*	*% identity*
M.musculus	AAH23307	94
G.gallus	BAA31514	80
X.laevis	AAH74283	72
D.rerio	AAH81685	57
D.melanogaster	AAY55132	32

Figure 1.2ii HNT at a glance
Human HNT proprotein sequence (NCBI NP_057606) annotated with features (C), and its percentage identity with orthologues and homologous sequences across species (D). Note that for homologous sequences there is not always a one-to-one match for a specific IgLON between species.

1.1.3 *LSAMP*

LSAMP, also known as LAMP, was first discovered using a monoclonal antibody that stained cortical and subcortical regions of the limbic system in rat brain[33]. Since then, it probably constitutes the most studied member of the IgLON family. *LSAMP* was initially cloned in the rat and shortly afterwards in the human[1,34]. The human *LSAMP* sequence contains an ORF of 1014 bp, and encodes a 338 aa protein with 3 immonoglobulin domains, an N-terminal signal peptide, a C-terminal GPI attachment site and 8 N-linked glycosylation sites. Human and rat sequences are reported to be 94% identical at the nucleotide level and 99% identical at the amino acid level. The chick *LSAMP* gene has been also cloned and is 91% identical to the rat nucleotide sequence[35]. Physically, human *LSAMP* has been mapped to chromosome 3q, whereas mouse *Lsamp* to chromosome 16, at a region of conserved synteny with the human[36]. Three transcripts have been identified in the human and chick, two in the rat and multiple in the mouse[11,37]. These isoforms differ mainly either in the signal peptide coding sequence or the C-terminal one.

The LSAMP protein was originally purified from rat and bovine hippocampus[38]. It was found to be an extracellular protein of 64-68 kDa, modified by N-linked glycosylation and tethered to the membrane by a GPI anchor.

The expression of *LSAMP* has been tightly linked with the limbic system since its discovery. In the adult rat brain, it localises post-synaptically on neuronal somata and dendrites, but not axons[38]. Generally, *Lsamp* is expressed heavily in areas of the forebrain and diencephalon that are considered limbic and only sparsely in non-limbic midbrain and hindbrain regions[39]. When the distribution of LSAMP was studied in the amygdaloid complex and the hippocampus of cynomolgus monkeys, it was found that staining of limbic structures is highly heterogeneous, and probably confined to very specific functional domains[40]. In the chick nervous system, *LSAMP* expression has been shown in the forebrain, cerebellum, tecta, retina and spinal cord[41]. It mostly localises in areas of interneuronal contact, such as the molecular layer in the cerebellum and the inner and outer plexiform layers in the retina. Furthermore, the distribution of LSAMP in the pigeon brain has been elucidated and found to be very similar to that in mammals[42]. Outside the CNS, the only organ where expression of *LSAMP* has been reported to date is the kidney[43].

It is known that *LSAMP* is expressed in neurones early in foetal development, as early as E13, and its pattern of temporal expression correlates with the formation of limbic pathways[44,45]. Interestingly, although in the adult LSAMP is present in post-synaptic sites, in development it is more widespread, being expressed on growing axons both pre- and post-synaptically[38]. Transplantation experiments, involving taking precursors of either perirhinal or sensorimotor cortex prior or just after the onset of *Lsamp* expression and placing them either homo- or heterotopically, have elegantly demonstrated that there is an initial developmental window during which cells are still "pluripotent" (until E12 in the rat) before they become committed to a limbic fate[46]. In the developing chick neural tube, *LSAMP* is expressed in the anterior midbrain and by most neural crest cells[47]. In the chick, there is some evidence of differential expression of *LSAMP* alternative transcripts in development[35].

With regard to its functions, the ability of LSAMP to affect neurite outgrowth has been studied extensively. More specifically, LSAMP is thought to play a bifunctional role: it facilitates neurite outgrowth of neurones that express it, such as limbic neurones, and it inhibits neurite outgrowth from neurones that do not express it[1,48,49]. LSAMP is thought to induce neurite outgrowth by modulating intracellular Ca^{2+} levels[50]. It has been demonstrated that the first Ig domain within the LSAMP protein is necessary and sufficient for its neurite-promoting acitivity in hippocampal neurones; this is also the domain that can interact homophilically[51]. The inhibition of neurite outgrowth from non-expressing neurones is mediated by heterophilic interactions and requires full length LSAMP, although is mostly dependent on the second Ig domain. Furthermore, administration of anti-LSAMP antibody to rats results in an abnormal growth of the mossy fibre projections from developing granule neurones of the dentate gyrus of the hippocampus[1]. Moreover, evidence for the involvement of LSAMP in both homo- and heterophilic adhesion and interactions is well documented[11,23,35,49,52]. The functional significance of the finding that *Lsamp* is up-regulated in rats with reduced exploratory activity remains to be clarified[53].

Additional information on the human *LSAMP* gene and the protein it encodes is shown in Figure 1.3; this is not based on published data, but on analysis undertaken for this thesis specifically.

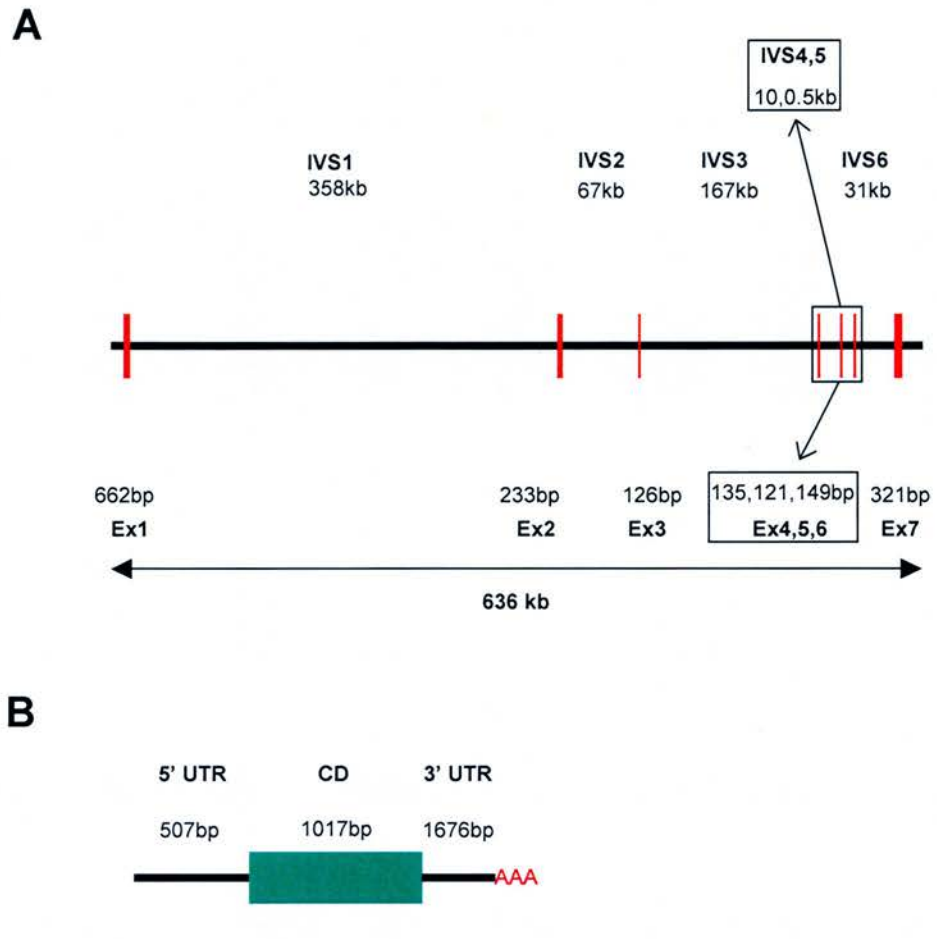

Figure 1.3i *LSAMP* at a glance
Gene structure (A) and mature mRNA structure (B) of human *LSAMP* based on NCBI 3q13.2-q21 sequence and NM_002338 (not to scale). IVS = intron; Ex = exon; UTR = untranslated region; CD = coding region; AAA = poly(A) track.

C

```
  1 MVRRVQPDRK QLPLVLLRLL CLLPTGLPVR SVDFNRGTDN ITVRQGDTAI LRCVVEDKNS
 61 KVAWLNRSGI IFAGHDKWSL DPRVELEKRH SLEYSLRIQK VDVYDEGSYT CSVQTQHEPK
121 TSQVYLIVQV PPKISNISSD VTVNEGSNVT LVCMANGRPE PVITWRHLTP TGREFEGEEE
181 YLEILGITRE QSGKYECKAA NEVSSADVKQ VKVTVNYPPT ITESKSNEAT TGRQASLKCE
241 ASAVPAPDFE WYRDDTRINS ANGLEIKSTE GQSSLTVTNV TEEHYGNYTC VAANKLGVTN
301 ASLVLFRPGS VRGINGSISL AVPLWLLAAS LLCLLSKC
```

signal peptide | Ig domains | glycosylation sites | GPI attachment site | cleaved in mature peptide

D

Species	*Accession number*	*% identity*
M.musculus	BAE34618	88
G.gallus	CAB08115	80
X.laevis	AAH74296	82
D.rerio	AAH81685	52
D.melanogaster	AAY55132	31

Figure 1.3ii LSAMP at a glance
Human LSAMP proprotein sequence (NP_002329) annotated with features (C), and its percentage identity with orthologues and homologous sequences across species (D). Note that for homologous sequences there is not always a one-to-one match for a specific IgLON between species.

1.1.4 *NEGR1*

The last member to be added in the IgLON family, NEGR1, most widely known as KILON, was originally isolated and cloned from a rat brain raft fraction after PI-PLC solubilisation[54]. It has also been independently cloned by a second group[55]. Like the rest of the IgLONs, it has three Ig domains and is subjected to post-translational glycosylation due to its 6 N-linked glycosylation sites, which results in an increase in the apparent molecular weight to 46 kDa relative to the predicted one of 36 kDa. The rat NEGR1 peptide sequence is 56% identical to the rat LSAMP sequence, 49% to OPCML and 48% to HNT[54]. The chick orthologue has also been identified and is commonly known as neurotractin[52]. Two isoforms have been described, a long (L) 50 kDa protein and a short (S) 37 kDa protein. The latter lacks the third Ig domain. Recently, mouse *Negr1* has been cloned[56].

In the rat, expression of *Negr1* has been documented in the cerebral cortex, hippocampus, diencephalon and cerebellum, with lower expression in the medulla oblongata and very low in the spinal cord[14,54]. More specifically, NEGR1 immunoreactivity has been demonstrated in magnocellular neurones of the supraoptic and paraventricular nuclei in the rat hypothalamus, where NEGR1 mainly localises in the dendrites of vasopressin-secreting neurones and to a lesser extent of oxytocin-secreting neurones[14,19]. NEGR1 is mainly found at post-synaptic sites in the adult rat cerebral cortex and hippocampus, co-localising with the vesicle-associated membrane protein 2 (VAMP-2), a synaptic protein marker. In the chick, NEGR1 has been described as an axonal glycoprotein; there is evidence that the long and short isoforms are not differentially expressed[52]. Outside the brain, *Negr1* expression has been reported only in the skull, intervertebral discs, intestine, ribs and visceral cranium of E17 rats at the RNA level[55].

NEGR1 expression is developmentally regulated, in the rat, chick and mouse[14,52,54,56]. In the rat, it is very low at E16 and starts rising from E19, peaking around P30-P70. In the developing chick, *NEGR1* expression is restricted to subsets of commissural and longitudinal axon tracts.

NEGR1 has been assigned a neurite outgrowth-promoting role in neurones that express it[52]. In addition, it has been shown to interact both homophilically and heterophilically with other IgLONs[14]. Interestingly, in the mouse, subsequent to a

lesion in the entorhinal cortex, *Negr1* expression was induced in reactive astrocytes in the denervated outer molecular layer of the dentate gyrus, where regenerative axon sprouting occurs[56]. This is the first report of an IgLON being expressed by non-neuronal cells in the brain. Consequently, a hypothesis was proposed that NEGR1 could function as a trans-neural growth-promoting factor for outgrowing axons following hippocampal denervation.

Additional information on the human *NEGR1* gene and the protein it encodes is shown in Figure 1.4; this is not based on published data, but on analysis undertaken for this thesis specifically.

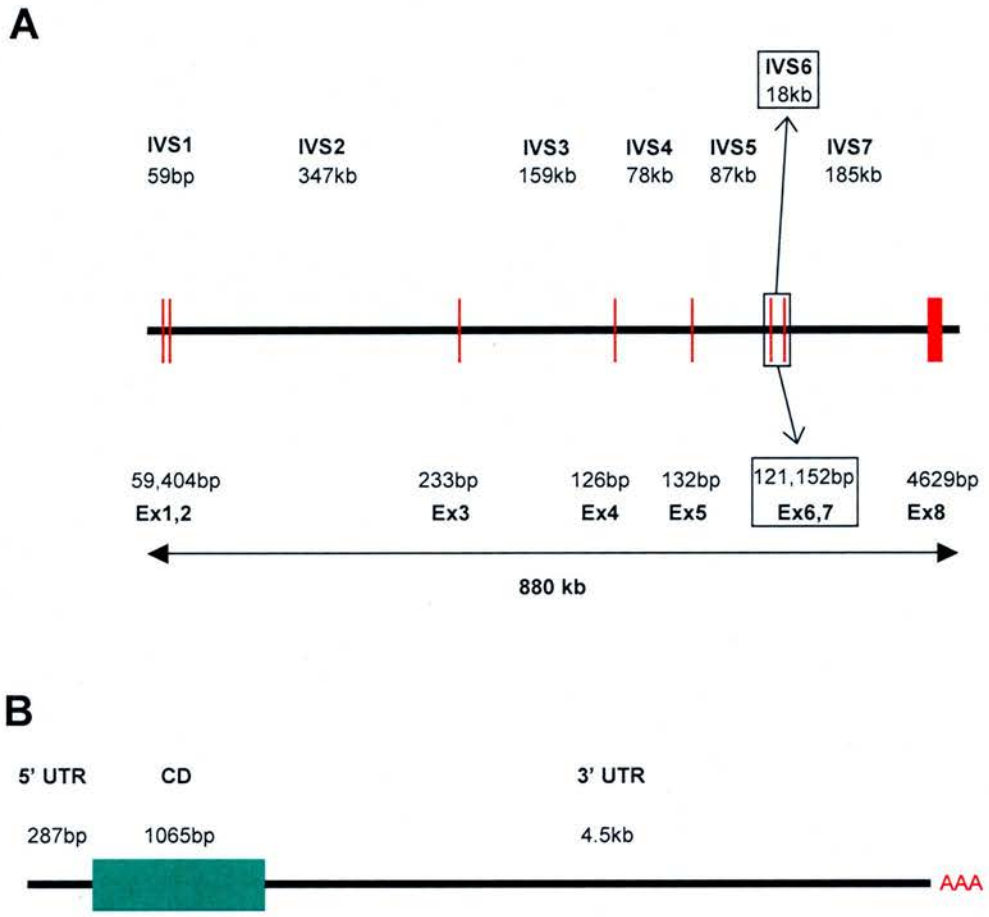

Figure 1.4i *NEGR1* at a glance
Gene structure (A) and mature mRNA structure (B) of human *NEGR1* based on NCBI 1p31.1 sequence and NM_173808 (not to scale). IVS = intron; Ex = exon; UTR = untranslated region; CD = coding region; AAA = poly(A) track.

C

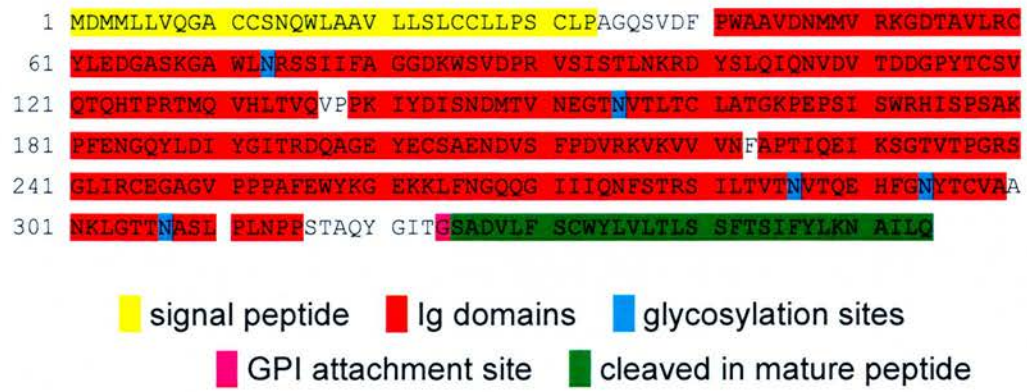

E

Species	Accession number	% identity
M.musculus	BAE27799	93
G.gallus	CAB44446	82
X.laevis	AAH74296	58
D.rerio	NP_001003851	62
D.melanogaster	AAK93253	33

Figure 1.4ii NEGR1 at a glance
Human NEGR1 proprotein sequence (NCBI NP_776169) annotated with features (C) and its percentage identity with orthologues and homologous sequences across species (D). Note that for homologous sequences there is not always a one-to-one match for a specific IgLON between species.

1.1.5 Interactions within the IgLON family

It has been mentioned that apart from the ability of each IgLON to participate in homophilic interactions, heterophilic binding is also possible: OPCML has been reported to interact with HNT, LSAMP and NEGR1; HNT with OPCML and LSAMP; LSAMP with OPCML, HNT and NEGR1; and NEGR1 with OPCML, HNT and LSAMP[11,14,52]. There has been a recent proposition that each IgLON protein is principally a subunit of a heterodimeric adhesion molecule, termed Diglon[57]. The four IgLON proteins can potentially form six Diglons: LSAMP-OPCML, LSAMP-HNT, HNT-OPCML, NEGR1-OPCML, NEGR1-HNT and LSAMP-NEGR1. Based on their relative adhesion affinities, the authors postulated that OPCML and LSAMP interact mostly heterophilically, whilst HNT can also function homophilically. The role of NEGR1 in these interactions remains to be confirmed. The ability of IgLONs to associate in dimeric complexes is reflected on their function: co-transfection of *OPCML* and *HNT* in CHO cells resulted in a significant reduction in their ability to modify neurite outgrowth from cerebellar granule cells.

1.1.6 The IgLON family in cancer

Sellar and colleagues have proposed that *OPCML* represents a novel tumour suppressor gene in sporadic epithelial ovarian cancer[21]. Their report was the first one to link an IgLON with disease, and indeed to focus on an area of IgLON biology that is not centred on the brain. *OPCML* was originally identified through a high rate of complete loss of heterozygosity (LoH) within its second intron on 11q25. *OPCML* was shown to be expressed in normal ovarian surface epithelium, the site of origin of EOC, but its RNA expression was abolished in 83% of a panel of ovarian tumours and 88% of a panel of ovarian cancer cell lines. Mutation screening identified only one somatic mutation in EOC, a C→G transversion that results in a missense P95R substitution in the first Ig domain of the protein. Nonetheless, extensive promoter hypermethylation was found in ovarian tumour samples and cancer cell lines, suggesting that the mechanism underpinning *OPCML* silencing is epigenetic. Furthermore, it was shown that OPCML has functional features of a tumour supressor: it suppresses cell growth *in vitro*, when expressed in the ovarian cancer

SKOV-3 cell line, and tumourigenicity *in vivo*, in intraperitoneal and subsutaneous xenografts. In SKOV-3 cells, it was also found to promote cell-cell aggregation, a function lost when mutant *OPCML*, harbouring the P95R mutation, was expressed.

The second IgLON to be linked with cancer is *LSAMP*. More specifically, *LSAMP* was identified by positional cloning to span a breakpoint in familial clear cell renal cell carcinoma (CCRCC)[43]. *LSAMP* RNA was down-regulated in all renal cell carcinoma cell lines examined relative to its levels in the normal kidney. The *LSAMP* promoter was found to be methylated in most of these cell lines, as well as in 26% of a panel of sporadic CCRCC samples and 4 familial CCRCC cases. In samples where methylation was found, RNA down-regulation was also shown relative to the normal kidney. Somatic mutations were not identified. When an *LSAMP-EGFP* construct was expressed in renal cell carcinoma cell lines, there was marked growth suppression. Hence, it was postulated that LSAMP might have a tumour suppressor function in CCRCC. It should be noted, however, that the growth suppression effect seen should be appreciated with some caution, as the observed localisation of LSAMP in the transfected cell lines was cytoplasmic, contrary to its common extracellular localisation.

1.2 Ovarian cancer

Ovarian cancer is the leading cause of death from gynaecological malignancy[58]. It ranks fourth or fifth as a cause of death from cancer in women (Figure 1.5), who have a 1 in 48 lifetime risk of developing it[59]. The incidence of the disease rises with age, peaking in around the seventh to eighth decade. 90% of ovarian cancers are epithelial ovarian cancers (EOCs), the rest originating in granulosa, or rarely stromal and germ cells. Cancer of the ovary is primarily a sporadic disease, with familial cases accounting for only 5-10% of patients[60,61].

In the following sections, an introduction on ovarian cancer biology will be presented. After discussing some relevant elements of normal ovarian biology, important aspects of ovarian cancer will be covered, including aetiology, histology and the genetics of the disease.

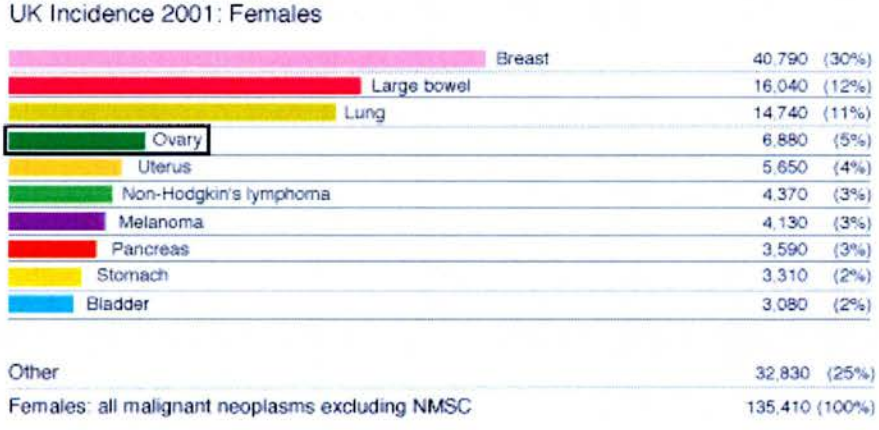

Figure 1.5 UK incidence of cancer in females
2001 figures of women's cancer incidence in the UK. Adapted from the Cancer Research UK Statistics website.

1.2.1 The ovarian surface epithelium

When examining the features of a human ovary, the ovarian surface epithelium seems to be obscured by more complex structures (Figure 1.6). It is relatively recently that this inconspicuous cell layer overlying the ovary, the OSE, has become the focus of intense study, with respect to both its normal physiology and pathology[62-64].

The OSE, also known as ovarian mesothelium or quite misleadingly as the "germinal" epithelium, is the single layer of squamous to cuboidal epithelial cells that is only tenuously attached to the ovary (Figure 1.7). Developmentally, the OSE is part of the coelomic epithelium, which is the mesoderm-derived epithelial lining of the intra-embryonic coelom. It remains controversial whether the foetal OSE is also the developmental source of ovarian granulosa cells. The mature OSE expresses various keratins (7, 8, 18 and 19), as well as mucin antigen 1, and 17β-hydroxysteroid dehydrogenase. It features cilia, apical microvilli and a basal lamina. It is separated from the ovarian stroma by a dense collagenous tissue layer, the tunica albuginea; this is what gives the ovary its off-white colour. Within the OSE layer, intercellular contact is maintained by desmosomes and incomplete tight junctions and facilitated by the presence of several integrins and N-cadherin.

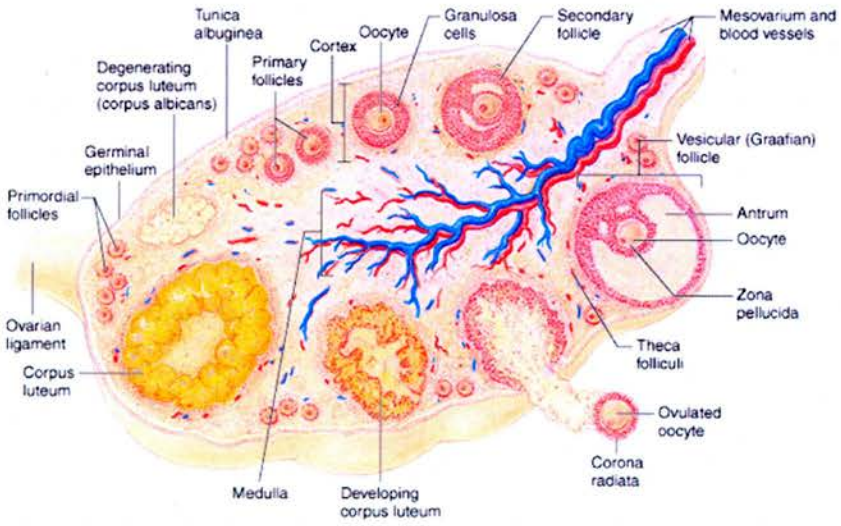

Figure 1.6 The human ovary
Diagram of the basic anatomical features of the human ovary. Reproduced from the Human Anatomy website of Lake Michigan College.

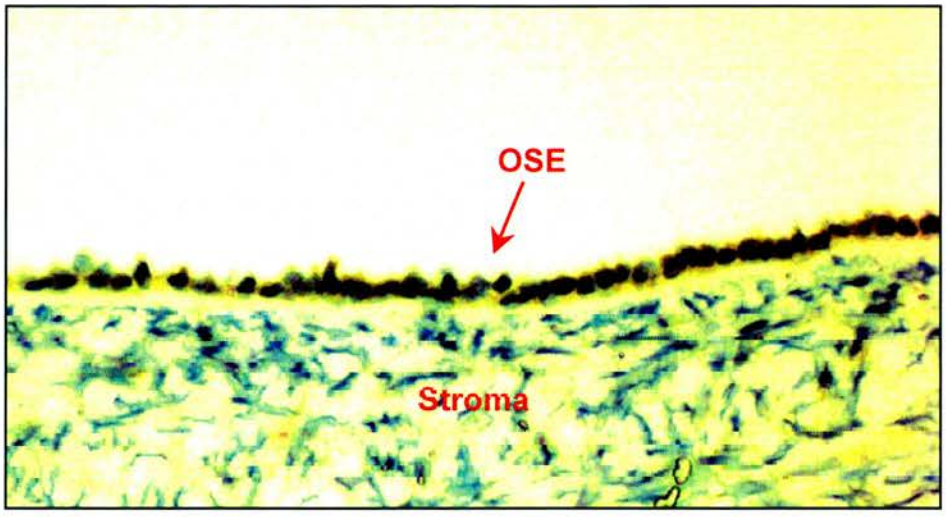

Figure 1.7 The ovarian surface epithelium
Human ovary section focusing on the OSE layer. Image courtesy of Dr M. Rae, Centre for Reproductive Biology, University of Edinburgh.

One of the defining characteristics of the ovarian surface epithelium is its limited degree of differentiation; it is therefore described as having both epithelial and mesothelial features. This might explain the current absence of OSE-specific markers. In response to stimuli that are not fully understood, but are usually part of a regenerative response, OSE cells undergo epithelial-to-mesenchymal conversion (EMC) and assume characteristics of stromal cells. These stimuli are exemplified by ovulatory rupture *in vivo* and explantation into culture. With age, the ovary tends to form OSE-lined invaginations, often manifesting as crypts. It is thought that the propensity of OSE cells to undergo EMC serves as a homeostatic mechanism that allows cells that have been trapped in cysts to be incorporated in the ovarian stroma as fibroblasts.

Functionally, the ovarian surface epithelium transports materials to and from the peritoneal cavity and plays an important role in cycles of ovulation and post-ovulatory repair. OSE functions are regulated by hormones and inflammatory mediators. Examples include: gonadotrophin releasing hormone (GnRH), which is an autocrine growth inhibitor for the normal OSE[65]; follicle stimulating hormone (FSH) and various steroid hormones, which interact with their respective receptors expressed by OSE cells[66-68]; epidermal growth factor (EGF), which stimulates OSE proliferation and affects its differentiation[69]; several members of the transforming

growth factor beta (TGFβ) family of growth factors, which inhibit OSE growth[70]; and various cytokines, such as IL-1, IL-6, macrophage colony stimulating factor (M-CSF) and granulocyte macrophage colony stimulating factor[71] (GM-CSF). A number of the aforementioned growth factors and hormones often signal through mitogen-activated protein kinases[72] (MAPKs). During ovulation, gonadotrophic stimulation of plasminogen activator secretion by the OSE part that is contiguous with the preovulatory follicle elicits a local increase in the concentration of tissue plasmin. This in turn activates latent collagenases and releases tumour necrosis factor alpha (TNFα) from the thecal endothelium, which precipitates collagenolysis by the induction of matrix metaloproteases. Consequently, the apical follicular wall weakens, leading to stigma formation and finally ovulatory rupture. In post-ovulatory repair, the OSE is likely to contribute to the restoration of the ovarian cortex through its capacity to synthesise both epithelial and connective tissue-type components of the extracellular matrix. The OSE's propensity to undergo epithelial to mesenchymal conversion is particularly advantageous during post-ovulatory repair, conferring increased cell motility and contractility and favourable proliferative and ECM-modifying responses.

1.2.2 Histological types and grades

Histologically, ovarian tumours are considered to be among the most complex[73]. Epithelial ovarian tumours are categorised into serous, endometrioid, mucinous, clear cell, Brenner, undifferentiated, mixed and unclassified types. Furthermore, they can be classified as benign, borderline (i.e. of low malignant potential; LMP) and malignant (carcinomas). As previously mentioned, normal OSE has both epithelial and mesenchymal features and hence can be considered not to be fully differentiated. Malignant transformation is accompanied by a differentiation process that drives the cells to acquire a more differentiated epithelial morphotype. The newly acquired epithelial characteristics are shared by Müllerian duct-derived epithelia and ovarian carcinomas are categorised according to the structure to which they resemble (Figure 1.8): serous carcinomas, which constitute the vast majority of ovarian tumours, resemble the structure of the fallopian tube; endometrioid tumours

have similar histology to the endometrium; mucinous tumours are reminiscent of the endocervix; and clear cell tumours resemble mesonephric structures.

In addition, the degree of differentiation of an ovarian tumour is reflected on its classification by histological grade. There are three grades: grade 1 is characterised by well-differentiated tumours, grade 2 by moderately-differentiated ones and grade 3 by poor differentiation status.

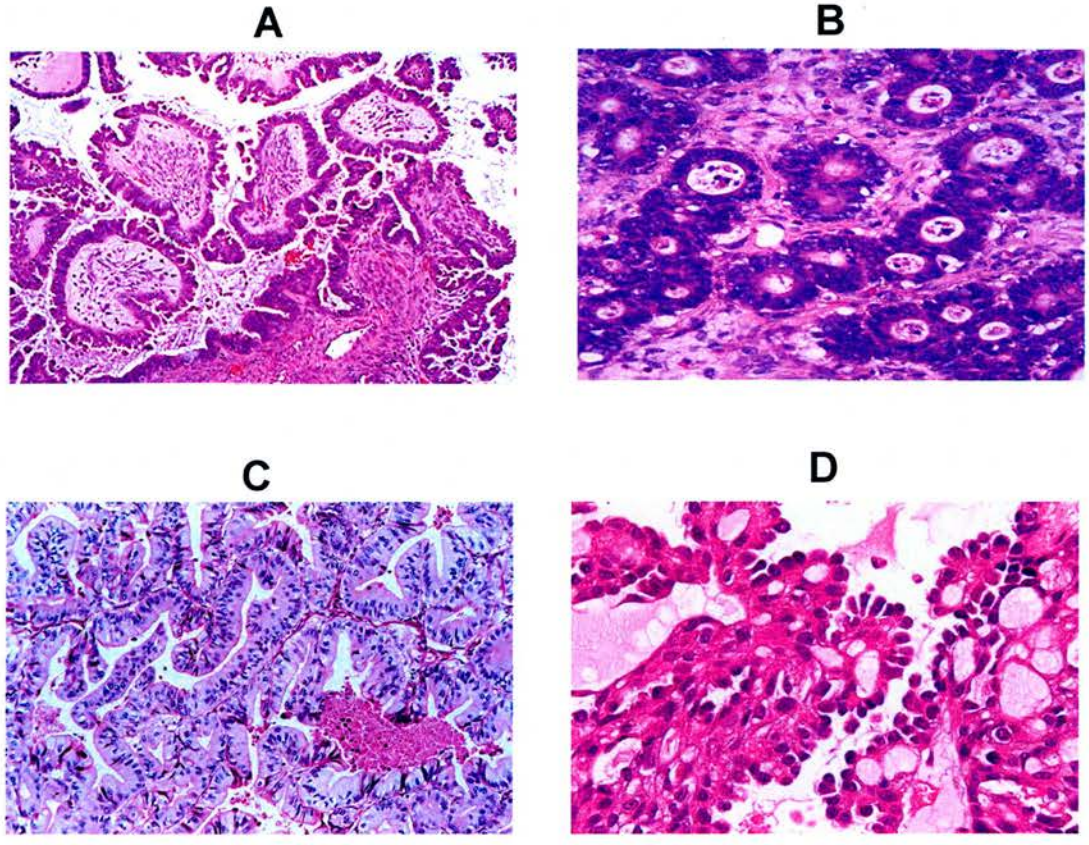

Figure 1.8 Epithelial ovarian cancer histological types
Sections of serous (A), endometrioid (B), mucinous (C) and clear cell (D) carcinomas. Images courtesy of Dr A. Al-Nafussi, Department of Pathology, University of Edinburgh (B,D) or reproduced from the Internet Pathology Laboratory for Medical Education, Florida State University website (A) and the "Borderline ovarian tumours: a web-based atlas" website (C).

1.2.3 FIGO staging

There are four basic stages of advancement in ovarian cancer according to its classification by the International Federation of Gynaecology and Obstetrics (FIGO). In stage I, the hallmark is the formation of inclusion cysts that invade the ovarian cortex. Malignant growth can be present in one (Ia) or both ovaries (Ib), or following rupture of a cyst, cancer cells can be extruded in the peritoneal cavity (Ic). Stage II disease is characterised by peritoneal dissemination to the fallopian tubes and/or the uterus (IIa) or to other tissues within the pelvis (IIb), which can be accompanied by the presence of ascitic fluid (IIc). In stage III, the disease has spread beyond the pelvis but is still restricted to the peritoneal cavity: there is only microscopic seeding (IIIa), or presence of nodules smaller than (IIIb) or larger than 2 cm (IIIc), or presence of positive retroperitoneal or inguinal nodes (IIIc). Finally, stage IV disease is defined by the presence of distant metastases, encompassing pleural effusion and parenchymal liver. On the whole, ovarian cancer is not an overtly metastatic disease, as it is mainly associated with locoregional dissemination, rather than spreading to distant sites. Thus, stage IV disease is quite rare.

1.2.4 Diagnosis, prognosis and treatment

Ovarian cancer is commonly initially indicated by suprapubic or transvaginal ultrasonography[74]. Initial findings are evaluated in combination with surgical exploration and histopathological examination, allowing the precise staging and grading of the disease. Ovarian cancer has been dubbed the "silent killer", as early stage disease is relatively asymptomatic and hence is rarely diagnosed by current means: only 20-25% of patients with invasive EOC are diagnosed with stage I or II disease. Generally, symptoms include prolonged swelling of the abdomen, which can be accompanied by pain, digestive problems and weight loss. The only validated marker in current use for the management of ovarian cancer is the CA125 glycoprotein: approximately 80% of patients with overt symptoms present with increased levels of immunoreactive CA125. However, the use of this marker in ovarian cancer diagnosis is problematic, due to the lack of specificity and sensitivity of tests, the fact that some ovarian cancer types are usually not associated with

elevated CA125 levels (mucinous tumours) and the detection of false positives in conditions such as pregnancy, pelvic inflammatory disease, endometriosis etc[75].

The following factors contribute to the prognosis of ovarian cancer: age, disease type, stage and grade, volume of residual tumour after initial surgical "debulking" and patient performance status. Although if diagnosed early ovarian cancer has a very good prognosis, with a 92% 5-year survival rate, most cases (75%) are diagnosed at a late stage of disseminated disease when the prognosis is much less favourable, with only a 25% 5-year survival rate.

Treatment of ovarian cancer varies according to the objectives that are to be met[76,77]. Upon initial diagnosis, previously untreated patients are offered treatment that aims at curing them and prolonging their survival. Subsequently, maintenance or consolidation therapy is offered, in order to prevent recurrence of the disease. If patients relapse after first-line treatment, the primary objective of treatment becomes mostly palliative, so as to control symptoms, improve quality of life, and increase disease-free interval, thus prolonging overall survival.

Most patients with early stage disease are cured with standard therapy. Staging laparotomy will indicate whether a patient has a high (stage I high-grade tumours, stage Ic tumours, and all stage II tumours) or low (stage Ia and Ib tumours) risk of recurrence. For the low-risk group, cytoreductive surgery alone is usually effective in curing more than 90% of patients. In contrast, patients in the high-risk category of early stage disease have a relapse rate of 40-50%, and many will die from recurrent disease. For these patients, surgery is commonly accompanied by adjuvant platinum-based chemotherapy. The value of this approach has been demonstrated by the ACTION (Adjuvant Chemotherapy in Ovarian Neoplasm) randomised clinical trial, which reported that immediate platinum-based chemotherapy improved overall and recurrence-free survival[78]. However, this treatment regime is still ineffective in 18% of patients, suggesting better options are needed.

With respect to the vast majority of patients, who are diagnosed with advanced-stage disease, treatment commonly consists of cytoreductive surgery and subsequent combination chemotherapy, employing a platinum-based compound, such as cisplatin or carboplatin, and either a taxane such as paclitaxel, or an

alkylating agent such as cyclophosphamide. Recent large prospective studies have favoured the use of carboplatin and paclitaxel, a combination that tends to become the standard of care for advanced-stage disease[79,80]. Nonetheless, approximately 75% of these patients will relapse in less than 5 years post treatment, with a median survival following recurrence of approximately 2 years.

Finally, in cases wherein platinum-resistance has developed, alternative treatments can be offered, including the administration of gemcitabine, topotecan, doxorubicin and taxanes. Unfortunately, the response rate of these chemotherapy options is particularly low, often below 15%.

1.2.5 Aetiology

It has been long established that parity, lactation and oral contraceptive use act as protective factors against ovarian cancer[81]. These factors are in agreement with the two major hypotheses regarding the aetiology of ovarian cancer that have shaped thinking on the disease pathogenesis. Moreover, recognised environmental risk factors in ovarian cancer include diet, talc, industrial pollutants, cigarette smoking, asbestos and infectious agents[82]. Family history is a strong determinant in 5 to 10% of ovarian cancer cases.

The original hypothesis of the aetiology of ovarian neoplasia is the incessant ovulation hypothesis, as formulated by Fathalla in 1971[83]. The principal idea of this hypothesis is that continuous ovulatory cycles are damaging to the ovarian surface epithelium. Consequently, ovarian cancer arises mainly in species such as human and chicken, wherein frequent cyclic ovulation occurs, in contrast with rats and mice for example[84]. Ovulation is accompanied by cell damage, which in turn translates into an enhanced potential for aberrant DNA repair, inactivation of tumour suppressor pathways and subsequent mutagenesis[85,86]. It has been demonstrated that a high number of ovulatory cycles may be associated with increased levels of proliferation-linked DNA damage and an increased risk of developing certain types of EOC[87]. Although the phenomenon of ovulation is widely accepted as central to the pathogenesis of ovarian cancer, some of the expectations of the incessant ovulation hypothesis have not been confirmed by epidemiologic evidence[88,89]. Notably, the link

between infertility and ovarian cancer risk is not properly established and factors that reduce ovulation do not proportionally reduce the risk of ovarian cancer.

The second major hypothesis is the pituitary gonadotrop(h)in hypothesis[90]. Key to this hypothesis is the entrapment of OSE in inclusion cysts within the ovarian stroma (Figure 1.9). The entrapped epithelium is thought to be subsequently stimulated by oestrogen or oestrogen precursors, particularly in the presence of high and persistent levels of luteinising hormone (LH) and follicle stimulating hormone (FSH), both of gonadotrophic function. As in the incessant ovulation hypothesis, not all the epidemiologic evidence is in concert with the gonadotrophin hypothesis. For example, one study that measured the serum levels of gonadotrophic hormones many years prior to outcome did not find an association between hormone levels and occurrence of ovarian cancer[91]. Even if the gonadotrophin hypothesis should not be accepted in its entirety, it is generally believed that steroid hormones play a role in ovarian tumourigenesis[92]. Furthermore, it has been postulated that ovarian cancer risk is increased by factors associated with excess androgen stimulation of OSE cells and reduced by factors linked to a greater progesterone stimulation[93].

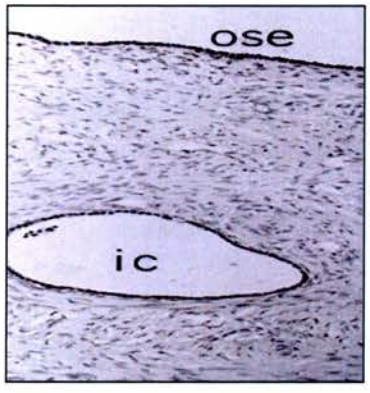

Figure 1.9 Ovarian inclusion cyst
Entrapped epithelium within the ovarian stroma. ic = inclusion cyst.
Reproduced from Auersperg *et al.*, 2001.

Increasingly, inflammation has been regarded as an essential element in the aetiology of ovarian neoplasia[94]. There is an array of epidemiologic evidence in support of a role by inflammation, exemplified by risks imposed by talc and asbestos exposure[95,96], endometriosis[97] and pelvic inflammatory disease[98] and protection by either hysterectomy without oophorectomy or tubal ligation[99]. Cytokines normally secreted by OSE cells, such as IL-1 and IL-6, are also produced by ovarian cancer cells[71,100]. The recruitment of these normally secreted cytokines into deregulated autocrine loops may be essential to the tumourigenic process and could be contributing to mutagenesis. Furthermore, ovulation is associated with a marked inflammatory response[101]. The epithelium in and around the site of ovulation may replicate more actively, come into contact with a plethora of cytokines and prostaglandins and be subjected to oxidative stress, thereby increasing the risk of mutagenesis. Hence, inflammation might be linked to ovarian carcinogenesis through the same processes that physiologically tie it to ovulation.

1.2.6 Origin, early events and disease progression

The study of early events leading to ovarian carcinogenesis has been greatly hampered by the lack of animal models until quite recently and methodological problems in the culture of ovarian surface epithelial cells[102]. However, with recent advances, our understanding of how ovarian cancer arises has become better.

It is now generally accepted that epithelial ovarian cancer arises in the OSE. Histologically, there have been various observations favouring an OSE origin: atypia is often found in the OSE adjacent to invasive carcinoma; there is an increased frequency of inclusion cysts in normal ovaries contralateral to malignant ones; the OSE adjacent to a carcinoma is more metaplastic and dysplastic; and ovaries that have been prophylactically removed due to a family history of ovarian cancer tend to have more inclusion cysts[103]. Nevertheless, it is quite rare to find OSE atypia without the presence of adjacent invasive carcinoma. This rarity, together with the fact that, morphologically, ovarian tumours resemble components of Müllerian rather than OSE origin has created in the past controversy over the true origin of epithelial ovarian cancer. It was once suggested that components of the secondary Müllerian system (such as paraovarian and tubal cysts, and rete ovarii) play a role in ovarian

carcinogenesis[104]. However, to understand why this argument has been mostly refuted, one has to appreciate the special nature of the OSE and examine the recent experimental evidence.

As previously discussed, the OSE is characterised by an incomplete differentiation, which confers it a propensity to undergo EMC following regenerative stimuli. EOC is unique among most epithelial cancers in that instead of the cells acquiring a less differentiated phenotype, ovarian cancer cells are generally more differentiated than OSE cells. How are these two issues linked and how can they be explained? It is known that with neoplastic progression, the tendency of OSE to undergo EMC diminishes and the cells become committed to epithelial phenotypes[102]. Cancerous cells acquire specialised epithelial features, exemplified by the expression of E-cadherin and various mucins, and the development of polarised epithelia, with papillae, cysts and glandular structures. Only in the late stages of disease advancement do these specialised features diminish, although they can persist even when tumours are metastatic or in the form of ascites[105]. This metaplasia is particularly evident in surface invaginations and inclusion cysts. Metaplastic cells express E-cadherin, which may act as a survival factor, while their expression of the *MET* oncogene increases, which is known to contribute to the growth and invasiveness of many types of cancer[106]. E-cadherin is central to this differentiation process. It is a transmembrane, calcium-dependent cell adhesion molecule, which promotes cell-cell adhesion and the formation of adherens junctions, stabilised by its association with α, β and γ catenins that are physically linked to F-actin[107,108]. Normal OSE cells rarely express E-cadherin, whereas metaplastic OSE cells often do[105,109]. Furthermore, although E-cadherin is scarce or absent in ovarian cancer metastases, it is almost always present in primary ovarian tumours[110-113]. When E-cadherin was expressed in SV40 large T-antigen immortalised OSE cells, the transfected cells did not undergo EMC; instead, they acquired more epithelial features, e.g. the expression of cytokeratins and CA125, which are associated with ovarian metaplasia and neoplasia, suggesting that E-cadherin plays a causal role[114].

Major progress has been made recently with respect to animal models in ovarian cancer by three independent groups. Orsulic and colleagues used p53-deficient transgenic mice that constitutively express the avian receptor TVA[115].

Ovarian cells were taken from these mice and were infected *ex vivo* with a replication-competent avian leucosis virus vector harbouring the coding sequence of selected oncogenes (*Myc* and/or *Kras* and/or *Akt1*). *In vitro*, the infected cells exhibited increased proliferation, especially when both *Myc* and *Akt1* were expressed. When infected cells were reintroduced in the mice, subcutaneously, intraperiotoneally or homotopically, expression of any two of the three oncogenes resulted in tumours that were of epithelial origin. The induced ovarian tumours resembled human ovarian carcinomas in their progression rate and peritoneal dissemination. Tumours also developed in a p53-proficient background, although with a much increased latency period. Connolly and co-workers used the *Misiir* (Müllerian inhibitory substance type II receptor; official symbol: *Amhr2*) promoter to drive the expression of the SV40 large T-antigen in female transgenic mice, taking advantage of the notion that *MISIIR* is expressed in ovarian cancer cells but not in normal OSE cells[116]. 50% of these mice developed ovarian tumours of epithelial origin that resembled human ovarian tumours of poor differentiation, with intraperitoneal dissemination, invasion of the omentum and formation of ascites. Ascite-derived cell lines exhibited expression of epithelial markers, anchorage independence, and tumourigenicity when xenografted in SCID mice. Finally, Flesken-Nikitin and colleagues created a conditional mouse model of ovarian cancer[117]. They used immunocompetent mice that are homozygous for floxed alleles of *Tp53* and *Rb1*, and by administering adenoviral constructs expressing Cre recombinase in the bursa, they achieved inactivation of the two transgenes in OSE cells. This resulted in the growth of epithelial ovarian tumours, mostly of serous histology, which spread intraperitoneally, forming ascites, and metastasised to the lung and the liver. Interestingly, even early dysplastic lesions had inactivation of both transgenes. So, what have these studies achieved collectively? Apart from providing valuable tools to study and understand ovarian cancer in the mouse, they have strengthened the theory that ovarian cancer arises in the OSE and have cast some light on the early molecular events that might be required in ovarian tumourigenesis.

In ovarian cancer, a stepwise sequence of molecular events that accompany tumourigenesis has not been described[103]. In contrast, it is a matter of debate whether

there is a progression from benign tumours to borderline tumours to ovarian carcinomas. The linear progression hypothesis posits that ovarian cancer arises from less malignant entities, which progress to full malignancy by the accumulation of genetic mutations[118-120]. According to this theory, tumours of low malignant potential, i.e. borderline tumours, represent precursor lesions. As an antithesis, it has been postulated that LMP tumours and carcinomas are independent, each arising *de novo* from the OSE[121]. The evidence to date, mostly based on comparative genomic hybridisation studies, does not entirely exclude either hypothesis, although the growing consensus is arguably leaning on the non-progression theory or a combination of both[122-125]. A dualistic model proposed by Shih Ie and Kurman proposes that ovarian neoplasms arise by two distinct pathways[126]. Type I carcinomas (low-grade serous, endometrioid, clear cell and mucinous) arise from precursor lesions of low-malignant potential, whilst type II carcinomas (high-grade serous and undifferentiated) arise *de novo*, evolve more rapidly and are more aggressive. It still remains a matter of debate whether there is progression in ovarian tumourigenesis, as well as to what extent divergence occurs among different histological types and between LMP tumours and invasive carcinomas. This problem might be resolved with the better and more rational classification of ovarian tumours, which is likely to be available in the future, based on molecular rather than morphological criteria. A number of microarray studies have already pointed to molecular separation between distinct histological types of ovarian cancer[127,128].

1.2.7 Genetics of EOC

Epithelial ovarian cancer manifests with tumours of clonal origin that arise due to multiple genetic changes[129,130]. The familial and sporadic types of epithelial ovarian cancer are thought to differ in their molecular pathogenesis. Hence, the genetics of each type will be introduced separately in the following sections.

1.2.7.1 Familial EOC

5-10% of ovarian cancer cases are thought to be familial[60,131]. Three distinct hereditary ovarian cancer syndromes have been described to date: hereditary site-specific ovarian cancer, hereditary breast/ovarian cancer and hereditary

non-polyposis colorectal cancer (HNPCC)[62]. The genetics of hereditary site-specific ovarian cancer remain obscure, apart from the fact that heredity is autosomal dominant as in the other two syndromes.

The high-penetrance genes associated with hereditary breast/ovarian cancer are the extensively studied *BRCA1* and *BRCA2* genes, both encoding proteins thought to regulate the DNA damage response[132,133]. More specifically, the BRCA1 and BRCA2 proteins are involved in the repair of double-stranded DNA breaks by homologous recombination[134]. This potentially error-free DNA repair mechanism requires the localisation of RAD51 to the site of damage, forming foci in the nucleus. BRCA2 interacts directly with RAD51, whereas BRCA1 is required for the formation of foci by an as yet unidentified interaction[135]. Cells lacking functional BRCA1 and BRCA2 are diverted to using more error-prone repair pathways, thus risking the occurrence of chromosomal abnormalities and genetic instability. Apart from a role in homologous recombination, which is best documented for BRCA2, additional functions have been proposed for BRCA1 in nucleotide excision repair, cell cycle checkpoint control, protein ubiquitination, chromatin remodelling and transcriptional activation of oxidative stress-responsive genes[136-138].

BRCA1 was first to be identified and cloned[139]. The human gene spans approximately 80 kb on 17q12-21, encoding a protein of 1863 aa. To date, more than 250 *BRCA1* mutations have been described, which span the entire coding sequence of the gene. The majority of these mutations have been identified in families with multiple cancer cases. 87% of all described germ-line mutations result in either truncation or absence of the protein, brought about by frameshift, nonsense, splice-site, and genomic deletion changes. *BRCA2* is located on human chromosome 13q12-13[140]. It encodes a protein of 3418 aa. As in *BRCA1*, mutations in *BRCA2* have been described throughout its coding region. The majority of mutations are frameshifts resulting in protein truncation. Population-based studies have suggested that the lifetime risk of ovarian cancer is about 20-30% in *BRCA1* mutation carriers, albeit this increased risk is not manifest until around the age of 40[141]. *BRCA2* mutations were initially thought to play a much less important role in familial ovarian cancer, whereas newer evidence suggests that as much as 35% of hereditary ovarian cancer cases might be attributable to *BRCA2* mutations[142]. A cluster of

mutations in the *BRCA2* gene, known as the ovarian cancer cluster region, is associated with increased ovarian and decreased breast cancer risk[143]. The prevalence of mutations in 316 cases of British origin unselected for family history was found to be 2.5% for *BRCA1* and 2.2% for *BRCA2*[144].

The above-described high-penetrance genes are thought to account only for a proportion of familial risk. Although there are no reported estimates of the proportion of excess familial risk conferred by these genes, *BRCA1* will account for 16% of this excess risk, assuming a mutation frequency of 1:1000 and a 20-fold risk, whereas *BRCA2* will account for 8%, assuming a mutation frequency of 1:500 and a 10-fold increase in risk. Hence, these genes might be contributing only 30% of the known excess risk[131].

HNPCC is characterised by defects in the mismatch repair (MMR) system, which is responsible for the repair of nucleotide changes during DNA replication, thus preventing the propagation of mutations. The five main genes associated with MMR are *MLH1*, *MSH2*, *MSH3*, *PMS1* and *PMS2*. Mutations in *MSH2* and *MLH1* account for 70% of HNPCC cases, with *PMS1*, *PMS2* and *MSH3* accounting for some of the rest[145]. The cumulative risk of ovarian cancer in MMR gene mutation carriers from HNPCC families is 12%[146].

Low-penetrance susceptibility genes are more difficult to identify mainly due to issues of experimental design. The experimental approach usually employed involves association studies, which aim at discovering polymorphisms that confer risk of developing a disease. With respect to ovarian cancer, there have been numerous reports of case-control studies of polymorphisms, which have identified various risk-associated alleles. Examples include polymorphisms in *TP53*[147], *GSTM1*, *GSTT1*[148] and *HRAS*[149]. *TP53* would appear to be the best candidate thus far, although the case for this is not proven. The role of *TP53* will be elaborated upon in relation to sporadic EOC, although it is also associated with the familial type of the disease. It should be noted that problems associated with statistical power and significance, as well as the importance of modulation by other genes and environmental factors, have hampered the value of published association studies.

1.2.7.2 Sporadic EOC

Very few cases of *BRCA1* or *BRCA2* mutations have been reported in sporadic EOC[150,151]. Nonetheless, decreased expression of *BRCA1* has been documented, and accounted for by promoter hypermethylation[152]. In contrast, the same study found over-expression of *BRCA2* in sporadic EOC, which was also caused epigenetically, by promoter hypomethylation. The significance of this finding remains to be elucidated.

A multitude of other genes have been implicated in sporadic EOC[60]. Most of the recognized oncogenes are either genes that are implicated in other types of cancer and were thus chosen for study in ovarian cancer or have been identified by being over-expressed or amplified and were subsequently pursued in functional studies. It should be noted that little is known about how and at what level oncogenes participate in the malignant transformation of the ovarian surface epithelium[153]. Tumour suppressor genes have been identified by positional cloning based on cytogenetic, linkage and LoH studies; expression and/or promoter methylation profiling; differential display; and functional analysis[154]. LoH studies are the most common approach for identifying TSGs in sporadic cancers. *OPCML* is one example of a gene originally identified by LoH and now regarded as a novel TSG in sporadic EOC[21]. Interestingly, this gene also exemplifies a growing list of TSGs that are inactivated primarily or exclusively by epigenetic silencing through promoter hypermethylation, rather than somatic mutations.

Tables 1.2 and 1.3 illustrate the genes that have been linked to sporadic EOC to date. These genes were identified by literature searches using the following criteria: up-regulation and/or activating mutations and/or oncogenic properties for genes putatively termed oncogenes; down-regulation and/or inactivating mutations and/or anti-oncogenic properties for genes putatively termed tumour suppressor genes. These tables exclude genes that have been solely identified by cell line analyses or microarray evidence, or have been reported by studies focusing exclusively on chemoresponse or clinical outcome. References are given as examples and are not exhaustive.

More detailed information is provided below on the two most extensively studied oncogenes and TSGs in sporadic EOC.

Oncogenes

- *ERBB2*

ERBB2 is an oncogene located on 17q21.1 encoding a member of the epidermal growth factor (EGF) receptor family of receptor protein kinases[155]. The ERBB2 protein does not have a ligand-binding domain and therefore binds to other ligand-bound EGF receptor family members, forming heterodimers that enhance kinase-mediated activation of downstream signalling pathways[156]. Examples include the MAPK and PI3K pathways.

Amplification and/or over-expression of *ERBB2* have been extensively documented in ovarian cancer (see references in Table 1.2), with conflicting data regarding associations with clinicopathologic variables. A recent study has reported a prevalence of 27% for over-expression of the gene[157], which is representative of the central tendency in most studies. Functionally, the oncogenic properties of ERBB2 have been demonstrated in ovarian cancer, by transfection of the gene in rat OSE cells[158].

- *KRAS*

The *KRAS* gene, which is located on 12p12.1, encodes an oncoprotein that belongs to the small GTPase superfamily[159-161]. It is thought to have a crucial function in the regulation of growth in eukaryotic cells, by being involved in the control of cell proliferation, differentiation and apoptosis.

KRAS is frequently mutated in ovarian cancer, in particular mucinous carcinomas, wherein it has a mutation prevalence of approximately 50% (see references in Table 1.2). Interestingly, *KRAS* mutations are also frequent in borderline tumours, again especially of the mucinous type, suggesting that these tumours represent a precursor lesion of the invasive carcinoma.

Tumour suppressor genes

- *TP53*

The *TP53* gene on 17p13.1 encodes a nuclear protein that is pivotal in the regulation of the cell cycle, particularly in the transition from G0 to G1[162]. Upon cellular stress, particularly DNA damage, the p53 protein can arrest cell cycle progression, thus allowing DNA repair, or lead to apoptosis. p53 is a DNA-binding protein containing DNA binding, oligomerisation and transcription

activation domains. It is postulated to bind as a tetramer to specific *cis* elements and activate expression of downstream genes that inhibit growth and/or invasion, thereby exhibiting tumour suppressor properties. The protein also has transcription-independent tumour suppressor functions, in DNA repair and recombination[163]. *TP53* is expressed at very low levels in normal cells; however, in a variety of transformed cell lines, its expression increases, which is believed to contribute to transformation and malignancy. Mutations in the *TP53* gene result in the loss of proliferation controls and hence inefficient DNA repair and genetic instability. The most common alterations in the *TP53* gene are missense mutations in its DNA-binding domain, which result in the loss of its tumour suppressor activity and over-expression of non-functional p53 in the nucleus. Alterations of the *TP53* gene occur not only as somatic mutations in human malignancies, but also as germ-line mutations in some cancer-prone families with Li-Fraumeni syndrome.

TP53 represents the TSG that is most frequently associated with ovarian cancer[163]. In ovarian cancer, pooled data show *TP53* over-expression in 17% of borderline tumours, 39% of early and 55% of advanced stage cases. Over-expression of *TP53* is more frequent in serous carcinomas (56%) than other histological types and p53 immunopositivity is highest among grade 3 tumours. *TP53* mutations are met in 45% of all carcinomas, again being more prevalent in the serous type and advanced-stage disease. In contrast, only 5% of LMP tumours have *TP53* mutations. The majority of studies have not found associations between aberration of *TP53* and ovarian cancer prognosis.

- *PTEN*

This gene was identified as a TSG on 10q23 that is mutated in a large number of cancers at high frequency[164]. It encodes a protein that contains a tension-like domain, as well as a catalytic domain similar to that of dual specificity protein tyrosine phosphatases[165]. Unlike most of the protein tyrosine phosphatases, however, PTEN preferentially dephosphorylates phosphoinositide substrates. It negatively regulates intracellular levels of phosphatidylinositol-3,4,5-trisphosphate, thereby functioning as a tumour suppressor by inhibiting the AKT/PKB signalling pathway[166].

Mutations in the *PTEN* gene are well documented in ovarian cancer, although the overall data regarding their frequency and importance are conflicting[167]. A number of studies have reported mutations and/or loss of *PTEN* expression (see references in Table 1.3), whereas others did not find a role for this gene in EOC[168]. Aberrations are often associated with endometrioid histology and arise through diverse mechanisms, such as allelic loss, intragenic deletion and epigenetic silencing[169]. Functionally, *PTEN* expression in ovarian cancer cell lines results in growth suppression and inhibition of migration[170,171].

Gene	Evidence	Histological type	References
AKT2	Amplification		172
	Expression		173
BRAF	Mutation	LMP serous	174
	Expression		175
CCND1	Expression		176
	Amplification	Mucinous	177
EEF1A2	Expression+Function		178
EIF5A2	Expression+Function		179
	Amplification		180
	Amplification		181
	Amplification	Serous	182
	Expression		183
ERBB2	Amplification		184
	Amplification		185
	Expression	Mucinous+Endometrioid	186
	Expression	Clear cell	187
	Function		188
	Expression		157
FGF3	Amplification		184
HRAS	Function		189
KIT	Expression	Serous	190
	Mutation	LMP mucinous	191
	Mutation	Mucinous	192
	Amplification		181
	Mutation	Mucinous	193
	Mutation	Serous	194
KRAS	Mutation	Mucinous	195
	Mutation	Mucinous	196
	Mutation	Mucinous	197
	Mutation	Mucinous	198
	Mutation	Mucinous	199
	Mutation	Mucinous	200
MDM2	Expression	Mucinous+Endometrioid	186
MET	Expression+Function		201
MST1R	Expression+Function		201
	Amplification		202
MYC	Expression	Serous	203
	Amplification		181
	Amplification		204
MYCL1	Amplification+Expression		205
PAK1	Amplification+Expression		206
PIK3CA	Amplification+Function		207
	Mutation	Clear cell+Mucinous	208
PIK3R1	Mutation		209
PTGS2	Expression	Serous	210
	Expression	Serous	211
WFDC2	Expression	Serous+Endometrioid	212

Table 1.2 Putative oncogenes involved in sporadic EOC
Potential oncogenes reported in sporadic ovarian cancer. Gene symbols displayed according to the HUGO Gene Nomenclature Committee.

Gene	Evidence	Histological type	References
ADPRH	Expression		213
BCL2	Expression	Serous	214
BCL2L1	Expression	Serous	214
CAV1	Expression+Function		215
CD82	Expression		216
	Expression(methylation)		217
	Mutation		218
CDKN2A	Expression		219
	Expression(methylation)	Serous	220
	Expression	Serous	221
	Methylation		222
DCC	Expression	Serous	223
DIRAS3	Expression+Function		224
DOC2	Expression+Function		225
DPH1	Expression+Function		226
HTRA1	Expression+Function		227
MAP2K4	Expression+Function		228
MYO18B	Mutation+Expression(methylation)		229
OPCML	LoH+Expression(methylation)+Function		21
PLAGL1	LoH+Expression		230
	Expression(methylation)+Function		231
PRDM5	Expression+Function		232
PTEN	Mutation	Endometrioid	233
	LoH+Mutation		234
	LoH+Expression		169
	Mutation+Expression	Endometrioid	235
PYCARD	Expression(methylation)		236
RB1	Expression		237
RNASET2	Expression+Function		238
	Function		239
SEPT9	Expression(methylation)		240
SFRP1	Expression(methylation)		241
SMAD4	LoH+Mutation		242
SPARC	Expression+Function		243
TACC1	Expression	Endometrioid	244
TACC2	Expression	Serous	244
TCEAL7	Expression(methylation)+Function		245
TFAP2A	Function		246
TP53	Expression		247
	Mutation		248
	Expression		183
	Mutation		249
	Mutation+Expression		250
	Expression	Serous	195
	Mutation	Endometrioid	251
	LoH+Mutation	Serous	192
	Mutation	Serous	252
TP73	LoH+Expression		253
WT1	Expression(methylation)	Clear cell	254
	Expression	Mucinous+Clear cell	255
WWOX	Mutation		256
	Expression		257

Table 1.3 Putative TSGs involved in sporadic EOC

Potential tumour suppressor genes reported in sporadic ovarian cancer. Gene symbols displayed according to the HUGO Gene Nomenclature Committee.

1.3 The project

1.3.1 Rationale

The hypothesis that *OPCML* is a tumour suppressor gene in epithelial ovarian cancer incurred the realisation that the knowledge of the biology of this gene and the family where it belongs is very limited. The IgLON family has been historically associated with the central nervous system due to the fact that its members are prototypically expressed in this locality. Furthermore, the emphasis of IgLON study has been primarily placed on chick and rat models of neural function. In contrast, our appreciation of what OPCML and its relatives do outside the brain is rather obscure. This is mainly due to the fact that until recently there was limited interest on exploring the biology of the IgLON family at a more generalised level. Nonetheless, assuming that OPCML plays a role in ovarian carcinogenesis, it has to do so in a way whereby it has functions in the normal ovary that are impaired in ovarian cancer. It is imperative that these potential functions be explored; this realisation provided the momentum for the conception of this project. Not only is there a need to understand why and how OPCML is linked with ovarian cancer, but also to establish the role of OPCML in normal ovarian physiology. These issues should be addressed in the context of the position of OPCML within the IgLON family and its interactions with the rest of the family.

1.3.2 Objectives

In view of the aforementioned reasoning, the project that is presented in this thesis has focused on aspects of OPCML and IgLON biology that have not been previously studied. The primary aim has been the functional characterisation of OPCML, in particular with regard to roles that are relevant in normal ovarian physiology and ovarian tumourigenesis. What attributes does OPCML have in order to function as a tumour suppressor? How does its dysfunction contribute to ovarian carcinogenesis? In addition to the identification of novel functions, the secondary objective of this work has been the characterisation of not only *OPCML*, but also the IgLON family as a whole, at the level of gene expression. More specically, questions regarding the expression of the family in development, in normal adult tissues, and

also in ovarian cancer were raised. Overall, the project was developed to address issues of OPCML function and IgLON expression. Attempts to meet these objectives were shaped by consideration of models and ideas that are significant in ovarian cancer.

1.3.3 Approach

In order to explore the functions of OPCML *in vitro*, the gene was expressed in two different contexts. Firstly, an inducible system of expression was created and characterised for the purposes of this work. The inducible system used was a Tet-On system of regulated expression in the cervical cancer HeLa cell line. The HeLa Tet-On cell line was used to express the wild-type *OPCML* sequence. Secondly, a previously generated resource was also used, an over-expression system based on the ovarian cancer SKOV-3 cell line. Both wild-type and mutant (harbouring the P95R mutation) *OPCML* were expressed in SKOV-3 cells. Hence, the functional characterisation of OPCML was undertaken both at a regulated and an over-expression level, in two different contexts. To allow the study of OPCML in an ovarian cancer cell line in a regulated fashion of expression, a SKOV-3 based Tet-On system was also developed. However, due to time constraints, this system was not ready for use in functional work.

Issues of IgLON expression were addressed in both mouse and human using a variety of experimental approaches at both the RNA and protein levels. IgLON expression was examined developmentally, in adult life, in cancer cell lines and in sporadic EOC. Methodologically, it was attempted to use a diverse range of approaches, covering expression from the molecular to the histological level.

Chapter 2

Materials and methods

2.1 Cell culture

2.1.1 Transfected cell line resources

The following transfected cell lines were used, which had been previously generated by members of the research group (Table 2.1):

Designation	Cell line	Vector	Insert
SKOV-3 OPCML^{WT}	SKOV-3 derivative clone	pcDNA3.1/Zeo (Invitrogen)	wild-type human *OPCML*[i]
SKOV-3 OPCML^{Mut}	SKOV-3 derivative clone	pcDNA3.1/Zeo (Invitrogen)	mutant human *OPCML*[ii]
SKOV-3 HNT	SKOV-3	pcDNA3.1 (Invitrogen)	human *HNT*[iii]
SKOV-3 LSAMP	SKOV-3 derivative clone	pcDNA3.1/Zeo (Invitrogen)	human *LSAMP*[iv]
SKOV-3 NEGR1	SKOV-3 derivative clone	pcDNA3.1/Zeo (Invitrogen)	human *NEGR1*[v]

Table 2.1 Available transfected cell lines
Cell lines used in this project that had been previously generated. HeLa is a cervical cancer cell line; SKOV-3 is an ovarian cancer cell line. Vector maps are shown in Appendix C.

2.1.2 Maintenance of cell lines

All cell lines were maintained at 37°C in a humidified atmosphere of 5% CO_2 in an open-air incubator. Cell culture plasticware was purchased from Nunc™. Media, PBS (Appendix A) and dissociation solutions were prewarmed to 37°C prior to use.

The SKOV-3 derivative cell line, as well as SKOV-3 HNT, was maintained in RPMI 1640 medium (Invitrogen), containing 10% (v/v) heat-inactivated foetal calf serum (FCS), penicillin (100 units/ml), streptomycin (100 µg/ml), and geneticin (600 µg/ml). The cell lines transfected with the other IgLON constructs were maintained in the same medium, with the addition of zeocin (125 µg/µl).

[i] Nucleotides 24-1110 of GenBank NM_002542.2
[ii] As above, but with C>G at position 334 of the sequence
[iii] Nucleotides 248-1600 of GenBank AF126426.1
[iv] Nucleotides 484-1520 of GenBank NM_002338.2
[v] Nucleotides 84-1233 of GenBank NM_173808.2

Double stable HeLa Tet-On cells harbouring an inducible *OPCML* construct were cultured in DMEM (Invitrogen) containing 10% (v/v) FCS, as well as the following antibiotics: penicillin (100 units/ml), streptomycin (100 μg/ml), geneticin (100 μg/ml) and hygromycin B (100 μg/ml). SKOV-3 Tet-On cell lines were maintained in RPMI 1640 medium (Invitrogen) supplemented with 10% (v/v) FCS, as well as the following antibiotics: penicillin (100 units/ml), streptomycin (100 μg/ml), and geneticin (300 μg/ml). SKOV-3 Tet-On OPCML cells were maintained in the same medium, with the addition of hygromycin B (50 μg/ml)

The medium was changed twice a week.

2.1.3 Cell passage

Cells were routinely passaged when reaching confluency. The medium was removed, cells were washed twice with PBS and an appropriate amount of trypsin was added. Cells were placed in an incubator at 37°C / 5% CO_2 until completely detached. The effect of trypsin was counteracted with the addition of medium containing 10% (v/v) FCS. An appropriate volume of the cell suspension was transferred to a fresh cell culture container, the medium was replenished, and the cells were returned to the incubator.

2.1.4 Stable and transient transfections of cell lines

Two rounds of stable transfections were undertaken in order to create the SKOV-3 Tet-On cell line expressing wild-type *OPCML*. In the first round, the pTet-On vector was introduced in SKOV-3 cells; in the second round, the pTRE-Tight OPCML construct was introduced in the selected SKOV-3 Tet-On clone.

Transfections into cells were carried out using Lipofectin® Reagent (Invitrogen), according to the manufacturer's guidelines. For stable transfections, $2x10^5$ cells were plated out in 6 cm petri dishes, in quadruplicate. The cells were incubated in the appropriate medium supplemented with 10% (v/v) FCS at 37°C / 5% CO_2 for 18-24 h, until 40-60% confluent. The following day, two sets of 1.5 ml eppendorf tubes were prepared. The first set contained 100 μl of serum-free medium without any antibiotics, 2 μg of vector DNA (for the first transfection) or the same

amount of construct DNA (for the second transfection) and 0.11 μg of Linear Hygromycin Marker (for the second transfection; from BD Biosciences). The second set contained 100 μl of serum-free medium without any antibiotics and 12 μl of Lipofectin. The tubes were allowed to stand at room temperature for 30 min. The contents of one tube from the first set and one tube from the second set were mixed in a 15 ml tube and allowed to stand at room temperature for a further 15 min. During this time, the plates containing the cells were drained and rinsed once with serum-free medium. 1.8 ml of serum-free medium without any antibiotics were added to each 15 ml tube, which was then tapped gently to mix. The contents of each tube were poured onto the appropriate plate. The plates were placed in an incubator at 37°C / 5% CO_2. After six hours, the medium was replaced with serum-containing medium without any antibiotics and the plates were returned to the incubator. After 48 h, the cells were trypsinised and transferred into a 175 cm^2 flask. 50 ml of selection medium was added [RPMI 1640 (Invitrogen) containing 10% (v/v) FCS, penicillin (100 units/ml), streptomycin (100 μg/ml) and geneticin (600 μg/ml) for transfection with pTet-On; as above, but with the addition of hygromycin B (50 μg/ml) for transfection with pTRE-Tight OPCML]. The flasks were refilled with 30 ml selection medium every 3-4 days until all the cells in the control flask had completely died and colonies were clearly visible in the other flasks. At that point, the medium was removed from the flasks, which were washed twice with PBS. A drop of trypsin was added to each colony with a fine pastette. Using the pastette, the colony was gently scraped while being aspirated and transferred to a 24-well plate. When all colonies had been transferred, the 24-well plates were placed in an incubator at 37°C / 5% CO_2.

For transient transfections, the same protocol was followed, however, instead of selection medium, the cells were grown for 48 h in medium containing 10% (v/v) FCS, but no selection antibiotics. After this period, the cells were assayed for gene activity.

2.1.5 Cryopreservation of cells: freezing and recovery

Prior to being frozen, cells were grown until 70-80% confluent. They were washed twice with PBS, trypsinised and pelleted. The cell pellets were resuspended in an appropriate volume of ice-cold freezing medium [1% (v/v) DMSO in FCS] and transferred into cryovials in 1.5 ml aliquots. The cryovials were placed in a –70°C freezer for one to two days and then transferred to a liquid nitrogen tank for permanent storage.

In order to recover cells from liquid nitrogen storage, they were thawed at 37°C in a water bath. When almost thawed, cells were slowly added to tubes containing 10 ml of medium with 10% (v/v) FCS. The cell suspensions were pelleted by centrifugation at 500 g for 5 min, washed with 10 ml of medium containing 10% (v/v) FCS and respun. Upon resuspension in the appropriate medium, the cell suspension was transferred to cell culture flasks and placed in an incubator at 37°C / 5% CO_2. The following day, if confluent, the cells were passaged; otherwise, the medium was replaced.

2.2 Cloning and general nucleic acid manipulation

2.2.1 Cloning overview

In order to generate riboprobes for the detection of mouse IgLON messages by whole-mount *in situ* hybridisations, the respective cDNAs were amplified from mouse brain and cloned into the pGEM®-T Easy Vector (Promega; Appendix C). This vector contains SP6 and T7 promoter sites, enabling *in vitro* transcription.

For the generation of inducible human IgLON constructs, the respective cDNAs were excised from pGEM®-T Easy, wherein they had been previously cloned, and cloned into pTRE-Tight (BD Biosciences; Appendix C).

2.2.2 Digestion of DNA with restriction endonucleases

Digestion with restriction enzymes (REs) was used widely in this project for three main purposes: linearization of plasmids, obtaining nucleic acid fragments for cloning and screening for integration of inserts. Restriction enzymes and accompanying digestion buffers were purchased from Roche. DNA was mixed with an appropriate amount of RE and incubated from 1.5 to 3 h at 37°C. Complete digestion was confirmed by agarose gel electrophoresis of the digestion reaction.

2.2.3 Extraction of DNA fragments from agarose gels

In order to extract DNA from an agarose gel, the QIAquick® Gel Extraction Kit was used (Qiagen). DNA fragments were subjected to electrophoresis on a low-melting SeaPlaque® (BMA) agarose-TAE gel stained with ethidium bromide. The bands were visualised by UV light and excised from the gels using a clean scalpel. The gel slices were transferred to 1.5 ml microcentrifuge tubes and weighed. A volume of Buffer PB equivalent to three times the weight of each slice was added. The tubes were heated at 50°C and vortexed periodically until the gel slices dissolved. One gel volume of isopropanol was added to each tube and the samples were mixed. The samples were applied to columns placed on collection tubes, which were centrifuged for 1 min at 13,000 rpm in a microcentrifuge. The flow-through was discarded. To remove all traces of agarose, 0.5 ml of Buffer QG was added to

the columns, which were centrifuged for 1 min at 13,000 rpm in a microcentrifuge. The columns were washed by adding 0.50 ml of Buffer PE and letting stand for 3 min. They were then centrifuged for 1 min at 13,000 rpm in a microcentrifuge. The flow-through was discarded and the columns were centrifuged for an additional 1 min at 13,000 rpm in a microcentrifuge, to remove residual Buffer PE. The columns were transferred to clean 1.5 ml microcentrifuge columns. To elute DNA, 30 µl of Buffer EB were added to the centre of each column; the columns were let to stand for 1 min and were spun for 1 min at 13,000 rpm in a microcentrifuge. Eluted DNA was quantified (section 2.2.10) and then stored at –20°C.

2.2.4 Phenol extraction and ethanol precipitation of DNA

In order to purify DNA from a solution, an equal volume of 24:24:1 (v/v/v) phenol/chloroform/isoamyl alcohol (Sigma) was added to it in a 1.5 ml microcentrifuge tube. The tube was vortexed rigorously for 10 s and microcentrifuged for 30 s at 13,000 rpm and room temperature. The aqueous phase was carefully removed and transferred to a fresh 1.5 ml microcentrifuge tube. An equal volume of 24:1 (v/v) chloroform/isoamyl alcohol (Sigma) was added, the tube was vortexed rigorously for 10 s and microcentrifuged for 30 s at 13,000 rpm and room temperature. The aqueous phase was carefully removed and transferred to a fresh 1.5 ml microcentrifuge tube. 1/10 volume of 3 M sodium acetate pH 5.2 was added and the solution was mixed by flicking several times. 2 to 2.5 volumes of ice-cold absolute ethanol were added; the solution was vortexed and placed at –70°C for an hour. Following microcentrifugation for 15 min at 13,000 rpm and 4°C, the supernatant was discarded and the pellet was washed with 1 ml of 70% (v/v) ethanol for 10 min at 13,000 rpm at room temperature. The supernatant was removed by pipetting and the pellet was dried in a SpeedVac® Plus (Savant) evaporator. The pellet was finally dissolved in an appropriate volume of ultra-pure water and stored at –20°C.

2.2.5 Dephosphorylation of vector DNA

Before setting ligation reactions between a vector and an insert, the former needs to be dephosphorylated in order to minimise its propensity for self-ligation. 50 µl of purified linearised vector (equivalent to 20 µg before purification) were mixed with 2 U of Shrimp Alkaline Phosphatase (Roche), 6 µl of 10x Dephosphorylation Buffer (Roche) and 2 µl of ultra-pure water. The mixture was incubated for 30 min at 37°C. After dephosporylation and before the vector was considered ready to use in ligations, it was subjected to a further round of purification.

2.2.6 Ligation reactions

Ligation reactions were performed using the components of the pGEM®-T Easy Vector System (Promega). Reactions were set up by combining the following (Table 2.2):

Component	Amount
2x Rapid Ligation Buffer	5 µl
Vector	50 ng
Purified PCR product	3 µl
T4 DNA Ligase (3 Weiss units/µl)	1 µl

Table 2.2 Ligation reaction

Reactions were mixed by pipetting and incubated over-night at 4°C.

2.2.7 Transformation of bacteria

JM109 High Efficiency Competent Cells (Promega) were used as a bacterial system that is compatible with blue/white colour screening and standard ampicillin selection. Aliquots of the above cells were removed from storage at –70°C and thawed on ice, until just thawed. The cells were mixed by gently flicking the tubes. Meanwhile, 2 µl of a ligation reaction or 1 ng of plasmid DNA were added to sterile 17x100 mm polypropylene tubes on ice. 50 µl of thawed cells were added to each tube; the tubes were gently mixed by flicking and placed on ice for 20 min. The cells were then heat-shocked for 45-50 s in a water bath at exactly 42°C. After the heat shock, the tubes were returned on ice for 2 min. 950 µl of room temperature SOC

medium (Appendix A) were added to each tube. The cells were incubated with shaking for 1.5 h at 37°C and 180 rpm. 100 or 900 µl of each transformation culture were plated onto LB plates, containing the appropriate selection additives: ampicillin at 100 mg/ml, X-gal at 80 mg/ml and 0.5 mM IPTG. The plates were incubated over-night at 37°C.

2.2.8 Preparation of bacterial glycerol stocks

10 ml of over-night cultures were centrifuged at 3,220 g for 10 min. Each cell pellet was resuspended in 3 ml of 20-30% (v/v) glycerol in LB medium, divided into two 1.5 ml aliquots and stored at –20°C.

2.2.9 Purification of plasmid DNA

Small-scale purifications of plasmid DNA were prepared using the QIAprep® Spin Miniprep kit (Qiagen), according to the manufacturer's instructions. 5 ml of over-night bacterial cultures were centrifuged at 3,220 g for 10 min. The pellets were resuspended in 250 µl Buffer and transferred to 1.5 ml microcentrifuge tubes. 250 µl of Buffer P2 were added and the tubes were inverted 6 times. 350 µl of Buffer N3 were added and the tubes were inverted 6 times. The tubes were then centrifuged for 10 min at 13,000 rpm in a microcentrifuge. The supernatants were transferred into spin columns placed on a vacuum manifold and vacuum was applied. The columns were washed by adding 0.5 ml of Buffer PB and applying vacuum. The columns were then washed with 0.75 ml of Buffer PE and by applying vacuum. The columns were transferred to their receptacles and centrifuged for 1 min at 13,000 rpm in a microcentrifuge. The columns were placed in 1.5 ml microcentrifuge tubes. Finally, 50 µl of Elution Buffer were added to the centre of each column; the columns were incubated for 1 min and centrifuged at 13,000 rpm in a microcentrifuge to elute the DNA. The DNA samples were quantified (section 2.2.10) and then stored at –20°C.

2.2.10 Quantification of DNA

In order to determine the concentration and purity of DNA samples, appropriate dilutions were made (usually 1 in 200) in ultra-pure water. The optical densities of the diluted samples were then measured at 260 and 280 nm in a Unicam UV2 Spectrometer. The concentration was calculated according to the rule that DNA with an optical density (OD) at 260 nm of 1 has a concentration of 50 mg/ml. Purity was determined by the OD_{260}/OD_{280} ratio, with acceptable ratios being between 1.6 and 2.1.

2.2.11 Treatment of PCR products prior to sequencing

Prior to being sequenced, PCR products were subjected to enzymatic removal of excess primers and unincorporated nucleotides. 3 µl of a PCR product were combined with 5 U of Exonuclease I (Amersham Biosciences), 1 U of Shrimp Alkaline Phosphatase (Amersham Biosciences) and 3.5 µl of ultra-pure water. The reactions were incubated at 37°C for 15 min and then at 80°C for 15 min. The purified products were then either prepared for sequencing or stored at –20°C until used.

2.2.12 Preparation of reactions for fluorescent cycle sequencing

In order to prepare sequencing reactions, the BigDye® v3.1 Dye Terminator Cycle Sequencing Kit (Applied Biosystems) was used, according to the manufacturer's instructions. For a 10 µl reaction, the following were combined in a 0.5 ml eppendorf tube: 100 ng of DNA or 3 µl of PCR product, 1.6 pmol of primer, 2 µl of BigDye and ultra-pure water to the final volume. The reaction was mixed by vortexing and incubated in a thermal cycler. The conditions were as below:

- 96°C hot start
- 96°C 30 s
- 50°C 15 s
- 60°C 4 min

} 24 cycles

- 4°C hold

The reactions were removed from the thermal cycler and briefly spun. 2.5 µl of 125 mM EDTA and 30 µl of absolute ethanol were added to each tube. After vortexing, the tubes were incubated for 15 min at room temperature and spun in a microcentrifuge at 13,000 rpm for 20 min. The ethanol was removed by pipetting and 30 µl of 70% (v/v) ethanol was added. The tubes were spun in a microcentrifuge at 4°C and 13,000 rpm for 5 min. The ethanol was removed and the tubes were allowed to air-dry.

The pellets were given to the Wellcome Trust Clinical Research Facility, Western General Hospital, for automated processing in a 3730 Genetic Analyser (Applied Biosystems).

2.2.13 RNA extraction and DNase I treatment from cultured cells

RNA was extracted from cells in culture using the Absolutely RNA™ RT-PCR Miniprep Kit (Stratagene), according to the manufacturer's instructions. The medium was removed from exponentially-growing cells, usually growing in a 75 cm^2 flask or a 10 cm dish. A mixture of 600 µl of Lysis Buffer and 4.3 µl of beta-mercaptoethanol was added per flask and spread evenly over the surface. The lysates were mixed and collected by repeated pipetting and transferred to 1.5 ml microcentrifuge tubes. The tubes were vortexed and stored at –70°C for future processing.

To isolate RNA, the homogenates were thawed and transferred to Prefilter Spin Cups seated in 2 ml receptacle tubes and spun in a microcentrifuge at 13,000 rpm for 5 min. An equal volume of 70% (v/v) ethanol was added to each filtrate and the tubes were vortexed for 5 s. Half of each mixture was transferred to a Fibre-Matrix Spin Cup seated in a fresh 2 ml receptacle and spun in a microcentrifuge at 13,000 rpm for 1 min. The filtrates were discarded and the centrifugation was repeated for the remainder of the mixtures.

600 µl of Low-Salt Wash Buffer were added to each sample. The samples were spun in a microcentrifuge at 13,000 rpm for 1 min. The filtrates were discarded and the samples were spun for 2 min. 55 µl of DNase solution (5 µl of RNase-Free

DNase I and 50 µl of DNase Digestion Buffer) were added directly onto each fibre matrix. The samples were incubated at 37°C for 30 min in an air incubator.

600 µl of High-Salt Wash Buffer were added to each spin cup and the samples were spun in a microcentrifuge at 13,000 rpm for 1 min. The filtrates were discarded, 600 µl of Low-Salt Wash Buffer were added, and the samples were spun again as previously. The filtrates were discarded, 300 µl of Low-Salt Wash Buffer were added and the samples were spun in a microcentrifuge at 13,000 rpm for 2 min to dry the fibre matrix.

The spin cups were transferred to 1.5 ml microcentrifuge tubes. Elution Buffer was warmed at 60°C and 50 µl were added directly onto the centre of the fibre matrix. The samples were incubated at room temperature for 2 min and then spun in a microcentrifuge at 13,000 rpm for 1 min. The elution step was repeated with a further 50 µl of Elution Buffer.

The purified RNA was quantified (section 2.2.15) and stored at –70°C.

2.2.14 RNA extraction from mouse brain

Total RNA was prepared from tissue using the RNeasy® Midi Kit (Qiagen), according to the manufacturer's instructions. A whole mouse brain was firstly weighed and then divided in two using a sterile disposable scalpel. Each piece of tissue was transferred to a 15 ml tube, into which 1 ml of Buffer RLT was added. The tissue was dismembranated at 180 rpm for 1 min. 3 ml of Buffer RLT were added and the lysates were centrifuged at 21,885 g and 23°C for 10 min. The supernatants were transferred to 15 ml centrifuge tubes. 4 ml of 70% (v/v) ethanol were added and the tubes were mixed immediately by rigorous shaking. Each sample was then split into two and applied to RNeasy columns placed on 15 ml centrifuge tubes. The tubes were centrifuged at 21,885 g and 23°C for 5 min. After discarding the flow-through, each column was washed with 4 ml of Buffer RW1. The tubes were again centrifuged as above. The flow-through was discarded and each column was washed with 2.5 ml of Buffer RPE. The tubes were centrifuged at 21,885 g and 23°C for 2 min. The wash was repeated, followed by an extended centrifugation for 5 min. The columns were then transferred onto fresh 15 ml centrifuge tubes. RNA was eluted in two elution steps. Each step involved the

addition of 150 µl of ultra-pure water, incubation at room temperature for 1 min and centrifugation at 21,885 g and 23°C for 3 min. At the end of the elution, the contents of each tube were mixed together.

The purified RNA was quantified (section 2.2.15) and stored at –70°C.

2.2.15 Quantification of RNA

In order to determine the concentration and purity of purified RNA samples, appropriate dilutions were made (usually 1 in 100) in ultra-pure water. The optical densities of the diluted samples were measured at 260 and 280 nm in a Unicam UV2 Spectrometer. The concentration was calculated according to the rule that RNA with an optical density (OD) at 260 nm of 1 has a concentration of 40 mg/ml. The purity was determined by the OD_{260}/OD_{280} ratio, with acceptable ratios being between 1.6 and 2.1.

2.2.16 DNase I treatment of RNA

When samples had not been DNase I-treated during the RNA extraction process, they were treated using the DNA-free™ DNase Treatment and Removal Reagents (Ambion), as per the manufacturer's instructions. 0.1 volume of 10x DNase I Buffer and 1 µl of DNase I (i.e. 2 units) were added to 10 µg of RNA. The sample was mixed gently and incubated at 37°C for 30 min. 0.1 volume or 5 µl (whichever was greater) of DNase Inactivation Reagent were added to the sample. After mixing well, the sample was incubated at room temperature for 2 min and centrifuged at 10,000 g for 1 min to pellet the DNase Inactivation Reagent. The DNase-treated sample (supernatant) was then transferred to a fresh tube and stored at –70°C.

2.2.17 First strand cDNA synthesis from total RNA

cDNA was synthesised from total RNA using the 1st Strand cDNA Synthesis Kit for RT-PCR (AMV) by Roche, following the manufacturer's guidelines. 1 µg of DNase I-treated total RNA was mixed with ultra-pure water to a final volume of 8.2 µl.

The following components were mixed in a sterile 0.5 ml microcentrifuge tube (Table 2.3):

Reagent	Volume for 1 sample (µl)
10x Reaction Buffer	2
25 mM $MgCl_2$	4
Deoxynucleotide Mix	2
Random Primer $p(dN)_6$	2
RNase Inhibitor	1
AMV Reverse Transcriptase	0.8
RNA	8.2

Table 2.3 First strand cDNA synthesis reaction

The above volumes are for synthesis of 20 µl of cDNA. For lower or higher scales of synthesis, these volumes were adapted as appropriate.

The mixture was briefly vortexed and centrifuged to collect it at the bottom of the tube. The reaction was incubated at 25°C for 10 min and then at 42°C for 60 min on a PCR block. Finally, the reverse transcriptase was denatured by incubation at 99°C for 5 min, followed by cooling on ice for 5 min.

Samples were stored at –70°C.

2.2.18 Agarose gel electrophoresis

DNA or RNA fragments were visualised using agarose-TAE gel electrophoresis. Gels were prepared by dissolving 1% or 2% (w/v) agarose in 1x TAE buffer (Appendix A). Ethidium bromide was added to a final concentration of approximately 0.5 µg/ml. Samples were mixed with gel loading dye (Appendix A), loaded and run in 1x TAE buffer. Bands were visualised by UV illumination and their sizes were determined by comparison to markers (Ready-Load™ 1 kb and 100 bp DNA Ladders from Invitrogen).

2.3 Biological material

2.3.1 Multiple-tissue cDNA panels

The following multiple tissue cDNA panels were used (all purchased from BD Biosciences): Human MTC™ Panels I and II; Human Foetal MTC™; and Mouse MTC™ Panels 1 and III.

2.3.2 Mouse embryos

Embryos were collected from CD1 mice observing good animal handling practices. Time of conception was estimated by cervical smearing of mated female mice.

2.3.3 Mouse sections

Mouse embryo sections were purchased from Zyagen. Mouse tissue arrays were purchased from Chemicon International.

2.3.4 Human ovarian samples

Primary ovarian tumour material and non-malignant tissues were obtained from patients having undergone gynaecological surgery in the Lothian University Hospitals NHS Trust under ethical approval granted by the Lothian NHS Board Local Research Ethics Committee. Tissue samples were excised and stored in liquid nitrogen. Non-malignant tissue samples were derived from patients that underwent bilateral oophorectomies for suspected malignancy, but were found to have benign histologies; samples were collected from apparently normal contralateral ovaries.

2.3.5 Human embryo sections

Human embryo sections were provided by the Human Developmental Biology Resource. Ethical approval for the use of these sections was granted specifically for this work by the Lothian NHS Board Local Research Ethics Committee.

2.4 Reverse transcription polymerase chain reaction

2.4.1 General

RT-PCR was carried out extensively in this project, either to amplify cDNA fragments for cloning purposes, or to detect RNA messages of interest in expression studies. The same principles of optimisation were applied for both kinds of experiments: specificity of target amplification and sensitivity of the reaction to the desired extent. Reactions were prepared as follows: 0.5 μM of each primer, 0.2 mM of dNTPs, 1x reaction buffer, 1.5 mM of $MgCl_2$ [all three aforementioned reagents were included in the 1st Strand cDNA synthesis kit for RT-PCR (AMV) from Roche], 1 U of Pic *Taq* polymerase (Cancer Research UK) and 1/12.5 volume of cDNA. Cycling consisted of an initial denaturation for 5 min at 94°C, followed by a 4-cycle touchdown (30 s at 94°C, 30 s at 67°C decreasing by 3°C per additional cycle, and 45 s at 72°C) and then 30 cycles of 30 s at 94°C, 30 s at 55°C and 45 s at 72°C, and a final extension for 5 min at 72°C. MJ Research DNA Engine Tetrad thermal cyclers were used for all RT-PCR. All primers that were used are listed in Appendix B. These were designed using Primer3 v0.2 (Whitehead Institute of Biomedical Research).

2.4.2 Real-time quantitative RT-PCR

2.4.2.1 General considerations

In designing real-time PCR experiments, several factors were taken under consideration. A basic requirement was that the target sequence be short, around 100 bp. The conditions of cycling were optimised such that the reactions could be satisfactory with respect to both sensitivity and specificity. The RNA sources (cell line or tissue) for the standard curves were carefully chosen based on high levels of expression for the respective genes of interest. An additional requirement was that the melt curves of the products were specific to each gene having one clearly distinguishable peak corresponding to a specific melting temperature.

2.4.2.2 *Performing qRT-PCR*

Quantitative RT-PCR was performed using Rotorgene 2000 and 3000 real-time cyclers (Corbett Research). 15 µl reactions were set up using 40 ng of RNA, 0.3 µM of each primer and the QuantiTect SYBR Green one-step RT-PCR kit (Qiagen), according to the manufacturer's guideline. Reactions were set up in quadruplicate for reverse-transcribed samples and non-template PCR contamination controls, in triplicate for the standard curve points and in duplicate for the non-reverse-transcribed DNA contamination controls (beta actin runs). Fluorescence was detected using the FAM channel (source 470 mm; detector 510 nm). Analysis and quantification was performed using Rotorgene v4.6, v5.0 and v6.0 software. The criteria for acceptability of a run were: R-value of at least 0.99; R2-value of at least 0.89; efficiency value from 0.99 to 1.10; melting curves with the same and specific peak; absence of PCR contamination; and in actin runs, absence of DNA contamination. Inter-run variation was corrected for by the use of a "normaliser" sample that was included in all runs.

Cycling conditions were set as follows: Reverse transcription at 50°C for 30 min, followed by a 15 min polymerase activation at 95°C, and 40 cycles of denaturation at 94°C for 15 s, annealing at 57°C for 30 s and extension at 72°C for 30 s. After a final extension at 72°C for 1 min, product melting was set across a 72 to 99°C temperature ramp, with 5 s steps of 1°C.

All primers that were used are listed in Appendix B. These were designed using Primer3 v0.2 (Whitehead Institute of Biomedical Research).

2.5 General manipulation of protein

2.5.1 Protein extraction from cultured cells

Cells to be harvested for protein extraction were firstly rinsed in ice-cold PBS. The PBS was drained and residual amounts were removed by a pastette. An appropriate amount of protein extraction buffer (Appendix A) was added in order to completely cover the surface of the flask or plate. The flasks or plates were placed on ice for 10 min. The cells were detached with a scraper and then collected into 1.5 ml microcentrifuge tubes. These were spun at 13,000 rpm in a microcentrifuge for 10 min. The supernatants, i.e. the cell lysates, were transferred into fresh tubes and stored at –20°C.

2.5.2 Protein quantification

Total protein concentration in cell lysates was measured using the Bio-Rad Protein Assay. The assay dye was prepared by diluting the stock solution 1:5 in deionised water and filtration through a Whatman No 1 filter paper. Protein standards were prepared by making serial dilutions of BSA in deionised water, starting from a known concentration. The samples to be assayed were also diluted to a range of 1:3 to 1:5 in deionised water. 20 µl of standards or samples were transferred to test tubes, into which 1 ml of the dye was added. The tubes were vortexed and 200 µl of samples or standards were transferred to a 96-well plate in triplicate. The plate was read in a BP 800 Biohit plate reader at 595 nm. A standard curve was calculated from the absorbance readings of the standards and the protein content of each of the lysates was determined by comparison thereto.

2.5.3 Deglycosylation of protein lysates

Deglycosylation of protein lysates was undertaken using a peptide N-Glycosidase (PNGase F) kit (New England Biolabs). 20 µg of total protein were denatured in 1x Glycoprotein Denaturing Buffer at 100°C for 10 min. 1/10 of volume of each 10x G7 Buffer and 10% NP-40 were added, together with 1000 U of PNGase F. The reaction was incubated at 37°C over-night.

2.5.4 Western blotting

2.5.4.1 SDS-polyacrylamide gel electrophoresis of protein samples

Discontinuous acrylamide gels were prepared as follows: For the resolving gel, the following were combined in deionised water: an appropriate volume of 37.5:1 acrylamide/bis acrylamide depending on the final concentration desired, usually 10% (v/v); 0.4 mM Tris pH 8.85; 0.1% (w/v) SDS; 0.25% (v/v) TEMED; and 0.03% (w/v) AMPS. For the stacking gel, the following were combined in deionised water: 3.5% or 5% (v/v) acrylamide/bis acrylamide; 131 mM Tris pH 6.8; 0.1% (w/v) SDS; 0.1% (v/v) TEMED; and 0.1% (w/v) AMPS. The gel system used was the Mini-PROTEAN 3 (Bio-Rad). Firstly, the resolving gel was poured into the casting apparatus and allowed to polymerise under a layer of isopropanol. Once set, the isopropanol was drained, the stacking gel was poured, the appropriate comb was inserted into it and the gel was allowed to polymerise.

To prepare the protein samples, an appropriate amount of each lysate (usually 10 or 20 μg) was denatured by heating at 95°C for 10 min with 1x denaturing sample buffer (Appendix A). After denaturation, the samples were placed on ice to cool, then spun briefly and placed again on ice. Deglygosylated samples had already been denatured; hence, they were not mixed with denaturing sample buffer, but only with 1/10 vol glycerol.

The samples were loaded into the gel and run in gel running buffer (Appendix A) for approximately 1 h at 200 W, alongside a molecular weight marker (New England Biolabs).

2.5.4.2 Transfer of proteins onto membrane

Proteins were transferred from the gel to an Immobilon-P membrane (Millipore) using the Mini-PROTEAN 3 Trans-Blot Cell (Bio-Rad). The transfer was performed either over-night at 30 V and 4°C in transfer buffer (Appendix A) or at 100 V for 1.5 h in transfer buffer containing 20% (v/v) methanol.

2.5.4.3 *Blocking, antibody incubations and washes*

The membranes were rinsed twice in TBS (Appendix A) containing 0.1% (v/v) Tween-20 (TBS/Tween) and then washed three times by rocking in the same solution, 5 min each wash, at room temperature. The membranes were then blocked by rocking in 1% (v/v) Blocking Agent [contained in the BM Chemilluminescence Blotting Substrate kit (Roche)] in TBS/Tween for 1 h at room temperature. The blocking agent was drained and the membranes were probed with an appropriate dilution of the primary antibody in TBS/Tween, by rocking over-night at 4°C.

The following day, the membranes were rinsed twice in TBS/Tween and then washed three times in TBS/Tween and twice in 0.5% (v/v) blocking agent in TBS/Tween: these washes were done by rocking for 5 min each time, at room temperature. The membranes were then probed with an appropriate dilution of the secondary antibody in TBS/Tween, by rocking for 1 h at room temperature. Following this incubation, the membranes were rinsed twice in TBS/Tween; washed three times by rocking in TBS/Tween, 5 min each wash, at room temperature; rinsed twice in TBS; and washed three times in TBS as previously.

The following primary/secondary antibody combinations were used in western blotting (Table 2.4):

Primary antibody	Dilution	Secondary antibody	Dilution
anti-OPCML[vi]	1/2000	goat anti-chick (Abcam)	1/2000
anti-ACTIN (Calbiochem)	1/500000	goat anti-mouse (Calbiochem)	1/4000

Table 2.4 Antibodies used in immunoblotting

[vi] Custom-made IgY polyclonal antibody, raised in chicken against an OPCML peptide sequence (Biosource)

2.5.4.4 *Signal detection*

The signal was detected using the BM Chemilluminescence Blotting Substrate (Roche), according to the manufacturer's instructions. The luminol was prepared by combining 10 ml of Luminescence Substrate A and 100 µl of Starting Solution B and was let to stand at room temperature for half an hour before use. The membranes were treated with luminol for 1 min and then transferred to an X-ray film cassette. In a dark room, the membranes were overlaid with Hyperfilm™ (Amersham Biosciences) for a period ranging from 1 s to 5 min, depending on signal intensity. Films were developed in a Curix 60 developer (Agfa).

2.6 Whole-mount *in situ* hybridisation

2.6.1 Synthesis of digoxygenin-labelled riboprobes

2.6.1.1 In vitro transcription

Firstly, the plasmid DNA was linearised using a restriction endonuclease that digests downstream of the appropriate promoter. Linearised plasmid DNA was subjected to phenol extraction and ethanol precipitation (section 2.2.4).

In order to produce digoxygenin-labelled RNA probes, the DIG RNA Labelling Kit (SP6/T7) (Roche) was used, according to the manufacturer's instructions. The following components were combined with ultra-pure water to a final volume of 20 µl on ice:

- 1 µg of linearised plasmid DNA
- 2 µl of 10x NTP Labelling Mixture
- 2 µl of 10 x Transcription Buffer
- 1 µl of Protector RNase Inhibitor
- 2 µl of appropriate RNA polymerase

The restriction enzyme and RNA polymerase (Pol) used for each construct can be seen in Table 2.5.

Construct	Orientation to be transcribed	RE	Pol
Opcml	Antisense	SalI	SP6
	Sense	NcoI	T7
Hnt	Antisense	SalI	SP6
	Sense	NcoI	T7
Lsamp	Antisense	SalI	SP6
	Sense	NcoI	T7
Negr1	Antisense	NcoI	T7
	Sense	SalI	SP6
Shh	Antisense	HindIII	T3
Fgf8	Antisense	HindIII	T3

Table 2.5 *In vitro* transcription for the creation of labelled probes

The reaction components were mixed gently, spun briefly and incubated for 2 h at 37°C.

After the incubation, 1 µl of each reaction was run on a 2% (w/v) agarose gel stained with EtBr to visually inspect the synthesised probes.

2 µl of DNase I were added to each sample and reactions were incubated for 15 min at 37°C. The reactions were then stopped by the addition of 2 µl of 0.2 M EDTA pH 8.0.

2.6.1.2 Quantification of synthesised probes

Standards were prepared using the DIG-labelled riboprobe control of known concentration from the kit used for the synthesis of the probes. The RNA was diluted in RNA dilution buffer [5:3:2 (v:v:w) H_2O:20xSSC[vii]:formaldehyde] to give concentrations ranging from 10 ng/µl to 0.01 pg/µl. The synthesised probes were diluted to an approximate concentration of 10 ng/µl based on the appearance of probe bands when run on an agarose gel (see previous section). 1 µl from the standards and the probe dilutions was applied to spots on a positively-charged nylon membrane.

[vii] DEPC-treated and autoclaved (Sigma)

The RNA on the membrane was fixed by UV cross-linking in a Bio-Rad GS Gene Linker UV Chamber, using the appropriate programme. The membrane was washed twice in PBT (Appendix A), for 1 min each time, and then blocked with 1x Blocking Reagent (Roche) in maleic acid buffer (Appendix A) for 2 min. The membrane was probed with a 1:5000 dilution of anti-digoxigenin-AP, Fab fragments (Roche) in 1x Blocking Reagent for 3 min and then washed twice in PBT, for 1 min each time. The membrane was treated with BM Purple (Roche) at room temperature for approximately 30 min, until the staining developed. Finally, the membrane was rinsed with deionised water and dried between paper towels. Riboprobe concentrations were estimated according to which standards matched the spots of unknown concentrations in colour intensity.

2.6.1.3 Precipitation of probe RNA

10 µl of TE buffer pH 8.0 (Appendix A), 10 µl of 4 M LiCl[viii] and 300 µl of ethanol were added to each sample, which was then mixed and incubated at –20°C for 30 min. The samples were then spun in a microcentifuge at 13,000 rpm and 4°C for 10 min. The pellets were washed with 70% (v/v) ethanol and air-dried. Finally they were redissolved in TE Buffer pH 8.0 to an approximate final concentration of 0.1 mg/ml, aliquoted and stored at –20°C.

2.6.2 Collection & fixation of mouse embryos

Embryos were collected at the following ages: E8.5, E9.5, E10.5, E11.15, E12.5 and E13.5[ix]. The extra-embryonic membranes and the amnion were removed from the embryos in ice-cold PBS. The brain and heart of embryos older than E8.5 were pierced by a needle. Samples were fixed in ice-cold 4% (w/v) paraformaldehyde for at least 4 h; the fixative was changed once. Samples were washed twice in PBT at 4°C for 5 min each wash. Samples were then dehydrated by successive washes by rocking in 25%, 50% and 75% (v/v) methanol in PBT at room temperature, for 5 min each wash. Finally, samples were washed twice with 100% methanol, for 5 min each wash, and stored after the second wash in the same solution at –20°C until used. All the above steps were undertaken in RNase-free conditions.

[viii] DEPC-treated and autoclaved

[ix] E corresponds to embryonic age (days post coitum)

2.6.3 Whole-mount *in situ* hybridisations of mouse embryos

All the steps until and including hybridisation were carried out in RNase-free conditions. All washes were done at room temperature and by rocking, unless otherwise stated.

The fixed embryos were rehydrated by successive washes in descending grades of methanol to PBT: 100%, 75%, 50% and 25% (v/v). The embryos were then washed three times in PBT, for 5 min each time and digested with 10 μg/μl Proteinase K (Sigma) in PBT at room temperature for the following times (Table 2.6):

Age	Digestion time
E8.5-9.5	15 min
E10.5	20 min
E11.5	25 min
E12.5	30 min
E13.5	35 min

Table 2.6 Duration of proteinase K digestion

After the digestion, the samples were post-fixed with freshly prepared 4% (w/v) paraformadehyde with 0.2% (v/v) glutaraldehyde in PBT for 45 min on ice. Warm prehybridisation solution (Appendix A) was added and the embryos were allowed to sink in their containers. This was repeated and then the solution was removed and an appropriate volume of warm prehybridisation solution was added. The embryos were incubated for 1 h at 65°C by rocking. The solution was changed and incubation continued for a further 3 h. The solution was then replaced with hybridisation solution containing 250 ng/ml DIG-labelled riboprobe, enough to cover the samples. Hybridisation was carried out at 65°C over-night by rocking.

The following day, the hybridisation solution was removed and kept at 4°C to be reused for a maximum of three further times. Post-hybridisation solution (Appendix A) was added and the samples were washed at 65°C for 10 min. The

embryos were then washed with 25% (v/v) 2x SSC, pH 4.5[x] in post-hybridisation solution at 65°C for 10 min. The washes were repeated with 50% and then 70% (v/v) 2x SSC, pH 4.5 similarly. The samples were washed twice, for 30 min each time, in 0.1% (v/v) CHAPS[xi] / 2x SSC at 65°C, followed by another two 30 min washes at the same temperature in 0.1% (v/v) CHAPS / 0.2x SSC, pH 4.5. The samples were then washed with TNT buffer (Appendix A) at room temperature for 10 min.

In order to block the samples, they were incubated for at least 4 h in blocking solution at 4°C. They were then incubated with a 1:2000 dilution of anti-digoxigenin-AP, Fab fragments (Roche), in blocking solution at 4°C over-night with gentle agitation.

The following day, samples were washed with 0.1% (w/v) BSA in TNT buffer five times, 1 h each time and left to wash in fresh solution at 4°C over-night.

In the final day of the protocol, the embryos were washed twice, for 30 min each time, in NTMT buffer (Appendix A) and then twice in NTM buffer (Appendix A), for 10 min each time. To visualise the hybrids, the samples were incubated in BM Purple (Roche) in the dark. The samples were rocked for the first 20 min of development and then monitored by eye until staining developed. Finally, the stain was fixed in 4% (w/v) paraformaldehyde at 4°C over-night.

Stained embryos were photographed using an AxioCam camera (Carl Zeiss) and AxioVision v3.1 software (Carl Zeiss).

[x] Made from a 20x DEPC-treated and autoclaved stock solution (Sigma)
[xi] Made from a 2x stock solution (Sigma)

2.7 Immunohistochemistry of paraffin-embedded sections

For immunohistochemical experiments, sections were first dewaxed in xylene, by two 5 min washes. Then they were rehydrated in descending grades of ethanol to water, as can be seen in Table 2.7:

Step	Duration
1. 100% (v/v) ethanol	2 min
2. 100% (v/v) ethanol	5 min
3. 100% (v/v) ethanol	2 min
4. 95% (v/v) ethanol	2 min
5. 70% (v/v) ethanol	3 min
6. Water	3 min

Table 2.7 Rehydration of sections

The rehydrated sections were then treated with fresh 3% (v/v) hydrogen peroxide [made from diluting a 30% stock solution in water] for 30 min. Following a 5 min wash in water, antigen retrieval was performed by heating the sections in citrate buffer pH 6.0 (10 mM citric acid monohydrate) in a microwave oven at 700 W. This was done in three 5 min steps, after each of which cold citrate buffer was used to top up the boiling solution. At the end of antigen retrieval, the sections were left immersed in citrate buffer to cool down for 20 min.

The sections were washed in 0.05 M TBS by rocking for 5 min and then blocked with 20% (v/v) foetal calf serum in TBS (TBS/FCS) for 10 min at room temperature. Excess blocking solution was drained and the sections were incubated with a 1/60 dilution of the anti-OPCML antibody in TBS/FCS for 2 h at room temperature.

After two 5 min washes in TBS by rocking, the sections were incubated with a 1/250 dilution of a pre-absorbed goat anti-chick IgY (Abcam) in 20% (v/v) FCS/TBS for 30 min at room temperature.

The sections were washed twice in TBS by rocking, for 5 min each time, incubated with a 1/20 dilution of the tertiary antibody [Link antibody from the Multilink® Super Sensitive™ Link-Label IHC Detection System (Biogenex)] in TBS for 30 min at room temperature, and washed again twice in TBS as previously.

To develop the stain, the sections were treated with Liquid DAB (Biogenex) for 5 min in the dark. Subsequently, the sections were subjected to the following washes and treatments:

- Wash in water for a few minutes
- Counterstaining with haematoxylin for 2 min
- Wash in water for 2 min
- Treatment with acid alcohol [0.1% (v/v) concHCl in 70% (v/v) EtOH] for 30 s
- Wash in water for 2 min
- Wash in Scott's tap water (Appendix A) for 1 min

Finally, the stained sections were dehydrated in ascending grades of ethanol to water, in reverse of the rehydration steps; cleared in xylene, for 5 min each time; and mounted in DPX medium (Fisher Scientific).

Stained sections were photographed using a SPOT™ Insight 14.2 Color Mosaic camera (Diagnostic Instruments Inc.) and SPOT™ v4.1.2 software (Diagnostic Instruments Inc.).

2.8 Cell biology assays

2.8.1 Migration assay

Migration assays were performed using the QCM^{TM}-Collagen I, -Fibronectin and -Vitronectin Quantitative Cell Migration Assays (Chemicon International), according to the manufacturer's instructions. These assays utilise Boyden chambers with an 8 μm pore size to measure haptotaxis towards an immobilised ECM protein gradient. The assay chambers are precoated with either an ECM molecule or BSA, the latter serving as a negative control. For each assay, two microplates are used: one test plate, containing ECM-coated chambers, and one control plate, with ECM-coated wells (serving as an adhesion control) and BSA-coated chambers.

The cells to be assayed were serum-starved, i.e. grown in media lacking FCS, for 48 h prior to the experiments. The assay plates were equilibrated to room temperature. The cells were washed twice with PBS, and trypsinised. Trypsin was counteracted by the addition of quenching medium [DMEM with 5% BSA (w/v)]. The cells were counted and resuspended in quenching medium. Single-cell suspensions were created by passing the cells three times through a 21G needle. 300 μl of quenching medium were added to the first row of wells of the test plate, beneath the Boyden chambers. Similarly, quenching medium was added to the second row of wells in the control plate. After pipetting the cells gently to resuspend, 2.5 x 10^5 cells of the first sample were placed into an ECM-coated Boyden chamber on the test plate. The same number of cells were added to ECM-coated wells in the first row of the control plate and the BSA-coated Boyden chambers on the control plate. The above steps were repeated for the rest of the samples. All the samples were done in duplicate. The plates were then incubated for approximately 22 h at 37°C / 5% CO_2.

The following day, 6 drops of Cell Stain Solution were added to each well of the second row of wells in the test plate and the third row of wells in the control plate. Using a clean pipette for each well, the medium was removed from the ECM-coated control wells in the first row of the control plate, and 6 drops of Cell Stain Solution were added to each of these wells. The medium was carefully

removed from the ECM-coated Boyden chambers in the first row of the test plate. Using forceps, the first ECM-coated Boyden chamber was removed from the test plate, without touching the underside of the chamber. The medium from the inside of the chamber was gently swabbed using a flattened cotton bud, taking care not to puncture the chamber membrane. The cleaned chamber was then placed into a well containing cell stain and the process was repeated for the next chamber. After cleaning all the test chambers, the same was done for the BSA-coated control chambers, placing each chamber in its respective stain well once completed (second row of wells in the test plate and third row of wells in the control plate). The plates were then incubated for 30 min at room temperature. The cell stain was removed from the ECM-coated control row with a pipette and wells in this row were washed three times with 1 ml PBS per well. 300 µl of PBS were added to each ECM-coated control well. 300 µl of Extraction Buffer were added to all the wells in the empty third row of the test plate and the empty fourth row of the control plate. Using forceps, one ECM-coated chamber was removed each time from the stain, and washed thoroughly in deionised water by submersion. The inside of each chamber was then cleaned with a flattened cotton bud as before and the cleaned chambers were placed in Extraction Buffer. The test and control plates were placed on a shaker and the stain was eluted for 10 min. 100 µl of stain solution from elution wells were removed per sample and transferred into a microplate. Optical density was read at 570 nm in a BP 800 Biohit plate reader.

The results were analysed by subtracting the BSA-coated readings from the ECM-coated ones.

2.8.2 Invasion assay

Invasion assays were carried out using Biocoat™ Matrigel™ Invasion Chambers and Control Inserts (BD Biosciences). Invasion chambers contain 8 µm pore size PET membranes with a thin layer of Matrigel basement membrane matrix: these allow cell invasion. In contrast, control inserts only have the membrane, and thus allow cell migration.

After matrigel and control inserts were allowed to come to room temperature, 0.5 ml of DMEM was added to the bottom of the wells and to the interior of matrigel

inserts. The matrigel chambers were rehydrated for 2 h in an incubator at 37°C / 5% CO_2. Meanwhile, exponentially-growing cells were washed twice with PBS, trypsinised and counted. Single-cell suspensions were prepared at 5 x 10^4 cells/ml in DMEM, by passing the cells three times through a 21G needle. The medium was removed from the bottom of the wells and the matrigel inserts and 0.75 ml DMEM with 5% (v/v) FCS was added to the wells of the companion plate, in order to act as a chemoattractant. Using sterile forceps, the inserts were transferred to the wells, avoiding the creation of bubbles. Immediately, 0.5 ml of single-cell suspension was added to each chamber and the plates were placed for 24 h in an incubator at 37°C / 5% CO_2.

The following day, non-invading cells were scrubbed from the upper surface of the membranes using cotton buds: firstly, using dry cotton buds and then using cotton buds moistened with DMEM. The inserts were transferred onto wells containing 0.5 ml MTT at 0.2 mg/ml (Sigma) in PBS, the plate was covered with aluminium foil and placed in an incubator for 3 h at 37°C / 5% CO_2. The crystals were removed from the lower surface of membranes using cotton buds. The tips of the cotton buds were cut and placed in tubes containing 1 ml spectrometric grade DMSO (Sigma). The tubes were vortexed in order to solubilise the crystals. Three 200 µl aliquots per sample were transferred to a microplate and optical density was measured at 570 nm in a BP 800 Biohit plate reader.

The results were calculated as follows:

$$\% \text{ invasion} = \frac{\text{OD (invading cells)}}{\text{OD (migrating control cells)}} \times 100\%$$

2.8.3 Cell-ECM adhesion assay

In order to measure the adhesion of cells on proteins of the extracellular matrix, the CytoMatrix™ Screen Kit (Chemicon International) was used, according to the manufacturer's instructions. This kit uses 8-well removable strips in a 96-well plate frame. The wells in the first seven rows of each strip are coated with an ECM component, namely Fibronectin, Vitronectin, Laminin, Collagen I or Collagen IV.

The last well of each strip is coated with BSA, which serves as a negative assay control.

The strips were rehydrated with 200 µl of PBS per well for at least 15 min at room temperature. Before the assay, the PBS was removed from the rehydrated strips. Exponentially-growing cells were washed twice with PBS, trypsinised and counted. Single-cell suspensions at 2.5 x 10^5 cells/ml were created by passing the cells three times through a 21G needle. 100 µl of each cell suspension was added to the ECM-coated wells in duplicate or the BSA-coated well. The plate was incubated at 37°C / 5% CO_2 for 45 min. The plate was gently washed three times with PBS containing Ca^{2+}/Mg^{2+} (200 µl per well). 100 µl of 0.2% (w/v) crystal violet in 10% (v/v) ethanol were added to each well. The plate was incubated for 5 min at room temperature. The stain was removed from the plate, which was then gently washed five times with PBS containing Ca^{2+}/Mg^{2+} (200 µl per well). 100 µl of solubilisation buffer [a 1:1 mixture of 0.1 M NaH_2PO_4, pH 4.5 and 50% (v/v) ethanol] were added to each well. The strips were allowed to incubate by gently shaking at room temperature for 5 min, until the cell-bound stain was solubilised. The absorbance at 570 nm was read in a BP 800 Biohit microplate reader.

2.8.4 Cell-cell adhesion assay

The cell-cell adhesion assay measures the adhesion of fluorescently-labelled cells on non-labelled cell monolayers. For each assay, two plates were used, a test and a control. Washing steps were omitted for the control plate in order to determine total cell fluorescence. Each plate also contained non-labelled cells incubated on cell monolayers, so that background fluorescence could be measured.

In order to prepare the monolayers, cells were washed twice with PBS, trypsinised and counted. 2.5 x 10^4 cells were added to each well. The plates were incubated over-night at 37°C / 5% CO_2.

Cells to be labelled were washed twice with PBS, trypsinised and counted. They were resuspended in serum-free medium at 5 x 10^5 cells/ml and passed three times through a 21G needle. Calcein AM (Molecular Probes) was added to the single-cell suspensions to a final concentration of 5 µM. The suspensions were mixed well and incubated at 37°C / 5% CO_2 for 30 min. Unlabelled cell suspensions were

also prepared and incubated alongside the labelled ones. After the incubation, both labelled and unlabelled cells were washed twice with serum-free medium and resuspended to 5 x 10^5 cells/ml.

The medium was removed from the monolayers by aspiration. 100 µl of either labelled or unlabelled cell suspension (i.e. 5 x 10^4 cells) were added to each well. The cells were incubated at 37°C / 5% CO_2 for 90 min. The non-adherent cells were removed from the test plate only by carefully washing five times: 200 µl of serum-free medium were added to each well and the plate was gently swirled. The plate was inverted and excess liquid was blotted onto paper towels. 200 µl of PBS were added to each well of the test plate, whereas 100 µl of PBS were added to each well of the control plate. Fluorescence was measured using a filter with an excitation wavelength of 485 nm and an emission wavelength of 520 nm in a Fluoroskan Ascent FL (Labsystems) plate reader. The percentage of cell-cell adhesion was determined by dividing the background-corrected fluorescence of adherent cells by the total background-corrected fluorescence of cells and multiplying by 100%.

2.8.5 Growth assay

Exponentially-growing cells were washed twice with PBS, trypsinised and counted. Single-cell suspensions were created by passing the cells three times through a 21G needle. 100 cells were plated in 1 ml medium supplemented with 10% (v/v) FCS and the appropriate antibiotics in triplicate in 24-well plates. At each time-point, one plate of cells was washed twice with PBS, trypsinised and resuspended in medium. The cells were syringed as above to create a single-cell suspension and counted using a Coulter counter.

2.8.6 Cell proliferation assay by dual colour flow cytometry

Cell proliferation was measured using the Absolute-S™ Kit (Chemicon International), according to the manufacturer's guidelines. The protocol used was as follows. Exponentially-growing cells were seeded at a specific density in 175 cm^2 flasks one or two days prior to performing the experiment, depending on the cell line. SKOV-3 cells were seeded one day before the experiment at 10^6 cells per flask,

whereas HeLa cells were seeded two days before the experiment at 2 x 10^6 cells per flask.

In the first day of the assay, cells were washed twice with PBS, trypsinised and counted. 10 ml single-cell suspensions were made by passing the cells three times through a 21G needle and 20 µl of the BrdUrd Photolyte™ stock solution were added per suspension. The cells were incubated at 37°C / 5% CO_2 for 30 min. Following this incubation, DMSO was added to the cell suspensions, to a final concentration of 2% (v/v). Immediately, 20 µl of Photolyte Enhancer™ were added per suspension and the cells were incubated for an additional 20 min at 37°C / 5% CO_2.

The cells were then centrifuged for 5 min at 300 g and the supernatant was removed by aspiration. The cells were resuspended in 1 ml of Wash Buffer and the centrifugation step was repeated. After removing the supernatant by aspiration, the cells were resuspended in the residual Wash Buffer by gently vortexing the tubes. 3 ml of 70% (v/v) ice-cold ethanol were added and the cells were stored at –20°C over-night.

The following day, 1 ml of the BrdUrd-incorporated cells was transferred to 12x75 mm polystyrene test tubes. The tubes were centrifuged at 300 g for 5 min, and the supernatant was removed by aspiration being careful not to disturb the cell pellets. 2 ml of Wash Buffer were added in each tube and the tubes were centrifuged at 300 g for 5 min. The supernatants were removed by aspiration and the cell pellets were resuspended in 0.5 ml of Wash Buffer. The cells were irradiated on a UV light box for 5 min.

[NB All the above steps were performed with minimal exposure to light]

After illumination, 1 ml of Wash Buffer was added to each tube and the tubes were centrifuged at 300 g for 5 min. The supernatants were removed by aspiration.

Each cell pellet were resuspended in 50 µl of the DNA labelling solution prepared as described below (Table 2.8):

Component	Volume per sample (µl)
TdT Reaction Buffer	10
TdT Enzyme	0.75
Br-dUTP	8
dH_2O	32.25

Table 2.8 DNA labelling solution

The cells were incubated in the DNA labelling solution for 60 min at 37°C in a water bath. Every 15 min the tubes were shaken in order to resuspend the cells.

At the end of the incubation, 2 ml of Rinse Buffer were added to each tube and the tubes were centrifuged at 300 g for 5 min. The supernatants were removed by aspiration.

The cells were then resuspended in 100 µl of FITC~BrdU antibody solution, prepared by combining 5 µl of FITC~BrdU with 100 µl of Rinse Buffer per sample. The cells were incubated in the FITC~BrdU antibody solution in the dark for 30 min at room temperature. 0.5 ml of the Propidium Iodide / RNase A Solution was then added per tube and the cells were incubated in the dark for a further 30 min at room temperature.

Finally, the cells were analysed in a FACSCalibur™ flow cytometer (BD Biosciences), using Cellquest™ v3.2.1 software (BD Biosciences). Samples were run in triplicate; for each replicate, 10,000 events were acquired. A dot plot of linear red fluorescence against log green fluorescence was gated on FL2A *versus* FL2W to exclude DNA doublets and on FSC *versus* SSC to exclude cellular debris. Cells in S phase were identified by high green fluorescence, whereas G0/G1 or G2/M populations were defined by a combination of low green fluorescence and low or high red fluorescence respectively. Results were expressed as percentages of the total gated events in the dot plot.

2.8.7 Annexin V assay by flow cytometry

FACS-based apoptosis studies were undertaken using the TACS™ Annexin V-FITC Apoptosis Detection Kit (R&D Systems). Cells to be assayed were seeded on 175 cm^2 flasks and the following day the medium was changed. If required, camptothecin (used from a 2 mM stock solution in DMSO) was added in the medium to the final concentration of 1 μM. After approximately 48 h, the media, containing floating cells, were emptied from the flasks and set aside. The cells were washed twice with PBS and trypsinised. To counteract the effect of trypsin, the media that were saved were re-introduced in their respective flasks. The combined suspensions of trypsinised and floating cells were pelleted, resuspended and counted in a Coulter counter. 5 x 10^5 cells were transferred to a 12x75 mm polystyrene test tube. The tubes were spun down at 400 g for 5 min. The cells were resuspended in ice-cold PBS and then spun down as previously. The cells were gently respunded in 100 μl of 1x Binding Buffer (made by diluting the 10x stock solution in deionised water). 10 μl of Propidium Iodide and 2 μl of Annexin V-FITC were added to each tube. Alongside the experimental samples, three controls were prepared: with only Propidium Iodide or Annexin V-FITC, or without either. The cells were incubated in the dark for 15 min at room temperature.

Finally, the cells were analysed in a FACSCalibur™ flow cytometer (BD Biosciences), using Cellquest™ v3.2.1 software (BD Biosciences). Samples were run in triplicate; for each replicate, 10,000 events were acquired. A dot plot of log red fluorescence against log green fluorescence was gated on FSC *versus* SSC to exclude cellular debris. Quadrant markers were used to distinguish the different populations. Early-stage apoptotic cells were defined as the population with high green fluorescence and low red fluorescence, whereas late-stage apoptotic or necrotic cells as having high green and high red fluorescence. Results were expressed as percentages of the total gated events in the dot plot.

2.9 Statistical analysis

Except in the expression study in ovarian cancer, all other statistical comparisons were undertaken in Microsoft Excel by Student's *t* test.

In the aforementioned expression study, all statistical analyses were conducted in SPSS v12 (SPSS Inc.). Non-parametric comparisons between unmatched samples were made using the Mann-Whitney (*U*) test for two samples or the Kruskal-Wallis (χ^2) test for more than two samples. Non-parametric correlations were tested using the Spearman rank (r_s) test. Regression models were made using linear regression analysis. Survival curves were produced using the Kaplan-Meier method and tested with the log-rank test. Survival models were estimated using Cox proportional hazards regression analysis.

Chapter 3

Creation and characterisation of inducible cell lines expressing OPCML

3.1 Introduction

Historically, mammalian systems of inducible gene expression have relied on a family of prokaryotic DNA binding proteins, exemplified by the *E. coli* Tet repressor protein (TetR)[258]. TetR negatively regulates the genes of the tetracycline-resistance operon on the Tn*10* transposon. It inhibits transcription of these genes by binding to the tet operator sequences *tetO* in the absence of tetracycline. Tetracycline-inducible systems are based on this transcriptional regulation. They are categorised into Tet-Off and Tet-On systems. In a Tet-Off system, the regulatory protein is a 37 kDa fusion of amino acids 1-207 of TetR and the C-terminal 127 amino acids of the HSV VP16 activation domain[259]. VP16 converts the TetR repressor into an activator. The fusion protein is called the tetracycline-controlled transactivator (tTA). In Tet-On systems, four amino acid changes in TetR convert it into a "reverse" TetR (rTetR), with the fusion protein termed rtTA. Thus, in Tet-Off systems tTA activates genes in the absence of tetracycline, whilst in Tet-On systems rtTA activates genes in the presence of tetracycline.

Inducible systems have two components: a regulatory component, based on a plasmid encoding the TetR-derived regulatory protein; and a response component, based on a plasmid that allows the tetracycline-responsive expression of a gene of interest. Hence, the regulatory plasmid either encodes tTA or rtTA (for Tet-Off and Tet-On systems respectively) and the response plasmid harbours the gene of interest driven by a minimal promoter placed under the influence of a tetracycline response element (TRE). The TRE derives from the *tetO* sequences, thus allowing binding of the regulatory protein in the absence (Tet-Off) or presence (Tet-On) of tetracycline.

Since the groups of Bujard and Hillen first demonstrated the efficacy of this regulated system in mammalian cells, the unparalleled advantages of inducible systems have established their usage as a tool of remarkable potential[260,261]. Firstly, as the critical regulatory elements are prokaryotic, tetracycline-inducible systems have no effects on host genes. The interpretation of any observed phenotypes is thus simplified by the absence of pleiotropic effects. Moreover, the inducer is incorporated in the transcription factor complex and hence its concentration directly

correlates with the concentration of the latter allowing the expression of genes of interest at narrowly defined levels. This greatly simplifies the study of genes encoding products that are growth-inhibitory or toxic, or whose functions are tightly linked to their level of expression. It also becomes possible to study the effect of genes at expression levels approximating physiological ones, avoiding over-expression artefacts. Another advantage of inducible systems is that comparisons can be made within the same clone, between the induced and uninduced state, thus obliterating the issue of clonal variation. Finally, as tetracyclines are antibiotics whose use is extensively documented in humans, they can be excellent candidates for gene regulation in gene therapy.

Tet-inducible systems have been extensively used, both *in vitro* and *in vivo*, to study a variety of genes and their functions. *In vitro*, important cancer-related genes, such as *TP53*, have been placed under the regulation of tet-responsive systems[262]. Studies have focused on such diverse areas as cell signalling[263], the immune response[264] and microarray comparisons between induced and uninduced states[265]. Recent advances have made the study of two genes possible by an inducible system[266]. *In vivo*, retroviral derivatives of tet systems have been extensively used in the generation of inducible models of gene expression in animal studies[267]. Recently, Belteki and colleagues have combined a conditional transgene expression system, based on Cre-loxP, with an inducible system, based on Tet-Off, to study *Vegfa* during embryonic development and postnatally in mice[268].

This chapter presents the work carried out in order to create two inducible systems of *OPCML* expression: a Tet-On system based on the HeLa cervical cancer cell line and a Tet-On system based on the SKOV-3 ovarian cancer cell line. The former was created using a commercially-available HeLa Tet-On cell line and was characterised in order to be used in further analysis and functional studies as will be discussed in later chapters. The latter was developed *ab initio* and will be used in future studies. Overall, the main objective of this part of the project was to create an inducible resource of *OPCML* expression to complement the existing over-expression system in studies of *OPCML* and IgLON expression as well as OPCML function.

3.2 The HeLa Tet-On system

3.2.1 Background to the creation of a double stable HeLa Tet-On OPCML cell line

In order to identify the functions of OPCML, the inducible system that was employed is the commercial HeLa Tet-On system available by BD Biosciences. The reason behind the choice of a non-ovarian cell line to study the functions of a potential tumour suppressor gene in ovarian cancer is that when this work commenced there was no commercially available ovarian inducible cell line. The HeLa system was therefore chosen as an alternative that could provide an *in-vitro* model of gynaecological cancer. The HeLa Tet-On system should allow exploiting the advantages offered by any inducible system, i.e. the achievement of near-physiological levels of expression and the avoidance of clonal variation. Having a SKOV-3 over-expression system in addition would help address the issue of context specificity in any phenotype that would be identified.

Figure 3.1 shows the basic features of the HeLa Tet-On system. As supplied, the HeLa Tet-On stable cells harbour the pTet-On plasmid (Appendix C), which encodes the rtTA regulator protein and also has a neomycin-resistance gene. These cells can be transfected with a response plasmid, which in the case of this work was pTRE2hyg, a vector that contains a hygromycin-resistance gene (Appendix C). When the gene of interest is cloned in pTRE2hyg, it is placed under the control of the tetracycline-response element, TRE. This consists of seven direct repeats of a 42 bp sequence containing the *tetO,* located just upstream of the minimal CMV promoter. In the Tet-On system, rtTA binds the TRE and activates transcription in the presence of doxycycline (dox; an antibiotic of the tetracycline family).

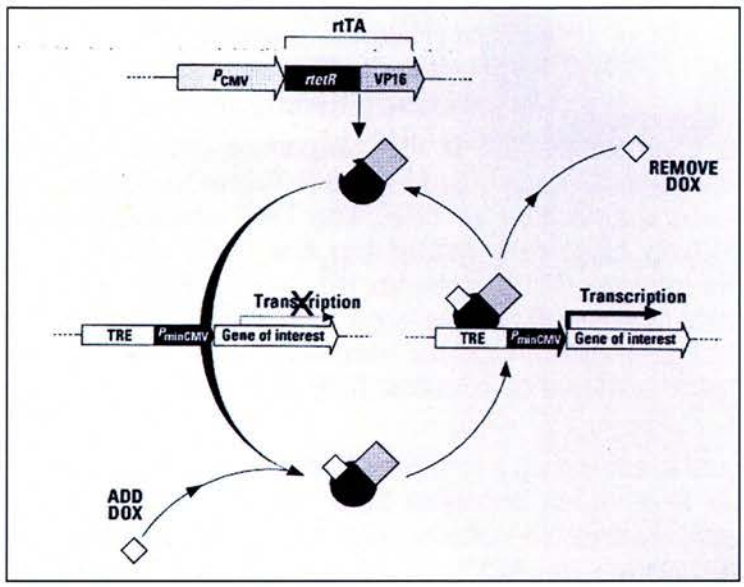

Figure 3.1 The BD Tet-On system
The system comprises two plasmids: a regulatory plasmid and a response plasmid. The former produces the regulatory protein, which upon addition of dox, binds the TRE in the latter, which then drives the transcription of the gene of interest. (reproduced from the BD Tet-Off and Tet-On Gene Expression Systems User Manual).

The creation of double stable clones had been previously undertaken. In brief, either a wild-type human OPCML coding sequence or a sequence harbouring the P95R mutation (the only identified somatic mutation in sporadic EOC to date[21]) had been cloned in the pTRE2hyg vector. The vector had been transfected in HeLa Tet-On cells and the present project commenced with the screening of double stable clones.

3.2.2 Selection of inducible HeLa Tet-On OPCML clones

In order to select inducible double stable clones the following strategy was employed (Figure 3.2). Each clone was treated with 1 μg/ml dox for 48 h or left untreated. Lysates were collected, RNA was extracted and DNase I-treated, and cDNA was synthesised. The assay used to demonstrate induction was an RT-PCR using a forward primer that anneals on the *OPCML* sequence and a reverse primer

that anneals on pTRE2hyg, thereby amplifying specifically the dox-induced *OPCML* transcript. The criteria for acceptable clones were high fold-induction, i.e. a sufficient difference between uninduced and induced expression levels of *OPCML*, and absent or minimal "leaky" (uninduced) expression.

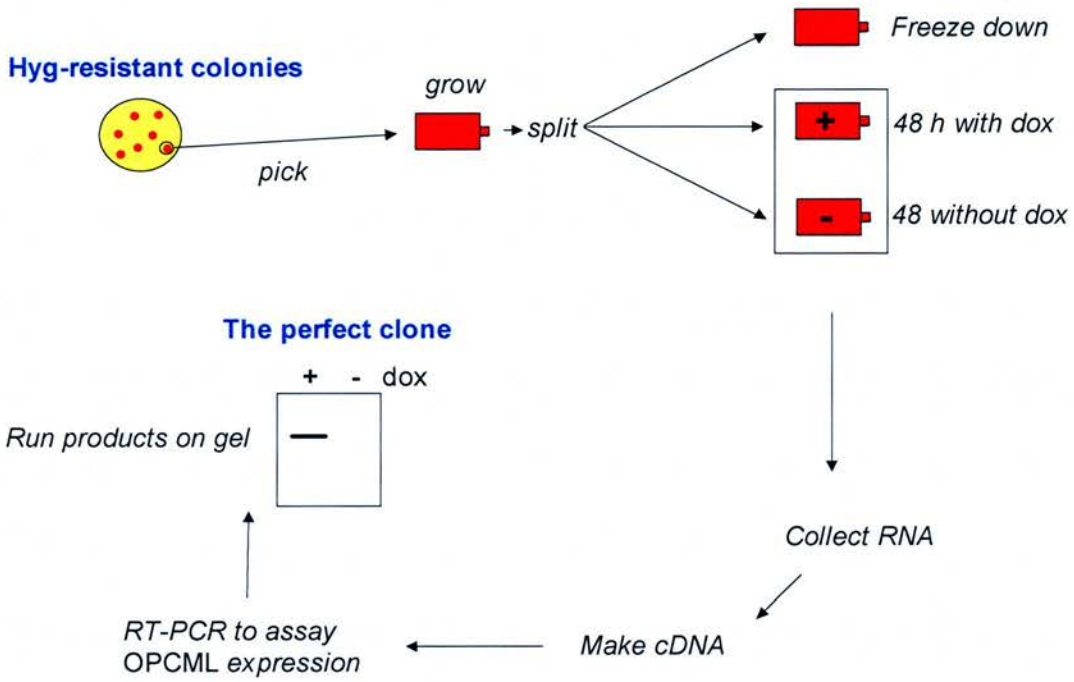

Figure 3.2 Screening strategy for HeLa Tet-On OPCML clones
Diagrammatic representation of the strategy used to select inducible HeLa Tet-On OPCML clones. Clones were grown for 48 h in the presence or absence of dox, and assayed by RT-PCR for *OPCML* expression.

More than fifty clones for each genotype were screened by RT-PCR; Figure 3.3 shows one experiment as an example. Clone 1 demonstrated moderate *OPCML* expression in the induced state and a high uninduced level; clone 2 had no expression at all; clone 3 had almost equal levels of non-induced and induced expression; clone 4 had slightly stronger induced expression, but high uninduced expression as well; and clone 5 had only very low induced expression. This experiment is very representative of the inducibility patterns of most of the clones that were screened. The vast majority of the clones that were screened failed to satisfy the criteria of acceptability. In fact, there was not any clone that satisfied both criteria absolutely.

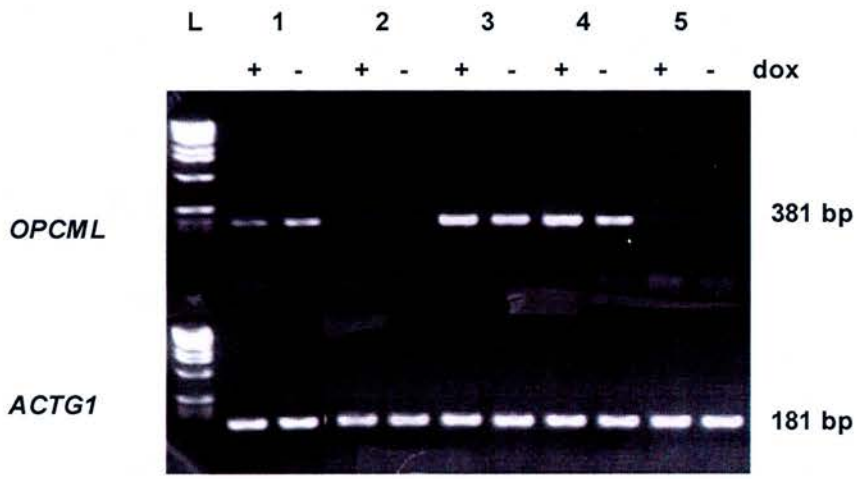

Figure 3.3 Screening for inducible HeLa Tet-On OPCML clones
Clones were grown for 48 h with or without dox and then assayed for *OPCML* induction by RT-PCR. Products were run on a 2% (w/v) agarose gel stained with EtBr. DNA and PCR contamination controls were negative (data not shown). Numbers represent different clones. L = 100 bp DNA ladder; *ACTG1* = gamma actin.

After extensive screening, the two most promising clones that were identified are shown in Figure 3.4. One wild-type and one mutant *OPCML* clone are shown, both exhibiting an acceptable fold-induction, although both also having some uninduced expression. The absence of clones that strictly satisfied the criteria of selection led to the selection of these two clones for further characterisation.

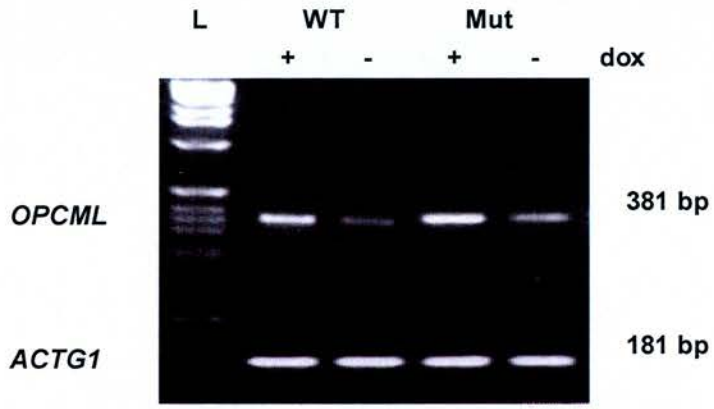

Figure 3.4 The two selected HeLa Tet-On OPCML clones
The two selected clones were grown for 48 h with or without dox and then assayed for *OPCML* induction by RT-PCR. Products were run on a 2% (w/v) agarose gel stained with EtBr. DNA and PCR contamination controls were negative (data not shown).
WT = wild type; Mut = mutant; L = 100 bp DNA ladder; *ACTG1* = gamma actin.

3.2.3 Characterisation of the selected HeLa Tet-On OPCML clones

The two selected clones were subjected to further characterisation so as to investigate quantitatively the induction of *OPCML* at both the RNA and the protein levels. Firstly, the wild-type and the mutant clones were treated with increasing amounts of dox (ranging from 100 to 1000 ng/ml) and 48 h post-induction, protein and RNA lysates were collected. Expression at the protein level was measured by western blotting using the anti-OPCML antibody. Expression at the RNA level was quantified by qRT-PCR, using an assay similar to the one used in screening. As can be seen in Figure 3.5, both clones expressed *OPCML* upon induction with dox and expression increased in line with the concentration used. OPCML was clearly detectable after induction with as little as 100 ng/ml in the wild-type and 500 ng/ml in the mutant. In both the wild-type and the mutant clones, there was a very good positive correlation between dox concentration and amount of protein detected by densitometry ($r = 0.98$ for the wild-type and 0.99 for the mutant). In order to validate

the specificity of the anti-OPCML antibody, two controls were used: the SKOV-3 *OPCML*-transfected cell line as a positive control and the untransfected parental cell line as negative control. Presence of immunoreactivity in the positive control and absence thereof in the negative control confirmed the specificity of the antibody employed. Notably, OPCML was detected as a doublet in all lysates. The approximate size of the doublet is 55 kDa. At the RNA level, *OPCML* expression rose as the concentration of dox increases (r = 0.98 for both the wild-type and the mutant). Low levels of uninduced expression were also observed, in accordance with the non-quantitative RT-PCR data. It is also important to note that a comparison between the protein and RNA data confirmed that they were well correlated (r = 0.97 for both the wild-type and the mutant). Moreover, it is interesting that although the mutant clone exhibited overall lower expression levels at the protein level in comparison to the wild-type one, at the RNA level the converse was seen.

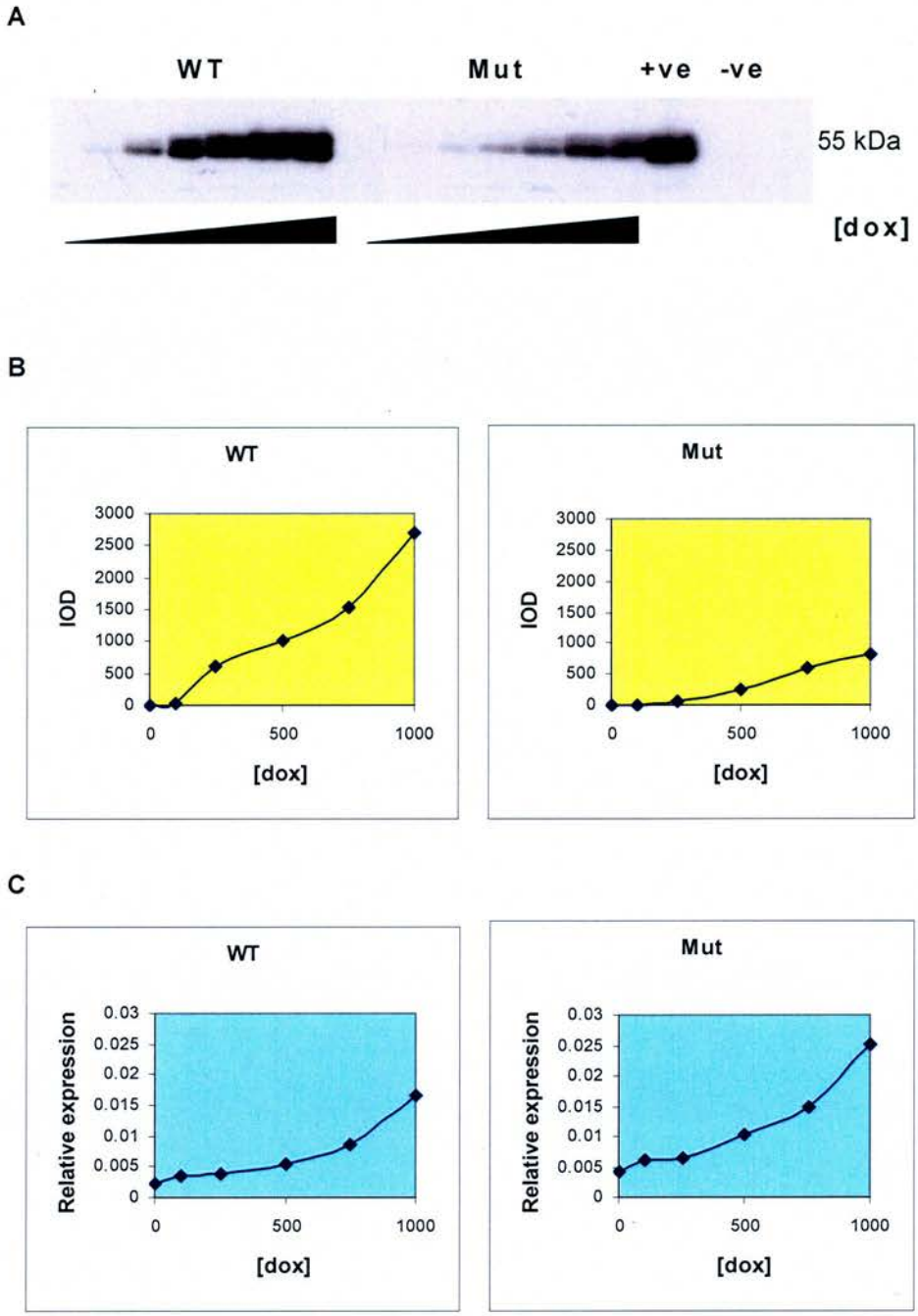

Figure 3.5 Characterisation of the selected HeLa Tet-On OPCML clones at the protein and RNA level

The two selected clones were induced for 48 h with a gradient of dox concentrations and assayed for *OPCML* expression by western blotting (A, B) and qRT-PCR (C). Panel B shows the densitometric quantification of panel A. RNA expression was calculated relative to beta actin. DNA and PCR contamination controls were negative (data not shown).

WT = wild type; Mut = mutant; +ve = positive control (SKOV-3 OPCML);

-ve = negative control (SKOV-3 parental); [dox] = dox concentration ranging from 100 to 1000 ng/ml; IOD = integrated optical density.

Having established the concentration of dox needed for OPCML protein induction in the selected clones based on the above experiment, the minimum dox concentration required for each clone was subsequently examined. This would facilitate the expression of *OPCML* at a level approximating the physiological one, which previous work had suggested to be low in the human ovary. The previous experiment was therefore repeated, but the concentrations of dox used for each clone were centred around the lowest ones identified in the previous experiment that were sufficient to induce detectable OPCML protein. Hence, for the wild-type clone a dox range of 50 to 500 ng/ml was used, whereas for the mutant clone the range was 100 to 750 ng/ml. The two clones were treated with dox for 48 h, and protein lysates were collected. Figure 3.6 shows this experiment's western blot with the anti-OPCML antibody and its quantification. As can be seen, the OPCML doublet was strongly visible after induction with 250 ng/ml for the wild-type and 500 ng/ml for the mutant.

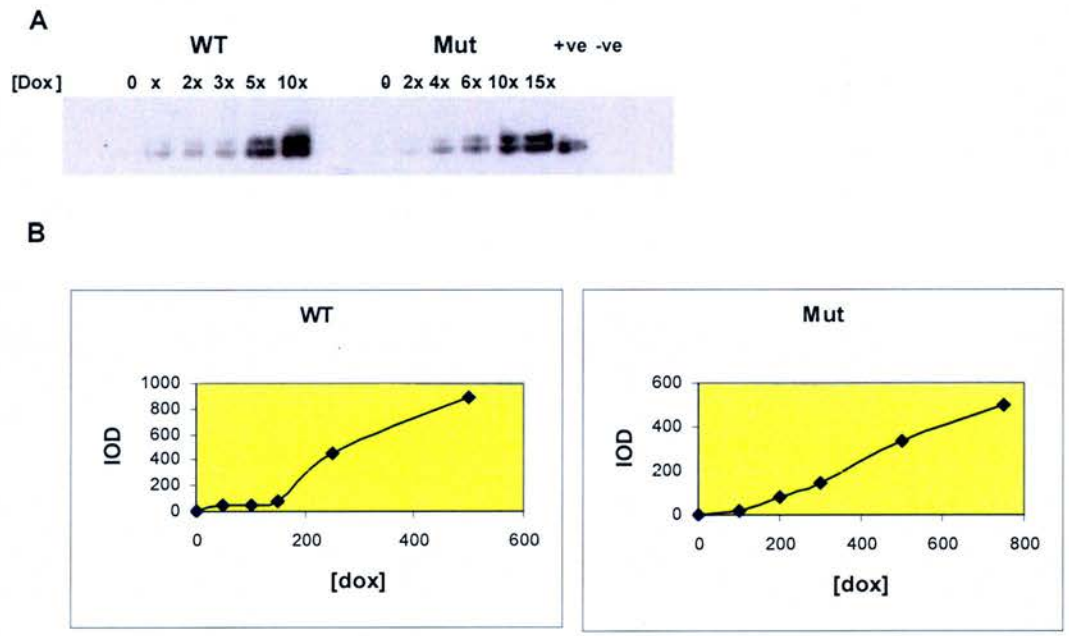

Figure 3.6 Finding the minimal dox concentration required to induce *OPCML* expression in the selected HeLa Tet-On OPCML clones
The two selected clones were induced for 48 h with a gradient of dox concentrations and assayed for *OPCML* expression by western blotting (A, B). Panel B shows the densitometric quantification of panel B.
WT = wild type; Mut = mutant; +ve = positive control (SKOV-3 OPCML);
-ve = negative control (SKOV-3 parental); [dox] = dox concentration in multiples of x, where x = 50 ng/ml; IOD = integrated optical density.

It is known that OPCML is a glycosylated protein; the detection of a doublet by western blotting is likely to indicate isoforms bearing different degrees of glycosylation, as has been previously reported. To demonstrate this, protein lysates prepared for the two HeLa Tet-On clones, as well as the SKOV-3 OPCML cell line and the SKOV-3 untransfected parent, were treated with a deglycosylation enzyme, PNGase F. The treated samples were immunoblotted alongside untreated samples. Deglycosylation resulted in the two bands of each doublet merging into a single band of a reduced size, approximately 38 kDa (Figure 3.7). Notably, it was evident in this blot, as in previous ones (e.g. Figure 3.6), that only one band of the SKOV-3 doublet is met in the doublet of the HeLa Tet-On cells. Hence, it appeared that the OPCML glycoprotein species differ in the two cell lines.

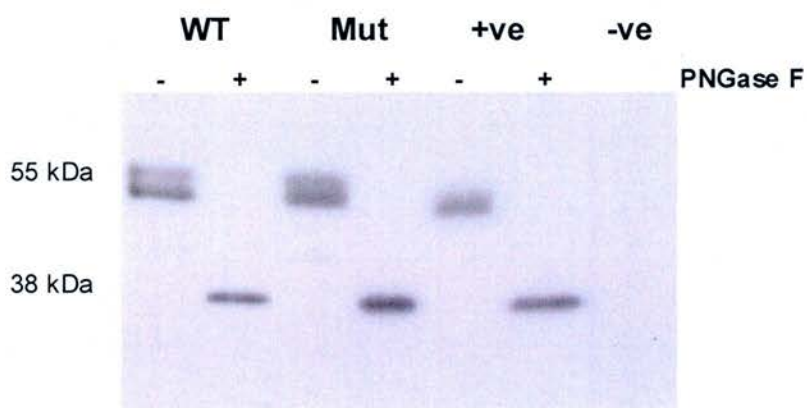

Figure 3.7 Deglycosylation experiment
Lysates from the two selected HeLa Tet-On OPCML clones were collected after induction with dox for 48 h. The lysates were treated with PNGase F or left untreated and were immunoblotted with the anti-OPCML antibody.
WT = wild type; Mut = mutant; +ve = positive control (SKOV-3 OPCML);
-ve = negative control (SKOV-3 parental).

3.3 The SKOV-3 Tet-On system

As previously mentioned, the reasons for choosing an inducible system so as to study the functions of OPCML included the ability to work at a level of expression that is comparable to the physiological level and hence avoids over-expression artefacts, as well as being able to make comparisons in the same clone without the issue of clonal variation. Furthermore, the choice of a non-ovarian cell line was based on availability constraints. The hope was that HeLa cells transfected with *OPCML* would behave similarly as SKOV-3 cells as a model of gynaecological cancer *in vitro*, and if not, comparisons would be valuable in respect with context specificity. However, some serious problems were encountered that led to a change of direction for the future. Firstly, both selected HeLa Tet-On OPCML clones exhibited "leaky", uninduced, expression (Figure 3.5), which as will be seen in chapter 4 is actually comparable to the expression of *OPCML* in the human ovary (Figure 4.12) and thus likely to be functional. Secondly, as will be discussed in chapter 5, transfection of *OPCML* into the non-ovarian HeLa cells does not incur the same phenotypic attributes as those in the ovarian SKOV-3 cells. As a result, the HeLa system is not an optimal tool to study a tumour suppressor gene in ovarian cancer. It was therefore important to change strategy for the future and try to establish an inducible system in an ovarian cell line. This would have to be undertaken in two steps: initially, creating a SKOV-3 Tet-On cell line by transfection of a regulatory plasmid; and then creating a double stable cell line by a further transfection of an OPCML-encoding response plasmid. The regulatory plasmid used was the same pTet-On plasmid that the commercial HeLa Tet-On cells contain (Appendix C); however, the response plasmid was a second generation version, which is reported to offer a tighter regulation of gene expression, avoiding "leakiness" typical of its older version. The plasmid used was pTRE-Tight from BD Biosciences (Appendix C).

3.3.1 Creation of a stable SKOV-3 Tet-On cell line

The first step in the creation of a successful SKOV-3 based inducible system was to stably transfect SKOV-3 cell with the pTet-On plasmid. The cells were subjected to three independent transfections and selection based on neomycin resistance. Approximately 30 clones were picked from each transfection, expanded and subjected to screening.

3.3.2 Selection of an inducible SKOV-3 Tet-On clone

The selection of an inducible stable SKOV-3 Tet-On clone was based on screening by three independent methods: reporter assays, growth curves and transient transfections with *OPCML*.

The principle behind screening by reporter assays is that the temporary introduction of a luciferase-encoding response plasmid into the SKOV-3 Tet-On clones should allow to test which clones exhibit favourable inducibility profiles by examining luciferase extivity. The screening was performed after transiently transfecting the clones under test with pTRE2hyg-Luc, which is a response plasmid harbouring the luciferase gene as a reporter. Following the transient transfections, the clones were treated with dox for 48 h or left untreated and then assayed for luciferase activity. The criteria for selection were as previously: high fold-induction (more than 20-fold) and low uninduced activity. Figure 3.8 shows the four clones that were selected after screening based on the aforementioned criteria. All four SKOV-3 Tet-On clones exhibited more than 20-fold induction, as well as a low uninduced luciferase activity. It was therefore inferred that these clones have the potential to provide an optimal SKOV-3 Tet-On system in terms of inducibility.

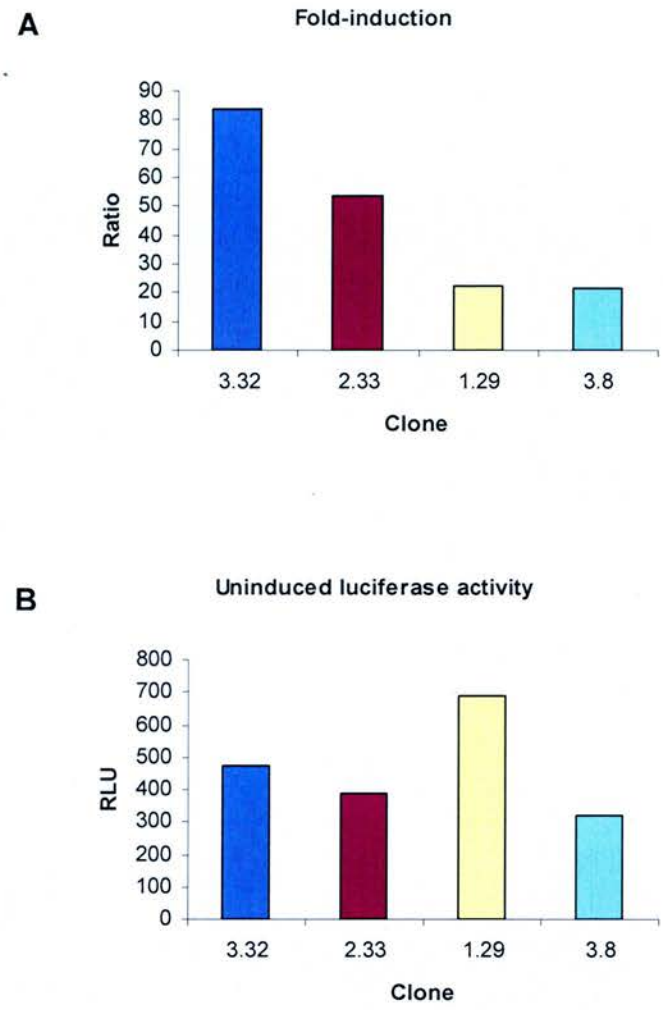

Figure 3.8 The four selected SKOV-3 Tet-On clones based on reporter assays

SKOV-3 Tet-On clones were transiently transfected with pTRE2hyg-Luc, grown in the presence or absence of dox for 48 h and assayed for luciferase activity by a reporter assay.

Fold-induction = ratio of induced over uninduced luciferase levels;

RLU = relative luminescence units.

The next round of screening aimed at examining the growth characteristics of the selected clones in order to ensure that they grow similarly to the parental cell line. The four clones were thus used in a growth curve experiment, whereby Tet-On cells were seeded and counted over a 9-day period so that their growth characteristics could be compared to the parental cells. As can be seen in Figure 3.9, all clones grew relatively similarly to the SKOV-3 parent, apart from clone 3.8 that grew substantially faster, and clone 3.32 that grew more slowly than 3.8 but still faster than the parent.

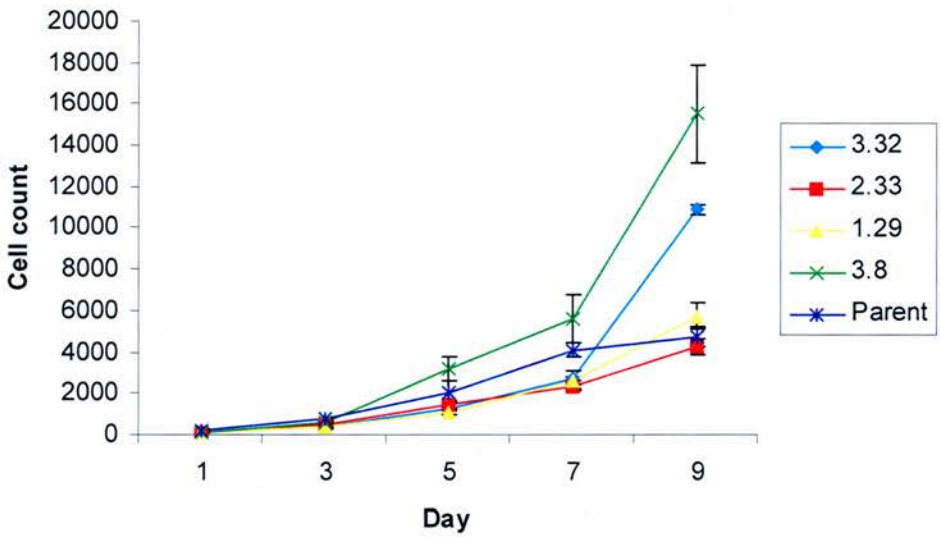

Figure 3.9 Growth curves of selected SKOV-3 Tet-On clones
The four selected SKOV-3 Tet-On clones were tested in growth characteristics against their parental cell line. Cells were seeded and counted over a period of nine days. Error bars represent the SD of three replicates.

The ultimate selection assay examined the potential of the four Tet-On clones to allow induction of our specific gene of interest, i.e. *OPCML*. To this end, the four clones were subjected to transient transfections with the pTRE-Tight vector containing the human *OPCML* sequence (see following section). The transiently-transfected clones were treated with dox for 48 h or left untreated and RNA was collected. Inducibility was examined by RT-PCR using a forward *OPCML*-specific primer and a reverse vector-specific primer. As is evident in Figure 3.10, the Tet-On clone that satisfied best the selection criteria was clone 2.33: it exhibited minimal uninduced expression and sufficiently strong induction of *OPCML*, in this transient transfection assay. SKOV-3 Tet-On clone 2.33 was therefore finally selected for the second round of stable transfections.

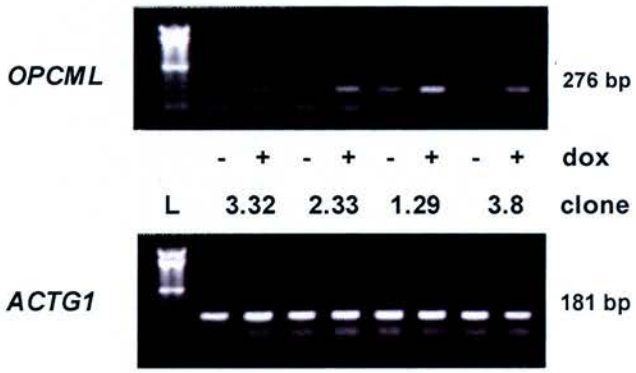

Figure 3.10 Transient transfections of selected SKOV-3 Tet-On clones with pTRE-Tight OPCML
The four selected SKOV-3 Tet-On clones were transiently transfected with a response plasmid encoding OPCML, grown for 48 h with or without dox and assayed for expression of *OPCML* by RT-PCR. Products were run on a 2% (w/v) agarose gel stained with EtBr. DNA and PCR contamination controls were negative (data not shown). L = 100 bp DNA ladder; *ACTG1* = gamma actin.

3.3.3 Creation of a double stable SKOV-3 Tet-On OPCML cell line

As the response vector to be used in the second round of transfections was not the same as the one used in the HeLa Tet-On OPCML cells, the *OPCML* sequence had to be cloned in the new vector, pTRE-Tight (Appendix C). The respective cDNA fragment was excised from the pcDNA3.1/Zeo construct (used in the SKOV-3 OPCML cell line; see chapter 2) and cloned into pTRE-Tight. Figure 3.11 shows plasmid DNA from six potentially insert-containing colonies digested with a restriction endonuclease that allows separation of the vector and the insert. As can be seen, five out of six colonies did actually contain the insert. In order to confirm the sequence integrity of the inserts and also determine the orientation of insert integration in the vector, these five positive clones were sequenced (data not shown). Finally, one clone was selected that was sequence-perfect and where the insert had ligated in the sense orientation.

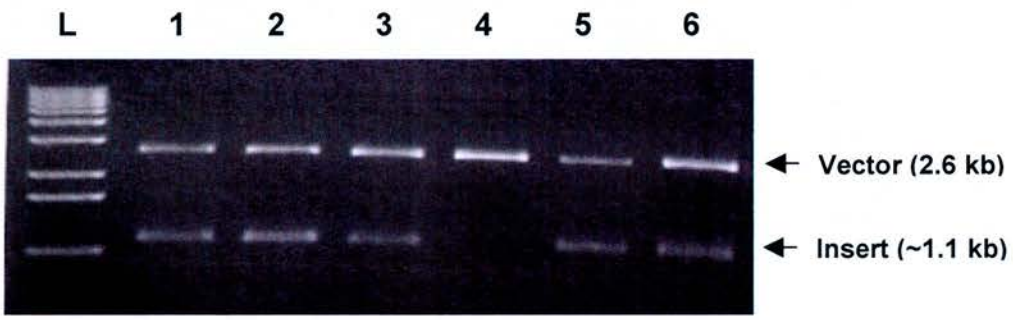

Figure 3.11 Cloning of *OPCML* into pTRE-Tight
The wild-type *OPCML* sequence was cloned into pTRE-Tight. After transformation of competent bacteria, potentially positive colonies were picked, plasmid DNA was prepared and digested with NotI to release the insert.
Products were run on a 1% (w/v) agarose gel stained with EtBr.
L = 1 kb DNA ladder; numbers 1 to 6 represent six individual colonies.

The pTRE-Tight *OPCML* construct was co-transfected into the SKOV-3 Tet-On 2.33 clone in combination with a linear cDNA encoding a hygromycin-resistance marker. Three independent stable transfections were carried out, and the cells were placed under hygromycin selection. Hygromycin-resistant colonies were picked and expanded for further analysis. SKOV-3 Tet-On OPCML double stable clones are currently under test for inducibility profiles by qRT-PCR, using an *OPCML*-specific primer set. Figure 3.12 shows an experiment representative of data that have been thus far acquired.

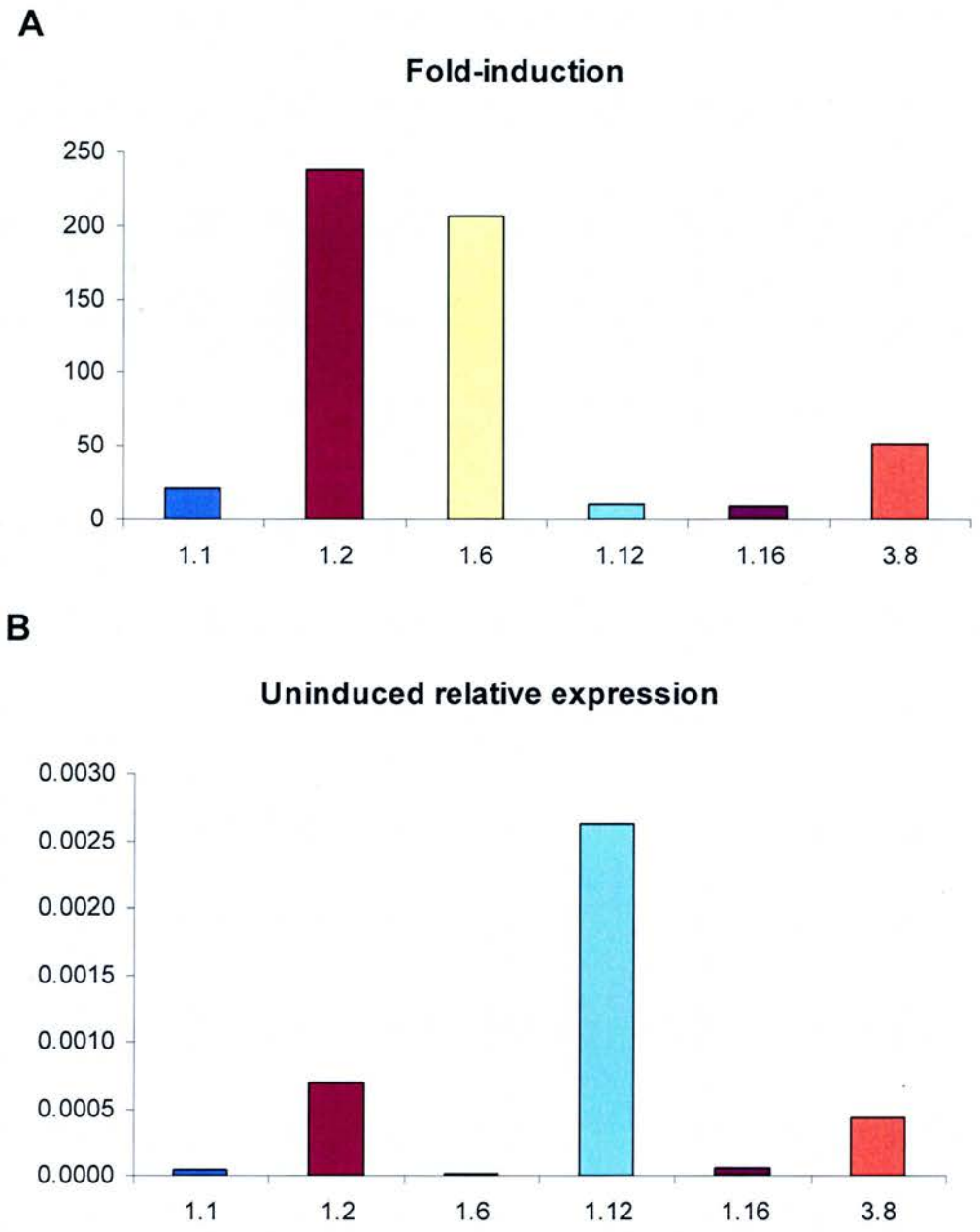

Figure 3.12 Screening of SKOV-3 Tet-On OPCML clones
Clones were grown for 48 h with or without dox and then assayed for *OPCML* induction by qRT-PCR. Expression is shown relative to beta actin. DNA and PCR contamination controls were negative (data not shown). Numbers represent different clones. Fold-induction = ratio of induced over uninduced relative expression.

3.4 Discussion

In the quest to understand better what OPCML does and identify functions that have not been studied before in the locality with which it has been typically associated, i.e. the brain, an inducible system of expression was developed to complement an already-existing over-expression system[21]. The parallel use of the two systems would allow the investigation of OPCML biology from different perspectives. An inducible system offers advantages that a traditional system lacks: it allows the study of a gene of interest in a regulated fashion, such that level of expression can be linked to function; working at expression levels that are not exaggerated renders functional characterisation potentially more reliable avoiding over-expression artefacts and better approximating physiological roles; and finally, comparisons between induced and uninduced states within the same clone surpass concerns of clonal variation.

Even though the over-expression system is based on a SKOV-3 ovarian cancer cell line, arguably offering a better-suited platform to investigate a novel tumour suppressor gene in ovarian cancer, the inducible resource used is a HeLa cervical cancer Tet-On system. HeLa cells are considered to be particularly stable tet responders[260]. Another advantage in using the HeLa system is that even if transfection of *OPCML* results in a different phenotype than in SKOV-3 cells, any differences identified would underpin the significance of context specificity.

When an inducible system of expression is created, the ultimate expectation is the identification of clones that do not exhibit "leaky", uninduced expression, but offer robustly regulated induced expression. Extensive screening of HeLa Tet-On OPCML clones did not yield any clones of such characteristics. The clones that were selected, one wild-type and one mutant *OPCML*-expressing clones, both exhibit some level of uninduced expression. The selection of these two clones relied on the assumption that the levels of uninduced expression were sufficiently low to be functionally insignificant. Reported work is often based on such less-than-optimal systems[269].

In both the wild-type and mutant Tet-On clones, doxycycline induction results in a well-regulated expression of *OPCML* both at the RNA and protein levels.

RNA was induced in concert with the amount of the inducer used, supporting the hypothesis that in defined circumstances transcription can occur in a graded rather than threshold manner[270]. Protein levels are also in concert with the amount of doxycycline used to induce *OPCML* expression. Importantly, for each clone, there is a clear correlation between RNA and protein levels, suggesting that the regulated transcription of *OPCML* can be used to achieve a regulated functional expression. Interestingly, even though the same amount of doxycycline induces a higher *OPCML* RNA expression in the mutant than the wild-type clone, the converse is true for protein expression. This probably suggests that, as a clone, HeLa OPCML^{Mut} Tet-On has lower translation efficiency than its wild-type counterpart; alternatively, the mutant OPCML protein might be less stable. In contrast, HeLa OPCML^{WT} Tet-On is generally more responsive to doxycycline induction at the protein level, with much lower amounts of the inducer needed.

OPCML is reported to have six putative N-linked glycosylation sites[9], although our *in silico* analysis has identified five. In fact all IgLONs undergo post-translational glycosylation and this has been confirmed by deglycosylation experiments for multiple members of the family[8,54]. In both the HeLa cells and the SKOV-3 cells the OPCML protein is detected as a doublet of an approximate molecular weight of 55 kDa. Removal of glycosylation results in the detection of OPCML as a single band at approximately 38 kDa. This is in fact the predicted molecular weight of the native protein, confirming that the apparent size of the 55 kDa protein is due to glycosylation. The two bands of the doublet are likely to exemplify processed proteins of different degrees of glycosylation. Of potential interest is the fact that there is a difference in the appearance of the HeLa doublet in comparison to the SKOV-3 one. This disparity in the OPCML protein is the first example of divergence between the two systems and might be a contributing factor in any functional differences identified and discussed in chapter 5. Differences in glycosylation, which are conferred post-translationally, often have functional consequences[271].

Despite the usefulness of the effort devoted in the development of the HeLa Tet-On OPCML system, issues that are related to the link of *OPCML* with ovarian cancer are better addressed by the use of an ovarian system, such as the SKOV-3

OPCML resource. In addition, potential obstacles arising from the "leakiness" that has been identified in the HeLa Tet-On system prompt the use of a more refined inducible system. These two factors have made the consideration of a SKOV-3 inducible system imperative, albeit with a priority that became evident towards the end of this work. Hence, the generation of a SKOV-3 Tet-on cell line was undertaken.

In order to maximise the chances of a successful system, the selection of a favourable SKOV-3 Tet-On clone was thee-fold. Clones were initially selected on the basis of inducibility after transient transfections with a response plasmid that encodes luciferase, the activity of which can be easily measured by reporter assays. Four clones were selected, all with high fold-induction and low background levels. These clones were further tested to ensure that they grow similarly to their parental cell line. Finally, transient transfections with a response plasmid encoding OPCML demonstrated how these four clones would potentially act as hosts that allow the regulated expression of an exogenous gene. Taken together, the data from the three independent selection methods pointed to the most favourable SKOV-3 Tet-On clone.

The creation of a SKOV-3 inducible system of *OPCML* expression would have to ensure that precautions were taken to minimise the risk of "leaky", i.e. uninduced, expression. To this end, *OPCML* was cloned in a second-generation response plasmid, pTRE-Tight, which should offer a tighter regulation of the exogenous gene by the inducer than its predecessor. After stably transfecting pTRE-Tight OPCML into the selected SKOV-3 Tet-On clone, extensive qRT-PCR screening is currently being performed. Thus far, several clones with favourable inducibility profiles have been identified. In spite of the fact that these clones became available at the end of this work and thus were not further characterised, it is hoped that they will be a valuable resource for the study of OPCML function in the future. If more time were available, the screening would continue until selecting a few clones that satisfied best the inducibility criteria. Subsequently, these clones would be further characterised at both the RNA and protein levels, similarly to the HeLa Tet-On clones. Finally, the selected and characterised SKOV-3 Tet-On OPCML clones could be used in functional studies.

Overall, the work desrcribed in this chapter has established two important tools that would allow the study of OPCML function. Firstly, an inducible system of gene expression in HeLa cells was created and characterised fully. This system was subsequently used in the functional characterisation of OPCML, alongside the SKOV-3 over-expression system, as will be presented in chapter 5. Secondly, a SKOV-3 inducible system was also created in order to provide a better platform to study the functions of OPCML in an ovarian context. This resource has not been fully developed yet, but once the screening and characterisation is complete, it will provide a valuable tool for the future.

Chapter 4

Studies on IgLON expression

4.1 Introduction

The exploration of the expression profiles of the IgLON family has been a central theme in this work. In its pursuit, the ultimate aim was to build a detailed picture of the expression patterns of the four IgLONs in order to complement and extend existing data. A holistic characterisation of the IgLON family at the level of expression will enhance our understanding of the biology of this group of adhesion molecules and add essential information to the knowledge that has been thus far acquired mainly by studies in the chick and rat nervous systems.

So, what is currently known about the expression of IgLON family members? Briefly reiterating what has been extensively presented in chapter 1, it is known that IgLON expression patterns in the brain are distinct but also overlapping: *OPCML* is mainly expressed in the grey matter[18], *HNT* in the sensorimotor cortex and the cerebellum[27], *LSAMP* in the cortical and subcortical neurones of the limbic system[33] and *NEGR1* in the cerebrum and brain stem[54].

This chapter presents results that extend the study of IgLON expression to additional levels. Expression studies were undertaken in two species, namely mouse and human, as well as various human cancer cell lines. In the mouse and human, studies were undertaken both in adult tissues, and also in development. Moreover, the expression of the family was established in epithelial ovarian cancer, in addition to the normal ovary. All these diverse expression analyses were approached by a multitude of methods, ranging from the molecular to the histological level.

4.2 IgLON expression in cell lines

As a starting point of IgLON expression profiling, the first line of experiments focused on establishing the expression levels of the family in various human cancer cell lines of both ovarian and non-ovarian origin. The only similar data to date exist with respect to *OPCML*, as reported by Sellar *et al.*[21]. Hence, establishing the profiles of the other family members in a wider panel of cell lines can be regarded as a pilot experiment before addressing expression in cancer.

4.2.1 IgLON RNA expression in a panel of cancer cell lines

In order to determine the RNA levels of the four IgLONs in cancer cell lines, a panel comprising 17 ovarian and 14 non-ovarian cell line samples was used. Expression of each IgLON was measured in the panel by qRT-PCR. Figure 4.1 illustrates the results. *OPCML* expression was not detected in any cell line. Significant *HNT* RNA expression was only detected in two cell lines, namely CaOV-3 and 59M, both of ovarian origin. *LSAMP* was expressed in 11 out of the 14 ovarian cell lines, showing a range of expression levels, from extremely high to low. In addition, it was expressed highly in only one non-ovarian cell line, PANC-1, which is of pancreatic origin; it also exhibited low expression in other two non-ovarian cell lines. Finally, there appeared to be three groupings in *NEGR1* expression in ovarian cell lines: six cell lines exhibited high expression, five cell lines exhibited low expression and the remaining seven minimal to none. With respect to non-ovarian cell lines, there were three high-expressers, one low-expresser and the rest did not have any *NEGR1* expression.

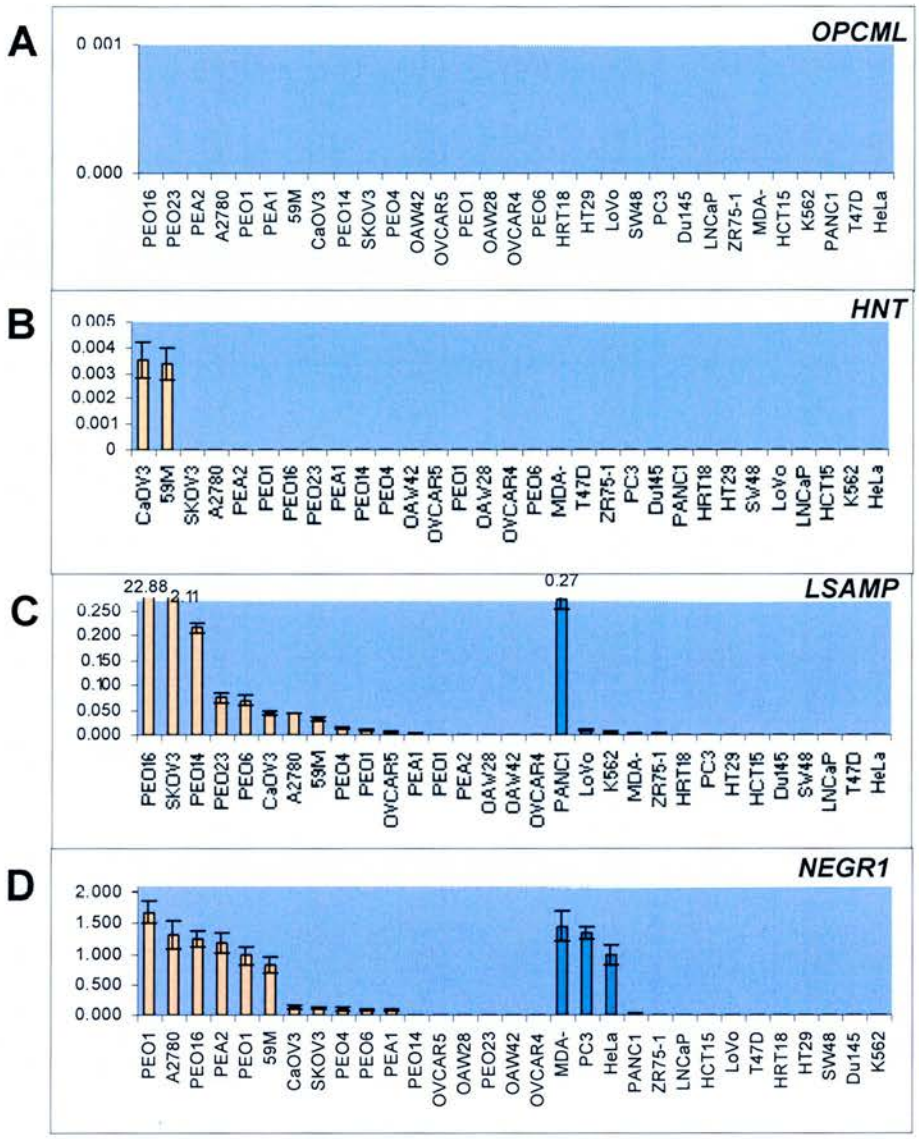

Figure 4.1 IgLON RNA expression in a panel of cell lines
RNA levels of *OPCML* (A), *HNT* (B), *LSAMP* (C) and *NEGR1* (D) in a panel of cancer cell lines, as measured by qRT-PCR. IgLON expression in ovarian (salmon) and non-ovarian (turquoise) cell lines is shown relative to beta actin expression, in decreasing order. DNA and PCR contamination controls were negative (data not shown). Error bars represent the SEM of three independent experiments.

4.2.2 IgLON RNA expression in *OPCML*-transfected cell lines

The functional characterisation of *OPCML*, as will be presented in chapter 5, is based on the use of two cell line resources: an over-expression system in SKOV-3 ovarian cancer cells and an inducible expression system in HeLa cervical cancer Tet-On cells. There is considerable homology within the IgLON, both at the level of the structure of the genes and the protein sequence they encode, as well as the postulated functions of the latter. A lot of these functions are thought to be mediated by IgLONs interacting with each other[57]. Thus, the examination of the relative levels of all the IgLONs in the *OPCML*-transfected cell lines was a necessary step in order to be able to point to differences between the two systems that might be reflected on phenotypic divergence. It also directly addresses any potential expression relationships that IgLONs might have, in addition to how these are affected by *OPCML*.

The examination of IgLON expression was restricted to the RNA level, as fully optimised antibodies were not available for all the IgLONs. As shown in Figure 4.2, parental SKOV-3 cells did not express *OPCML*; after transfection with either wild-type or mutant *OPCML*, there was high expression of both cDNAs, with mutant *OPCML* expression being lower than that of the wild-type. How did this reflect on the expression of the rest of the IgLONs? *HNT* RNA was not detectable in the SKOV-3 cell lines. *LSAMP* expression showed a 43-fold drop in the wild-type *OPCML* expresser ($p = 0.002$) and a 25-fold decrease in the mutant ($p = 0.002$) relative to the parental cell line. *NEGR1* expression was halved after expression of *OPCML*, both in the wild-type ($p = 0.001$) and mutant ($p < 0.001$) expressers. In HeLa Tet-On cells, significant expression of *OPCML* was demonstrated at the high level of induction. Like SKOV-3 cell lines, HeLa Tet-On cells did not express *HNT* at the RNA level. *LSAMP* RNA expression was very low, whilst *NEGR1* expression was much higher than in SKOV-3 cells; it did not differ after induction of *OPCML* though.

It is interesting to note that in the SKOV-3 cell lines, *OPCML* expression was negatively correlated with both *LSAMP* and *NEGR1* (r = -0.97 for both). *LSAMP* expression was directly proportional to that of *NEGR1* (r = 1.00). In HeLa Tet-On cells, *OPCML* expression did not correlate with either *LSAMP* or *NEGR1*. The expression of the latter two however did correlate positively as in SKOV-3 cells (r = 0.96).

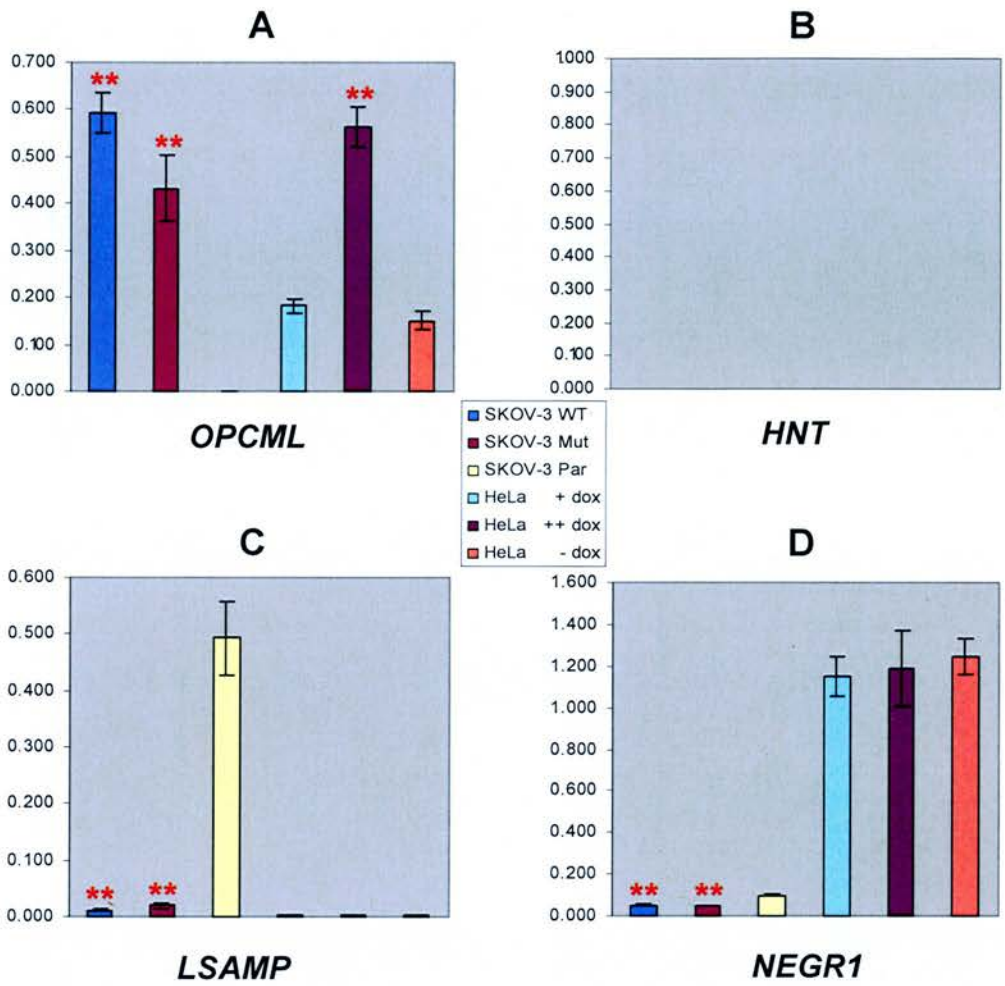

Figure 4.2 IgLON expression in the *OPCML*-transfected cell lines
Expression of *OPCML* (A), *HNT* (B), *LSAMP* (C) and *NEGR1* (D) in the SKOV-3 OPCML and HeLa Tet-On OPCML cell lines. RNA expression is shown relative to beta actin. DNA and PCR contamination controls were negative (data not shown). Error bars represent the SEM of three independent experiments.
** $p < 0.01$ as compared to parental/uninduced cell lines by Student's *t* test.
WT = wild type; Mut = mutant; Par = parent;
+ dox, ++ dox, - dox = 48 h treatment with 100 ng/ml dox, 1000 ng/ml dox and no dox respectively.

4.2.3 Confirmation of the transcriptional effect of *OPCML*

The effect of *OPCML* expression on the expressions of *LSAMP* and *NEGR1* was quite pronounced, even if only demonstrated at the RNA level. It was decided to investigate this transcriptional effect further, by attempting to reproduce it in an independent context. A first test was to examine the expression of IgLONs in an alternative SKOV-3 OPCML clone, deriving from an independent transfection of the same wild-type *OPCML* construct used in the SKOV-3 OPCML^{WT} clone. To be able to distinguish them, let this alternative clone be called SKOV-3 OPCML$^{WT.2}$.

As can be seen in Figure 4.3, *OPCML* expression influenced the expression of both *LSAMP* and *NEGR1* in the SKOV-3 OPCML$^{WT.2}$ clone. Relative to the parental cell line, there was a three-fold decrease in the expression of *LSAMP* and a four-fold decrease in the expression of *NEGR1*. Notably, the expression of *OPCML* in this clone was six-fold lower than in the default clone.

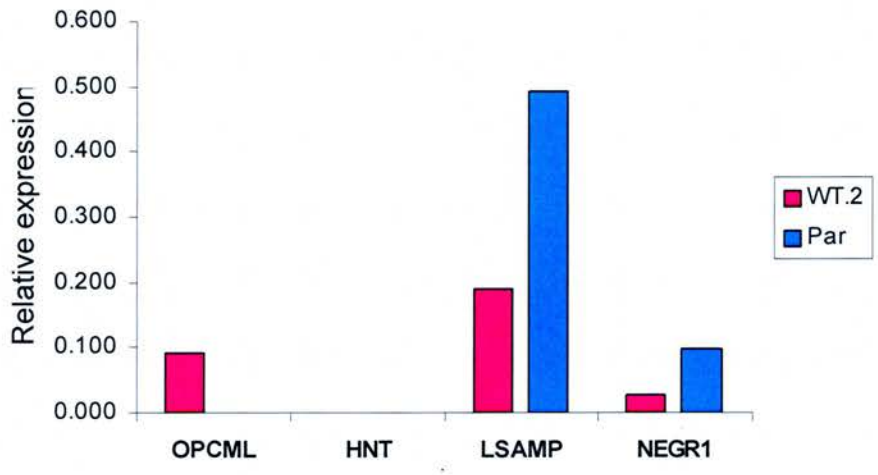

Figure 4.3 The effect of *OPCML* expression on the transcription of *LSAMP* and *NEGR1*: confirmation on an independent SKOV-3 OPCML clone

Expression of the four IgLONs at the RNA level in the SKOV-3 OPCML$^{WT.2}$ clone and its parent as determined by qRT-PCR. RNA expression is shown relative to beta actin. DNA and PCR contamination controls were negative (data not shown). WT.2 = wild-type clone 2; Par = parent.

Having confirmed the effect of *OPCML* expression on *LSAMP* and *NEGR1* expression in SKOV-3 cells, two questions emerged: firstly, whether this effect is a feauture of this particular cell line; secondly, whether the effect on *LSAMP* is independent of the effect on *NEGR1* or the effect on one secondarily results in an effect on the other as the two are correlated. In order to address these two issues, two other ovarian cancer cell lines were used. PEA2, a cell line expressing very little *LSAMP* RNA, and PEO23, a cell line expressing minimal *NEGR1* RNA. To express *OPCML* in these cell lines, transient transfections were undertaken, with the same wild-type *OPCML* construct used in SKOV-3 OPCML cells.

Figure 4.4 shows the RNA levels of the IgLONs in the two ovarian cell lines following transient transfections with the *OPCML*-containing plasmid. In both PEA2 and PEO23 cell lines, the transient transfections caused successful expression of *OPCML*. In PEA2 cells, expression of *OPCML* resulted in a 1.8-fold decrease in the RNA level of *LSAMP* and a 1.5-fold decrease in the level of *NEGR1*. In PEO23 cells, expression of *OPCML* was accompanied by a 2-fold drop in *LSAMP* RNA expression, whereas the minimal *NEGR1* expression was abolished. It should be noted that the transfection efficiencies were not estimated for these experiments. Thus, the observed fold-differences are likely to be an under-estimation of a more pronounced effect of *OPCML*.

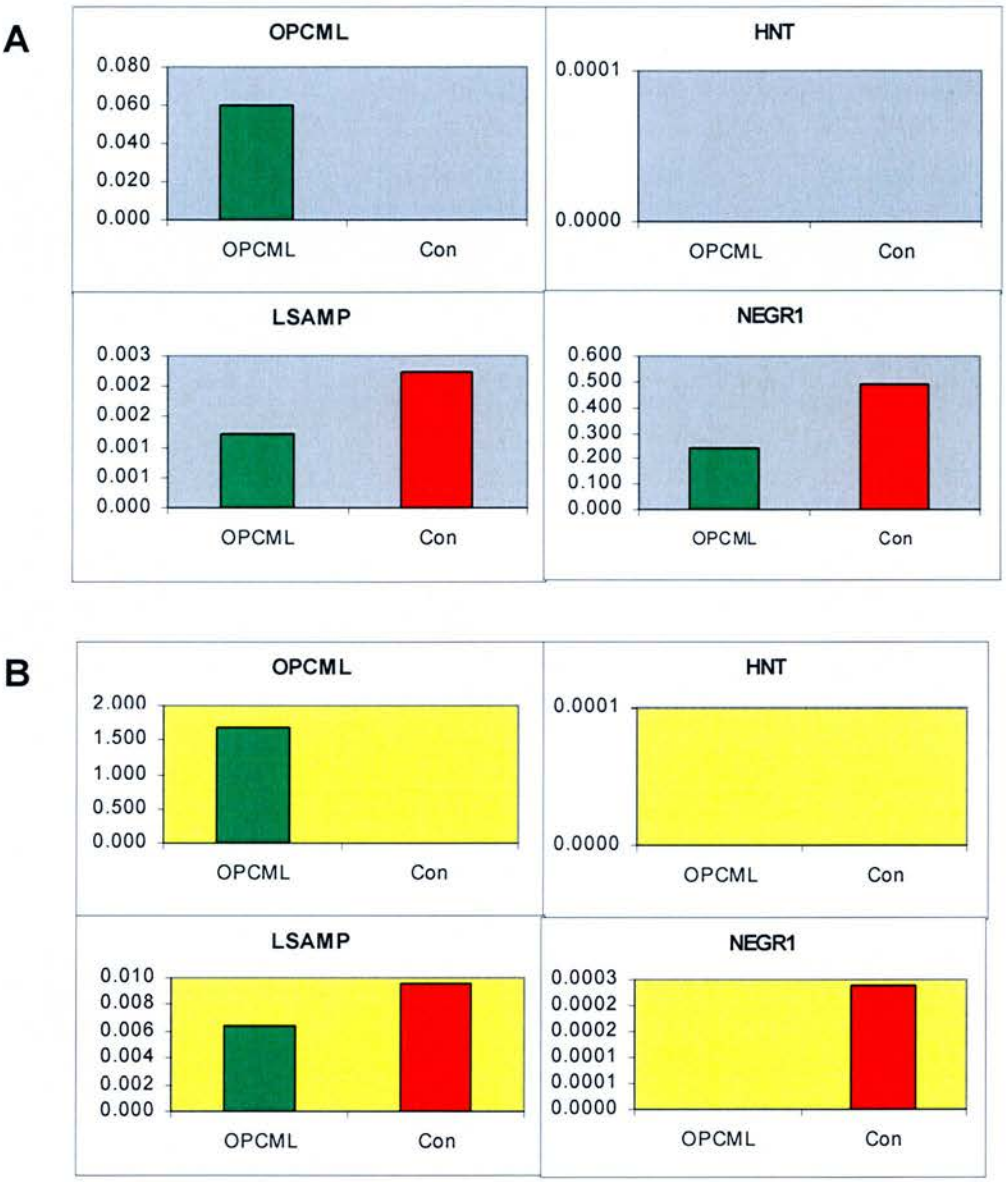

Figure 4.4 The effect of *OPCML* expression on the transcription of *LSAMP* and *NEGR1*: confirmation on two additional ovarian cell lines
Expression of the four IgLONs at the RNA level after transiently expressing *OPCML* in PEA2 (A) and PEO23 (B) cells as determined by qRT-PCR. RNA expression is shown relative to beta actin. DNA and PCR contamination controls were negative (data not shown). Note differences in y-axis scale.
Con = untransfected control.

4.3 IgLON expression in the mouse

The first species wherein extensive expression studies were undertaken was the mouse. The mouse was initially chosen as a well-suited organism to address the issue of developmental expression. Studies were subsequently extended in the adult mouse.

4.3.1 Developmental study of IgLON expression by whole-mount *in situ* hydridisations

One of the most suitable ways to study expression patterns of genes of interest is by *in situ* hybridisation. This technique is widely used to profile the expression of genes at the RNA level and is particularly suited for developmental studies. Developmental profiling is useful in two ways. Firstly, it provides evidence for whether a gene is developmentally regulated and hence is likely to play a role in normal development. Secondly, associations between expression of genes and specific developmental windows can suggest potential functions.

Whole-mount *in situ* hybridisation (WISH) can be used as a means to acquire developmental profiles when previous knowledge is limited and there is no particular tissue of interest. One can thus establish where and when genes are expressed by using one sample for each developmental time-point.

The technique of whole-mount *in situ* hybridisation was used in order to profile the expression of the four IgLON genes in mouse development. In brief, the work consisted of three stages: the generation of mouse IgLON-specific riboprobes, the collection of sufficient numbers of mouse embryos at different stages of development and the implementation of the *in situ* protocol.

In order to generate the mouse IgLON RNA probes, the individual mouse sequences were firstly identified by comparison to the respective human sequences. At the time, there were complete mouse coding sequences for *Hnt*, *Lsamp* and *Negr1*, but not for *Opcml*. For the latter, the sequence used was derived from two separate sequences (GenBank NM_177906.2 and XM_134679.2), which were merged to give the complete *Opcml* coding sequence. The criteria for selection of target regions consisted of a size restriction, aiming at targets of up to 1 kb, but most importantly target specificity. IgLON sequences are highly similar and also there are various potential alternative isoforms based on *in silico* evidence. These criteria had to be applied when designing the primers to amplify the targets regions, which would then be cloned in the appropriate expression vector. Hence, primer-annealing sites had to be unique for one particular IgLON, i.e. in areas of acceptable sequence divergence within the family, and representative of all potential isoforms, i.e. in areas where all these isoforms are identical. These criteria restricted the number of potential probes to only one probe per gene. The alignment of mouse IgLON coding sequences, highlighting the targets for probe design, is illustrated in Figure 4.5.

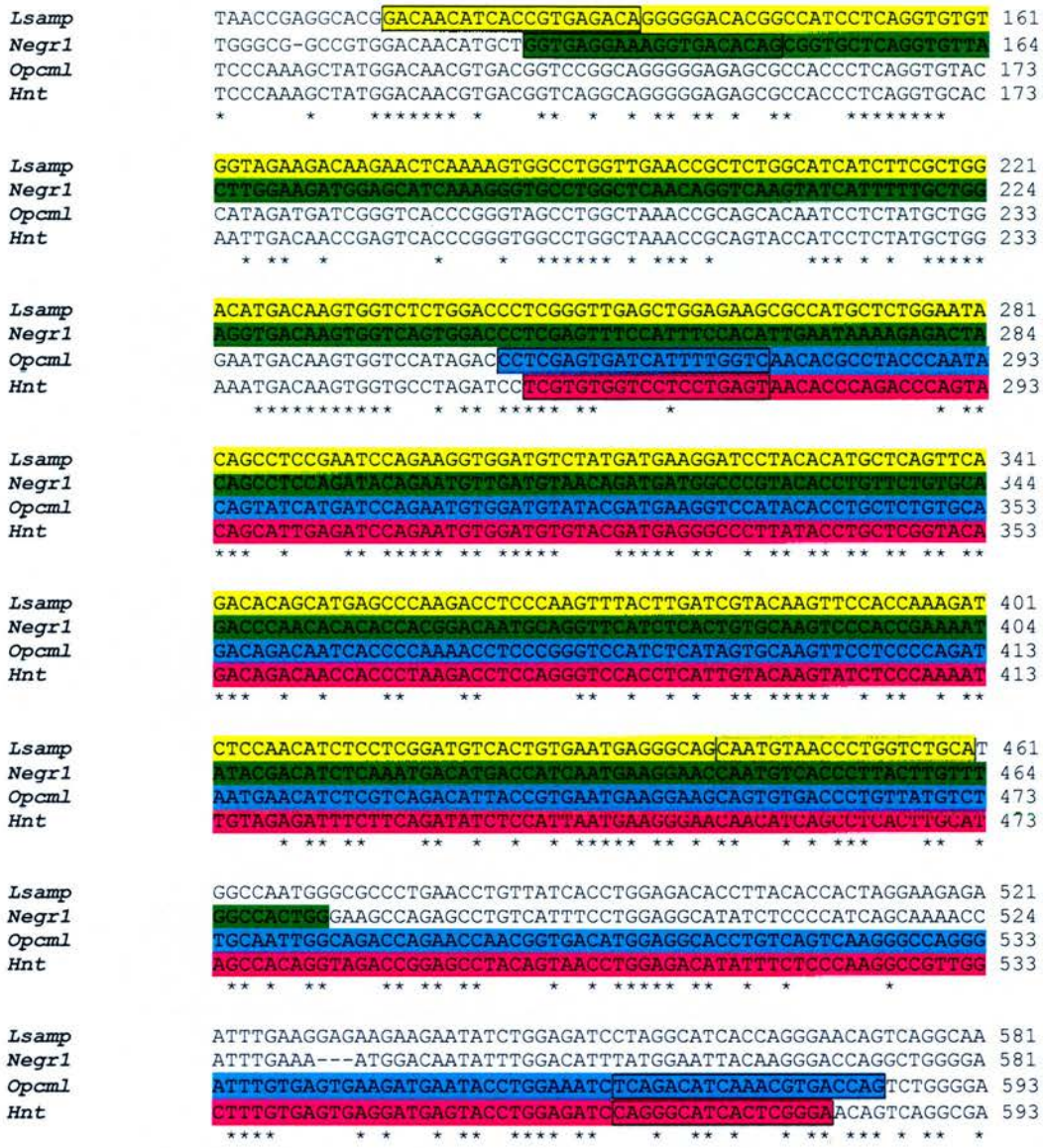

Figure 4.5 Target regions for mouse WISH probes
ClustalW multiple sequence alignment of partial mouse IgLON coding sequences. Highlighted sequences show selected target regions. Boxed sequences indicate primer-annealing sites. Asterisks denote identical nucleotides in all four sequences.

Once the target regions had been chosen, they were amplified from mouse brain cDNA using the specific primers. Brain was chosen, as this locality is where the IgLONs are prototypically expressed. The amplified targets can be seen in Figure 4.6.

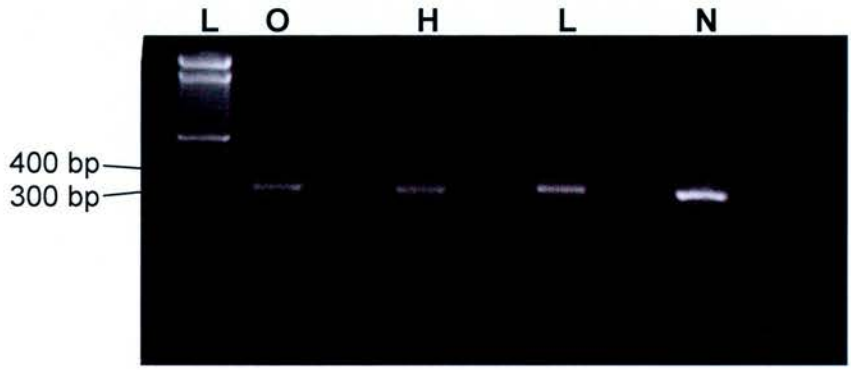

Figure 4.6 Mouse IgLON products for cloning in expression vector
Mouse cDNAs for cloning in expression vector for generation of IgLON riboprobes. The targets regions were amplified from mouse brain cDNA and the PCR products run on a 2% (w/v) agarose gel stained with EtBr.
L = 100 bp DNA ladder; O = *Opcml*; H = *Hnt*; L = *Lsamp*; N = *Negr1*.

The above sequences were cloned into pGEM-T easy, which is both a basic cloning as well as an expression vector, containing the appropriate promoters (Appendix C). DIG-labelled riboprobes were generated in antisense and sense orientations, the latter to serve as negative controls.

Various WISH protocols were attempted. However, none of the generated riboprobes was successful (data not shown). There was no signal with any of the probes tested in any developmental stage. In contrast, two probes used as positive controls worked as expected (Figure 4.7). These probes recognised their respective transcripts, namely *Shh* and *Fgf8*, revealing the involvement of these two genes in limb bud development.

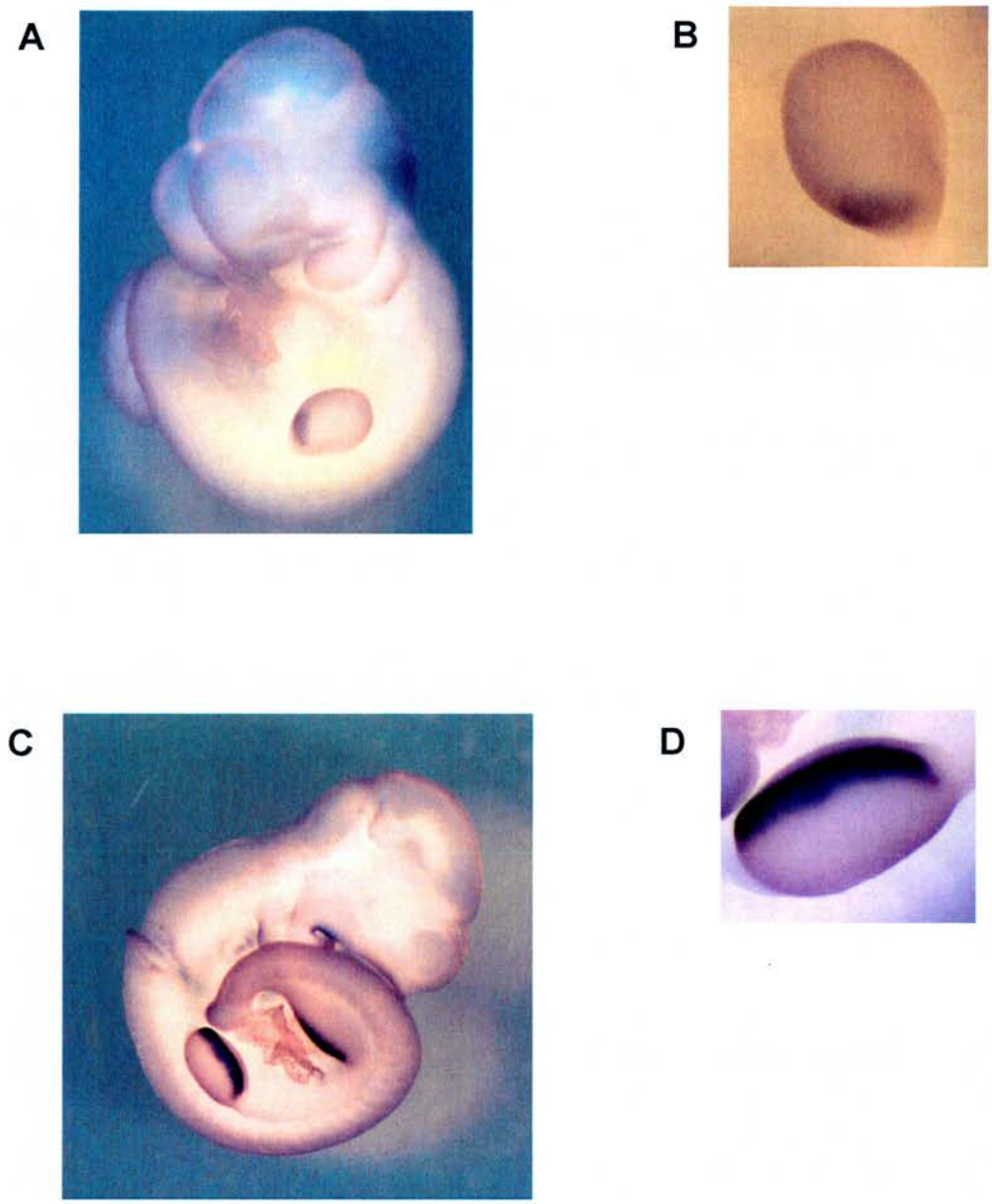

Figure 4.7 Staining of mouse embryos with the control probes
E10.5 mouse embryos stained with positive control riboprobes by WISH. Images taken after 1 h of signal development. Staining with the *Shh* antisense probe (A,B) and the *Fgf8* antisense probe (C,D); details showing limb bud signal (B,D).

4.3.2 IgLON expression in multiple-tissue cDNA panels

In order to examine the expression of the IgLON family in the mouse at the RNA level, panels of cDNAs from multiple adult tissues, as well as embryonic stages, were used. As can be seen in Figure 4.8, *Opcml* was strongly expressed in the

brain and testis; its expression level varied in the rest of the tissues, being undetectable only in the lymph node, the liver and the kidney. *Hnt* was strongly expressed in the eye, the uterus and the brain and to a varying degree in all other tissues apart from smooth muscle. *Lsamp* was detected strongly in the eye, the prostate, the uterus and the brain, with again varying expression across the rest of the panel and negative expression in the bone marrow and the spleen. *Negr1* exhibited strong expression in the brain, and varying levels of expression elsewhere except in the placenta and the spleen where no expression was detected. Notably, all the IgLONs seemed to be developmentally regulated, with expression levels that increased with embryonic age. This trend was particularly pronounced for *Opcml* and *Negr1*. Moreover, although at E7 there was hardly any *Opcml* or *Negr1* expression, *Hnt* and *Lsamp* were visibly expressed.

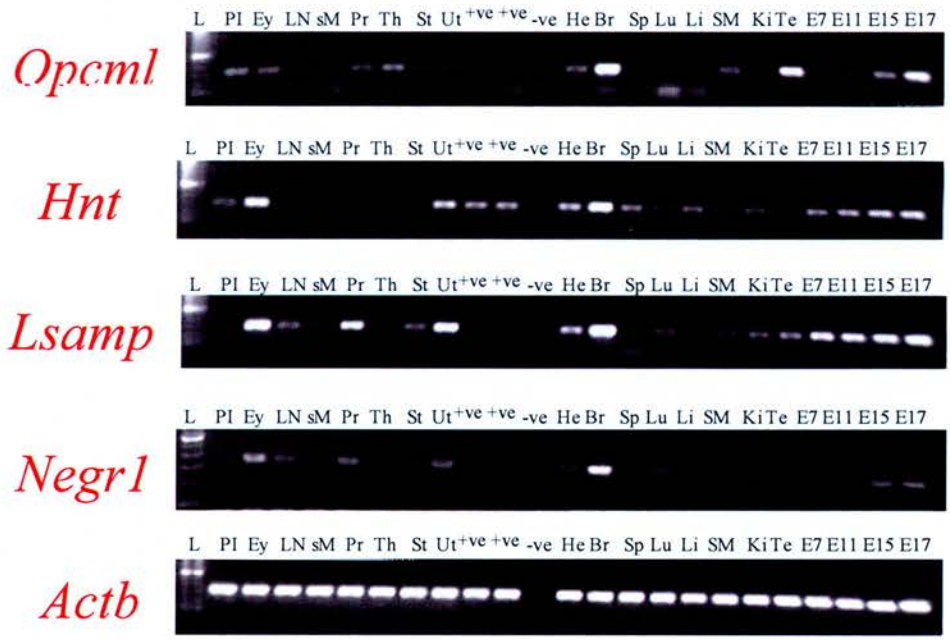

Figure 4.8 Mouse IgLON expression in multiple-tissue panels
Expression of the four IgLONs in multiple-tissue mouse cDNA panels by RT-PCR. L = 100 bp DNA ladder; Actb = beta actin; Pl = placenta; Ey = eye; LN = lymph node; sM = smooth muscle; Pr = prostate; Th = thymus; St = stomach; Ut = uterus; He = heart; Br = brain; Sp = spleen; Lu = lung; Li = liver; SM = skeletal muscle; Ki = kidney; Te = testis; E7-11 = embryonic days 7 to 11; +ve = panels' positive controls; -ve = PCR contamination control.

4.3.3 Expression of *Opcml* in embryo sections

As the attempt to establish the expression patterns of the IgLON family in mouse development by WISH was not fruitful, the issue of developmental expression was addressed by an immunohistochemical approach. More specifically, this was restricted to the study of *Opcml* only, due to antibody availability limitations.

The expression of *Opcml* was examined in the developing mouse embryo, from the age of E11 to E17. Staining in these embryo sections can be seen in Figure 4.9. As can be seen, *Opcml* expression was very low at E11 and increased gradually until E17. Various tissues were positive for *Opcml* staining, including: parts of the brain, muscle, heart, liver, skin, and epithelia of the intestine and kidney.

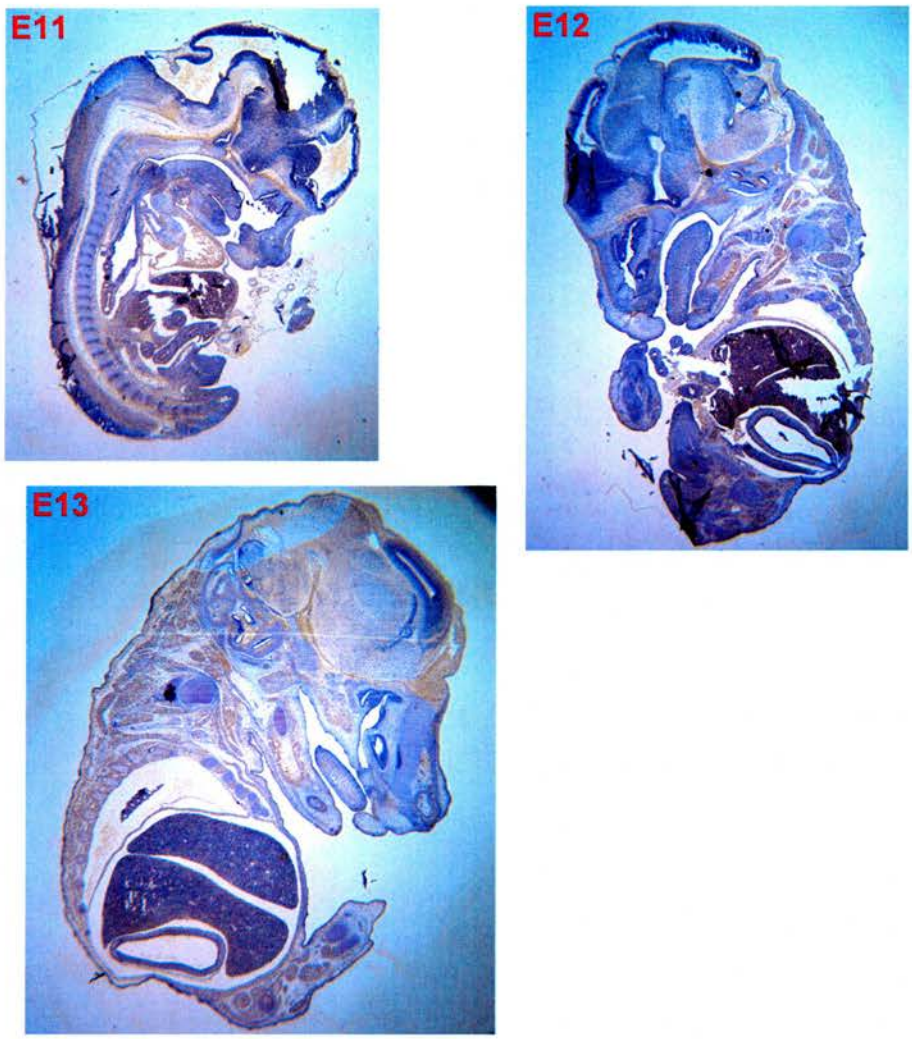

Figure 4.9i *Opcml* expression in mouse development
Staining of mouse embryo sections for *Opcml* expression by immunohistochemistry. Antibody controls were negative (data not shown). Images are at 1.6x magnification and have the same aspect ratio.

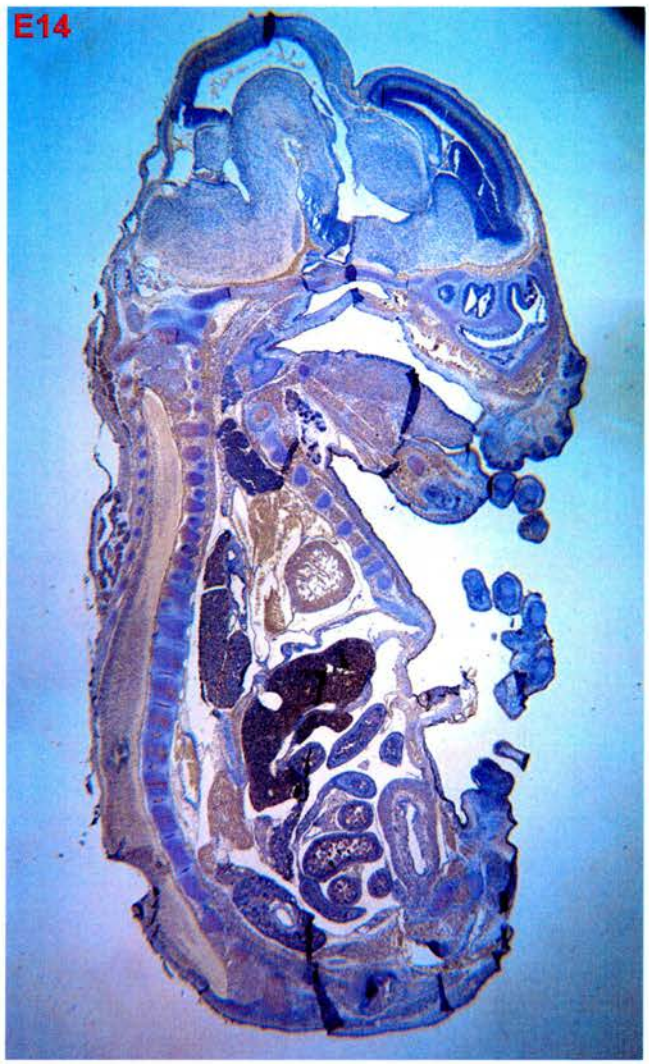

Figure 4.9ii *Opcml* expression in mouse development (continued)
Staining of mouse embryo sections for *Opcml* expression by immunohistochemistry. Antibody controls were negative (data not shown). Images are at 1.6x magnification and have the same aspect ratio.

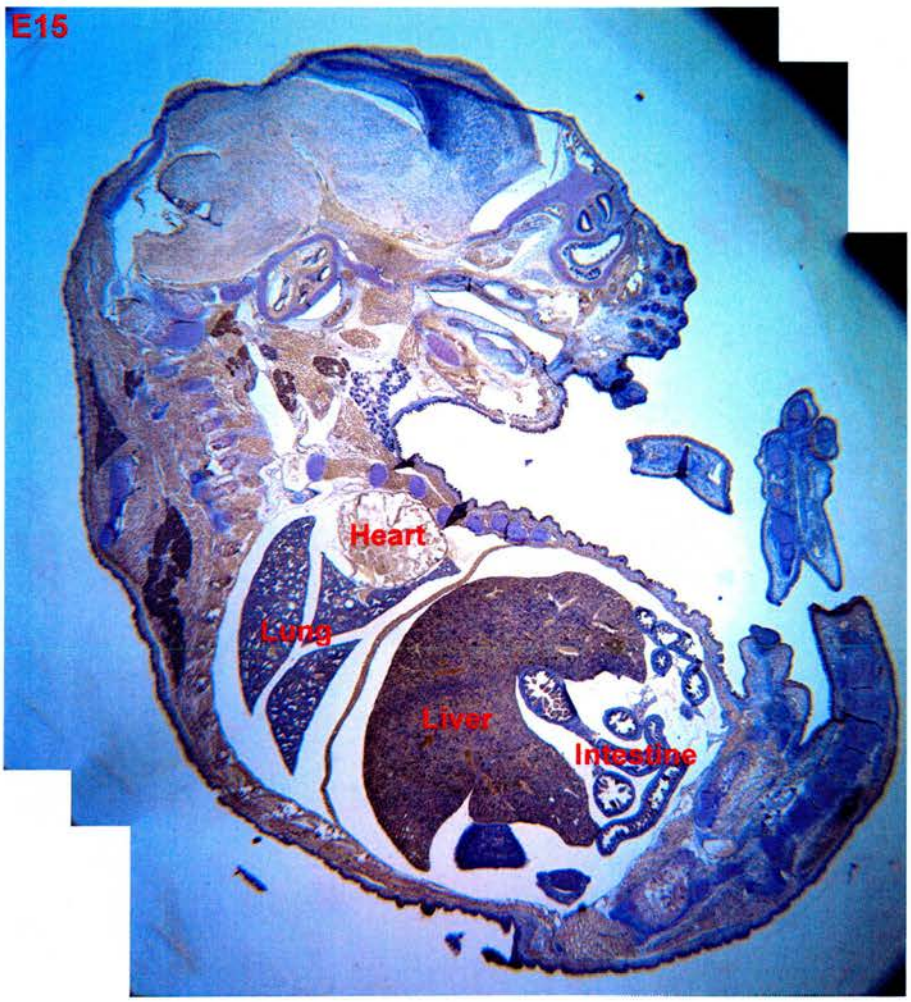

Figure 4.9iii *Opcml* expression in mouse development (continued)
Staining of mouse embryo sections for *Opcml* expression by immunohistochemistry. Antibody controls were negative (data not shown). Images are at 1.6x magnification and have the same aspect ratio.

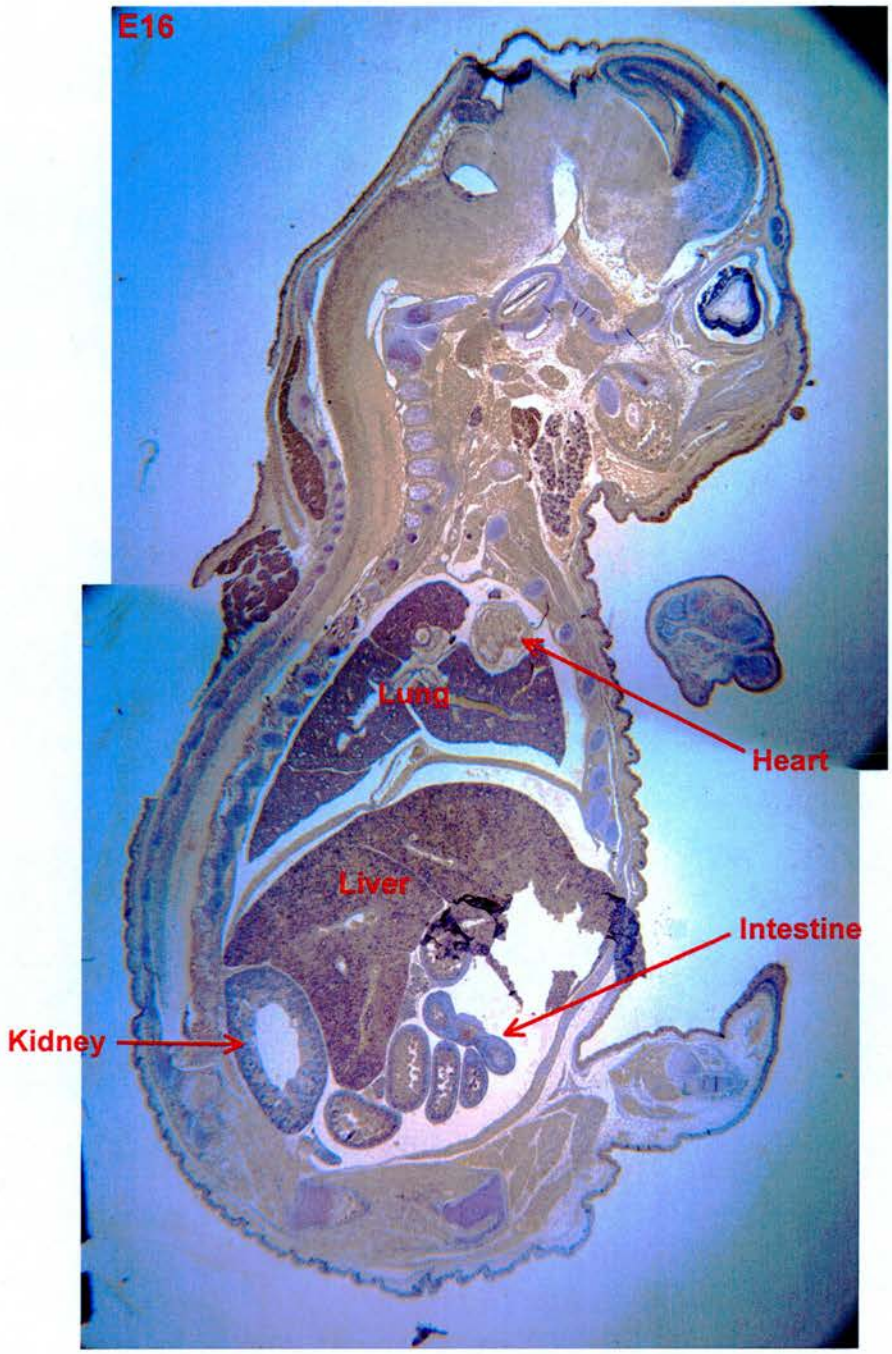

Figure 4.9iv *Opcml* expression in mouse development (continued)
Staining of mouse embryo sections for *Opcml* expression by immunohistochemistry. Antibody controls were negative (data not shown). Images are at 1.6x magnification and have the same aspect ratio.

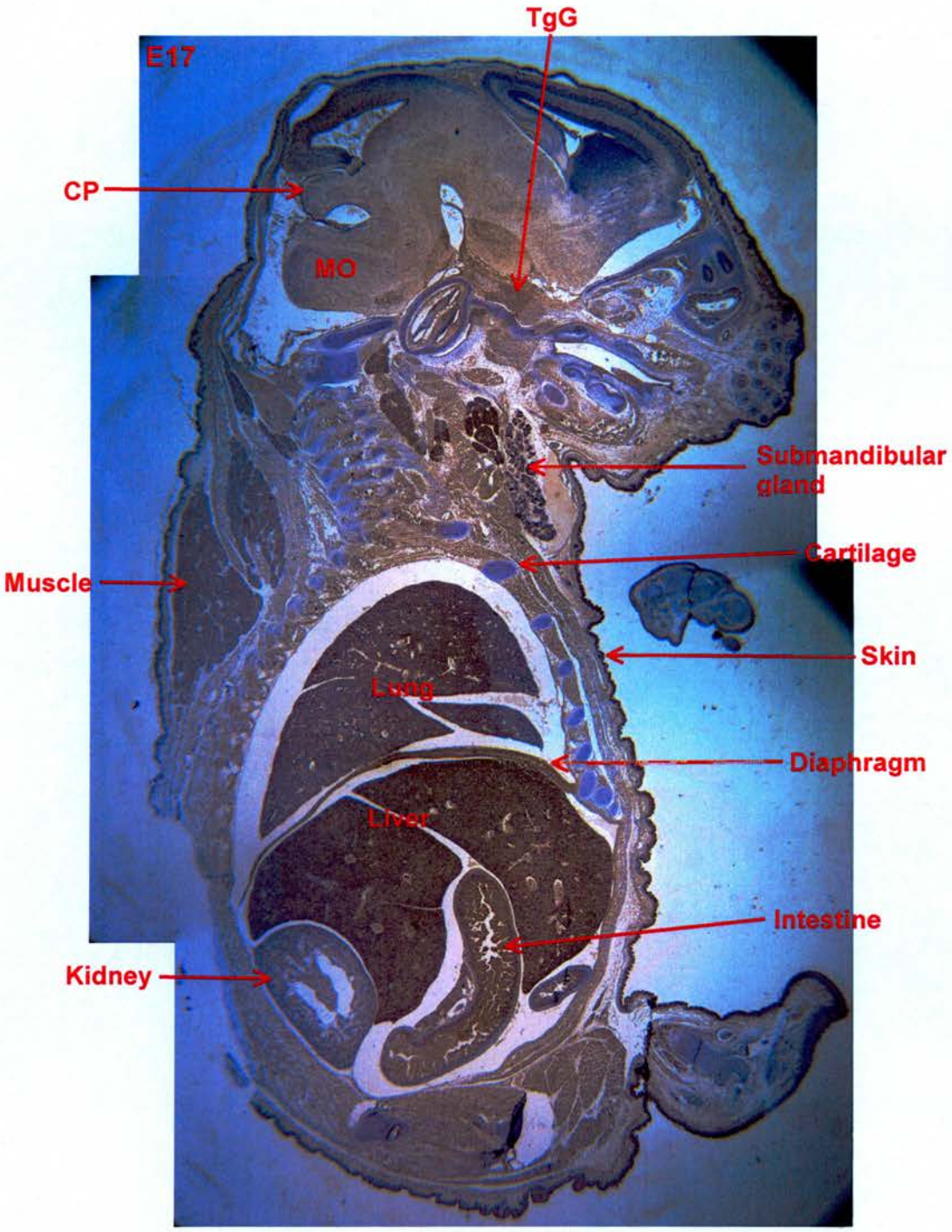

Figure 4.9v *Opcml* expression in mouse development (continued)
Staining of mouse embryo sections for *Opcml* expression by immunohistochemistry. Antibody control was negative (see Figure 4.9vi). Images are at 1.6x magnification and have the same aspect ratio. CP = cerebellar primordium; Mb = midbrain; Fb = forebrain; TgG = trigeminal ganglion; MO = medulla oblongata.

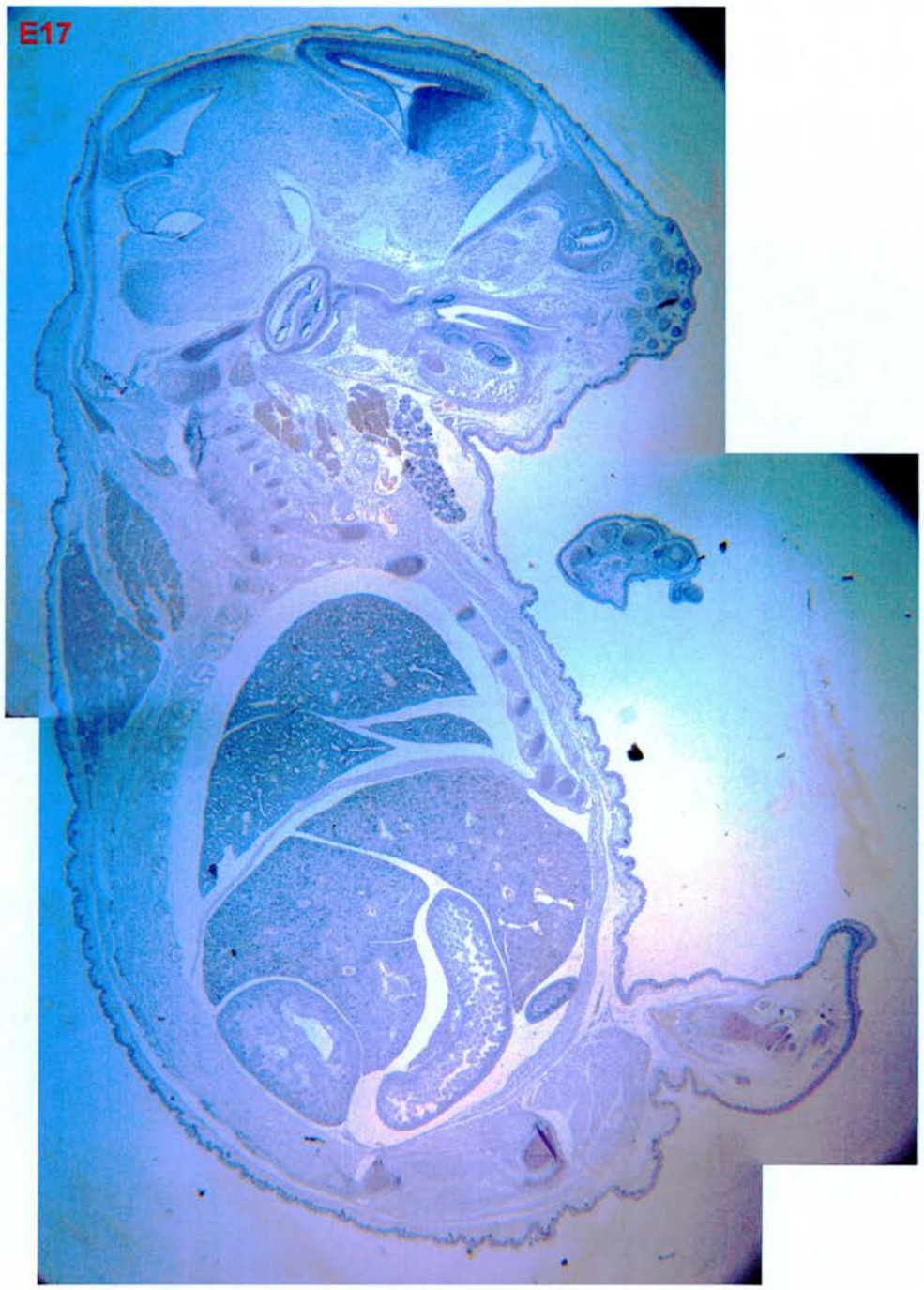

Figure 4.9vi *Opcml* expression in mouse development (continued)
Staining of mouse embryo sections for *Opcml* expression by immunohistochemistry: an example of negative antibody control staining. Images are at 1.6x magnification and have the same aspect ratio.

4.3.4 Expression of *Opcml* in tissue arrays

In order to complete the profiling of *Opcml* in the mouse, its expression was examined histologically in tissue arrays representing 26 different organs. The results are summarised in Table 4.1 and shown in Figure 4.10.

Organ	Opcml expression
Bladder	Strong epithelial and moderate smooth muscle staining.
Bone marrow	Undefined staining.
Breast	Epithelial/myoepithelial staining in lobular structures.
Cerebral cortex	Diffuse staining.
Cerebellum	Diffuse staining throughout; strong in specific cell types, e.g. Purkinje cells.
Eye	Strong retinal staining in ganglion cell layer, of neuronal processes in outer and inner plexiform layers, of inner segments in photoreceptor layer and of pigment cells.
Fallopian tube	Strong epithelial and some weak stromal staining.
Heart	Staining of all main cardiac tissue types; might be unspecific (weaker antibody control staining).
Kidney	Staining in tube and duct structures; might be unspecific (weaker antibody control staining).
Large intestine	Strong epithelial staining in villi and crypts. Moderate staining in muscularis mucosa.
Liver	Strong staining of outermost epithelium.
Lymph node	Staining of undefined cell populations.
Lung	Moderate staining around bronchial/alveolar structures.
Muscle	Staining throughout.
Ovary	Staining in follicular and derivative structures. Undetermined OSE staining due to "edge effects".
Pituitary	Staining throughout.
Spinal cord	Staining in grey matter, probably of central horns.
Skin	Staining of epidermis only.
Spleen	Staining in red pulp mostly.
Stomach	Staining in glands, i.e. of mucous and peptic cells.
Thyroid	Staining of undefined cell populations.
Uterus	Negative.

Table 4.1 *Opcml* expression in a mouse tissue array: data synopsis
Notes on the staining of a mouse normal tissue array for *Opcml* expression by immunohistochemistry. Tissues with definite unspecific staining are excluded.

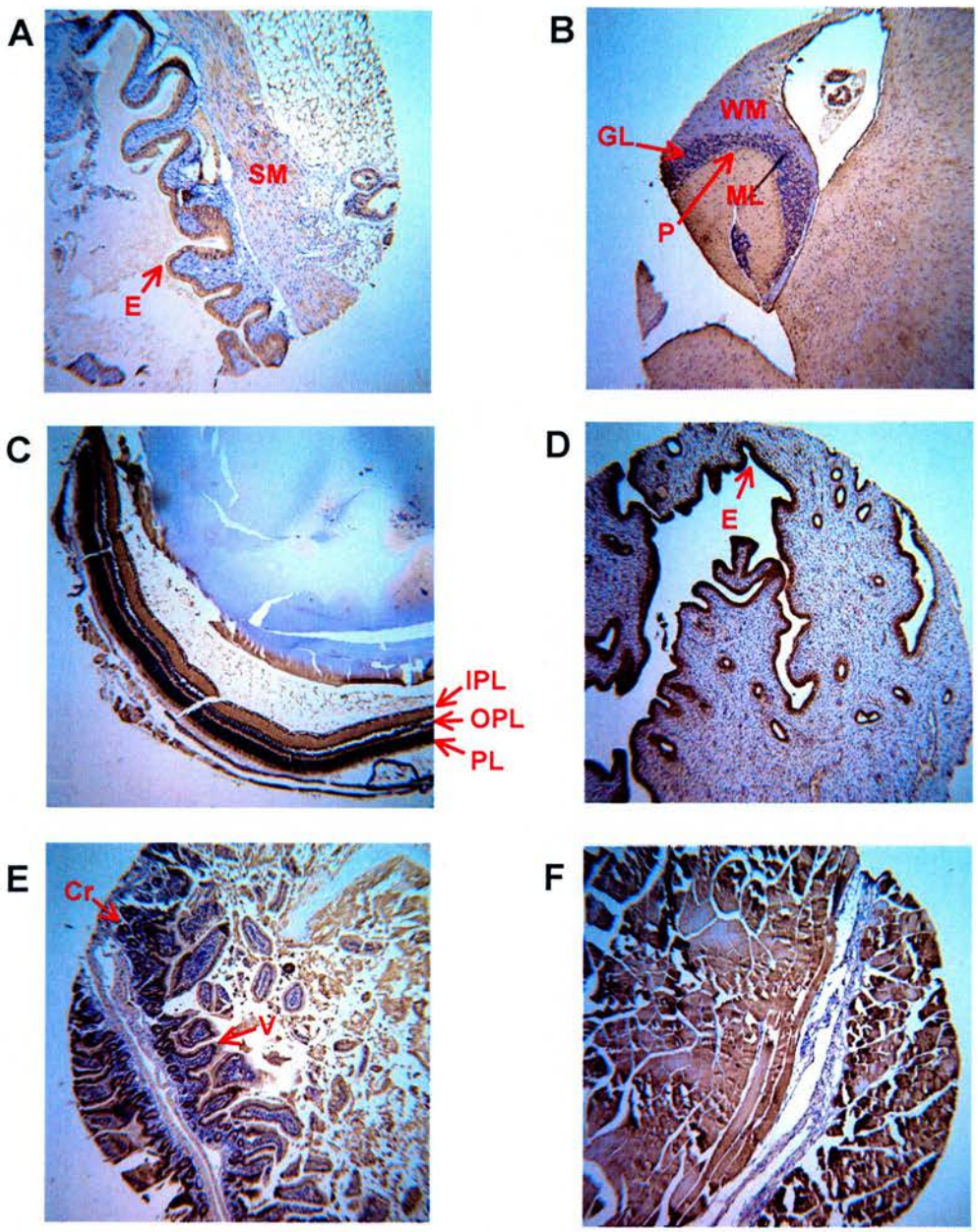

Figure 4.10i *Opcml* expression in a mouse tissue array
Examples of positive specific staining of a mouse normal tissue array for *Opcml* expression by immunohistochemistry. Antibody controls were negative (see examples in Figure 4.10iii). All images are at 10x magnification. Bladder (A); cerebellum (B); eye (C); fallopian tube (D); large intestine (E); muscle (F).
E = epithelium; SM = smooth muscle; WM = white matter; GL = granular layer; ML = molecular layer; P = Purkinje cells; OPL = outer plexiform layer; IPL = inner plaxiform layer; PL = photoreceptor layer; Cr = crypt; V = villus.

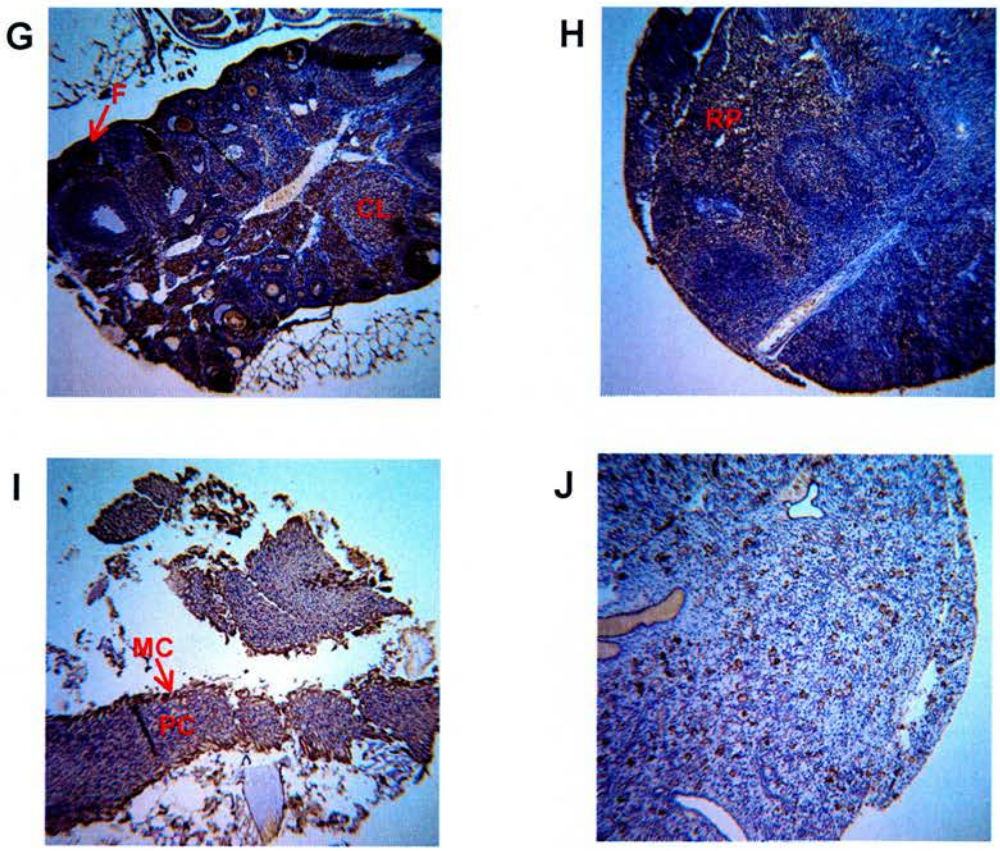

Figure 4.10ii *Opcml* expression in a mouse tissue array (continued)
Examples of positive staining of a mouse normal tissue array for *Opcml* expression by immunohistochemistry. Antibody controls were negative (see example in Figure 4.10iii). All images are at 10x magnification. Ovary (G); spleen (H); stomach (I); thyroid (J).
F = follicle; CL = corpus luteum; RP = red pulp; MC = mucous cells; PC = peptic cells.

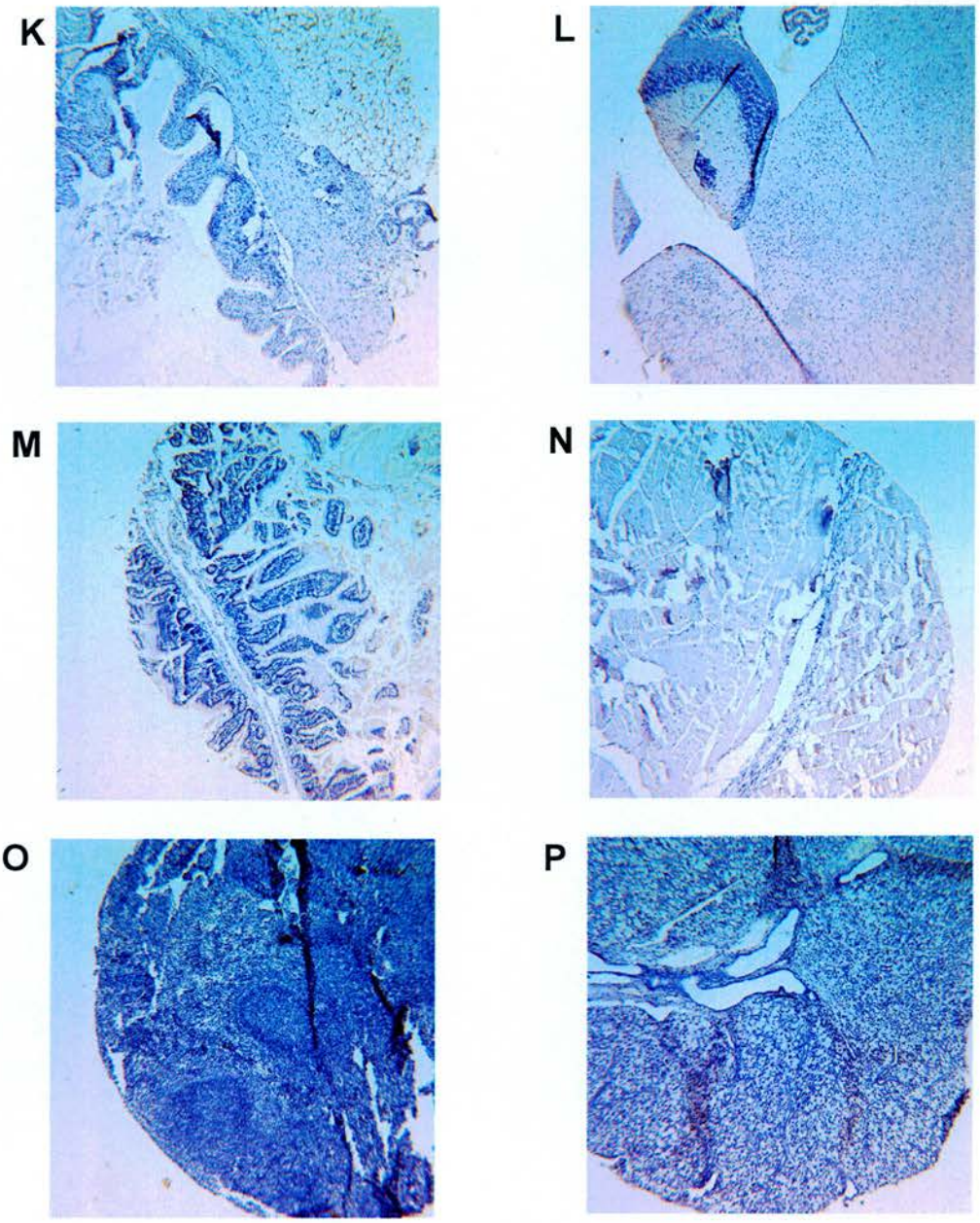

Figure 4.10iii *Opcml* expression in a mouse tissue array (continued)
Examples of negative antibody controls in the mouse normal tissue array. All images are at 10x magnification. Bladder (K); cerebellum (L); large intestine (M); muscle (N); spleen (O); thyroid (P).

4.4 IgLON expression in the human

The second species wherein the issue of IgLON expression was addressed is the human. With *OPCML* being a putative TSG in epithelial ovarian cancer, particular attention was paid to the expression of *OPCML* and its relatives in EOC as well as the normal ovary.

4.4.1 IgLON RNA expression in epithelial ovarian cancer

Expression of *OPCML* is reported to be reduced in sporadic EOC[21]. Another IgLON, *LSAMP*, has been reported to exhibit reduced expression in another type of cancer, namely clear cell renal cell carcinoma[43]. Moreover, the IgLONs are thought to participate in heterophilic interactions[57]. All these clues prompted for an examination of the IgLON family as a whole in sporadic epithelial ovarian cancer so as to judge whether family members other than *OPCML* are relevant. Thus, a study was undertaken to examine the expression of the four IgLONs in a well-characterised panel of 11 normal human ovaries and 57 EOC samples (Appendix D)[272]. The details of the panel can be seen in Table 4.2.

Description	*n*
All samples	68
Normal	11
Tumours	57
Serous	29
Clear Cell	12
Mucinous	4
Endometrioid	8
Mixed	1
Unclassified	3
Median age at diagnosis (years)	64
FIGO Stage	
I	8
II	4
III	37
IV	8
Grade	
1	2
2	11
3	41
Median survival (years)	2.25

Table 4.2 The panel of normal ovaries and EOC samples
Details of the panel used in the expression study of the IgLON family in EOC.
FIGO = *Fédération Internationale de Gynécologie et d'Obstétrique*.

In order to evaluate the RNA expression levels of the four IgLON family members in the panel, a real-time qRT-PCR approach was followed. *OPCML*, *LSAMP* and *NEGR1* exhibited reduced expression in the majority of tumour samples as compared with the normal ovaries (Figure 4.11). In contrast, tumour samples had elevated *HNT* expression in relation to the normal ones. The distribution of data for all four genes was not normal, hence non-parametric approaches were chosen for all subsequent statistical analyses.

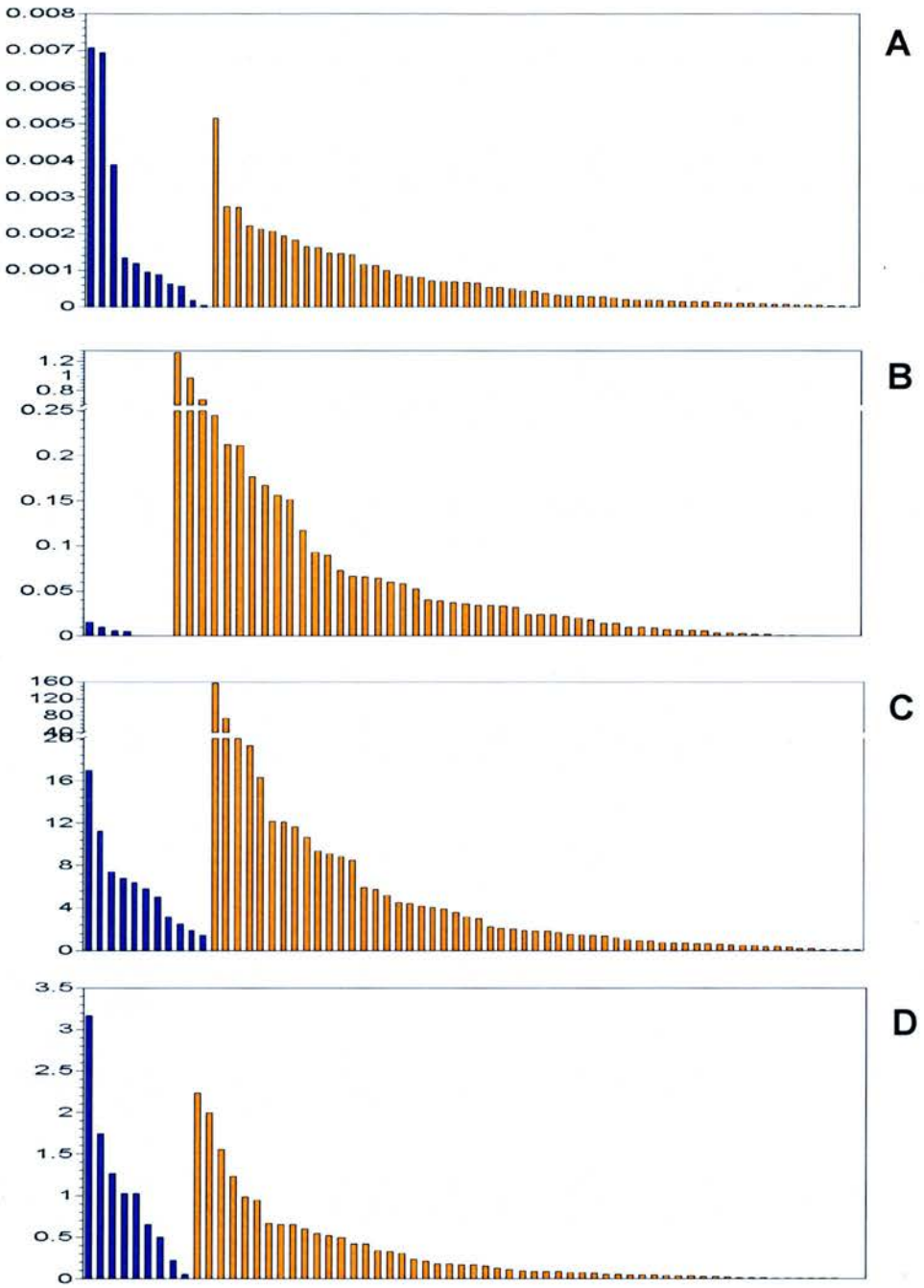

Figure 4.11 IgLON RNA expression in EOC and normal ovary samples
RNA expression levels of *OPCML* (A), *HNT* (B), *LSAMP* (C) and *NEGR1* (D) in the panel of EOC samples and normal ovaries as determined by qRT-PCR. IgLON expression in normal ovaries (blue) and ovarian tumour samples (orange) is shown relative to beta actin expression, in decreasing order. DNA and PCR contamination controls were negative (data not shown).

Upon observing graphs illustrating the median values of the four genes in the EOC samples collectively and the normal ovaries, the aforementioned trends become clearer (Figure 4.12). There was a 2.5-fold decrease in *OPCML* RNA levels in the EOC samples as compared to the normal ovaries (not significant). *LSAMP* expression was reduced by 3-fold ($p = 0.038$) and *NEGR1* expression by 11-fold ($p = 0.022$). *HNT* was found to exhibit an 11-fold increase ($p = 0.011$).

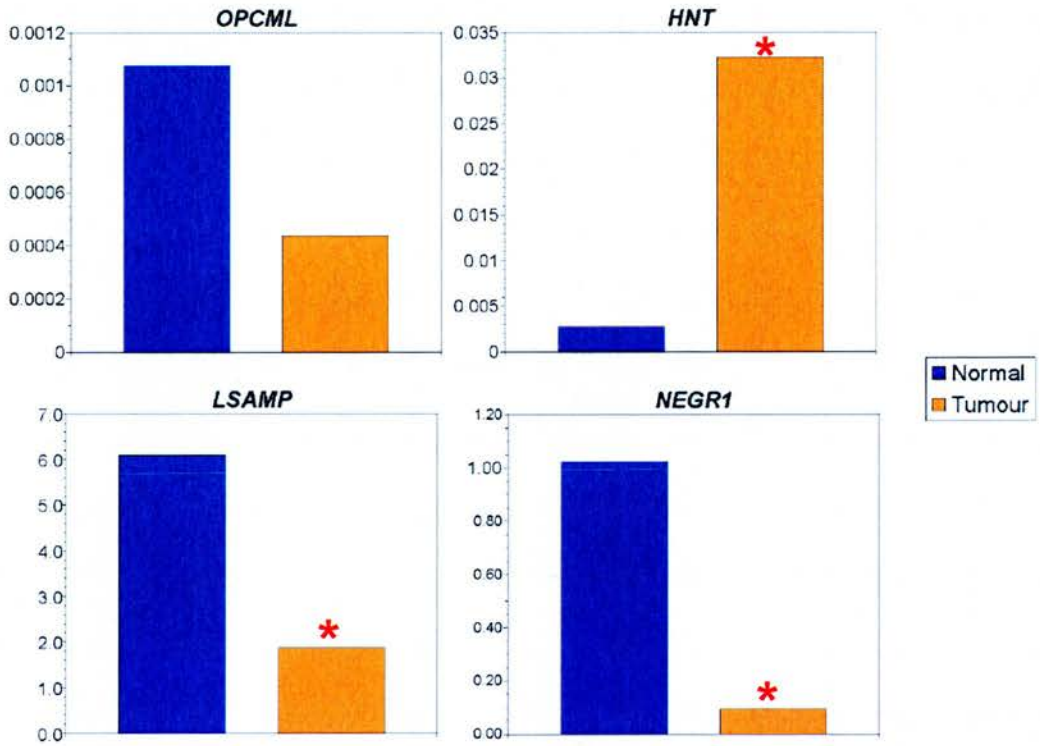

Figure 4.12 IgLON RNA levels in EOC and the normal ovary
Median expression levels of the IgLONs in the EOC samples collectively *versus* normal ovaries. The y-axis denotes expression relative to beta actin.
* $p < 0.05$ as compared by Mann-Whitney test.

Observing the expression data more closely, there were statistically significant differences between normal ovaries and tumour histological subgroups for all four IgLONs (Figure 4.13). More specifically, *OPCML* expression was significantly reduced in clear cell carcinomas ($p = 0.039$); *LSAMP* expression was reduced in endometrioid tumours ($p = 0.012$); and *NEGR1* expression was decreased in serous ($p = 0.014$), clear cell ($p = 0.009$) and endometrioid ($p = 0.001$) tumours. On the contrary, *HNT* expression was increased in serous carcinomas with respect to normal ovaries ($p = 0.008$).

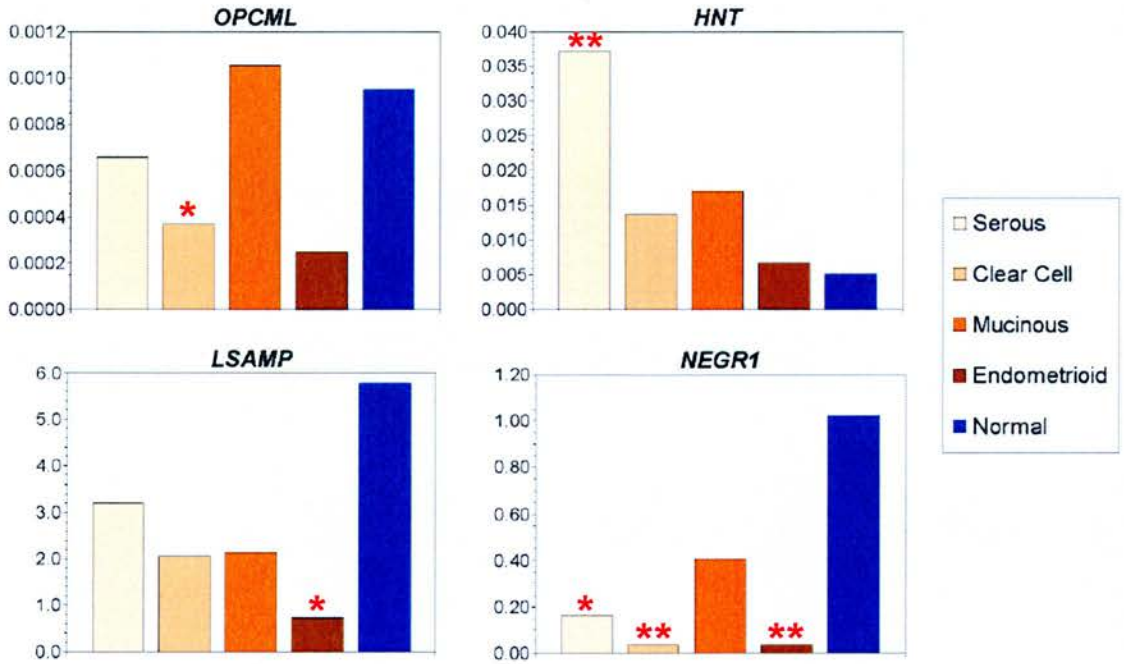

Figure 4.13 IgLON RNA levels in EOC according to histology
Median expression levels of the IgLONs in EOC histological subtypes *versus* normal ovaries. The y-axis denotes expression relative to beta actin.
* $p < 0.05$, ** $p < 0.01$ compared to normal ovaries by Mann-Whitney test.

Does expression of one IgLON influence that of the others in the panel? To address this question, potential correlations were tested non-parametrically. The strongest correlation found was a positive correlation between the expressions of *LSAMP* and *NEGR1* ($r_s = 0.55, p < 0.001$).

In addition, IgLON expression was tested for associations with clinicopathologic variables. Firstly, to establish whether IgLON expression was a function of age in the panel, the expression of each gene was tested for correlation with age as a continuous variable. However, significant correlations were not found. With respect to the categorical variables, stage was not found to differentiate IgLON expression. Nonetheless, there was a statistically significant difference in *LSAMP* expression among tumours of different grades ($p = 0.035$). In fact, as can be seen in Figure 4.14, this difference was even more significant when comparing grade 3 tumours (i.e. poorly-differentiated tumours) to the rest of the panel: poorly-differentiated carcinomas had lower levels of *LSAMP* than moderately- or well-differentiated ones ($p = 0.017$).

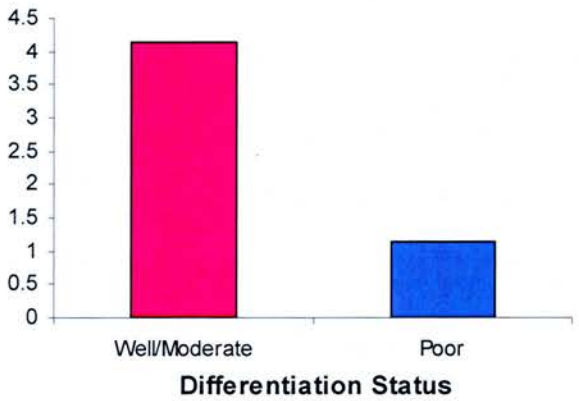

Figure 4.14 *LSAMP* expression according to differentiation status
Median expression levels of *LSAMP* in histological grade subgroups. The tumour group was divided into grade 3 samples (i.e. poorly differentiated tumours) and grades 1+2 samples (i.e. well- and moderately-differentiated tumours). The y-axis denotes expression relative to beta actin.

The effect of IgLON expression on the survival of patients was tested at two levels. Firstly, correlation between expression of each gene and overall survival was examined. This highlighted *LSAMP* as having a negative correlation (r_s = -0.30, p = 0.025). Secondly, patients were divided into high and low expressers for each gene, using the median values of the normal samples as cut-off points. Survival curves were plotted and the two groups compared (data not shown). However, statistically significant differences were not found for any of the four genes on this split.

In order to investigate whether the expression level of an IgLON gene can predict survival, the expression variables, as well as the clinicopathologic ones, were tested for prognostic value by Cox regression analysis. As can be seen in Table 4.3, in univariate analyses, *LSAMP* expression and stage were both found to be negative predictors of overall survival. Both variables were still found to be significant predictors of overall survival when tested together by multivariate analysis.

	Variable	Odds ratio	95% Confidence Interval		Significance
			Lower	Upper	
U	*OPCML*[1]	0.84	0.50	1.41	0.506
	HNT[1]	1.15	0.84	1.57	0.376
	LSAMP[1]	**1.63**	1.10	2.41	**0.015**
	NEGR1[1]	1.30	0.86	1.96	0.221
	Stage[2]	**8.86**	2.10	37.82	**0.003**
	Grade[3]	22.06	0.04	13126	0.343
M	*LSAMP*[1]	**1.85**	1.14	3.02	**0.013**
	Stage[2]	**10.21**	2.40	43.77	**0.002**

Table 4.3 Survival models
IgLON expression and clinicopathologic variables tested for prediction of overall survival in the panel by Cox regression analysis.
U = univariate; M = multivariate.
[1] Log-transformed.
[2] Early (i.e. stages I and II) *versus* late (i.e. stages III and IV).
[3] High (i.e. grade 3) *versus* rest (i.e. grades 1 and 2).

4.4.2 IgLON RNA expression in an OSE-enriched sample

As discussed in chapter 1, epithelial ovarian cancer arises in the single-cell layer overlying the ovary, the ovarian surface epithelium. The study undertaken to examine IgLON expression in the normal ovary and EOC was based on whole ovary samples, hence an issue that logically arose was at what levels IgLON expression is detected in OSE cells. One of the ways this issue can be addressed is by using an ovarian sample that is known to be representative of that cell population. Thus, IgLON RNA expression was examined in an OSE-enriched sample. The results are shown in Figure 4.15. In the OSE sample, *OPCML* and *LSAMP* exhibited approximately double the expression as compared to the median expression in the normal ovaries. *NEGR1* showed an even higher increase in the OSE sample, of approximately 9 times. In contrast, *HNT* expression is approximately 6 times lower in the OSE sample relative to the normal ovary median.

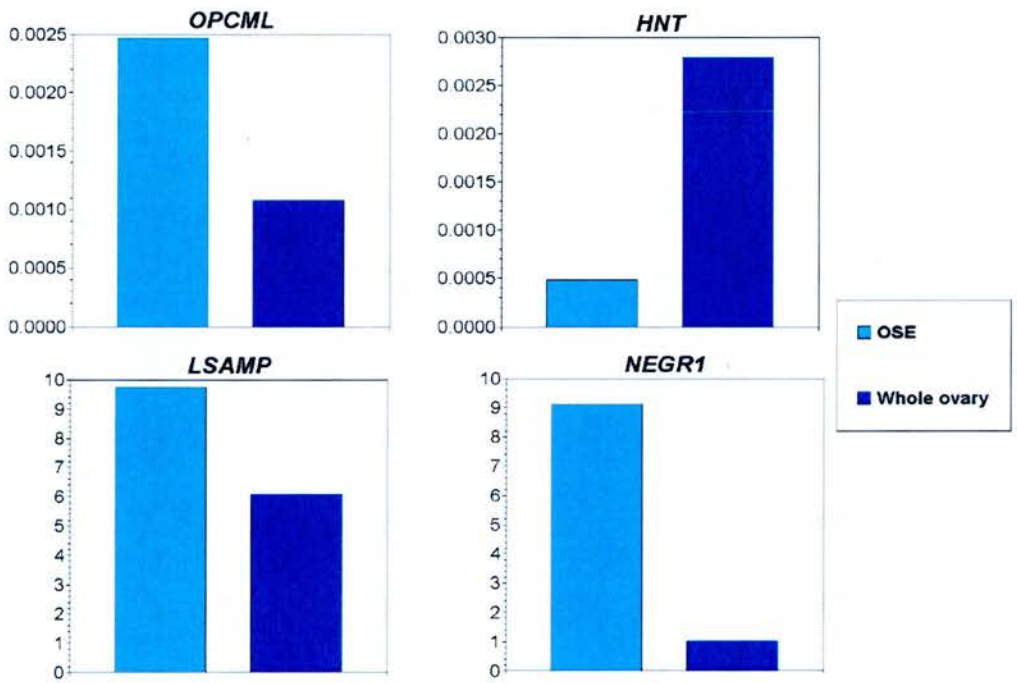

Figure 4.15 IgLON RNA expression in an OSE sample
Expression levels of the four IgLONs in an OSE-enriched sample as determined by qRT-PCR. Expression is shown relative to beta actin. DNA and PCR contamination controls were negative (data not shown). For comparison, the median relative expression in whole normal ovaries is also shown.

4.4.3 IgLON expression in multiple-tissue cDNA panels

As in the mouse, the expression of IgLON genes was investigated in panels representing various organs by RT-PCR. In the human, foetal panels were used in addition to adult ones.

Figure 4.16 shows the results for the foetal panel. As can be seen, expression of *OPCML* was detected mainly in the brain, but also the kidney and spleen. *HNT* was expressed mostly in the brain, the lung, the kidney and the heart, with minimal expression detected in the rest of the organs. *LSAMP* expression was very similar to that of *HNT*, whereas *NEGR1* was robustly expressed in all tissues apart from the liver and spleen where expression was minimal.

In the adult (Figure 4.17), *OPCML* expression was detected in the heart, the brain, the pancreas, the small intestine and the colon. *HNT* exhibited a very similar pattern. *LSAMP* was expressed in the heart, the brain, the pancreas, the prostate, the testis and the colon, with low expression in the ovary and the small intestine. Finally, *NEGR1* expression was only detected in the testis and colon. Although the two bands were apparently slightly different in size, this was probably a gel artefact, as sequencing did not indicate any differences (data not shown).

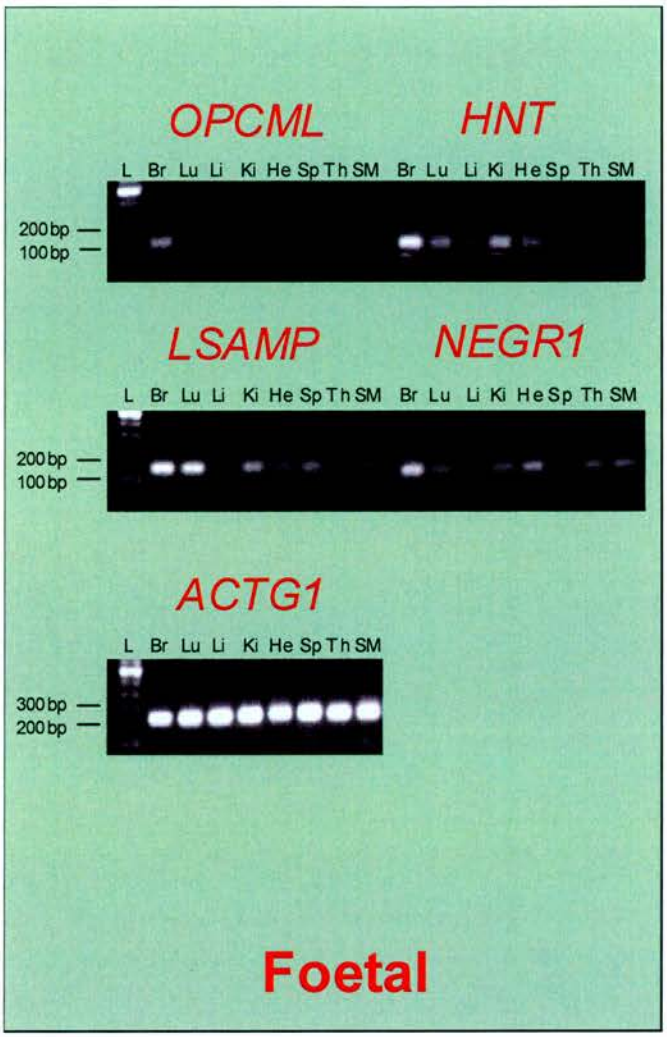

Figure 4.16 Human IgLON expression in a foetal multiple-tissue panel
Expression of the four IgLONs in a cDNA panel of foetal human tissues by RT-PCR. PCR controls were negative (data not shown).
L = 100 bp DNA ladder; *ACTG1* = gamma actin; Br = brain; Lu = lung; Li = liver; Ki = kidney; He = heart; Sp = spleen; Th = thymus; SM = skeletal muscle.

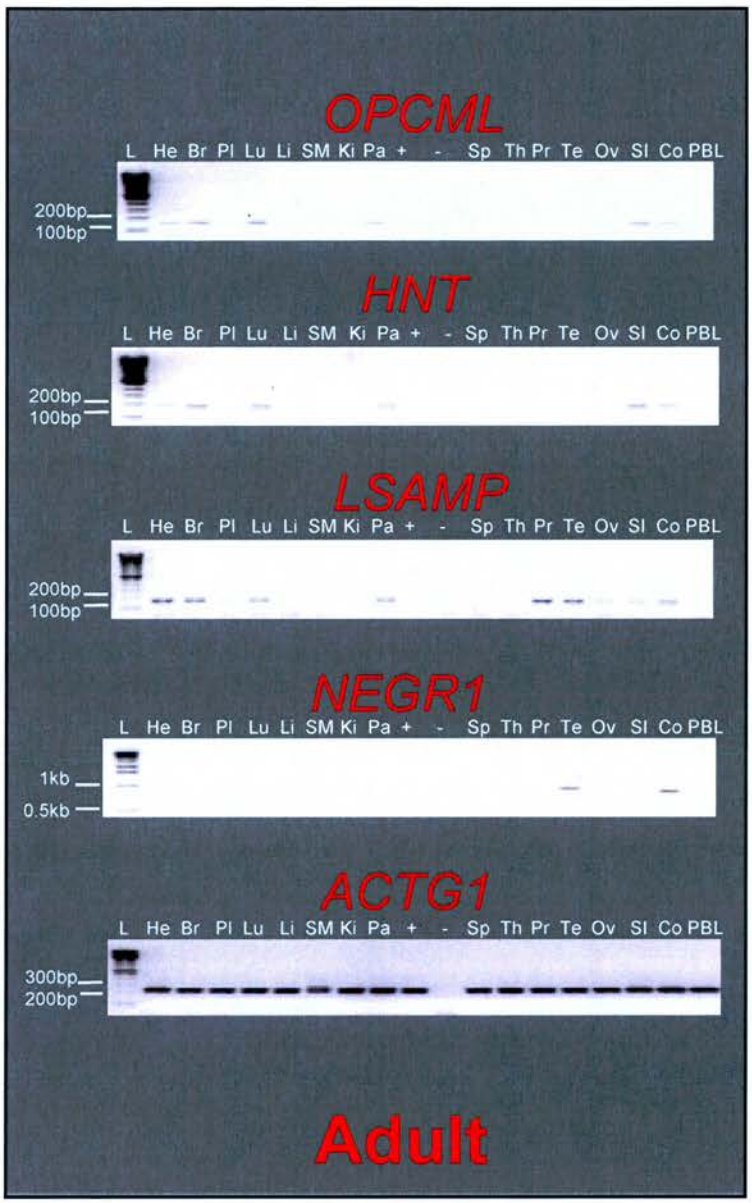

Figure 4.17 Human IgLON expression in an adult multiple-tissue panel
Expression of the four IgLONs in a cDNA panel of adult human tissues by RT-PCR. L = 100 bp DNA ladder; *ACTG1* = gamma actin; He = heart; Br = brain; Pl = placenta; Lu = lung; Li = liver; SM = skeletal muscle; Ki = kidney; Pa = pancreas; + = panel's positive control; - = PCR contamination control; Sp = spleen; Th = thymus; Pr = prostate; Te = testis; Ov = ovary; Sl = small intestine; Co = colon; PBL = peripheral blood lymphocyte.

4.4.4 Expression of *OPCML* in embryo sections

In the mouse, an extensive study of *OPCML* expression in development was undertaken. In the human, the same immunohistochemical approach was followed to a more limited extent. The staining patterns of three different human embryonic stages can bee seen in Figure 4.18. The staining by CS21 was not as strong as in the latest mouse stage. Some parts of the brain were positive, as well as the heart, the epithelial lining of the intestine and the liver.

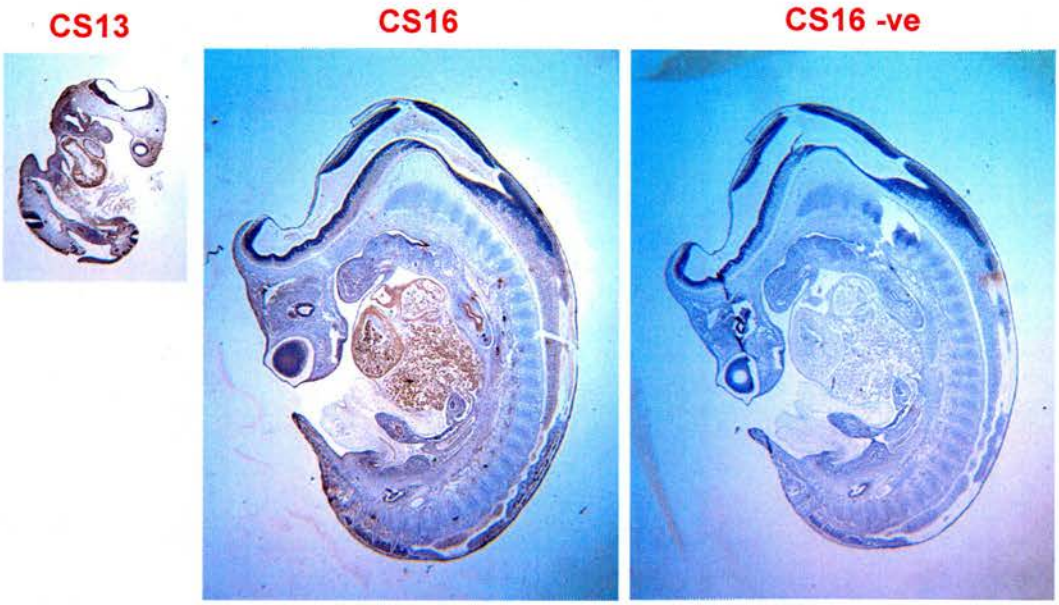

Figure 4.18i *OPCML* expression in human development
Staining of human embryo sections for *OPCML* expression by immunohistochemistry. Antibody controls were negative; one example shown. Images are at 1.6x magnification and have the same aspect ratio.
CS = Carnegie stage; -ve = antibody control.

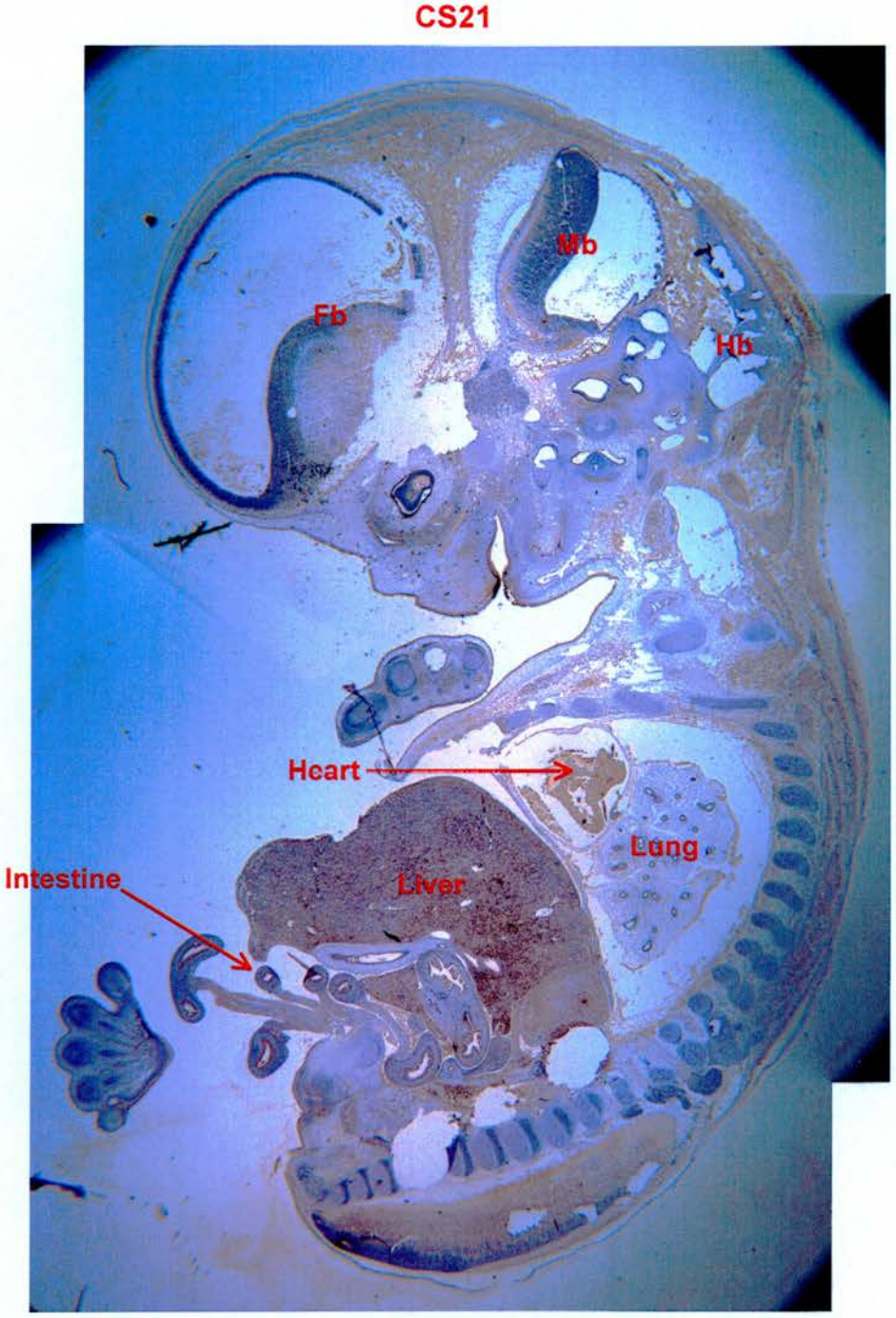

Figure 4.18ii *OPCML* expression in human development (continued)
Staining of human embryo sections for *OPCML* expression by immunohistochemistry. Antibody controls were negative (data not shown). Images are at 1.6x magnification and have the same aspect ratio.
CS = Carnegie stage; Fb = forebrain; Md = midbrain; Hb = hindbrain.

4.4.6 Expression of *OPCML* in normal ovary sections

Due to its potential role as a TSG in ovarian cancer, the expression of *OPCML* was also examined specifically in sections of human normal ovaries. As can be seen in Figure 4.19, *OPCML* was expressed in the ovarian surface epithelium, as well as the stroma. In the former, it was strongly expressed, whereas in the latter it was weakly expressed, apart from some undefined patches of strong staining.

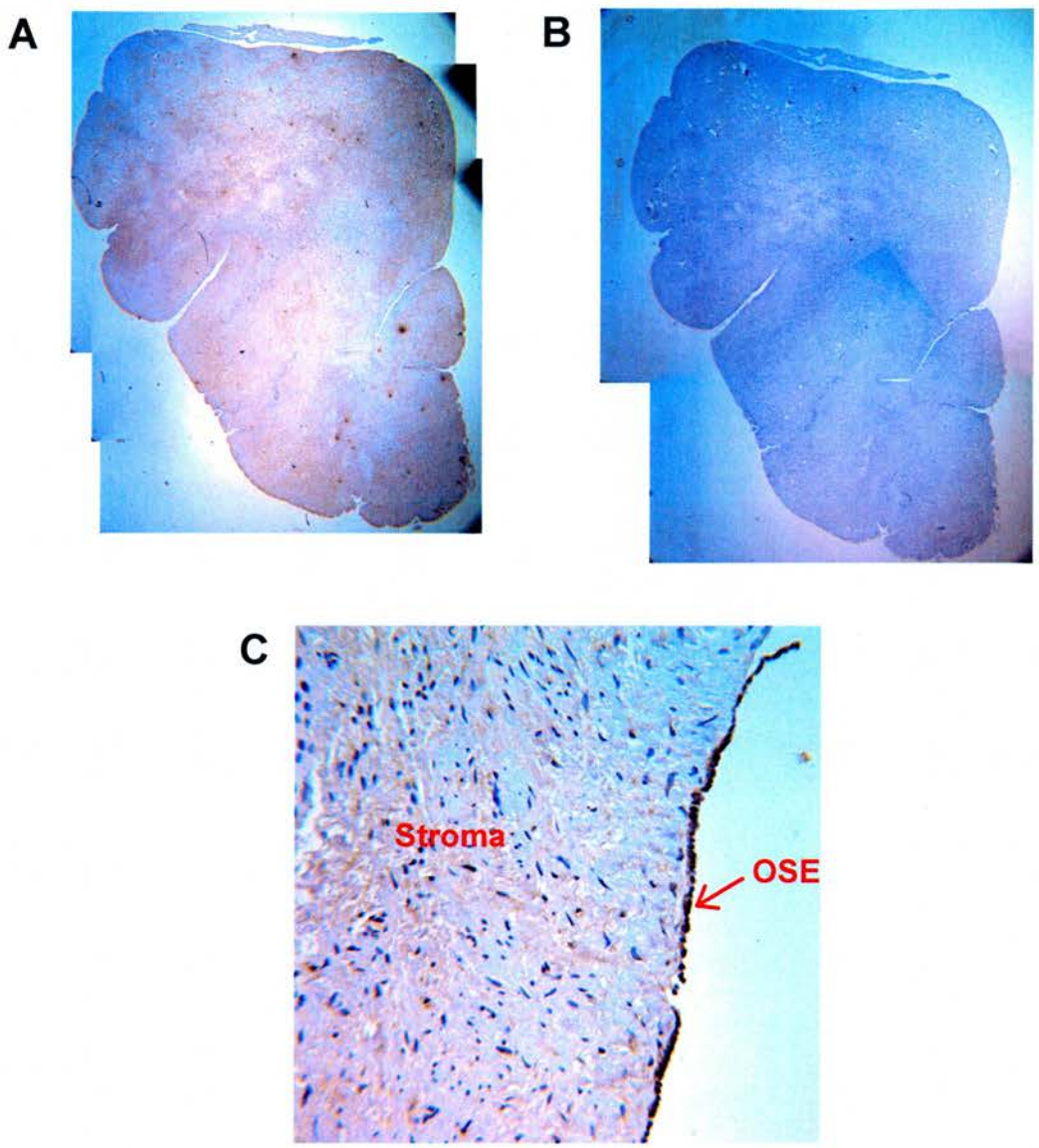

Figure 4.19 *OPCML* expression in the human ovary
Staining of human normal ovary sections for *OPCML* expression by immunohistochemistry. Whole ovary section, 1.6x (A) and its negative antibody control (B); detail showing epithelial staining, 40x (C).

4.5 Discussion

All the studies described in this chapter had a common aim: the acquisition of information regarding the patterns of expression of the IgLON family. By taking an approach that is multilateral and accommodates a variety of methods and levels of examination, a lot of useful knowledge has been gathered.

IgLON expression was firstly examined in human cancer cell lines. Information on cell line expression can often provide valuable hints on whether a gene might be subjected to expression alterations in cancer. A surprising finding was the fact that *OPCML* expression was not detectable in any of the examined cell lines by qRT-PCR. This partially disagrees with a previous report by Sellar and colleagues wherein, although most cell lines did not express *OPCML*, six did exhibit expression at varying levels[21], and these cell lines were represented in the panel used in this work. The experimental approach used in the original study was the same as in the present one, i.e. a qRT-PCR based method employing the same primer set. However, two factors differed: the real-time thermal cycler and the standard curve. As the expression of experimental samples is calculated against a standard curve, which derives from an over-expressing cell line or tissue, the choice of standard curve source sets a sensitivity threshold. This could be accentuated by the use of a different PCR machine. The qRT-PCR protocol has integral quality-assurance measures, for example the standard curve also serves a positive control; hence, the absence of *OPCML* expression in cell lines in the present study cannot be accounted for by PCR failure. Hence, the most likely explanation for the discrepancy between the two studies is related to sensitivity. There is also a possibility that the data from the present study are genuinely representative of cell line expression, despite being surprising. Preliminary protein data support the absence of OPCML in cell lines (E. Miller, personal communication). If the absence of *OPCML* expression were a true feature, it might be explained by the promoter methylation status of the cell lines, as it has been reported to be the case when *OPCML* is silenced, or it might actually be an effect incurred by cell culture *per se*. Another IgLON, namely *HNT*, was found to have a very restricted expression in the panel of cell lines. Only two cell lines, both of ovarian origin, were found to express *HNT*. On the other hand, the expression

levels of *LSAMP* and *NEGR1* were more variable across the panel. *LSAMP* was found to be strongly expressed in a minority of cell lines, whereas most of them had very low *LSAMP* expression. The establishment of the promoter methylation status in these cell lines will indicate if epigenetic silencing accounts for this low expression or absence thereof, as in renal carcinoma cell lines reported by Chen and colleagues[43]. Finally, the expression of *NEGR1* in the panel of cell lines could be grouped into high, low and absent, with particular samples exemplifying each of these groups.

When examining the expression of IgLONs in the two transfected cell line systems that were used in studies of OPCML function, it became evident that the SKOV-3 cell lines differ to the HeLa inducible one in the complement of IgLONs at the RNA level. SKOV-3 cells express *LSAMP* robustly and little *NEGR1*, in contrast to HeLa cells that have minimal *LSAMP* and high *NEGR1* expression. This might partially account for the phenotypic differences that will be presented in chapter 5. More interestingly, in the SKOV-3 cells, *OPCML* transfection was shown to have a striking effect on the expression of both *LSAMP* and *NEGR1* at the RNA level. When *OPCML* is expressed in SKOV-3 cells, it significantly reduces the expression of *LSAMP* and *NEGR1*. This effect would have to be corroborated at the protein level once IgLON antibodies are available and fully optimised. Nonetheless, the fact that the effect of *OPCML* on the expression of *LSAMP* and *NEGR1* was confirmed both in an independent SKOV-3 clone, but also in two alternative ovarian cancer cell lines, makes it likely to be significant. Not only does *OPCML* have an effect on *LSAMP* and *NEGR1*, which most likely is independent for each, but also there is a striking positive correlation between *LSAMP* and *NEGR1* RNA expression. The extent to which these relationships between IgLON expression levels are context-dependent remains to be clarified. This could be addressed using the same experimental approach but in cell lines of different origin. Overall, these findings are noteworthy in being the first reported trends of transcriptional coordination within the IgLON family.

One of the objectives of this work was to establish the expression of the IgLON family in development. This was initially attempted in the mouse by whole-mount *in situ* hybridisations. Unfortunately, this approach was not successful.

It is likely that the probes that were used were not optimal, since the protocol *per se* worked when used with two positive control probes. The limb bud-specific signal that was acquired using these two control probes is in agreement with published data[273,274]. The IgLON probes used were unique, as they had to account for issues of IgLON homology and potential isoforms; the design of alternative probes would be very difficult. Hence, the issue of developmental expression was tackled by IHC. Due to the fact that within the available time-frame only the anti-OPCML antibody had been fully optimised for use in histology, the expression of only this IgLON was examined. *Opcml* expression was found to be minimal in the first embryonic age examined, E11, and was found to rise with age. Indeed, by E17, *Opcml* was expressed in most of the tissues that is shown to be expressed in adult life. This developmental activation of *Opcml* was also evident at the RNA level, as was the case for *Negr1* as well, in agreement with reported evidence of IgLON expression increasing with age in development[22,54]. By E17, OPCML was found to localise in a variety of tissues, and it was only completely absent in bone and cartilage.

In the adult mouse, OPCML was histologically detected in three broad groups: nervous tissue, epithelial cell populations and muscle. At the RNA level, the IgLON genes were detected in a variety of different organs, with high expressions in the brain and eye.

In the human, the overall picture is quite similar. It was evident that by Carnegie stage 21 (embryonic day 54), *OPCML* has not reached its peak of expression. This in not surprising given that this stage of human development corresponds to mouse embryonic day 15, which is earlier relative to the latest mouse stage examined, i.e. embryonic day 17. Hence, it is likely that the expression of *OPCML* will be rising after CS21 to reach its peak at a subsequent stage of embryonic/foetal developmental or even early adult life. At the RNA level, the rest of the IgLONs are expressed again in variety of foetal and adult tissues. Paradoxically, *NEGR1* was only detected in the colon and testis in the adult human. This is likely to be due to a PCR or cDNA problem rather than being a genuine result, as it would be very unconventional for *NEGR1*, being an IgLON, not to be expressed in the adult brain.

Overall, both in the mouse and human the IgLON genes demonstrate quite similar patterns of expression, suggesting that more often than not, the individual genes are co-expressed at the organ level. There are however examples of divergence, such as in the mouse liver and placenta, and in the human prostate and testis, indicating that even though overall similar, IgLON expression patterns can also be distinct. This notion does not take into account the sub-organ localisation. At the level of particular cell types the IgLONs might exhibit more distinct expression patterns. Confirmation of this would require the histological examination of the other members of the family. In addition, expression in mouse and human was found to be generally conserved. Again, some exceptions were recorded, such as in the kidney, muscle, prostate and testis. These exceptions are in agreement with the postulation that one of the IgLONs, *HNT*, has expression disparities between rat and human[30]. Developmentally, the presented data are in agreement with reports of the IgLON family being developmentally regulated[22,30,54]. In the human, there were some instances where the expression was more restricted in the adult as opposed to the foetus. This observation renders the scenario of specific developmental windows when IgLONs can be switched on or off attractive. It has been reported that *OPCML* expression is higher in the visual cortex of kittens than of older cats and this was linked to a developmental window of plasticity[24,25]. The extent that similar developmental switching occurs in the rest of the IgLON family merits further investigation.

One of the most striking conclusions based on the expression data is that IgLON expression is not as restricted as has been widely reported. There are tissues such as the heart and the lung where IgLON expression seems to be as omnipresent as in the brain. Even though there were instances where the present study was in agreement with published data, e.g. in the localisation of OPCML in the eye, there were also instances of complete disagreement, e.g. in the expression of *Opcml* by cerebellar Purkinje cells. As the present study used a variety of different methods, tissues and ages, and was undertaken in two species, it has become evident that results can change based on the method of expression detection and its sensitivity and specificity. For example although in the multiple tissue cDNA panel *OPCML* was not detected in the ovary by standard RT-PCR, it was clearly detected by

qRT-PCR in other ovarian samples. Apart from the method, the other factor that might influence results is the tissue or organ under examination itself. Potential problems can arise due to issues such as the cell representation in a particular preparation, but also age, as we have seen that IgLON expression might fluctuate with age. Finally, the importance of isoforms should not be underestimated, especially as some approaches focus on particular isoforms, whilst others examine expression collectively, like the present study. Not only is it an issue of alternative transcripts, but also it can be an issue of alternative post-translational modifications. In the rat brain, it has been shown that the two commonly detected OPCML protein species show differential patterns of developmental expression[14].

One of the IgLON genes, *OPCML*, has been proposed as a tumour suppressor in sporadic epithelial ovarian cancer[21]. Its expression, as well as the expression of the rest of the family members, was examined in sporadic EOC and the normal human ovary, in order to investigate the relevance of the family as a whole in this type of human cancer[272]. The unselected patient cohort whereon the study was based, albeit relatively small, is very representative of the Scottish population, as described in larger studies[275]. What became evident is that with respect to EOC, it is not just OPCML, but the other IgLONs as well that might be playing a role. It was shown that the expression of all the IgLONs differs between normal ovaries and EOC at the RNA level. The expression levels of *OPCML*, *LSAMP* and *NEGR1* are all significantly decreased in EOC, in contrast to that of *HNT*, which is significantly increased. Confirmation of these differences at the protein level will merit investigating whether, apart from *OPCML*, *LSAMP* and *NEGR1* could also act as TSGs in sporadic EOC. Interestingly, a recent microarray study has also identified *HNT* as being up-regulated in clear cell endometrial carcinoma[276].

It is known that the cause of reduction in the expression of *OPCML* in EOC is mainly epigenetic[21], as is of *LSAMP* in clear cell renal cell carcinoma[43]. Hence, it is likely that the reduction in *LSAMP* and *NEGR1* expression in EOC is accounted for by epigenetic mechanisms. Although epigenetic changes are often age-dependent, age was not found to affect IgLON expression in the EOC panel.

Moreover, a significant positive correlation between the expressions of *LSAMP* and *NEGR1* was identified. The same correlation was evident in the

OPCML-transfected SKOV-3 cell lines. Consequently, it can be postulated that both genes need not be genetically or epigenetically silenced in EOC; the reduction in the expression of the one could result in a reduction in the expression of the other, potentially through a mechanism of coordinated transcriptional regulation. Interestingly, although when *OPCML* is introduced in SKOV-3 cells, its expression is accompanied by a decrease in the RNA expression of both *LSAMP* and *NEGR1*, in the EOC study this negative correlation was not seen. This is probably a reflection of the more complicated nature of a tumour as opposed to a clonal cell line that is genetically homogeneous.

There is currently debate regarding the most suitable normal control in EOC expression studies[277]. One might argue that as the present EOC study was based on whole-ovary preparations, the differences in expression seen might be due to the presence of stroma in the normal ovary. Examination of IgLON expression levels in an OSE-enriched sample provided evidence against this possibility. The three genes that were found to have a reduced expression in EOC, namely *OPCML*, *LSAMP* and *NEGR1*, all exhibited high expression in the OSE sample; *NEGR1*, the gene that exhibited the highest reduction in EOC, was the one that had the highest expression in the OSE sample relative to the median expression in the panel's normal ovaries. In contrast, *HNT*, which exhibited highly elevated expression in EOC, was very lowly expressed in the OSE sample. It is also worth stressing that the observed variability of the data for the normal ovary samples could be partially accounted for by the fragile nature of the OSE, which renders it susceptible to accidental removal during surgery. Moreover, *OPCML* was shown to be strongly expressed in the epithelial layer of normal human ovary sections. Hence, it is likely that all differences observed in the EOC are genuine and not due to the fact that microdissected tissue was not used.

It was demonstrated that in EOC the importance of each IgLON might be specific to histological type. *OPCML* expression is reduced in clear cell carcinomas, *LSAMP* in endometrioid, and *NEGR1* in all but the mucinous tumours. In contrast, *HNT* expression is elevated in serous carcinomas. It should be noted, however, that with respect to mucinous carcinomas, the lack of statistical significance could be due to the under-representation of this type of tumour in the panel. In EOC, malignant

transformation is characterised by a differentiation process, whereby the tissue of origin, the ovarian surface epithelium, acquires specialised differentiated features of specific histological morphology, depending on the type of tumour[62]. As IgLONs have partially distinct patterns of histological subtype expression, they could be part of different malfunctioning pathways that underpin this differentiation process. Notably, *LSAMP* expression was found to be higher in differentiated tumours. This suggests that the level of *LSAMP* expression is likely to be a biological function of differentiation. It can be argued that the significance of the reduction in *LSAMP* expression in the process of OSE transformation could lie in the cells' acquiring a less differentiated morphotype, which is considered to be of higher malignant potential.

Furthermore, *LSAMP* was found to be a negative prognostic factor in addition to being negatively correlated with overall survival. At both levels of statistical testing, the impact of *LSAMP* on survival is not high. This connexion might seem paradoxical, given that its overall tumour levels are significantly lower in the EOC than in normal ovaries. Nevertheless, the role of residual *LSAMP* in a tumour might be antithetical to its original function in the normal ovary. In terms of the multifactorial outcome described as survival, ovarian tumours might be disadvantaged by not expressing *LSAMP* and losing its novel functions. The true explanation of this paradoxical finding remains as yet undetermined.

Chapter 5

Studies on OPCML function

5.1 Introduction

Having developed the necessary tools to allow the study of OPCML biology, the next major strand of this work was devoted to using these tools in order to identify key functions of the gene, and understand the mechanisms behind its link with ovarian cancer.

To sum up the current knowledge on the functions of OPCML, as was extensively presented in chapter 1, here is what is known to date: There is indirect evidence that OPCML might have a role in cell recognition and cell adhesion[12], in dendritic plasticity[18,19,25], and the inflammatory response[26]. Functional studies in the brain of the rat and chick have indicated potential roles in cell-cell adhesion and cell recognition, effected by homophilic and/or heterophilic interactions with other IgLONs[11,14,23,26,57]. Finally, *OPCML* has been proposed as a tumour suppressor gene in sporadic epithelial ovarian cancer, in view of growth suppression properties *in vitro* and tumourigenicity suppression properties *in vivo*[21]. Although the mechanism of *OPCML* silencing in EOC is mainly epigenetic, one somatic mutation has been reported, resulting in a proline to arginine substitution at position 95 of the amino acid sequence (P95R).

Ultimately aiming at furthering our understanding of OPCML, its functions were examined in two expression systems: the ovarian cancer SKOV-3 over-expression system and the cervical cancer HeLa inducible system. In the former, the phenotypic effects of both wild-type and mutant (P95R) OPCML were examined, whilst in the latter the effects of wild-type OPCML were examined at low and high levels of induction. Apart from identifying the phenotypic consequences of expressing *OPCML* in these cell lines, comparisons made between the two systems can be useful in addressing the issue of context specificity. Furthermore, an important aspect of the functional characterisation of OPCML was to investigate how potential functions might comply with the role of a tumour suppressor.

This chapter presents the functional characterisation of OPCML in the SKOV-3 and HeLa Tet-On cell lines. A multitude of phenotypic assays were undertaken, and the results are presented and discussed. Finally, the significance of these findings is elaborated in the context of the role of *OPCML* as a TSG in epithelial ovarian cancer.

5.2 Haptotactic cell migration

Migration is a fundamental phenomenon of normal cellular activity, manifesting in a variety of processes, such as embryonic development, angiogenesis, and the immune response[278]. Cells mainly migrate within the extracellular matrix (ECM), due to interactions between cell surface adhesion receptors and ECM ligands. Cells can migrate both on the extracellular matrix (haptotaxis) and towards chemical signals, such as growth factors and chemokines (chemotaxis). Cell surface receptors, exemplified by the integrin family, govern a range of different cell functions, such as adhesion and migration, as well as cell attachment and polarity, growth and differentiation. In addition, cell migration is an important aspect of cancer pathogenesis, as it intrinsically linked to invasion[279]. Cancer cell motility involves integrin signalling, focal contact formation and actomyosin-dependent contractility. Cancer cells are motile due to the activation or deregulation of a variety of proteins, such as MET, EGF receptors, RAS proteins and PTEN. In addition to these intrinsic factors, determinants of cell motility are provided in the context of the tumour microenvironment.

Cell migration towards components of the ECM is the cellular property that was investigated by Boyden chamber-based migration assays. The principle of these assays is that cells migrate through the porous membrane of the Boyden chamber by haptotaxis towards an immobilised ECM protein gradient. More specifically, the effect on haptotactic migration that expression of *OPCML* confers on cells was examined. Hence, comparisons where made between *OPCML*-expressing SKOV-3 cells and their parental non-expressing controls, and between doxycycline-induced HeLa Tet-On cells and their uninduced counterparts.

In SKOV-3 cells, OPCML did not have any significant effect on haptotactic cell migration (Figure 5.1). SKOV-3 cells exhibited minimal migration to Collagen I. There was a very weak trend of increased migration to vitronectin, by both the wild-type and mutant *OPCML* expressing cells relative to the parental cell line, which was, however, not significant. There was also a weak trend of decreased migration to fibronectin by SKOV-3 $OPCML^{Mut}$ cells, which was again not significant.

In HeLa Tet-On cells, induction of *OPCML*, at both low and high levels of expression, resulted in an increase in migration towards Collagen I. There was no clear-cut effect on migration to either vitronectin or fibronectin. Overall, HeLa cells were more migratory than SKOV-3 cells, irrespective of *OPCML* status.

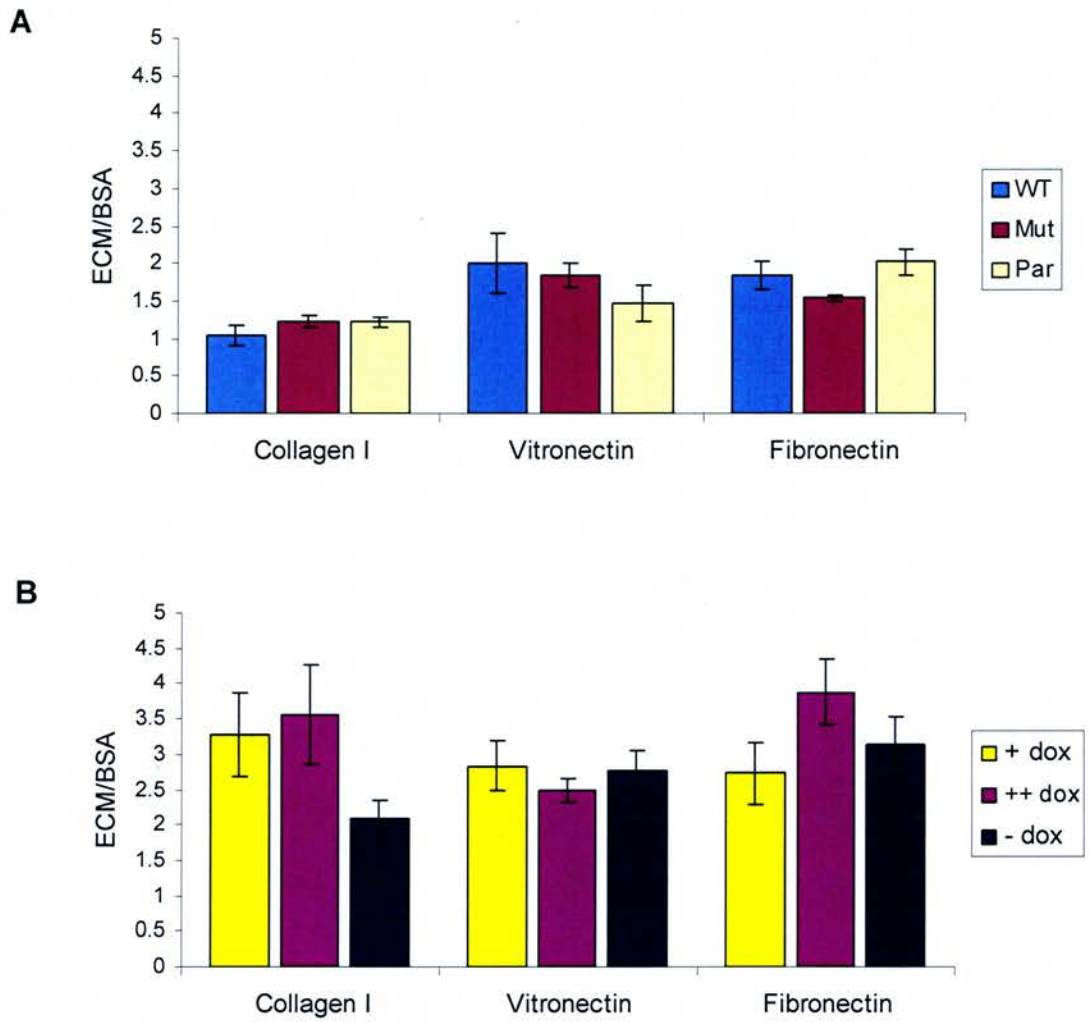

Figure 5.1 The effect of OPCML on haptotactic migration

Haptotactic cell migration in the SKOV-3 OPCML (A) and HeLa Tet-On OPCML (B) cell lines as quantified by migration assays. Assays were performed using Boyden chambers, where cells were allowed to migrate on ECM gradients for a period of approximately 22 h. Results are expressed as ratios of migration on ECM over migration on BSA, the latter serving as a background control. Error bars represent the SD of three replicates.

WT = wild type; Mut = mutant; Par = parent;

+ dox, ++ dox, - dox = 48 h treatment with 100 ng/ml dox, 1000 ng/ml dox and no dox respectively.

5.3 Invasion through matrigel

The property of invasiveness is one of the *sine qua non* features of all malignancy[280]. Cancer is malignant because cancerous cells can invade beyond the constraints of the normal tissue of origin into neighbouring tissues. Although the phenomenon of cell invasion occurs also in normal embryonic development, as well as in healthy adult organisms, it has been extensively studied with respect to cancer pathogenesis, in particular in the aspect of metastasis. In cancer, cells spread either as single cells, or as cell clusters, and can explore both lymphatic and haematogenous routes of dissemination.

As in cellular migration, interactions with the extracellular matrix are instrumental for the invasive cell, although in invasion, the ECM can be regarded as a barrier. Cells have specific strategies in order to overcome ECM resistance that involve changes in cell shape, contraction-dependent matrix remodelling and proteolysis. Hence, cell invasion can be considered to combine the aspects of adhesion, migration and proteolysis. More than being a barrier, however, the ECM also provides factors that will determine the survival of cells in their new environment.

Invasion assays are one of the tools to investigate the invasive potential of cells *in vitro*. A commonly used variation is based on the use of matrigel, which serves as a reconstituted basement membrane. Matrigel was developed from the supernatant of a Schwannoma cell line and predominantly contains laminin, collagen IV and nidogen[281]. The matrigel matrix is usually applied on a porous membrane, as part of a Boyden chamber. The occlusion of its pores blocks non-invasive cells from migrating through the membrane. In contrast, invasive cells can invade through the matrigel matrix and the membrane pores. In order to attract cells from one side of the membrane to the other, a chemoattractant is often employed. Essentially, this form of invasion assay is a chemotactic migration assay that has been modified by the addition of matrigel, which provides a physical barrier that the cells have to traverse. Comparisons can be made either between cells that are non-invasive and invasive cells, or between cells of different degrees of invasiveness.

In order to study the connexion of OPCML to cell invasion, the invasive potential of cells expressing *OPCML* was compared against that of non-expressing cells, in both the SKOV-3 and the inducible HeLa systems. When invasion assays were undertaken in the former, the effect of either wild-type or mutant OPCML on the invasive properties of cells was determined by comparison of the transfected to the parental cells. For the HeLa Tet-On system, comparisons were made between two different levels of wild-type *OPCML* induction and the uninduced state. In the particular type of invasion assays used, invasion through matrigel is measured relative to chemotactic migration.

As can be seen in Figure 5.2, in SKOV-3 cells, both wild-type and mutant OPCML significantly increased cell invasion. More specifically, SKOV-3 $OPCML^{WT}$ cells exhibited a 15% increase in invasion relative to the parental cell line (p = 0.040), while SKOV-3 $OPCML^{Mut}$ cells had an 11% increase (p = 0.020). In HeLa cells, both low- and high-level induction of *OPCML* resulted in a decrease in cell invasion, of approximately 7%, which was not statistically significant though.

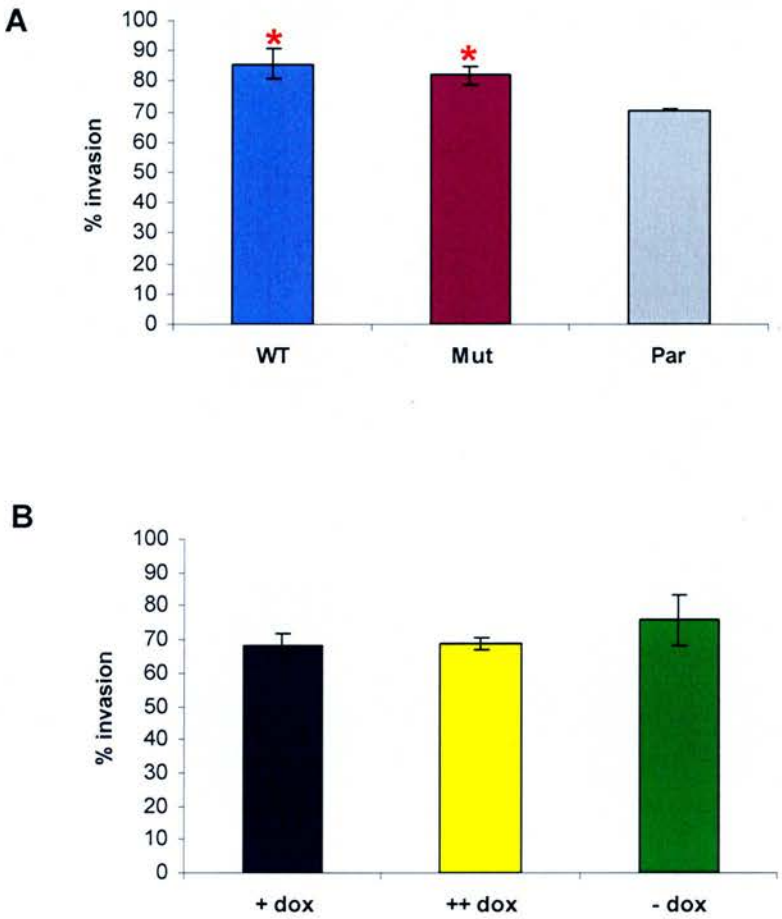

Figure 5.2 The effect of OPCML on cell invasion
Percentage invasion in the SKOV-3 OPCML (A) and HeLa Tet-On OPCML (B) cell lines as quantified by invasion assays. Assays were performed using Boyden chambers, where cells were allowed to either invade through a Matrigel matrix or migrate through a membrane without the matrix towards medium containing 5% FCS used as a chemoattractant for a period of 24 h. Invasion was calculated relative to migration. Error bars represent the SEM of three independent experiments.
* $p < 0.05$ compared to parental cell line by Student's t test.
WT = wild type; Mut = mutant; Par = parent;
+ dox, ++ dox, - dox = 48 h treatment with 100 ng/ml dox, 1000 ng/ml dox and no dox respectively.

Taking a closer look at the significant difference in invasion between SKOV-3 OPCML and SKOV-3 parental cells, it can be seen that this difference actually lay in the chemotactic migration of the cells, rather than the absolute invasion through matrigel (Figure 5.3). Percentage invasion was calculated as the ratio of the latter to the former and as chemotactic migration was smaller, the ratio was increased. In fact, SKOV-3 OPCML^{WT} cells exhibited a significantly reduced chemotactic migration relative to the parental cell line (p = 0.010) and so did the mutant *OPCML*-expressing cells (p = 0.004).

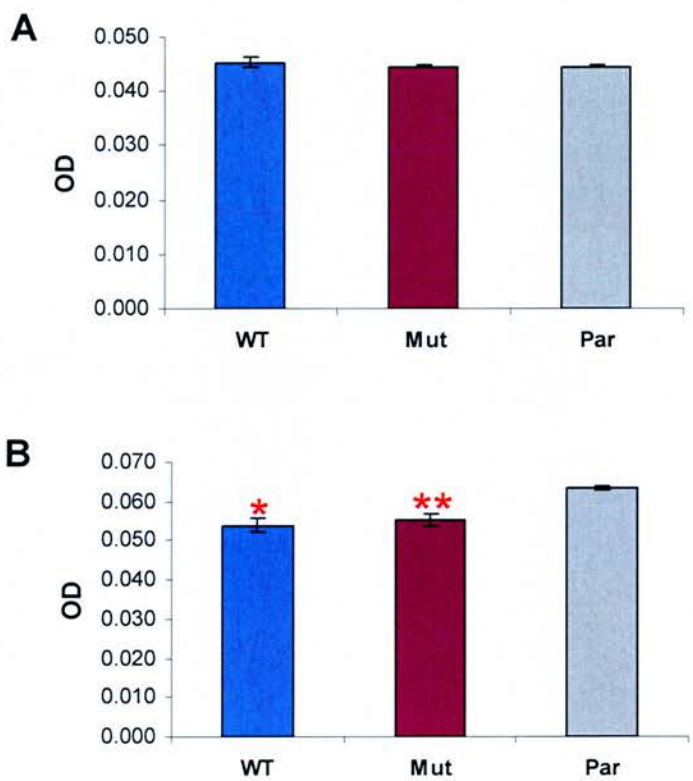

Figure 5.3 A closer look on the effect of OPCML on cell invasion in SKOV-3 cells

Absolute invasion through matrigel (A) and chemotactic migration (B) in the SKOV-3 OPCML cells as quantified by invasion assays. Error bars represent the SEM of three independent experiments.

* $p < 0.05$, ** $p < 0.01$ compared to parental cell line by Student's t test.

OD = optical density; WT = wild type; Mut = mutant; Par = parent.

5.4 Adhesion to the extracellular matrix

Apart from the role of cell-ECM interactions in the context of cellular migration and invasion, these interactions are also critical in "arresting" the cells inside the matrix. Whether it is normal tissue architecture, or the establishment of a tumour mass, the adhesion of cells to the extracellular matrix by means of cell surface receptors is a prerequisite.

Assays that measure the attachment of cells on ECM proteins are a useful aid in studying cell-ECM interactions directly. Attachment assays examine how the cells adhere onto surfaces coated with specific ECM molecules in a quantitative and/or qualitative manner.

In order to examine the effect of OPCML on cellular adhesion to the ECM, comparisons were made between *OPCML*-expressing SKOV-3 cells and their parental non-expressing controls, or between induced HeLa Tet-On cells and their uninduced counterparts.

As can be seen in Figure 5.4, in SKOV-3 cells, expression of wild-type *OPCML* significantly increased adhesion on fibronectin in relation to the parental cell line by approximately 30% ($p = 0.015$). In contrast, expression of mutant *OPCML* did not have an effect: SKOV-3 OPCML^{Mut} cells exhibited comparable adhesion on fibronectin as the parental cells. Hence, there was a significant difference between the wild-type and the mutant *OPCML*-expressing cells ($p = 0.021$). With respect to adhesion on vitronectin, expression of wild-type *OPCML* significantly increased adhesion by approximately 36% ($p = 0.010$), whilst of mutant *OPCML* by approximately 16% (not significant), as compared to the parental cell line. Again, there was a significant difference between the wild-type and the mutant *OPCML*-expressing cells ($p = 0.045$). *OPCML* expression was not found to significantly influence adhesion on laminin, collagen I or collagen IV, irrespective of being wild-type or mutant. There was however a trend for mutant *OPCML*-expressing cells to show less adhesion than wild-type ones. In HeLa Tet-On cells, expression of *OPCML* did not have any effect on adhesion to any ECM component at any level of induction.

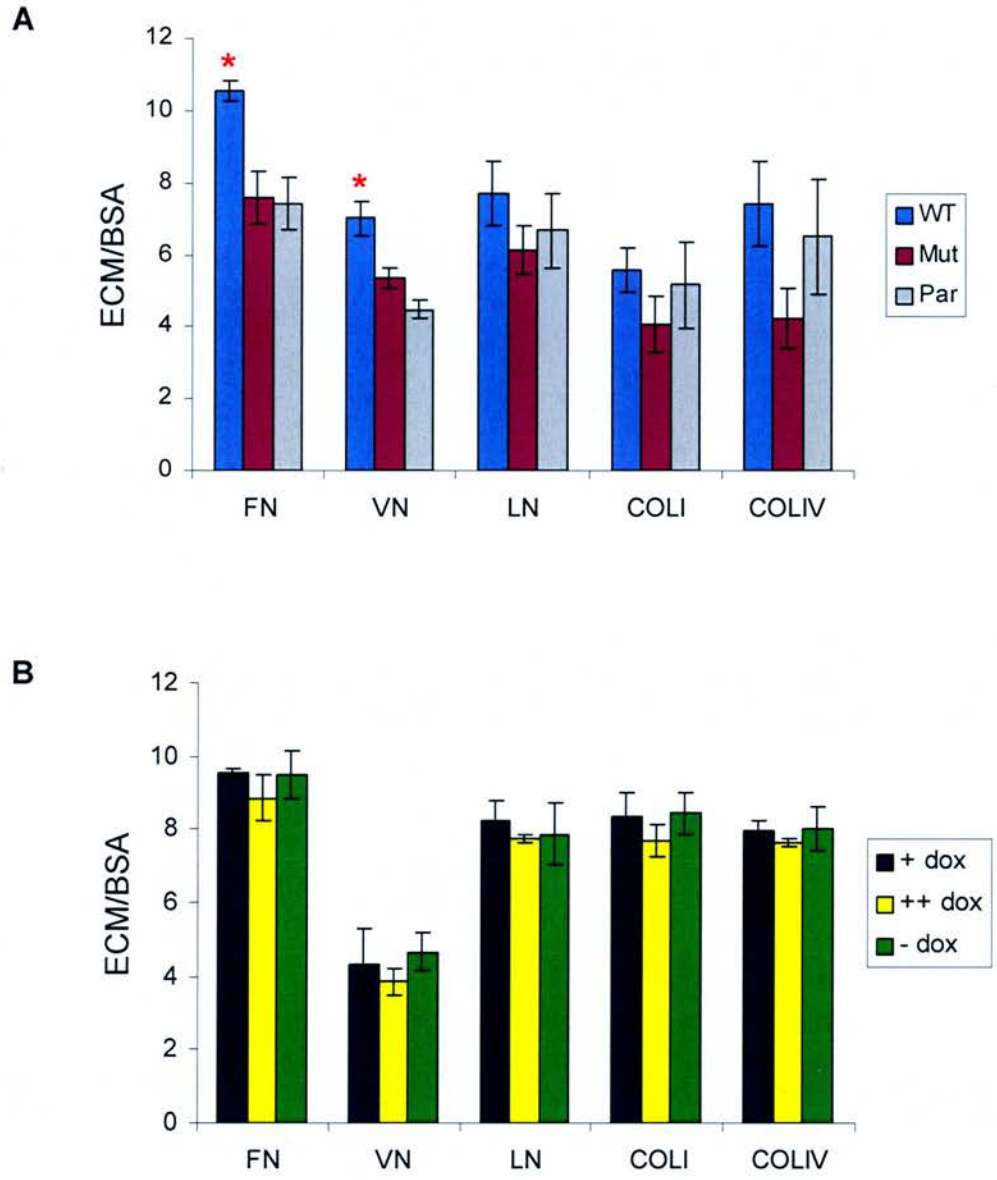

Figure 5.4 Effect of OPCML on adhesion to the ECM

Cell adhesion in the SKOV-3 OPCML (A) and HeLa Tet-On OPCML (B) cell lines as quantified by attachment assays. Cells were seeded and allowed to attach to either ECM-coated or BSA-coated strips for a period of 45 min. Results are expressed as ratios of attachment to ECM over attachment to BSA, the latter serving as a background control. Error bars represent the SEM of three independent experiments.

* $p < 0.05$ compared to parental cell line by Student's *t* test.

WT = wild type; Mut = mutant; Par = parent;

FN = fibronectin; VN = vitronectin; LN = laminin;

COLI = collagen I; COLIV = collagen IV;

+ dox, ++ dox, - dox = 48 h treatment with 100 ng/ml dox, 1000 ng/ml dox and no dox respectively.

5.5 Cell-cell adhesion

Thus far, the phenotypic properties of OPCML that were examined concerned cell-ECM interactions. Cells, though, and in particular epithelial cells, do not only form contacts with the ECM, but also with other cells. Cell-cell contacts, whether stabilized by tight, adherens or gap junctions, provide mechanical strength and polarization within any organised tissue, and can even promote the locomotion of cells. Apart from playing an important role in normal physiology, cell-cell adhesion is often the focus of study in tumour biology[282]. Homotypic epithelial cell-cell adhesion prevents the escape of cells into neighbouring tissues and can even withhold cell invasion by well-differentiated epithelial strands.

The measurement of cell-cell adhesion is commonly undertaken using commercially available fluorochrome probes[283]. Calcein AM is a soluble fluorescein derivative, which is taken up by cells as an ester and hydrolysed by internal esterases, reflecting cytoplasmic activity and hence indicating cell viability. A simple and sensitive cell-cell adhesion assay that involves the use of calcein AM is carried out in three steps: labelling of cells to be tested, adhesion of labelled cells to confluent unlabelled monolayers, and measurement of the fluorescent signal using microfluorimetry.

This section presents work that assessed the ability of OPCML as an adhesion molecule to influence cell-cell adhesion. Apart from investigating adhesion in cells that express *OPCML*, the role of the other IgLONs was also investigated in order to test whether interactions operate at the level of cell-cell adhesion.

5.5.1 In SKOV-3 OPCML cells

How does expression of *OPCML* influence the ability of cells to adhere to each other? To tackle this question, cell-cell adhesion assays were undertaken that examined the adhesion of cells expressing or not expressing *OPCML*. Due to the nature of these assays, which rely on two cell populations, the inducible system was not used, as it would have been difficult to fine-tune the induction timings to ensure that both populations had undergone the same degree of induction. Hence, these assays were only carried out in the SKOV-3 cells.

As is evident in Figure 5.5, expression of *OPCML* significantly increased cell-cell adhesion. More specifically, labelled SKOV-3 $OPCML^{WT}$ cells adhered twice as much to a monolayer of the same cell type ($p = 0.027$) or of SKOV-3 $OPCML^{Mut}$ cells ($p = 0.019$) than to a monolayer of the parental cell line. There was a trend for labelled SKOV-3 $OPCML^{Mut}$ cells to adhere more to a monolayer of the same type or of their wild-type counterpart than to the parental cells; however, differences were not statistically significant. Finally, labelled SKOV-3 parental cells adhered almost twice as much to a monolayer of cells expressing either wild-type ($p = 0.009$) or mutant ($p = 0.050$) *OPCML* than to the same cell type.

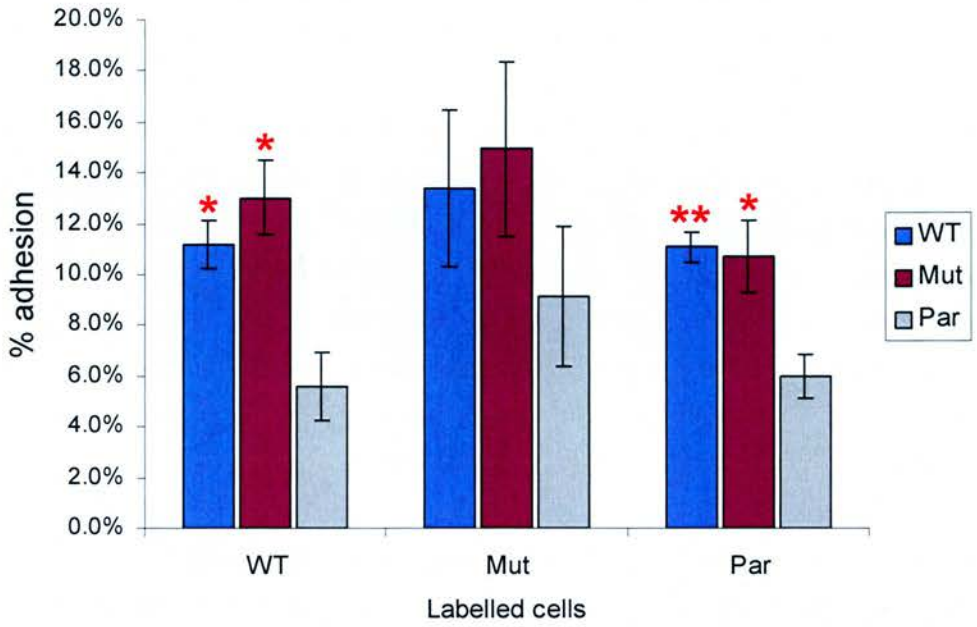

Figure 5.5 The effect of OPCML on cell-cell adhesion
Percentage cell-cell adhesion in the SKOV-3 OPCML cell lines as quantified by adhesion assays. Cells under test were fluorescently-labelled and allowed to attach on unlabelled cell monolayers for 90 min. Values are corrected for background fluorescence. Error bars represent the SEM of three independent experiments.
* $p < 0.05$, ** $p < 0.01$ compared to parental cell line by Student's *t* test.
WT = wild type; Mut = mutant; Par = parent.

5.5.2 In SKOV-3 IgLON cells

It has been hypothesised that IgLONs carry out their normal functions mainly by forming homodimers and also herodimers, termed Diglons. The availability of SKOV-3 cell lines transfected with members of the IgLON family other than *OPCML* offers an opportunity to test this hypothesis in an ovarian background. Having optimised the cell-cell adhesion assay, potential interactions could be examined by focusing on this particular functional aspect.

In order to test potential IgLON interactions, cell-cell adhesion assays were carried out using four IgLON-expressing SKOV-3 cell lines. Apart from the SKOV-3 cell line transfected with wild-type *OPCML*, SKOV-3 cell lines expressing *HNT*, *LSAMP* and *NEGR1* were used. However, as can be seen in Figure 5.6, statistically significant interactions were not identified. More specifically, labelled SKOV-3 $OPCML^{WT}$ cells attached better to monolayers composed of either cells of the same type or of *NEGR1*-expressing cells; *HNT*- and *LSAMP*-expressing monolayers were somewhat less favourable adhesion substrates. *HNT*-expressing labelled cells attached more to *OPCML*- and *LSAMP*-expressing monolayers; *LSAMP*-expressing labelled cells attached more to an *OPCML*-expressing monolayer; and *NEGR*-expressing labelled cells attached mostly to *OPCML*-expressing monolayers as well as homotypic monolayers. All these observations were merely trends, though, as none could be confirmed statistically.

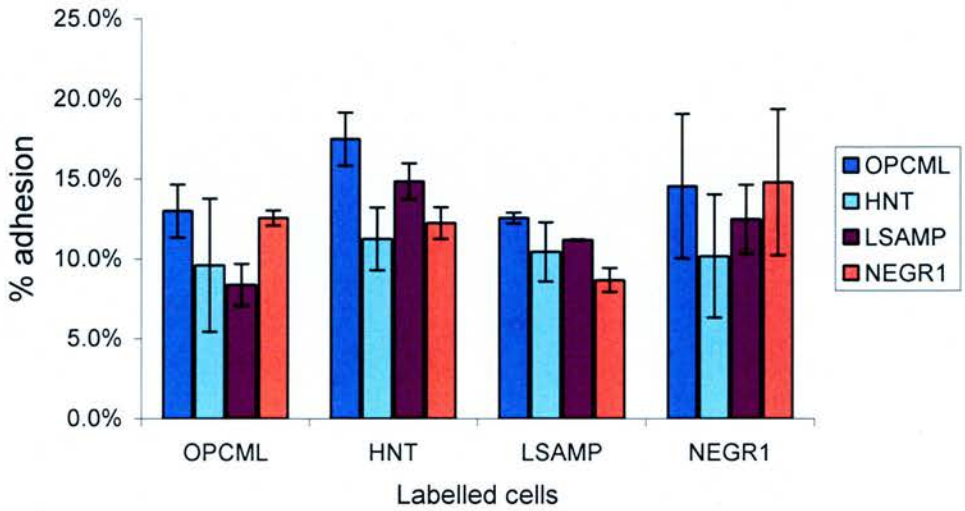

Figure 5.6 The effect of IgLONs on cell-cell adhesion
Percentage cell-cell adhesion in the SKOV-3 IgLON cell lines as quantified by adhesion assays. Cells under test were fluorescently-labelled and allowed to attach on unlabelled cell monolayers for 90 min. Values are corrected for background fluorescence. Error bars represent the SEM of three independent experiments.

5.6 Cell growth

The balance between cell proliferation and cell death is fundamental in any aspect of normal physiology and it is this balance that is disturbed in tumourigenesis by activation of oncogenic processes and suppression of protective mechanisms. Cancers arise by an evolutionary process whereby somatic cells mutate and escape the restraints that normally guard them against uncontrolled expansion. Hence, the aspect of cell growth is paramount in tumour biology, and any genes that are implicated in the processes underlying this aspect are commonly the focus of intense study.

Previous work had demonstrated that OPCML suppresses cell growth *in vitro*, when expressed in SKOV-3 cells[21]. Although this phenotypic effect has been described, what is not clear is why cells that express *OPCML* are growth-suppressed. A possible explanation could be that these cells exhibit reduced proliferation; alternatively, they could be subjected to increased cell death.

Before investigating the mechanism behind the growth suppression phenotype of *OPCML*, the growth characteristics of SKOV-3 clones transfected with *OPCML* were reassessed. Growth curves of the wild-type and mutant *OPCML*-expressing SKOV-3 cells, as well as the parental cell line, are shown in Figure 5.7. SKOV-3 $OPCML^{WT}$ cells are strongly growth-suppressed relative to the parental cells ($p < 0.001$). SKOV-3 $OPCML^{Mut}$ cells grow at a higher rate relative to their wild-type counterpart ($p < 0.001$), even though they still lag behind the parental cells ($p = 0.001$). In contrast, in HeLa Tet-On cells, OPCML does not have an effect on growth, irrespective of the level of induction.

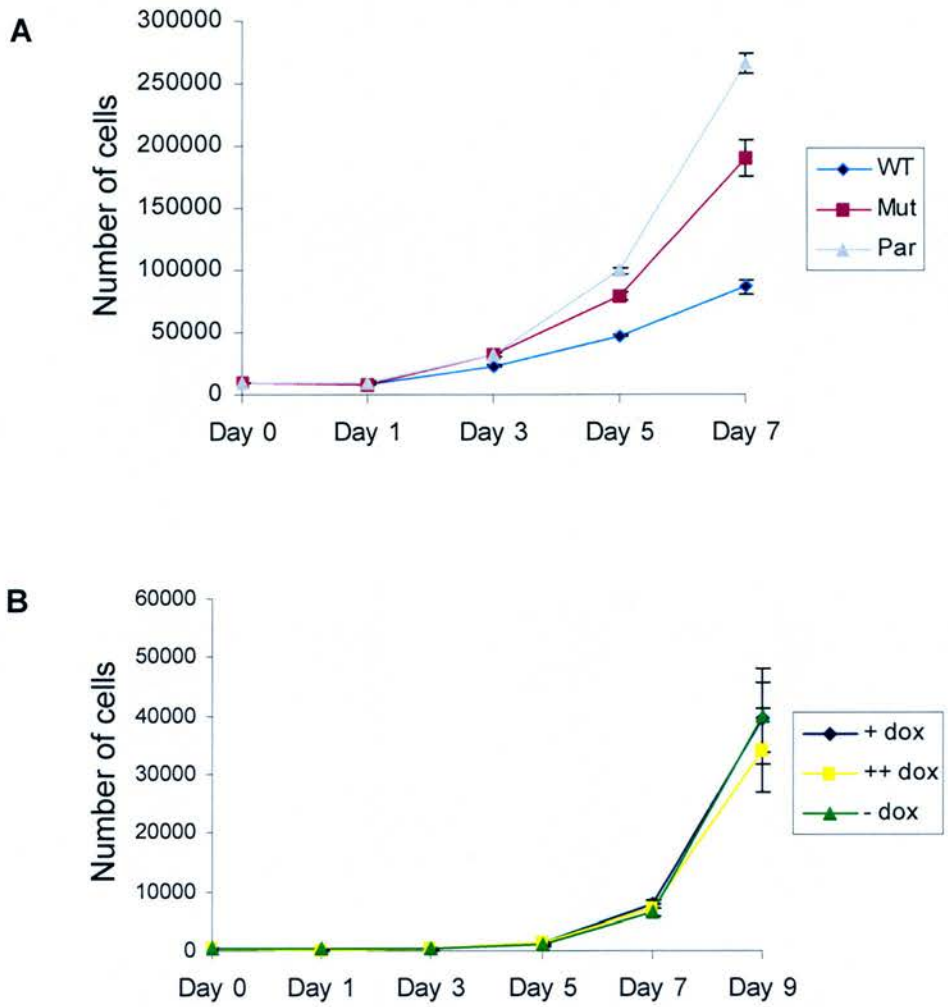

Figure 5.7 The effect of OPCML on cell growth
Growth curves of SKOV-3 OPCML (A) and HeLa Tet-On OPCML (B) cell lines. Error bars represent the SD of three replicates.
WT = wild type; Mut = mutant; Par = parent;
+ dox, ++ dox, - dox = medium with 100 ng/ml dox, 1000 ng/ml dox or no dox respectively.

5.7 Cell proliferation

One explanation for the growth suppression effect of OPCML on SKOV-3 cells could be that cells expressing *OPCML* are less proliferative. As a consequence, it would be expected that the cell cycle distribution and replicative capacity of SKOV-3 OPCML cells be skewed towards a less proliferative profile in comparison to the parental cells that do not express *OPCML*.

To test this hypothesis, proliferation was measured in SKOV-3 OPCML cells by FACS-based proliferation assays. More specifically, the technique used was a two-colour staining method for measuring cell proliferation by multiparameter analysis of DNA replication and cellular DNA content / cell cycle position by flow cytometry. This technique relies on the growth of cells in the presence of 5-bromo-2-deoxyuridine (BrdUrd), which is an accepted method for monitoring DNA replication. This is coupled with staining with propidium iodide, in order to acquire DNA cell cycle information.

As can be seen in Figure 5.8, OPCML did not have any significant effects on either DNA replication or cell cycle distribution. In fact, both the wild-type and the mutant *OPCML*-expressing SKOV-3 cells had similar profiles compared to their parental cell line.

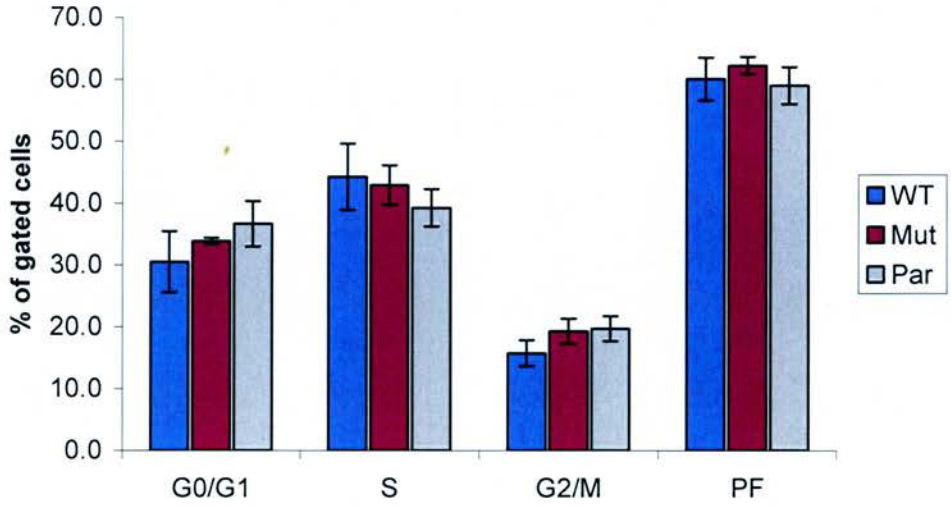

Figure 5.8 Effect of OPCML on cell proliferation
DNA replication and cell cycle distribution analysis in the SKOV-3 OPCML cell lines by flow cytometry. Error bars represent the SEM of three independent experiments; in each, a total of 30,000 events were acquired.
WT = wild type; Mut = mutant; Par = parent;
PF = proliferative fraction (i.e. S + G2/M).

5.8 Apoptosis

Another potential explanation for the growth suppression phenotype of *OPCML* could be related to apoptotic death. Apoptosis is a form of cell death crucial in the tumourigenic process, whereby a cell undergoes "programmed" cell death, triggered by a variety of intrinsic and extrinsic stimuli[284].

Apoptosis is characterised by certain features, detection of which can be used to identify it: DNA fragmentation, changes in cell size and granularity, changes in plasma permeability, cell surface modifications and formation of apoptotic bodies. An assay that is based on the detection of cell surface modifications is the annexin V assay[285]. Annexin V is an anti-coagulant protein that preferentially binds negatively charged phospholipids. Early in the apoptotic process, phospholipid asymmetry is disrupted, leading to the exposure of phosphatidylserine (PS) on the outer leaflet of the cell membrane. This event is thought to be important for macrophage recognition of cells undergoing apoptosis. Annexin V binding to PS is calcium-dependent, reversible and occurs with an affinity of approximately 5×10^{-10} M. As the event that annexin V assays measure occurs early in the apoptotic process, these assays can only accurately measure early apoptosis; late apoptosis cannot be distinguished from necrotic death.

The two SKOV-3 *OPCML*-expressing cell lines were analysed by the annexin V method and compared to the non-expressing parental cell line, as can be seen in Figure 5.9. Wild-type or mutant *OPCML*-expressing SKOV-3 cells underwent significantly more (early) apoptosis than the parental cell line ($p = 0.050$ for the wild-type; $p = 0.005$ for the mutant). The overall cell death levels were also elevated ($p = 0.043$ for the wild-type; $p = 0.048$ for the mutant). As the levels of background apoptosis in a cell line under normal growing conditions are generally low, in order to increase numbers and allow differences to be more distinctive, the SKOV-3 cell lines were subjected to treatment with a cytotoxic drug, camptothecin. After treatment with camptothecin, SKOV-3 $OPCML^{WT}$ cells exhibited a three-fold increase in early apoptosis compared to the parental cell line ($p < 0.001$). SKOV-3 $OPCML^{Mut}$ cells also showed an increase, albeit of a lower magnitude and not statistically significant. In fact, they did not differ significantly to their wild-type

counterpart. With respect to total cell death, both wild-type and mutant cell lines exhibited a statistically significant increase relative to the parental cell line ($p < 0.001$ for the wild-type; $p = 0.011$ for the mutant). Again, the effect of mutant OPCML was of a lower magnitude, albeit did not differ significantly from the effect of wild-type OPCML.

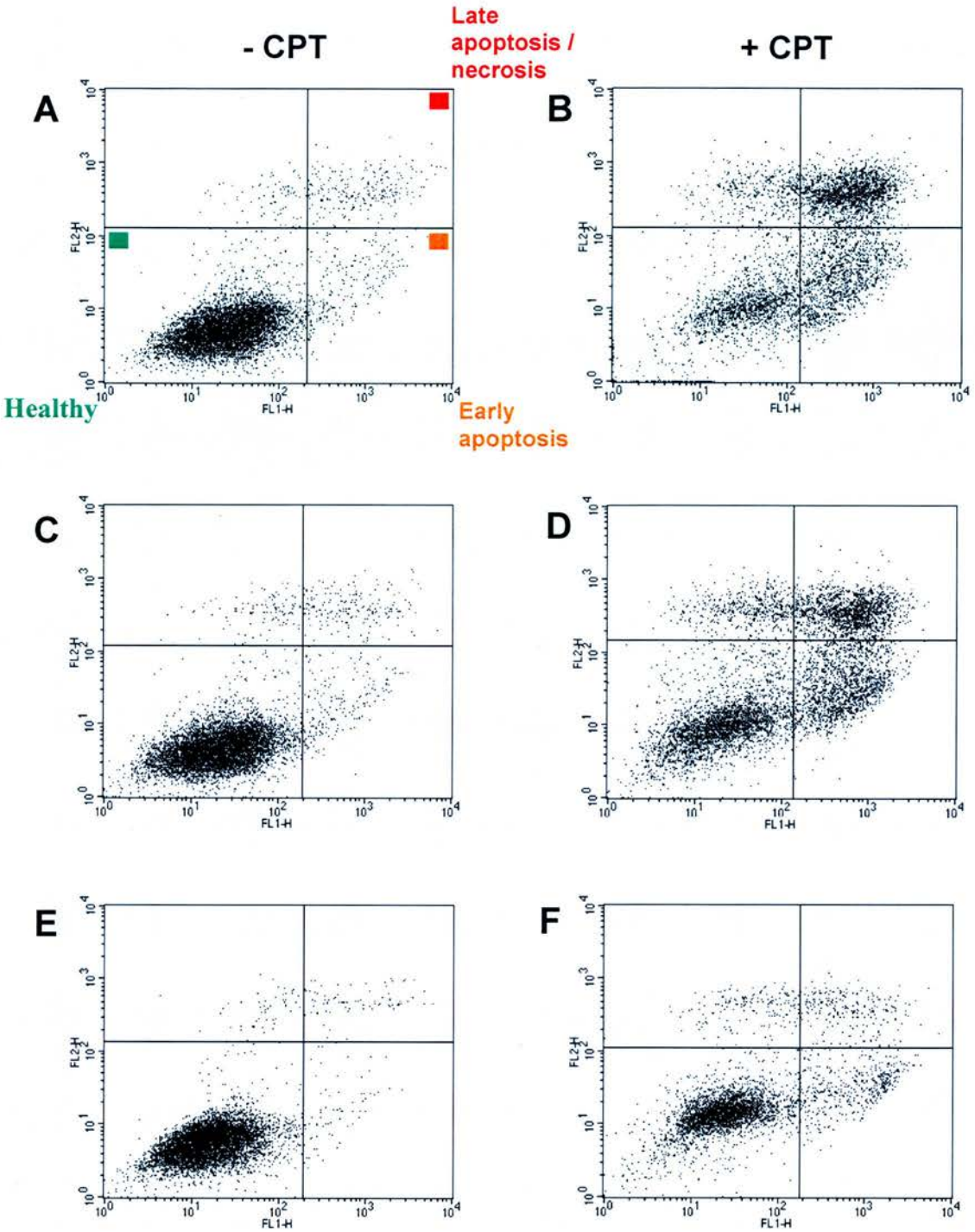

Figure 5.9i The effect of OPCML on apoptosis
Annexin V analysis by flow cytometry. Representative dot plots of SKOV-3 $OPCML^{WT}$ (A,B), SKOV-3 $OPCML^{Mut}$ (C,D) and SKOV-3 Par (E,F) cells, in the presence or absence of treatment with 1 μM camptothecin (CPT) for 48 h. Each dot plot corresponds to one replicate within an experiment (10,000 events acquired).

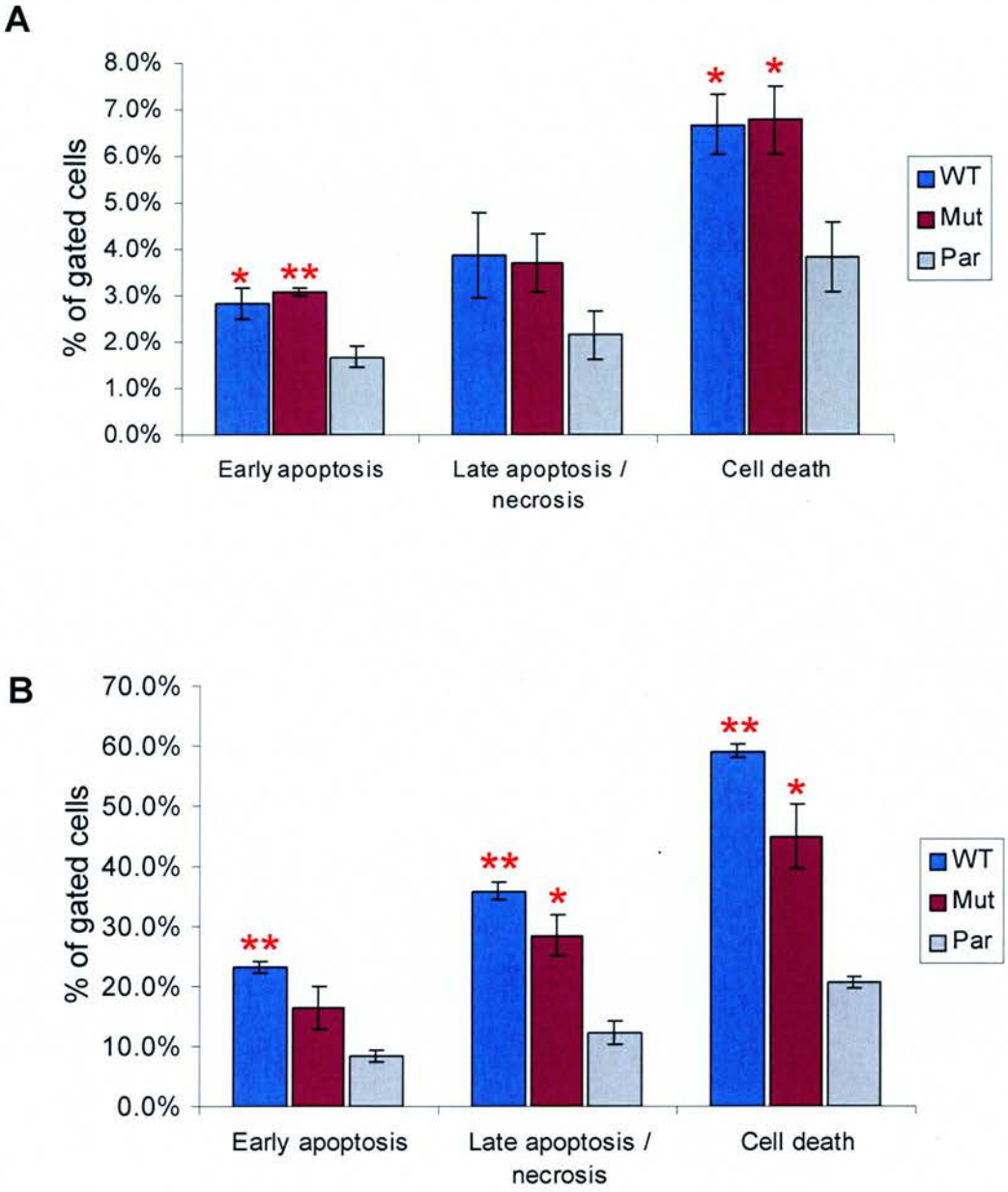

Figure 5.9ii The effect of OPCML on apoptosis (continued)
Annexin V analysis in the SKOV-3 OPCML cell lines by flow cytometry, measuring steady-state levels of apoptosis (A), and after treatment with 1 μM camptothecin for 48 h (B). Error bars represent the SEM of three independent experiments; in each, a total of 30,000 events were acquired.
* $p < 0.05$, ** $p < 0.01$ compared to parental cell line by Student's *t* test.
WT = wild-type; Mut = mutant; Par = parent.

5.9 Discussion

The functional characterisation of OPCML presented in this chapter was aimed at identifying novel functions for this protein and also exploring further what is currently known. In order to study the functions of OPCML, two alternative expression systems were used: an ovarian SKOV-3 over-expression system, expressing either wild-type or mutant *OPCML*, and a non-ovarian HeLa Tet-On inducible system expressing wild-type *OPCML* at two different levels of expression. A variety of phenotypic assays were used that focused on different aspects of cell biology.

Initially, attention was drawn to the interactions of cells with the extracellular matrix. It was found that wild-type OPCML increases significantly the adhesion of SKOV-3 cells to fibronectin and vitronectin. The adhesion of cells to the ECM is governed by receptor-mediated binding, involving surface receptors on cells and ligands on ECM components. The RHO signalling pathway is often implicated in the attachment of cells to a matrix[286]. Cell surface receptors typically belong to the integrin family, but can also be proteins such as CD44 and members of the immunoglobulin subfamilily of cell-adhesion molecules. For example, in ovarian cancer cells it has been shown that gonadotrophin stimulation of ovarian cancer MLS cells increases their adhesion to fibronectin due to CD44 and αv integrins[287]. More recently, Li and colleagues demonstrated by the very sensitive method of quartz crystal microbalance that strong ovarian cell adhesion to fibronectin and vitronectin is mostly mediated by αvβ3 integrins[288]. Hence, it can be postulated that the differential binding of cells expressing wild-type *OPCML* to components of the ECM could be attributed to an indirect effect via integrin signalling and/or the mere presence of OPCML if this protein can function as a receptor. The fact that OPCML is entirely extracellular makes the former postulation more likely.

Moreover, both wild-type and mutant OPCML were shown to significantly decrease chemotactic migration in SKOV-3 cells, without influencing haptotactic migration. Chemotactic cell migration is based on interactions between chemotactic molecules, such as growth factors, and their respective receptors. Motility-inducing cytokines and growth factors are known to signal via PI3K, RAC and RHO[289]. For

example, tuberin, the *TSC2* tumour suppressor gene product, decreases chemotactic cell migration in leiomyoma ELT3 cells through RHO activation[290]. The fact that OPCML has an effect on chemotactic, but not haptotactic cell migration is not unusual: there are examples of proteins affecting only one of the two phenomena[291] and even having an opposing effect[292]. In ovarian cancer, CXCR4 receptors are thought to influence peritoneal spread by chemotactic migration[293]. In contrast, integrin-mediated cell-ECM interactions are thought to be less important in facilitating ovarian cancer cell implantation onto the peritoneal mesothelium[294]. Interestingly, neurite outgrowth is closely related to cell migration and invasion, and OPCML is reported to inhibit neurite outgrowth in association with another IgLON, HNT[57]. It can be hypothesised that the effect of OPCML on chemotactic cell migration is likely to be linked to the expression of specific receptors and signalling through a pathway most probably associated with RHO. As OPCML affects cell adhesion to fibronectin and vitronectin, but not cell migration to these ECM components, it is important to note that in fact migration does not always correlate with adhesion[295,296]. Interestingly, chemotaxis is also important in physiological processes such as wound healing, which could be considered analogous to the process of ovulation. *OPCML* is known to be down-regulated by the proinflammatory cytokine interleukin-1β[26].

In addition, OPCML was demonstrated to promote cell-cell adhesion in SKOV-3 cells. The prototype homotypic epithelial cell-cell adhesion molecule functioning through homophilic interactions is E-cadherin, which operates in adherens junctions[297]. The E-cadherin gene *CDH1* is considered to be a tumour suppressor gene and prevent cell invasion in most cancers of epithelial origin. E-cadherin mediated cell-cell adhesion is lost concomitantly with progression towards malignancy[298]. This role of E-cadherin in epithelial tumourigenesis is connected to its aiding the process of epithelial to mesenchymal transition, a phenomenon characteristic of most epithelial tumours, whereby cancerous cells lose some of their differentiation features. However, ovarian cancer is an exceptional type of cancer in that respect: transformation of ovarian cells consists of their acquiring differentiated features towards a more epithelial morphotype[62]. Hence, ovarian cancer cells express E-cadherin, in contrast to OSE cells that express

N-cadherin[299,300]. Because of this unconventional relationship between E-cadherin and epithelial ovarian cancer, Sundfeldt argues that loss of normal cell-cell adhesion is a less important prerequisite in ovarian tumourigenesis[282]. However, this argument undermines the importance of other cell-cell adhesion molecules. As OPCML increases cell-cell adhesion when expressed in ovarian cancer cells, it could be part of the mechanism that ensures functional cell-cell adhesion in the normal ovary. Tumour suppressor genes are often reported to promote cell-cell adhesion[301-303]. A role in cell-cell adhesion could also involve cell signalling. For example, in OVCAR-3 cells, an ovarian cancer cell line that expresses E-cadherin, cell-cell adhesion is linked to the PI3K and EGFR pathways[304]. An interesting observation is that cell-cell adhesion in SKOV-3 cells that express *OPCML* is of the same magnitude as cell-cell adhesion between SKOV-3 cells that express *OPCML* and parental cells that do not express it. This indicates that OPCML can promote cell-cell adhesion by its presence on the surface of just one of the two interacting cell populations. This observation suggests that OPCML participates in heterophilic interactions; in the SKOV-3 parental cells its interacting partner is a protein other than OPCML. It could in fact be another IgLON, supporting the postulation that OPCML mainly functions through heterophilic interactions with other IgLONs[57]. The possibility of homophilic interactions in *OPCML*-expressing SKOV-3 cells cannot be excluded though. One apparent caveat in the cell-cell adhesion used was that the observed adhesion between labelled SKOV-3 cells expressing wild-type *OPCML* on an unlabelled monolayer of parental cells was not of the same magnitude as of labelled parental cells to an unlabelled monolayer of cells expressing wild-type *OPCML*. This could be accounted for by the nature of the particular type of cell-cell adhesion assay, which allows the accurate measurement of the adhesion of only the labelled cell population, which has been labelled using strictly defined conditions, as opposed to the creation of the monolayers, which is subject to inherent variability. Heterophilic interactions were examined with regard to cell-cell adhesion between SKOV-3 cell lines that express different IgLON proteins; however, the observed trends were inconclusive. It should be noted that the other IgLON expressing cell lines have not been characterised to the same extent as SKOV-3 OPCML cells.

Moreover, SKOV-3 cells already express high levels of *LSAMP*, so increasing its expression by transfecting the gene might not have phenotypic consequences.

One of the most significant aspects of OPCML function in SKOV-3 cells is growth suppression. *OPCML* expression in SKOV-3 cells causes marked growth suppression and the mechanism underlying this effect was investigated. It was found that OPCML significantly increases apoptosis, whereas it does not affect cell proliferation. The importance of pro-apoptotic proteins in preventing tumourigenesis is paramount and a variety of tumour suppressor genes play a role in apoptosis (see chapter 1 for TSGs in ovarian cancer). Apart from the direct role of OPCML in regulating cell growth by affecting apoptosis, it could also act as a deterrent for migrating cells, which, upon leaving their natural environment, need to switch on survival pathways in order to avoid anoikis. Furthermore, *OPCML* expression in SKOV-3 cells renders them significantly more chemosensitive to camptothecin due to elevated levels of apoptosis. Camptothecin is a cytotoxic drug that targets topoisomerase I-dependent DNA replication by reversibly inducing single-strand breaks[305]. Cell death by camptothecin requires an active S phase, a criterion that is satisfied in the SKOV-3 cells that express *OPCML*. Camptothecin-derived drugs, exemplified by topotecan and irinotecan, are widely used in clinical practice against diverse types of neoplasia, including ovarian cancer. It is worth investigating in the future whether the expression status of *OPCML* has an effect on the efficacy of these treatments. The chemoresponsiveness of SKOV-3 OPCML cells to other cytotoxic compounds also merits examination.

In SKOV-3 cells, the only clear-cut phenotypic difference between wild-type and mutant *OPCML* expression identified is regarding adhesion to the ECM: whereas wild-type *OPCML* expression increases adhesion to both fibronectin and vitronectin, mutant *OPCML* expression does not. SKOV-3 OPCML^{Mut} cells also grow somewhat slower that the parental cell line, but they are not overtly growth-suppressed as their wild-type counterpart. The difference with respect to cell-ECM adhesion could be explained by a potential loss of function of the mutant that affects either integrin signalling or the ability of the protein to act as a receptor for ECM ligands. Biomolecular modelling of the P95R mutation has suggested a conformational change in the first immunoglobulin domain[21]; this could in theory interfere with

cell-ECM interactions. In the same report, the mutation abolishes the effect of OPCML on cell-cell aggregation; in the present study, mutant *OPCML*-expressing cells did not exhibit different cell-cell adhesion properties relative to the wild-type *OPCML*-expressing cells. This probably is an indication of a difference in methodology, with cell-cell adhesion assays being more accurate and quantitative than aggregation assays. As far as the other phenotypic aspects of OPCML are concerned, the P95R mutation does not modify the behaviour of cells.

OPCML expression in the inducible HeLa cell line did not recapitulate any of the features identified in the SKOV-3 cells. In brief, in HeLa Tet-On cells *OPCML* expression resulted in an increase in adhesion to collagen I, had no effect on chemotactic migration or adhesion to the ECM and did not cause growth suppression. This could reflect the different genetic backgrounds between the cervical cancer HeLa cells and the ovarian cancer SKOV-3 cells. In fact, glycosylation of OPCML is evidently different, as was shown in chapter 3, as is the complement of IgLONs, as was shown in chapter 4. Finally, in the HeLa Tet-On system, all comparisons were made between the uninduced and the induced states. The fact that *OPCML* "leaky" expression is detected and is probably at functional levels could render some of these comparisons of questionable value. It can be assumed, though, that in so far as a tumour suppressor gene in ovarian cancer is being examined, the inferences based on the SKOV-3 cell lines are valid and more likely to reflect physiologically relevant aspects of OPCML biology.

There are two issues that might impose some caution in the interpretation of all the above phenotypes: the fact that enzymatic dissociation was used and the importance of the degree of cell-cell contact for a molecule like OPCML that might function via interactions *in trans*. Trypsin, which was the dissociation agent employed, has an effect on all cell surface molecules to varying degrees; however, it is assumed that consistently minimal exposure to trypsin, as was used in all the experiments described in this chapter, causes limited, if any, irreversible damage to cell surface molecules like OPCML, which is also stabilised by the attachment of the GPI anchor. Furthermore, the cells that were used in all the phenotypic assays had been seeded at standard and optimised densities to allow the appropriate degree of

confuency for each assay, but always more than 60% and less than 90%. Thus, lack of cell-cell contact has not been an issue.

OPCML is characterised by two intriguing features: it is a GPI-anchored protein (GPI-AP) and an immunoglobulin-like cell adhesion molecule (IgCAM). GPI-APs participate in a wide range of functions, from catalysis to adhesion[306]. Proteins tethered to the cell membrane by a GPI anchor are typically organised in membrane domains termed lipid rafts, which are thought to orchestrate the sorting of associated proteins and act as platforms for cell signalling[307]. There is a variety of GPI-APs that are implicated in cancer, such as the urokinase-type plasminogen activator receptor[308], GML, encoded by a p53-responsive gene[309] and HYAL2[310]. Roles of GPI-APs in cell-cell and cell-ECM adhesion[311], signal transduction[312] and invasion[313] are well documented. GPI-APs are extracellular, thus as signalling modulators they often interact *in cis* with transmembrane glycoproteins[314,315]. Furthermore, recent advances in our understanding of IgCAM biology have linked this important family of proteins with cell-cell and cell-matrix interactions, as well as cell signalling[316]. IgCAMs are able to associate with various membrane components *in cis*, such as growth factor receptors, integrins and cadherins. There also genes encoding IgCAMs that are down-regulated in diverse types of cancer; examples are *NCAM1*[317], *DCC*[318] and *CEACAM1*[319]. All these aspects of GPI-AP and IgCAM biology support the potential functions of OPCML identified in SKOV-3 cells and strengthen the hypothesis that it is a novel tumour suppressor gene in epithelial ovarian cancer.

Chapter 6

Conclusion

The conception of this project, which was inspired by earlier studies that identified *OPCML* as a novel tumour suppressor gene in epithelial ovarian cancer, was based on two broad objectives: the expression profiling of *OPCML* and other known members of the IgLON family in the mouse and human, and the functional characterisation of OPCML. Studies addressing both issues were designed in order to complement and expand on current knowledge. Functional studies relied on the creation and characterisation of suitable tools that would allow the examination of phenotypes incurred by the expression of *OPCML*.

The first major part of this work concerned the expression profiling of *OPCML* and the IgLON family in human cancer cell lines, in normal embryonic and adult tissues in the mouse and human and in ovarian cancer. Expression studies can be valuable in our understanding of the IgLON family, helping to further our knowledge and provide suggestions of potential functions. This is particularly useful with respect to a family that has been characterised in the brain mostly. So, what has been learnt from these diverse expression studies? Firstly, it has become evident that IgLON expression is not as restricted as previously thought. The IgLON genes might be primarily expressed in the nervous system, but are also expressed in other organ systems, an observation that suggests that they might have important functions outside the brain. It is known that in the brain IgLONs are involved in cell-cell recognition and cell adhesion, so it can be postulated that they could have similar functions in other localities. Furthermore, all IgLONs were shown to be developmentally regulated, a finding that reinforces previous knowledge and suggests that this family might be important in both developmental regulation and plasticity. Particularly pronounced was the developmental increase in expression of *Opcml* and *Negr1* in the mouse. With respect to *Opcml* specifically, this was also reflected on histological expression patterns, especially in the mouse. As embryonic development is longer in the human, the respective immunohistochemical detection of OPCML in human embryos has not identified high expression of the protein. A more thorough study of *OPCML* in human development is required, covering a broader period of embryonic and foetal life, although this might be difficult to achieve due to the restricted availability of human embryo sections. In addition, it

has been demonstrated that IgLON family members have both over-lapping and distinct expression patterns. At the level of the organ, there are examples wherein the family is expressed as a whole, such as the heart and the lung, again stressing that they must have important functions outside the brain. It is likely, however, that at a more narrow level, as in the individual cell type level, more divergence occurs, as has been previously reported. Moreover, this work has provided the first evidence of transcriptional coordination within the IgLON family. It has been shown that *OPCML* expression in three different ovarian cancer cell lines results in a decrease in the expression of both *LSAMP* and *NEGR1* at the RNA level. Additionally, the expressions of *LSAMP* and *NEGR1* exhibit a significant positive correlation, both in *OPCML*-transfected cell lines, but more importantly in normal and tumour ovarian samples. The significance of these trends is two-fold. They suggest that as a family, the IgLONs might share *cis* and/or *trans* regulatory elements. It is worth investigating in the future whether different transcription factors available in distinct tissue types could alter the expression relationships of the IgLON family. All the identified trends were in an ovarian context and they need to be investigated in other tissue types as well. The second important implication of these observations lies at the level of function: if IgLONs interact with each other then potential expression inter-relationships will have an impact on the availability of partners for the formation of functional complexes. Finally, we have established that in EOC it is not just *OPCML* that might be of relevance, but also the rest of the family. Like *OPCML*, *LSAMP* and *NEGR1* are down-regulated in sporadic EOC relative to the normal ovary, whilst *HNT* is up-regulated. Specific IgLONs are associated with distinct histological types of EOC. It is interesting to take a historical perspective of IgLON biology. The IgLON family was identified and has been typically studied in the brain. Subsequently, a study was reported that proposed *OPCML* as a TSG in sporadic EOC, followed by a second study proposing *LSAMP* in another type of cancer, clear cell renal cell carcinoma. Hence, it is becoming increasingly evident that the IgLON family might play diverse roles and might be associated with different types of cancer. OPCML in particular, was shown to be localised in the OSE, the site of origin of EOC, the site where it exhibits its strongest expression in the human ovary. This localisation is a prerequisite for the product of a TSG, which

is thought to be disrupted as an early event in ovarian tumourigenesis. Interestingly, OPCML also exhibits strong epithelial staining in other tissue types, such as the bladder.

Two distinct systems were used as means to study OPCML function. An inducible system of *OPCML* expression, based on the cervical cancer HeLa cell line was created and characterised so as to complement an over-expression system based on the ovarian cancer SKOV-3 cell line. Together, they provided *in vitro* models of gynaecological cancer from different perspectives. In developing the HeLa Tet-On system, the aim was to establish a resource that allows the regulated expression of *OPCML* exploiting the unparalleled advantages offered by inducible systems: expression at a defined level and lack of clonal variation. Despite the fact that the selected HeLa Tet-On OPCML clones had favourable inducibility profiles, as judged at both RNA and protein levels, the overall evaluation of this approach was not very promising. The clones were hampered by uninduced expression of *OPCML*, which was at a level not much lower to its expression in the ovary, indicating that even without induction functional protein was produced. In addition, differences between the HeLa and SKOV-3 cell lines were identified, highlighting the importance of context specificity. Disparity was evident both as expression of distinct OPCML glycoprotein species, but also as divergence in phenotype. In addition, HeLa and SKOV-3 cells differ in their complements of IgLONs. As a consequence, the creation of an ovarian cancer *in vitro* model was imperative. The SKOV-3 cell line was chosen as an obvious candidate, in view of its established use in the over-expression system. An inducible SKOV-3 resource will offer invaluable advantages in the study of genes associated with ovarian cancer, such as *OPCML*. This system was developed towards the end of this work, and was therefore not used in functional studies. Preliminary data suggest that the use of a second-generation response plasmid results in tighter regulation of *OPCML* expression, so it is expected that this system will lack the problems of uninduced expression that hampered the use of the HeLa Tet-On system. Overall, the use of inducible systems does entail counteracting numerous problems, mainly associated with "leakiness" and the

necessity of extensive screening; nonetheless, once established, these systems offer advantages that could not be offered by traditional over-expression *in vitro* models.

The second major part of this work was devoted in delineating the functions of OPCML, as a potential novel tumour suppressor in ovarian cancer. These studies were very important in thoroughly addressing for the first time the issue of OPCML function in an ovarian cancer model *in vitro*. The functional characterisation of OPCML has been very profitable. Several phenotypes were attributed to *OPCML* expression in SKOV-3 cells including an inhibitory effect on chemotactic migration and a stimulatory effect on adhesion to specific components of the extracellular matrix. Moreover, OPCML was shown to promote cell-cell adhesion, most likely by heterophilic interactions. The most significant finding, however, has been that OPCML has pro-apoptotic properties, which underlie the growth suppression phenotype that it incurs *in vitro*. Not only was OPCML found to play a pro-apoptotic role, but also, in so doing, it renders cells more chemosensitive to the cytotoxic drug camptothecin. If this effect were seen in response to additional drugs, then *OPCML* expression status might have considerable impact on patient outcome after chemotherapy in ovarian cancer. These identified functions reinforce the hypothesis that it acts as a tumour suppressor in ovarian cancer. In view of relevant aspects of GPI-AP and IgCAM biology as well as the biology of genes characterised by similar phenotypic profiles, the functions of OPCML imply that it participates in one or more signalling pathways; the identified phenotypes in adhesion, for example, have highlighted RHO signalling as one potential pathway.

Based on the above evidence, how can we accommodate *OPCML* in a model of ovarian tumourigenesis? It can be envisaged that in the normal ovary OPCML plays an important role in restricting cell growth as well as maintaining tissue architecture and confining OSE cells within their natural environment by cell-cell and cell-matrix interactions. It might also participate in the tissue remodelling that follows ovulation, as a response gene to pro-inflammatory cytokines such as IL-1β. In sporadic epithelial ovarian cancer, these functions are disturbed as *OPCML* expression is reduced or abolished, primarily by epigenetic silencing. Transformed

cells become less constrained and more migratory. By being less responsive to pro-apoptotic clues, they switch on survival pathways and can thus adapt to new circumstances. Participation of OPCML in cell signalling pathways almost certainly underlies these roles, which might be facilitated and/or stabilised by interactions with other members of the IgLON family.

Very recent evidence suggests that the expression of OPCML is likely to be influenced by hormones, such as oestrogen[320]. This new finding suggests that the link between OPCML and ovarian physiology might not only lie in the maintenance of tissue integrity, the regulation of cell growth, and the inflammatory response, but also in hormonal regulation, which is an additional facet to ovulation. As stressed previously, all these roles are likely to have a signalling component. This hypothesis is supported by a recent report that *OPCML* methylation and therefore expression status is affected by oncogenic RAS in OSE cells[321]. OPCML is a tumour suppressor gene silenced by methylation early and very frequently in the development of EOC, which makes it a good candidate marker, either alone or in combination with other methylated genes. Finally, the possibility of using a small mimetic molecule and thus replacing the lost functions of OPCML in ovarian cancer patients is very attractive as therapeutic intervention for the future. It remains to be established whether the loss of OPCML function occurs at a point of disease development that is reversible.

The observations and findings that this project has yielded pave the way that will eventually lead to a fuller understanding of OPCML and the IgLON family in normal physiology and cancer pathology. The work that was described and discussed in this thesis should be appreciated as a starting-point rather than an end in itself, as it has raised questions that need to be addressed in the future and has embraced only certain aspects of IgLON biology. The identified functions of OPCML need to be investigated further, in particular with respect to its specific involvement in apoptosis and potential cell signalling pathways. In regard with apoptosis, it would be worth examining the effect of OPCML using a different experimental approach, not based on the particular aspect of apoptosis which annexin V assays measure. With respect to cell signalling, potential pilot experiments could be designed focusing on pathways that were suggested by OPCML's identified functions, including the RHO

and PI3K pathways. Another promising approach to signalling studies could exploit the fact that OPCML is detected in lipid rafts and can therefore be isolated alongside other signalling molecules found in these domains. Proteomic identification of binding partners could discover interacting proteins and more importantly receptors that would be needed to convey signals intracellularly. Furthermore, an issue that has not been addressed in this work is that of alternative isoforms. Certain IgLON isoforms have been described in the literature; additionally, there is *in silico* evidence for the existence of more. What is not known, however, is whether these isoforms are differentially expressed in development and in adult tissues and more importantly if they have diverse functions. Hence, a number of the studies described in the previous chapters could be revisited in an isoform-specific manner. Moreover, a concept that is likely to contribute signficantly in future studies of IgLON function is that of interactions within the family. If IgLONs operate by forming heteromeric complexes, then future studies will have to account for this and be designed accordingly. It will become increasingly unfavourable to examine one family member in isolation, assuming it functionally depends on other IgLONs. Experiments could be based on *in vitro* models that either represent one particular IgLON only or a specific combination of IgLONs. Inducible systems are particularly suited for these kinds of experiments; a particular IgLON could be switched on at will against a defined complement of other IgLONs. Finally, the role of the IgLON family in ovarian and other types of human cancer needs to be addressed in a more thorough and systematic way. Intensification in the pursuit of IgLON function is imperative in order to assign the family roles in normal physiology and in cancer. More specifically, in the context of the human ovary, there is a need to understand the roles of OPCML and the other IgLONs, in adhesion, growth and any other aspect of their functions, by carefully-designed experiments that address these issues as well as the mechanisms underpinning them. If *OPCML* were confirmed to be a gene that is responsive to inflammatory clues, could the link between this gene and ovarian physiology lie in ovulation? The answers to this and the previous questions will hopefully provide suggestions of how loss of OPCML, LSAMP and NEGR1 function and over-expression of HNT contribute to ovarian carcinogenesis. Addressing all the aforementioned issues, of both expression and function, in

physiology and pathology, will not be a trivial task, as it will require a combination of approaches, but most importantly an increased awareness of the potential significance of the IgLON family outside the brain. Hopefully, this thesis has contributed towards this goal.

References

1. Pimenta, A. F. et al. The limbic system-associated membrane protein is an Ig superfamily member that mediates selective neuronal growth and axon targeting. *Neuron* **15**, 287-97 (1995).

2. Cho, T. M., Hasegawa, J., Ge, B. L. & Loh, H. H. Purification to apparent homogeneity of a mu-type opioid receptor from rat brain. *Proc Natl Acad Sci U S A* **83**, 4138-42 (1986).

3. Knapp, R. J. et al. Molecular biology and pharmacology of cloned opioid receptors. *Faseb J* **9**, 516-25 (1995).

4. Roy, S., Zhu, Y. X., Loh, H. H. & Lee, N. M. A monoclonal antibody that inhibits opioid binding to rat brain membranes. *Biochem Biophys Res Commun* **154**, 688-93 (1988).

5. Ann, D. K. et al. Specific reduction of delta-opioid receptor binding in transfected NG108-15 cells. *J Biol Chem* **267**, 7921-6 (1992).

6. Lane, C. M., Elde, R., Loh, H. H. & Lee, N. M. Regulation of an opioid-binding protein in NG108-15 cells parallels regulation of delta-opioid receptors. *Proc Natl Acad Sci U S A* **89**, 11234-8 (1992).

7. Lane, C. M., Jones, C. R., Reisine, T., Yu, L. & Lee, N. M. Alteration of OBCAM conformation as a result of opioid receptor expression and opioid ligand treatment. *Brain Res* **698**, 15-22 (1995).

8. Hachisuka, A., Yamazaki, T., Sawada, J. & Terao, T. Characterization and tissue distribution of opioid-binding cell adhesion molecule (OBCAM) using monoclonal antibodies. *Neurochem Int* **28**, 373-9 (1996).

9. Schofield, P. R. et al. Molecular characterization of a new immunoglobulin superfamily protein with potential roles in opioid binding and cell contact. *Embo J* **8**, 489-95 (1989).

10. Shark, K. B. & Lee, N. M. Cloning, sequencing and localization to chromosome 11 of a cDNA encoding a human opioid-binding cell adhesion molecule (OBCAM). *Gene* **155**, 213-7 (1995).

11. Lodge, A. P., Howard, M. R., McNamee, C. J. & Moss, D. J. Co-localisation, heterophilic interactions and regulated expression of IgLON family proteins in the chick nervous system. *Brain Res Mol Brain Res* **82**, 84-94 (2000).

12. Wick, M. J., Fan, G. & Loh, H. H. Expression of OBCAM-related cDNA clones in Cos 1 cells: evidence for a phosphatidylinositol linkage to the cell membrane. *Brain Res Mol Brain Res* **36**, 322-8 (1996).

13. Miyata, S., Taguchi, K. & Maekawa, S. Dendrite-associated opioid-binding cell adhesion molecule localizes at neurosecretory granules in the hypothalamic magnocellular neurons. *Neuroscience* **122**, 169-81 (2003).

14. Miyata, S. et al. Biochemical and ultrastructural analyses of IgLON cell adhesion molecules, Kilon and OBCAM in the rat brain. *Neuroscience* **117**, 645-58 (2003).

15. London, E. & Brown, D. A. Insolubility of lipids in triton X-100: physical origin and relationship to sphingolipid/cholesterol membrane domains (rafts). *Biochim Biophys Acta* **1508**, 182-95 (2000).

16. Pike, L. J. Lipid rafts: bringing order to chaos. *J Lipid Res* **44**, 655-67 (2003).

17. Simons, K. & Toomre, D. Lipid rafts and signal transduction. *Nat Rev Mol Cell Biol* **1**, 31-9 (2000).

18. Hachisuka, A., Nakajima, O., Yamazaki, T. & Sawada, J. Localization of opioid-binding cell adhesion molecule (OBCAM) in adult rat brain. *Brain Res* **842**, 482-6 (1999).

19. Miyata, S. et al. Expression of the IgLON cell adhesion molecules Kilon and OBCAM in hypothalamic magnocellular neurons. *J Comp Neurol* **424**, 74-85 (2000).

20. Miyata, S., Matsumoto, N. & Maekawa, S. Polarized targeting of IgLON cell adhesion molecule OBCAM to dendrites in cultured neurons. *Brain Res* **979**, 129-36 (2003).

21. Sellar, G. C. et al. OPCML at 11q25 is epigenetically inactivated and has tumor-suppressor function in epithelial ovarian cancer. *Nat Genet* **34**, 337-43 (2003).

22. Hachisuka, A., Nakajima, O., Yamazaki, T. & Sawada, J. Developmental expression of opioid-binding cell adhesion molecule (OBCAM) in rat brain. *Brain Res Dev Brain Res* **122**, 183-91 (2000).

23. McNamee, C. J., Reed, J. E., Howard, M. R., Lodge, A. P. & Moss, D. J. Promotion of neuronal cell adhesion by members of the IgLON family occurs in the absence of either support or modification of neurite outgrowth. *J Neurochem* **80**, 941-8 (2002).

24. Li, P. et al. Postnatal Expression Profile of OBCAM Implies its Involvement in Visual Cortex Development and Plasticity. *Cereb Cortex* (2005).

25. Prasad, S. S. et al. Gene expression patterns during enhanced periods of visual cortex plasticity. *Neuroscience* **111**, 35-45 (2002).

26. Vincenti, M. P. & Brinckerhoff, C. E. Early response genes induced in chondrocytes stimulated with the inflammatory cytokine interleukin-1beta. *Arthritis Res* **3**, 381-8 (2001).

27. Struyk, A. F. et al. Cloning of neurotrimin defines a new subfamily of differentially expressed neural cell adhesion molecules. *J Neurosci* **15**, 2141-56 (1995).

28. Spaltmann, F. & Brummendorf, T. CEPU-1, a novel immunoglobulin superfamily molecule, is expressed by developing cerebellar Purkinje cells. *J Neurosci* **16**, 1770-9 (1996).

29. Lodge, A. P., McNamee, C. J., Howard, M. R., Reed, J. E. & Moss, D. J. Identification and characterization of CEPU-Se-A secreted isoform of the IgLON family protein, CEPU-1. *Mol Cell Neurosci* **17**, 746-60 (2001).

30. Liu, J. et al. The cloning and preliminarily functional analysis of the human neurotrimin gene. *Sci China C Life Sci* **47**, 158-64 (2004).

31. Jungbluth, S., Phelps, C. & Lumsden, A. CEPU-1 expression in the early embryonic chick brain. *Mech Dev* **101**, 195-7 (2001).

32. Gil, O. D., Zanazzi, G., Struyk, A. F. & Salzer, J. L. Neurotrimin mediates bifunctional effects on neurite outgrowth via homophilic and heterophilic interactions. *J Neurosci* **18**, 9312-25 (1998).

33. Levitt, P. A monoclonal antibody to limbic system neurons. *Science* **223**, 299-301 (1984).

34. Pimenta, A. F., Fischer, I. & Levitt, P. cDNA cloning and structural analysis of the human limbic-system-associated membrane protein (LAMP). *Gene* **170**, 189-95 (1996).

35. Brummendorf, T., Spaltmann, F. & Treubert, U. Cloning and characterization of a neural cell recognition molecule on axons of the retinotectal system and spinal cord. *Eur J Neurosci* **9**, 1105-16 (1997).

36. Pimenta, A. F., Tsui, L. C., Heng, H. H. & Levitt, P. Assignment of the gene encoding the limbic system-associated membrane protein (LAMP) to mouse chromosome 16B5 and human chromosome 3q13.2-q21. *Genomics* **49**, 472-4 (1998).

37. Pimenta, A. F. & Levitt, P. Characterization of the genomic structure of the mouse limbic system-associated membrane protein (Lsamp) gene. *Genomics* **83**, 790-801 (2004).

38. Zacco, A. et al. Isolation, biochemical characterization and ultrastructural analysis of the limbic system-associated membrane protein (LAMP), a protein expressed by neurons comprising functional neural circuits. *J Neurosci* **10**, 73-90 (1990).

39. Reinoso, B. S., Pimenta, A. F. & Levitt, P. Expression of the mRNAs encoding the limbic system-associated membrane protein (LAMP): I. Adult rat brain. *J Comp Neurol* **375**, 274-88 (1996).

40. Cote, P. Y., Levitt, P. & Parent, A. Limbic system-associated membrane protein (LAMP) in primate amygdala and hippocampus. *Hippocampus* **6**, 483-94 (1996).

41. Hancox, K. A., Sheppard, A. M. & Jeffrey, P. L. Characterisation of a novel glycoprotein (AvGp50) in the avian nervous system, with a monoclonal antibody. *Brain Res Dev Brain Res* **70**, 25-37 (1992).

42. Yamamoto, K. & Reiner, A. Distribution of the limbic system-associated membrane protein (LAMP) in pigeon forebrain and midbrain. *J Comp Neurol* **486**, 221-42 (2005).

43. Chen, J. et al. The t(1;3) breakpoint-spanning genes LSAMP and NORE1 are involved in clear cell renal cell carcinomas. *Cancer Cell* **4**, 405-13 (2003).

44. Pimenta, A. F., Reinoso, B. S. & Levitt, P. Expression of the mRNAs encoding the limbic system-associated membrane protein (LAMP): II. Fetal rat brain. *J Comp Neurol* **375**, 289-302 (1996).

45. Horton, H. L. & Levitt, P. A unique membrane protein is expressed on early developing limbic system axons and cortical targets. *J Neurosci* **8**, 4653-61 (1988).

46. Barbe, M. F. & Levitt, P. The early commitment of fetal neurons to the limbic cortex. *J Neurosci* **11**, 519-33 (1991).

47. Kimura, Y., Katoh, A., Kaneko, T., Takahama, K. & Tanaka, H. Two members of the IgLON family are expressed in a restricted region of the developing chick brain and neural crest. *Dev Growth Differ* **43**, 257-63 (2001).

48. Mann, F., Zhukareva, V., Pimenta, A., Levitt, P. & Bolz, J. Membrane-associated molecules guide limbic and nonlimbic thalamocortical projections. *J Neurosci* **18**, 9409-19 (1998).

49. Zhukareva, V. & Levitt, P. The limbic system-associated membrane protein (LAMP) selectively mediates interactions with specific central neuron populations. *Development* **121**, 1161-72 (1995).

50. Zhukareva, V., Chernevskaya, N., Pimenta, A., Nowycky, M. & Levitt, P. Limbic system-associated membrane protein (LAMP) induces neurite outgrowth and intracellular Ca2+ increase in primary fetal neurons. *Mol Cell Neurosci* **10**, 43-55 (1997).

51. Eagleson, K. L. et al. Distinct domains of the limbic system-associated membrane protein (LAMP) mediate discrete effects on neurite outgrowth. *Mol Cell Neurosci* **24**, 725-40 (2003).

52. Marg, A. et al. Neurotractin, a novel neurite outgrowth-promoting Ig-like protein that interacts with CEPU-1 and LAMP. *J Cell Biol* **145**, 865-76 (1999).

53. Nelovkov, A., Philips, M. A., Koks, S. & Vasar, E. Rats with low exploratory activity in the elevated plus-maze have the increased expression of limbic system-associated membrane protein gene in the periaqueductal grey. *Neurosci Lett* **352**, 179-82 (2003).

54. Funatsu, N. et al. Characterization of a novel rat brain glycosylphosphatidylinositol-anchored protein (Kilon), a member of the IgLON cell adhesion molecule family. *J Biol Chem* **274**, 8224-30 (1999).

55. Brauer, A. U. et al. IG-molecule Kilon shows differential expression pattern from LAMP in the developing and adult rat hippocampus. *Hippocampus* **10**, 632-44 (2000).

56. Schafer, M., Brauer, A. U., Savaskan, N. E., Rathjen, F. G. & Brummendorf, T. Neurotractin/kilon promotes neurite outgrowth and is expressed on reactive astrocytes after entorhinal cortex lesion. *Mol Cell Neurosci* **29**, 580-90 (2005).

57. Reed, J., McNamee, C., Rackstraw, S., Jenkins, J. & Moss, D. Diglons are heterodimeric proteins composed of IgLON subunits, and Diglon-CO inhibits neurite outgrowth from cerebellar granule cells. *J Cell Sci* **117**, 3961-73 (2004).

58. Parkin, D. M., Pisani, P. & Ferlay, J. Global cancer statistics. *CA Cancer J Clin* **49**, 33-64, 1 (1999).

59. Runnebaum, I. B. & Stickeler, E. Epidemiological and molecular aspects of ovarian cancer risk. *J Cancer Res Clin Oncol* **127**, 73-9 (2001).

60. Wenham, R. M., Lancaster, J. M. & Berchuck, A. Molecular aspects of ovarian cancer. *Best Pract Res Clin Obstet Gynaecol* **16**, 483-97 (2002).

61. Stratton, J. F. et al. Contribution of BRCA1 mutations to ovarian cancer. *N Engl J Med* **336**, 1125-30 (1997).

62. Auersperg, N., Wong, A. S., Choi, K. C., Kang, S. K. & Leung, P. C. Ovarian surface epithelium: biology, endocrinology, and pathology. *Endocr Rev* **22**, 255-88 (2001).

63. Murdoch, W. J. & McDonnel, A. C. Roles of the ovarian surface epithelium in ovulation and carcinogenesis. *Reproduction* **123**, 743-50 (2002).

64. Choi, K. C. & Auersperg, N. The ovarian surface epithelium: simple source of a complex disease. *Minerva Ginecol* **55**, 297-314 (2003).

65. Kang, S. K. et al. Role of gonadotropin-releasing hormone as an autocrine growth factor in human ovarian surface epithelium. *Endocrinology* **141**, 72-80 (2000).

66. Karlan, B. Y., Jones, J., Greenwald, M. & Lagasse, L. D. Steroid hormone effects on the proliferation of human ovarian surface epithelium in vitro. *Am J Obstet Gynecol* **173**, 97-104 (1995).

67. Zheng, W., Magid, M. S., Kramer, E. E. & Chen, Y. T. Follicle-stimulating hormone receptor is expressed in human ovarian surface epithelium and fallopian tube. *Am J Pathol* **148**, 47-53 (1996).

68. Lau, K. M., Mok, S. C. & Ho, S. M. Expression of human estrogen receptor-alpha and -beta, progesterone receptor, and androgen receptor mRNA in normal and malignant ovarian epithelial cells. *Proc Natl Acad Sci U S A* **96**, 5722-7 (1999).

69. Siemens, C. H. & Auersperg, N. Serial propagation of human ovarian surface epithelium in tissue culture. *J Cell Physiol* **134**, 347-56 (1988).

70. Taipale, J., Saharinen, J. & Keski-Oja, J. Extracellular matrix-associated transforming growth factor-beta: role in cancer cell growth and invasion. *Adv Cancer Res* **75**, 87-134 (1998).

71. Ziltener, H. J., Maines-Bandiera, S., Schrader, J. W. & Auersperg, N. Secretion of bioactive interleukin-1, interleukin-6, and colony-stimulating factors by human ovarian surface epithelium. *Biol Reprod* **49**, 635-41 (1993).

72. Choi, K. C., Auersperg, N. & Leung, P. C. Mitogen-activated protein kinases in normal and (pre)neoplastic ovarian surface epithelium. *Reprod Biol Endocrinol* **1**, 71 (2003).

73. Van Niekerk, C. C., Ramaekers, F. C., Hanselaar, A. G., Aldeweireldt, J. & Poels, L. G. Changes in expression of differentiation markers between normal ovarian cells and derived tumors. *Am J Pathol* **142**, 157-77 (1993).

74. Kerbrat, P. et al. Ovarian cancer. *Br J Cancer* **84 Suppl 2**, 18-23 (2001).

75. Bast, R. C., Jr. et al. CA 125: the past and the future. *Int J Biol Markers* **13**, 179-87 (1998).

76. Ozols, R. F. Treatment goals in ovarian cancer. *Int J Gynecol Cancer* **15 Suppl 1**, 3-11 (2005).

77. Ozols, R. F. Update on the management of ovarian cancer. *Cancer J* **8 Suppl 1**, S22-30 (2002).

78. Trimbos, J. B. et al. International Collaborative Ovarian Neoplasm trial 1 and Adjuvant ChemoTherapy In Ovarian Neoplasm trial: two parallel randomized phase III trials of adjuvant chemotherapy in patients with early-stage ovarian carcinoma. *J Natl Cancer Inst* **95**, 105-12 (2003).

79. Ozols, R. F. et al. Phase III trial of carboplatin and paclitaxel compared with cisplatin and paclitaxel in patients with optimally resected stage III ovarian cancer: a Gynecologic Oncology Group study. *J Clin Oncol* **21**, 3194-200 (2003).

80. du Bois, A. et al. A randomized clinical trial of cisplatin/paclitaxel versus carboplatin/paclitaxel as first-line treatment of ovarian cancer. *J Natl Cancer Inst* **95**, 1320-9 (2003).

81. Cramer, D. W., Hutchison, G. B., Welch, W. R., Scully, R. E. & Ryan, K. J. Determinants of ovarian cancer risk. I. Reproductive experiences and family history. *J Natl Cancer Inst* **71**, 711-6 (1983).

82. Herbst, A. L. The epidemiology of ovarian carcinoma and the current status of tumor markers to detect disease. *Am J Obstet Gynecol* **170**, 1099-105; discussion 1105-7 (1994).

83. Fathalla, M. F. Incessant ovulation--a factor in ovarian neoplasia? *Lancet* **2**, 163 (1971).

84. Fredrickson, T. N. Ovarian tumors of the hen. *Environ Health Perspect* **73**, 35-51 (1987).

85. Eccles, D. M., Cranston, G., Steel, C. M., Nakamura, Y. & Leonard, R. C. Allele losses on chromosome 17 in human epithelial ovarian carcinoma. *Oncogene* **5**, 1599-601 (1990).

86. Russell, S. E., Hickey, G. I., Lowry, W. S., White, P. & Atkinson, R. J. Allele loss from chromosome 17 in ovarian cancer. *Oncogene* **5**, 1581-3 (1990).

87. Schildkraut, J. M., Bastos, E. & Berchuck, A. Relationship between lifetime ovulatory cycles and overexpression of mutant p53 in epithelial ovarian cancer. *J Natl Cancer Inst* **89**, 932-8 (1997).

88. Whittemore, A. S., Harris, R. & Itnyre, J. Characteristics relating to ovarian cancer risk: collaborative analysis of 12 US case-control studies. IV. The pathogenesis of epithelial ovarian cancer. Collaborative Ovarian Cancer Group. *Am J Epidemiol* **136**, 1212-20 (1992).

89. Risch, H. A., Weiss, N. S., Lyon, J. L., Daling, J. R. & Liff, J. M. Events of reproductive life and the incidence of epithelial ovarian cancer. *Am J Epidemiol* **117**, 128-39 (1983).

90. Cramer, D. W. & Welch, W. R. Determinants of ovarian cancer risk. II. Inferences regarding pathogenesis. *J Natl Cancer Inst* **71**, 717-21 (1983).

91. Helzlsouer, K. J. et al. Serum gonadotropins and steroid hormones and the development of ovarian cancer. *Jama* **274**, 1926-30 (1995).

92. Ho, S. M. Estrogen, progesterone and epithelial ovarian cancer. *Reprod Biol Endocrinol* **1**, 73 (2003).

93. Risch, H. A. Hormonal etiology of epithelial ovarian cancer, with a hypothesis concerning the role of androgens and progesterone. *J Natl Cancer Inst* **90**, 1774-86 (1998).

94. Ness, R. B. & Cottreau, C. Possible role of ovarian epithelial inflammation in ovarian cancer. *J Natl Cancer Inst* **91**, 1459-67 (1999).

95. Graham, J. & Graham, R. Ovarian cancer and asbestos. *Environ Res* **1**, 115-28 (1967).

96. Cramer, D. W., Welch, W. R., Scully, R. E. & Wojciechowski, C. A. Ovarian cancer and talc: a case-control study. *Cancer* **50**, 372-6 (1982).

97. Brinton, L. A., Gridley, G., Persson, I., Baron, J. & Bergqvist, A. Cancer risk after a hospital discharge diagnosis of endometriosis. *Am J Obstet Gynecol* **176**, 572-9 (1997).

98. Risch, H. A. & Howe, G. R. Pelvic inflammatory disease and the risk of epithelial ovarian cancer. *Cancer Epidemiol Biomarkers Prev* **4**, 447-51 (1995).

99. Rosenblatt, K. A. & Thomas, D. B. Reduced risk of ovarian cancer in women with a tubal ligation or hysterectomy. The World Health Organization Collaborative Study of Neoplasia and Steroid Contraceptives. *Cancer Epidemiol Biomarkers Prev* **5**, 933-5 (1996).

100. Auersperg, N., Maines-Bandiera, S. L. & Dyck, H. G. Ovarian carcinogenesis and the biology of ovarian surface epithelium. *J Cell Physiol* **173**, 261-5 (1997).

101. Espey, L. L. Current status of the hypothesis that mammalian ovulation is comparable to an inflammatory reaction. *Biol Reprod* **50**, 233-8 (1994).

102. Auersperg, N., Ota, T. & Mitchell, G. W. Early events in ovarian epithelial carcinogenesis: progress and problems in experimental approaches. *Int J Gynecol Cancer* **12**, 691-703 (2002).

103. Feeley, K. M. & Wells, M. Precursor lesions of ovarian epithelial malignancy. *Histopathology* **38**, 87-95 (2001).

104. Dubeau, L. The cell of origin of ovarian epithelial tumors and the ovarian surface epithelium dogma: does the emperor have no clothes? *Gynecol Oncol* **72**, 437-42 (1999).

105. Maines-Bandiera, S. L. & Auersperg, N. Increased E-cadherin expression in ovarian surface epithelium: an early step in metaplasia and dysplasia? *Int J Gynecol Pathol* **16**, 250-5 (1997).

106. Huntsman, D., Resau, J. H., Klineberg, E. & Auersperg, N. Comparison of c-met expression in ovarian epithelial tumors and normal epithelia of the female reproductive tract by quantitative laser scan microscopy. *Am J Pathol* **155**, 343-8 (1999).

107. Takeichi, M. Morphogenetic roles of classic cadherins. *Curr Opin Cell Biol* **7**, 619-27 (1995).

108. Huber, O. et al. Nuclear localization of beta-catenin by interaction with transcription factor LEF-1. *Mech Dev* **59**, 3-10 (1996).

109. Sundfeldt, K. et al. E-cadherin expression in human epithelial ovarian cancer and normal ovary. *Int J Cancer* **74**, 275-80 (1997).

110. Hashimoto, M., Niwa, O., Nitta, Y., Takeichi, M. & Yokoro, K. Unstable expression of E-cadherin adhesion molecules in metastatic ovarian tumor cells. *Jpn J Cancer Res* **80**, 459-63 (1989).

111. Inoue, M., Ogawa, H., Miyata, M., Shiozaki, H. & Tanizawa, O. Expression of E-cadherin in normal, benign, and malignant tissues of female genital organs. *Am J Clin Pathol* **98**, 76-80 (1992).

112. Darai, E. et al. Expression of cadherins in benign, borderline, and malignant ovarian epithelial tumors: a clinicopathologic study of 60 cases. *Hum Pathol* **28**, 922-8 (1997).

113. Fujimoto, J., Ichigo, S., Hirose, R., Sakaguchi, H. & Tamaya, T. Expression of E-cadherin and alpha- and beta-catenin mRNAs in ovarian cancers. *Cancer Lett* **115**, 207-12 (1997).

114. Auersperg, N. et al. E-cadherin induces mesenchymal-to-epithelial transition in human ovarian surface epithelium. *Proc Natl Acad Sci U S A* **96**, 6249-54 (1999).

115. Orsulic, S. et al. Induction of ovarian cancer by defined multiple genetic changes in a mouse model system. *Cancer Cell* **1**, 53-62 (2002).

116. Connolly, D. C. et al. Female mice chimeric for expression of the simian virus 40 TAg under control of the MISIIR promoter develop epithelial ovarian cancer. *Cancer Res* **63**, 1389-97 (2003).

117. Flesken-Nikitin, A., Choi, K. C., Eng, J. P., Shmidt, E. N. & Nikitin, A. Y. Induction of carcinogenesis by concurrent inactivation of p53 and Rb1 in the mouse ovarian surface epithelium. *Cancer Res* **63**, 3459-63 (2003).

118. Powell, D. E., Puls, L. & van Nagell, J., Jr. Current concepts in epithelial ovarian tumors: does benign to malignant transformation occur? *Hum Pathol* **23**, 846-7 (1992).

119. Link, C. J., Jr., Kohn, E. & Reed, E. The relationship between borderline ovarian tumors and epithelial ovarian carcinoma: epidemiologic, pathologic, and molecular aspects. *Gynecol Oncol* **60**, 347-54 (1996).

120. Wolf, N. G., Abdul-Karim, F. W., Schork, N. J. & Schwartz, S. Origins of heterogeneous ovarian carcinomas. A molecular cytogenetic analysis of histologically benign, low malignant potential, and fully malignant components. *Am J Pathol* **149**, 511-20 (1996).

121. Bell, D. A. & Scully, R. E. Early de novo ovarian carcinoma. A study of fourteen cases. *Cancer* **73**, 1859-64 (1994).

122. Wolf, N. G. et al. Analysis of ovarian borderline tumors using comparative genomic hybridization and fluorescence in situ hybridization. *Genes Chromosomes Cancer* **25**, 307-15 (1999).

123. Hu, J., Khanna, V., Jones, M. M. & Surti, U. Genomic imbalances in ovarian borderline serous and mucinous tumors. *Cancer Genet Cytogenet* **139**, 18-23 (2002).

124. Singer, G., Kurman, R. J., Chang, H. W., Cho, S. K. & Shih Ie, M. Diverse tumorigenic pathways in ovarian serous carcinoma. *Am J Pathol* **160**, 1223-8 (2002).

125. Tibiletti, M. G. et al. Genetic and cytogenetic observations among different types of ovarian tumors are compatible with a progression model underlying ovarian tumorigenesis. *Cancer Genet Cytogenet* **146**, 145-53 (2003).

126. Shih Ie, M. & Kurman, R. J. Ovarian tumorigenesis: a proposed model based on morphological and molecular genetic analysis. *Am J Pathol* **164**, 1511-8 (2004).

127. Schwartz, D. R. et al. Gene expression in ovarian cancer reflects both morphology and biological behavior, distinguishing clear cell from other poor-prognosis ovarian carcinomas. *Cancer Res* **62**, 4722-9 (2002).

128. Ono, K. et al. Identification by cDNA microarray of genes involved in ovarian carcinogenesis. *Cancer Res* **60**, 5007-11 (2000).

129. Jacobs, I. J. et al. Clonal origin of epithelial ovarian carcinoma: analysis by loss of heterozygosity, p53 mutation, and X-chromosome inactivation. *J Natl Cancer Inst* **84**, 1793-8 (1992).

130. Godwin, A. K. et al. Spontaneous transformation of rat ovarian surface epithelial cells: association with cytogenetic changes and implications of repeated ovulation in the etiology of ovarian cancer. *J Natl Cancer Inst* **84**, 592-601 (1992).

131. Pharoah, P. D. & Ponder, B. A. The genetics of ovarian cancer. *Best Pract Res Clin Obstet Gynaecol* **16**, 449-68 (2002).

132. Kote-Jarai, Z. & Eeles, R. A. BRCA1, BRCA2 and their possible function in DNA damage response. *Br J Cancer* **81**, 1099-102 (1999).

133. Sowter, H. M. & Ashworth, A. BRCA1 and BRCA2 as ovarian cancer susceptibility genes. *Carcinogenesis* **26**, 1651-6 (2005).

134. Tutt, A. & Ashworth, A. The relationship between the roles of BRCA genes in DNA repair and cancer predisposition. *Trends Mol Med* **8**, 571-6 (2002).

135. Sharan, S. K. et al. Embryonic lethality and radiation hypersensitivity mediated by Rad51 in mice lacking Brca2. *Nature* **386**, 804-10 (1997).

136. Kerr, P. & Ashworth, A. New complexities for BRCA1 and BRCA2. *Curr Biol* **11**, R668-76 (2001).

137. Venkitaraman, A. R. Cancer susceptibility and the functions of BRCA1 and BRCA2. *Cell* **108**, 171-82 (2002).

138. Venkitaraman, A. R. Tracing the network connecting BRCA and Fanconi anaemia proteins. *Nat Rev Cancer* **4**, 266-76 (2004).

139. Miki, Y. et al. A strong candidate for the breast and ovarian cancer susceptibility gene BRCA1. *Science* **266**, 66-71 (1994).

140. Wooster, R. et al. Identification of the breast cancer susceptibility gene BRCA2. *Nature* **378**, 789-92 (1995).

141. Whittemore, A. S., Gong, G. & Itnyre, J. Prevalence and contribution of BRCA1 mutations in breast cancer and ovarian cancer: results from three U.S. population-based case-control studies of ovarian cancer. *Am J Hum Genet* **60**, 496-504 (1997).

142. Frank, T. S. Hereditary Risk of Breast and Ovarian Carcinoma: The Role of the Oncologist. *Oncologist* **3**, 403-412 (1998).

143. Lubinski, J. et al. Cancer variation associated with the position of the mutation in the BRCA2 gene. *Fam Cancer* **3**, 1-10 (2004).

144. Risch, H. A. et al. Prevalence and penetrance of germline BRCA1 and BRCA2 mutations in a population series of 649 women with ovarian cancer. *Am J Hum Genet* **68**, 700-10 (2001).

145. Wheeler, J. M., Bodmer, W. F. & Mortensen, N. J. DNA mismatch repair genes and colorectal cancer. *Gut* **47**, 148-53 (2000).

146. Aarnio, M. et al. Cancer risk in mutation carriers of DNA-mismatch-repair genes. *Int J Cancer* **81**, 214-8 (1999).

147. Campbell, I. G., Eccles, D. M., Dunn, B., Davis, M. & Leake, V. p53 polymorphism in ovarian and breast cancer. *Lancet* **347**, 393-4 (1996).

148. Hengstler, J. G. et al. Glutathione S-transferase T1 and M1 gene defects in ovarian carcinoma. *Cancer Lett* **130**, 43-8 (1998).

149. Weitzel, J. N. et al. The HRAS1 minisatellite locus and risk of ovarian cancer. *Cancer Res* **60**, 259-61 (2000).

150. Lancaster, J. M. et al. BRCA2 mutations in primary breast and ovarian cancers. *Nat Genet* **13**, 238-40 (1996).

151. Takahashi, H. et al. Mutation analysis of the BRCA1 gene in ovarian cancers. *Cancer Res* **55**, 2998-3002 (1995).

152. Chan, K. Y., Ozcelik, H., Cheung, A. N., Ngan, H. Y. & Khoo, U. S. Epigenetic factors controlling the BRCA1 and BRCA2 genes in sporadic ovarian cancer. *Cancer Res* **62**, 4151-6 (2002).

153. Auersperg, N., Edelson, M. I., Mok, S. C., Johnson, S. W. & Hamilton, T. C. The biology of ovarian cancer. *Semin Oncol* **25**, 281-304 (1998).

154. Liu, Y. & Ganesan, T. S. Tumour suppressor genes in sporadic epithelial ovarian cancer. *Reproduction* **123**, 341-53 (2002).

155. Bargmann, C. I., Hung, M. C. & Weinberg, R. A. The neu oncogene encodes an epidermal growth factor receptor-related protein. *Nature* **319**, 226-30 (1986).

156. Rubin, I. & Yarden, Y. The basic biology of HER2. *Ann Oncol* **12 Suppl 1**, S3-8 (2001).

157. Verri, E. et al. HER2/neu oncoprotein overexpression in epithelial ovarian cancer: evaluation of its prevalence and prognostic significance. Clinical study. *Oncology* **68**, 154-61 (2005).

158. Davies, B. R., Auersperg, N., Worsley, S. D. & Ponder, B. A. Transfection of rat ovarian surface epithelium with erb-B2/neu induces transformed phenotypes in vitro and the tumorigenic phenotype in vivo. *Am J Pathol* **152**, 297-306 (1998).

159. Cox, A. D. & Der, C. J. The dark side of Ras: regulation of apoptosis. *Oncogene* **22**, 8999-9006 (2003).

160. Macaluso, M. et al. Ras family genes: an interesting link between cell cycle and cancer. *J Cell Physiol* **192**, 125-30 (2002).

161. Kerkhoff, E. & Rapp, U. R. Cell cycle targets of Ras/Raf signalling. *Oncogene* **17**, 1457-62 (1998).

162. Hofseth, L. J., Hussain, S. P. & Harris, C. C. p53: 25 years after its discovery. *Trends Pharmacol Sci* **25**, 177-81 (2004).

163. Sengupta, S. & Harris, C. C. p53: traffic cop at the crossroads of DNA repair and recombination. *Nat Rev Mol Cell Biol* **6**, 44-55 (2005).

164. Chu, E. C. & Tarnawski, A. S. PTEN regulatory functions in tumor suppression and cell biology. *Med Sci Monit* **10**, RA235-41 (2004).

165. Lee, J. O. et al. Crystal structure of the PTEN tumor suppressor: implications for its phosphoinositide phosphatase activity and membrane association. *Cell* **99**, 323-34 (1999).

166. Cantley, L. C. & Neel, B. G. New insights into tumor suppression: PTEN suppresses tumor formation by restraining the phosphoinositide 3-kinase/AKT pathway. *Proc Natl Acad Sci U S A* **96**, 4240-5 (1999).

167. Ali, I. U., Schriml, L. M. & Dean, M. Mutational spectra of PTEN/MMAC1 gene: a tumor suppressor with lipid phosphatase activity. *J Natl Cancer Inst* **91**, 1922-32 (1999).

168. Maxwell, G. L. et al. Mutation of the PTEN tumor suppressor gene is not a feature of ovarian cancers. *Gynecol Oncol* **70**, 13-6 (1998).

169. Kurose, K. et al. Frequent loss of PTEN expression is linked to elevated phosphorylated Akt levels, but not associated with p27 and cyclin D1 expression, in primary epithelial ovarian carcinomas. *Am J Pathol* **158**, 2097-106 (2001).

170. Minaguchi, T. et al. Growth suppression of human ovarian cancer cells by adenovirus-mediated transfer of the PTEN gene. *Cancer Res* **59**, 6063-7 (1999).

171. Saga, Y., Mizukami, H., Takei, Y., Ozawa, K. & Suzuki, M. Suppression of cell migration in ovarian cancer cells mediated by PTEN overexpression. *Int J Oncol* **23**, 1109-13 (2003).

172. Cheng, J. Q. et al. AKT2, a putative oncogene encoding a member of a subfamily of protein-serine/threonine kinases, is amplified in human ovarian carcinomas. *Proc Natl Acad Sci U S A* **89**, 9267-71 (1992).

173. Bellacosa, A. et al. Molecular alterations of the AKT2 oncogene in ovarian and breast carcinomas. *Int J Cancer* **64**, 280-5 (1995).

174. Ho, C. L., Kurman, R. J., Dehari, R., Wang, T. L. & Shih Ie, M. Mutations of BRAF and KRAS precede the development of ovarian serous borderline tumors. *Cancer Res* **64**, 6915-8 (2004).

175. Worsley, S. D., Ponder, B. A. & Davies, B. R. Overexpression of cyclin D1 in epithelial ovarian cancers. *Gynecol Oncol* **64**, 189-95 (1997).

176. Shigemasa, K. et al. Cyclin D1 overexpression and p53 mutation status in epithelial ovarian cancer. *J Soc Gynecol Investig* **6**, 102-8 (1999).

177. Dimova, I. et al. Association of CyclinD1 copy number changes with histological type in ovarian tumors. *Acta Oncol* **43**, 675-9 (2004).

178. Anand, N. et al. Protein elongation factor EEF1A2 is a putative oncogene in ovarian cancer. *Nat Genet* **31**, 301-5 (2002).

179. Guan, X. Y. et al. Oncogenic role of eIF-5A2 in the development of ovarian cancer. *Cancer Res* **64**, 4197-200 (2004).

180. Hruza, C. et al. HER-2 and INT-2 amplification estimated by quantitative PCR in paraffin-embedded ovarian cancer tissue samples. *Eur J Cancer* **29A**, 1593-7 (1993).

181. Bian, M., Fan, Q., Huang, S., Ma, J. & Lang, J. Amplifications of proto-oncogenes in ovarian carcinoma. *Chin Med J (Engl)* **108**, 844-8 (1995).

182. Afify, A. M., Werness, B. A. & Mark, H. F. HER-2/neu oncogene amplification in stage I and stage III ovarian papillary serous carcinoma. *Exp Mol Pathol* **66**, 163-9 (1999).

183. Anreder, M. B., Freeman, S. M., Merogi, A., Halabi, S. & Marrogi, A. J. p53, c-erbB2, and PCNA status in benign, proliferative and malignant ovarian surface epithelial neoplasms: a study of 75 cases. *Arch Pathol Lab Med* **123**, 310-6 (1999).

184. Seki, A. et al. Detection of c-erbB-2 and FGF-3 (INT-2) gene amplification in epithelial ovarian cancer. *Int J Oncol* **17**, 103-6 (2000).

185. Fukushi, Y. et al. Detection of numerical aberration in chromosome 17 and c-erbB2 gene amplification in epithelial ovarian cancer using recently established dual color FISH. *Eur J Gynaecol Oncol* **22**, 23-5 (2001).

186. Ginath, S. et al. Expression of heparanase, Mdm2, and erbB2 in ovarian cancer. *Int J Oncol* **18**, 1133-44 (2001).

187. Iwamoto, H., Fukasawa, H., Honda, T., Hirata, S. & Hoshi, K. HER-2/neu expression in ovarian clear cell carcinomas. *Int J Gynecol Cancer* **13**, 28-31 (2003).

188. Yang, G., Cai, K. Q., Thompson-Lanza, J. A., Bast, R. C., Jr. & Liu, J. Inhibition of breast and ovarian tumor growth through multiple signaling pathways by using retrovirus-mediated small interfering RNA against Her-2/neu gene expression. *J Biol Chem* **279**, 4339-45 (2004).

189. Yang, G., Thompson, J. A., Fang, B. & Liu, J. Silencing of H-ras gene expression by retrovirus-mediated siRNA decreases transformation efficiency and tumorgrowth in a model of human ovarian cancer. *Oncogene* **22**, 5694-701 (2003).

190. Lassus, H. et al. Genetic alterations and protein expression of KIT and PDGFRA in serous ovarian carcinoma. *Br J Cancer* **91**, 2048-55 (2004).

191. Mok, S. C. et al. Mutation of K-ras protooncogene in human ovarian epithelial tumors of borderline malignancy. *Cancer Res* **53**, 1489-92 (1993).

192. Fujita, M. et al. Alteration of the p53 tumor suppressor gene occurs independently of K-ras activation and more frequently in serous adenocarcinomas than in other common epithelial tumors of the human ovary. *Jpn J Cancer Res* **85**, 1247-56 (1994).

193. Cuatrecasas, M., Villanueva, A., Matias-Guiu, X. & Prat, J. K-ras mutations in mucinous ovarian tumors: a clinicopathologic and molecular study of 95 cases. *Cancer* **79**, 1581-6 (1997).

194. Haas, C. J., Diebold, J., Hirschmann, A., Rohrbach, H. & Lohrs, U. In serous ovarian neoplasms the frequency of Ki-ras mutations correlates with their malignant potential. *Virchows Arch* **434**, 117-20 (1999).

195. Morita, K. et al. Incidence of P53 and K-ras alterations in ovarian mucinous and serous tumors. *Pathol Int* **50**, 219-23 (2000).

196. Suzuki, M., Saito, S., Saga, Y., Ohwada, M. & Sato, I. Mutation of K-RAS protooncogene and loss of heterozygosity on 6q27 in serous and mucinous ovarian carcinomas. *Cancer Genet Cytogenet* **118**, 132-5 (2000).

197. Garrett, A. P. et al. k-ras mutation may be an early event in mucinous ovarian tumorigenesis. *Int J Gynecol Pathol* **20**, 244-51 (2001).

198. Gemignani, M. L. et al. Role of KRAS and BRAF gene mutations in mucinous ovarian carcinoma. *Gynecol Oncol* **90**, 378-81 (2003).

199. Hogdall, E. V. et al. K-ras alterations in Danish ovarian tumour patients. From the Danish "Malova" Ovarian Cancer study. *Gynecol Oncol* **89**, 31-6 (2003).

200. Semczuk, A. et al. K-ras gene point mutations and p21ras immunostaining in human ovarian tumors. *Eur J Gynaecol Oncol* **25**, 484-8 (2004).

201. Maggiora, P. et al. The RON and MET oncogenes are co-expressed in human ovarian carcinomas and cooperate in activating invasiveness. *Exp Cell Res* **288**, 382-9 (2003).

202. Baker, V. V. et al. c-myc amplification in ovarian cancer. *Gynecol Oncol* **38**, 340-2 (1990).

203. Tashiro, H., Miyazaki, K., Okamura, H., Iwai, A. & Fukumoto, M. c-myc over-expression in human primary ovarian tumours: its relevance to tumour progression. *Int J Cancer* **50**, 828-33 (1992).

204. Diebold, J. et al. DNA ploidy and MYC DNA amplification in ovarian carcinomas. Correlation with p53 and bcl-2 expression, proliferative activity and prognosis. *Virchows Arch* **429**, 221-7 (1996).

205. Wu, R. et al. Amplification and overexpression of the L-MYC proto-oncogene in ovarian carcinomas. *Am J Pathol* **162**, 1603-10 (2003).

206. Schraml, P. et al. Combined array comparative genomic hybridization and tissue microarray analysis suggest PAK1 at 11q13.5-q14 as a critical oncogene target in ovarian carcinoma. *Am J Pathol* **163**, 985-92 (2003).

207. Shayesteh, L. et al. PIK3CA is implicated as an oncogene in ovarian cancer. *Nat Genet* **21**, 99-102 (1999).

208. Campbell, I. G. et al. Mutation of the PIK3CA gene in ovarian and breast cancer. *Cancer Res* **64**, 7678-81 (2004).

209. Philp, A. J. et al. The phosphatidylinositol 3'-kinase p85alpha gene is an oncogene in human ovarian and colon tumors. *Cancer Res* **61**, 7426-9 (2001).

210. Shigemasa, K. et al. Expression of cyclooxygenase-2 and its relationship to p53 accumulation in ovarian adenocarcinomas. *Int J Oncol* **22**, 99-105 (2003).

211. Erkinheimo, T. L. et al. Elevated cyclooxygenase-2 expression is associated with altered expression of p53 and SMAD4, amplification of HER-2/neu, and poor outcome in serous ovarian carcinoma. *Clin Cancer Res* **10**, 538-45 (2004).

212. Drapkin, R. et al. Human epididymis protein 4 (HE4) is a secreted glycoprotein that is overexpressed by serous and endometrioid ovarian carcinomas. *Cancer Res* **65**, 2162-9 (2005).

213. Rosen, D. G. et al. Expression of the tumor suppressor gene ARHI in epithelial ovarian cancer is associated with increased expression of p21WAF1/CIP1 and prolonged progression-free survival. *Clin Cancer Res* **10**, 6559-66 (2004).

214. Wehrli, B. M., Krajewski, S., Gascoyne, R. D., Reed, J. C. & Gilks, C. B. Immunohistochemical analysis of bcl-2, bax, mcl-1, and bcl-X expression in ovarian surface epithelial tumors. *Int J Gynecol Pathol* **17**, 255-60 (1998).

215. Wiechen, K. et al. Caveolin-1 is down-regulated in human ovarian carcinoma and acts as a candidate tumor suppressor gene. *Am J Pathol* **159**, 1635-43 (2001).

216. Liu, F. S. et al. Frequent down-regulation and lack of mutation of the KAI1 metastasis suppressor gene in epithelial ovarian carcinoma. *Gynecol Oncol* **78**, 10-5 (2000).

217. Fujita, M. et al. Alteration of p16 and p15 genes in common epithelial ovarian tumors. *Int J Cancer* **74**, 148-55 (1997).

218. Kanuma, T., Nishida, J., Gima, T., Barrett, J. C. & Wake, N. Alterations of the p16INK4A gene in human ovarian cancers. *Mol Carcinog* **18**, 134-41 (1997).

219. Marchini, S., Codegoni, A. M., Bonazzi, C., Chiari, S. & Broggini, M. Absence of deletions but frequent loss of expression of p16INK4 in human ovarian tumours. *Br J Cancer* **76**, 146-9 (1997).

220. Niederacher, D., Yan, H. Y., An, H. X., Bender, H. G. & Beckmann, M. W. CDKN2A gene inactivation in epithelial sporadic ovarian cancer. *Br J Cancer* **80**, 1920-6 (1999).

221. Havrilesky, L. J., Alvarez, A. A., Whitaker, R. S., Marks, J. R. & Berchuck, A. Loss of expression of the p16 tumor suppressor gene is more frequent in advanced ovarian cancers lacking p53 mutations. *Gynecol Oncol* **83**, 491-500 (2001).

222. Katsaros, D. et al. Methylation of tumor suppressor gene p16 and prognosis of epithelial ovarian cancer. *Gynecol Oncol* **94**, 685-92 (2004).

223. Saegusa, M., Machida, D. & Okayasu, I. Loss of DCC gene expression during ovarian tumorigenesis: relation to tumour differentiation and progression. *Br J Cancer* **82**, 571-8 (2000).

224. Yu, Y. et al. NOEY2 (ARHI), an imprinted putative tumor suppressor gene in ovarian and breast carcinomas. *Proc Natl Acad Sci U S A* **96**, 214-9 (1999).

225. Mok, S. C. et al. DOC-2, a candidate tumor suppressor gene in human epithelial ovarian cancer. *Oncogene* **16**, 2381-7 (1998).

226. Bruening, W. et al. Expression of OVCA1, a candidate tumor suppressor, is reduced in tumors and inhibits growth of ovarian cancer cells. *Cancer Res* **59**, 4973-83 (1999).

227. Chien, J. et al. A candidate tumor suppressor HtrA1 is downregulated in ovarian cancer. *Oncogene* **23**, 1636-44 (2004).

228. Yamada, S. D. et al. Mitogen-activated protein kinase kinase 4 (MKK4) acts as a metastasis suppressor gene in human ovarian carcinoma. *Cancer Res* **62**, 6717-23 (2002).

229. Yanaihara, N. et al. Reduced expression of MYO18B, a candidate tumor-suppressor gene on chromosome arm 22q, in ovarian cancer. *Int J Cancer* **112**, 150-4 (2004).

230. Cvetkovic, D., Pisarcik, D., Lee, C., Hamilton, T. C. & Abdollahi, A. Altered expression and loss of heterozygosity of the LOT1 gene in ovarian cancer. *Gynecol Oncol* **95**, 449-55 (2004).

231. Kamikihara, T. et al. Epigenetic silencing of the imprinted gene ZAC by DNA methylation is an early event in the progression of human ovarian cancer. *Int J Cancer* **115**, 690-700 (2005).

232. Deng, Q. & Huang, S. PRDM5 is silenced in human cancers and has growth suppressive activities. *Oncogene* **23**, 4903-10 (2004).

233. Obata, K. et al. Frequent PTEN/MMAC mutations in endometrioid but not serous or mucinous epithelial ovarian tumors. *Cancer Res* **58**, 2095-7 (1998).

234. Saito, M. et al. Allelic imbalance and mutations of the PTEN gene in ovarian cancer. *Int J Cancer* **85**, 160-5 (2000).

235. Chen, Y., Zheng, H., Yang, X., Sun, L. & Xin, Y. Effects of mutation and expression of PTEN gene mRNA on tumorigenesis and progression of epithelial ovarian cancer. *Chin Med Sci J* **19**, 25-30 (2004).

236. Akahira, J. et al. Promoter methylation status and expression of TMS1 gene in human epithelial ovarian cancer. *Cancer Sci* **95**, 40-3 (2004).

237. Taylor, R. R. et al. Abnormal expression of the retinoblastoma gene in ovarian neoplasms and correlation to p53 and K-ras mutations. *Gynecol Oncol* **58**, 307-11 (1995).

238. Acquati, F. et al. Cloning and characterization of a senescence inducing and class II tumor suppressor gene in ovarian carcinoma at chromosome region 6q27. *Oncogene* **20**, 980-8 (2001).

239. Acquati, F. et al. Tumor and metastasis suppression by the human RNASET2 gene. *Int J Oncol* **26**, 1159-68 (2005).

240. Burrows, J. F. et al. Altered expression of the septin gene, SEPT9, in ovarian neoplasia. *J Pathol* **201**, 581-8 (2003).

241. Takada, T. et al. Methylation-associated silencing of the Wnt antagonist SFRP1 gene in human ovarian cancers. *Cancer Sci* **95**, 741-4 (2004).

242. Takakura, S. et al. Allelic imbalance in chromosome band 18q21 and SMAD4 mutations in ovarian cancers. *Genes Chromosomes Cancer* **24**, 264-71 (1999).

243. Mok, S. C., Chan, W. Y., Wong, K. K., Muto, M. G. & Berkowitz, R. S. SPARC, an extracellular matrix protein with tumor-suppressing activity in human ovarian epithelial cells. *Oncogene* **12**, 1895-901 (1996).

244. Lauffart, B. et al. Aberrations of TACC1 and TACC3 are associated with ovarian cancer. *BMC Womens Health* **5**, 8 (2005).

245. Chien, J. et al. Epigenetic silencing of TCEAL7 (Bex4) in ovarian cancer. *Oncogene* **24**, 5089-100 (2005).

246. Sumigama, S. et al. Suppression of invasion and peritoneal carcinomatosis of ovarian cancer cells by overexpression of AP-2alpha. *Oncogene* **23**, 5496-504 (2004).

247. Goff, B. A. et al. Overexpression and relationships of HER-2/neu, epidermal growth factor receptor, p53, Ki-67, and tumor necrosis factor alpha in epithelial ovarian cancer. *Eur J Gynaecol Oncol* **17**, 487-92 (1996).

248. Murphy, M., McManus, D. T., Toner, P. G. & Russell, S. E. TP53 mutation in ovarian carcinoma. *Eur J Cancer* **33**, 1281-3 (1997).

249. Tworek, H. et al. Mutation analysis of BRCA1, TP53, and KRAS2 in ovarian and related pelvic tumors. *Cancer Genet Cytogenet* **112**, 105-18 (1999).

250. Wen, W. H. et al. p53 mutations and expression in ovarian cancers: correlation with overall survival. *Int J Gynecol Pathol* **18**, 29-41 (1999).

251. Okuda, T. et al. p53 mutations and overexpression affect prognosis of ovarian endometrioid cancer but not clear cell cancer. *Gynecol Oncol* **88**, 318-25 (2003).

252. Leitao, M. M. et al. Mutation and expression of the TP53 gene in early stage epithelial ovarian carcinoma. *Gynecol Oncol* **93**, 301-6 (2004).

253. Ng, S. W. et al. Analysis of p73 in human borderline and invasive ovarian tumor. *Oncogene* **19**, 1885-90 (2000).

254. Kaneuchi, M. et al. WT1 and WT1-AS genes are inactivated by promoter methylation in ovarian clear cell adenocarcinoma. *Cancer* (2005).

255. Waldstrom, M. & Grove, A. Immunohistochemical expression of wilms tumor gene protein in different histologic subtypes of ovarian carcinomas. *Arch Pathol Lab Med* **129**, 85-8 (2005).

256. Paige, A. J. et al. WWOX: a candidate tumor suppressor gene involved in multiple tumor types. *Proc Natl Acad Sci U S A* **98**, 11417-22 (2001).

257. Gourley, C. et al. WWOX mRNA expression profile in epithelial ovarian cancer supports the role of WWOX variant 1 as a tumour suppressor, although the role of variant 4 remains unclear. *Int J Oncol* **26**, 1681-9 (2005).

258. Blau, H. M. & Rossi, F. M. Tet B or not tet B: advances in tetracycline-inducible gene expression. *Proc Natl Acad Sci U S A* **96**, 797-9 (1999).

259. Triezenberg, S. J., Kingsbury, R. C. & McKnight, S. L. Functional dissection of VP16, the trans-activator of herpes simplex virus immediate early gene expression. *Genes Dev* **2**, 718-29 (1988).

260. Gossen, M. & Bujard, H. Tight control of gene expression in mammalian cells by tetracycline-responsive promoters. *Proc Natl Acad Sci U S A* **89**, 5547-51 (1992).

261. Gossen, M. et al. Transcriptional activation by tetracyclines in mammalian cells. *Science* **268**, 1766-9 (1995).

262. Albertoni, M. et al. Anoxia induces macrophage inhibitory cytokine-1 (MIC-1) in glioblastoma cells independently of p53 and HIF-1. *Oncogene* **21**, 4212-9 (2002).

263. Zhu, H. J., Iaria, J. & Sizeland, A. M. Smad7 differentially regulates transforming growth factor beta-mediated signaling pathways. *J Biol Chem* **274**, 32258-64 (1999).

264. Dressel, R., Lubbers, M., Walter, L., Herr, W. & Gunther, E. Enhanced susceptibility to cytotoxic T lymphocytes without increase of MHC class I antigen expression after conditional overexpression of heat shock protein 70 in target cells. *Eur J Immunol* **29**, 3925-35 (1999).

265. Pedersen, M. W., Thykjaer, T., Orntoft, T. F., Damstrup, L. & Poulsen, H. S. Profile of differentially expressed genes mediated by the type III epidermal growth factor receptor mutation expressed in a small-cell lung cancer cell line. *Br J Cancer* **85**, 1211-8 (2001).

266. Baron, U. et al. Generation of conditional mutants in higher eukaryotes by switching between the expression of two genes. *Proc Natl Acad Sci U S A* **96**, 1013-8 (1999).

267. Bohl, D., Naffakh, N. & Heard, J. M. Long-term control of erythropoietin secretion by doxycycline in mice transplanted with engineered primary myoblasts. *Nat Med* **3**, 299-305 (1997).

268. Belteki, G. et al. Conditional and inducible transgene expression in mice through the combinatorial use of Cre-mediated recombination and tetracycline induction. *Nucleic Acids Res* **33**, e51 (2005).

269. Unterrainer, G., Molzer, B., Forss-Petter, S. & Berger, J. Co-expression of mutated and normal adrenoleukodystrophy protein reduces protein function: implications for gene therapy of X-linked adrenoleukodystrophy. *Hum Mol Genet* **9**, 2609-16 (2000).

270. Kringstein, A. M., Rossi, F. M., Hofmann, A. & Blau, H. M. Graded transcriptional response to different concentrations of a single transactivator. *Proc Natl Acad Sci U S A* **95**, 13670-5 (1998).

271. Viapiano, M. S., Bi, W. L., Piepmeier, J., Hockfield, S. & Matthews, R. T. Novel tumor-specific isoforms of BEHAB/brevican identified in human malignant gliomas. *Cancer Res* **65**, 6726-33 (2005).

272. Ntougkos, E. et al. The IgLON family in epithelial ovarian cancer: expression profiles and clinicopathologic correlates. *Clin Cancer Res* **11**, 5764-8 (2005).

273. Mahmood, R. et al. A role for FGF-8 in the initiation and maintenance of vertebrate limb bud outgrowth. *Curr Biol* **5**, 797-806 (1995).

274. Echelard, Y. et al. Sonic hedgehog, a member of a family of putative signaling molecules, is implicated in the regulation of CNS polarity. *Cell* **75**, 1417-30 (1993).

275. Clark, T. G., Stewart, M. E., Altman, D. G., Gabra, H. & Smyth, J. F. A prognostic model for ovarian cancer. *Br J Cancer* **85**, 944-52 (2001).

276. Zorn, K. K. et al. Gene expression profiles of serous, endometrioid, and clear cell subtypes of ovarian and endometrial cancer. *Clin Cancer Res* **11**, 6422-30 (2005).

277. Zorn, K. K. et al. Choice of normal ovarian control influences determination of differentially expressed genes in ovarian cancer expression profiling studies. *Clin Cancer Res* **9**, 4811-8 (2003).

278. Friedl, P. & Brocker, E. B. The biology of cell locomotion within three-dimensional extracellular matrix. *Cell Mol Life Sci* **57**, 41-64 (2000).

279. Sahai, E. Mechanisms of cancer cell invasion. *Curr Opin Genet Dev* **15**, 87-96 (2005).

280. Mareel, M. & Leroy, A. Clinical, cellular, and molecular aspects of cancer invasion. *Physiol Rev* **83**, 337-76 (2003).

281. Hendrix, M. J., Seftor, E. A., Seftor, R. E. & Fidler, I. J. A simple quantitative assay for studying the invasive potential of high and low human metastatic variants. *Cancer Lett* **38**, 137-47 (1987).

282. Sundfeldt, K. Cell-cell adhesion in the normal ovary and ovarian tumors of epithelial origin; an exception to the rule. *Mol Cell Endocrinol* **202**, 89-96 (2003).

283. Braut-Boucher, F. et al. A non-isotopic, highly sensitive, fluorimetric, cell-cell adhesion microplate assay using calcein AM-labeled lymphocytes. *J Immunol Methods* **178**, 41-51 (1995).

284. Lowe, S. W., Cepero, E. & Evan, G. Intrinsic tumour suppression. *Nature* **432**, 307-15 (2004).

285. van Engeland, M., Nieland, L. J., Ramaekers, F. C., Schutte, B. & Reutelingsperger, C. P. Annexin V-affinity assay: a review on an apoptosis detection system based on phosphatidylserine exposure. *Cytometry* **31**, 1-9 (1998).

286. Bobak, D., Moorman, J., Guanzon, A., Gilmer, L. & Hahn, C. Inactivation of the small GTPase Rho disrupts cellular attachment and induces adhesion-dependent and adhesion-independent apoptosis. *Oncogene* **15**, 2179-89 (1997).

287. Schiffenbauer, Y. S. et al. Gonadotropin stimulation of MLS human epithelial ovarian carcinoma cells augments cell adhesion mediated by CD44 and by alpha(v)-integrin. *Gynecol Oncol* **84**, 296-302 (2002).

288. Li, J., Thielemann, C., Reuning, U. & Johannsmann, D. Monitoring of integrin-mediated adhesion of human ovarian cancer cells to model protein surfaces by quartz crystal resonators: evaluation in the impedance analysis mode. *Biosens Bioelectron* **20**, 1333-40 (2005).

289. Friedl, P. & Wolf, K. Tumour-cell invasion and migration: diversity and escape mechanisms. *Nat Rev Cancer* **3**, 362-74 (2003).

290. Astrinidis, A. et al. Tuberin, the tuberous sclerosis complex 2 tumor suppressor gene product, regulates Rho activation, cell adhesion and migration. *Oncogene* **21**, 8470-6 (2002).

291. Yang, C. et al. Integrin alpha1beta1 and alpha2beta1 are the key regulators of hepatocarcinoma cell invasion across the fibrotic matrix microenvironment. *Cancer Res* **63**, 8312-7 (2003).

292. Hintermann, E., Bilban, M., Sharabi, A. & Quaranta, V. Inhibitory role of alpha 6 beta 4-associated erbB-2 and phosphoinositide 3-kinase in keratinocyte haptotactic migration dependent on alpha 3 beta 1 integrin. *J Cell Biol* **153**, 465-78 (2001).

293. Scotton, C. J., Wilson, J. L., Milliken, D., Stamp, G. & Balkwill, F. R. Epithelial cancer cell migration: a role for chemokine receptors? *Cancer Res* **61**, 4961-5 (2001).

294. Cannistra, S. A., Ottensmeier, C., Niloff, J., Orta, B. & DiCarlo, J. Expression and function of beta 1 and alpha v beta 3 integrins in ovarian cancer. *Gynecol Oncol* **58**, 216-25 (1995).

295. Palecek, S. P., Loftus, J. C., Ginsberg, M. H., Lauffenburger, D. A. & Horwitz, A. F. Integrin-ligand binding properties govern cell migration speed through cell-substratum adhesiveness. *Nature* **385**, 537-40 (1997).

296. Calof, A. L. & Lander, A. D. Relationship between neuronal migration and cell-substratum adhesion: laminin and merosin promote olfactory neuronal migration but are anti-adhesive. *J Cell Biol* **115**, 779-94 (1991).

297. Perez-Moreno, M., Jamora, C. & Fuchs, E. Sticky business: orchestrating cellular signals at adherens junctions. *Cell* **112**, 535-48 (2003).

298. Perl, A. K., Wilgenbus, P., Dahl, U., Semb, H. & Christofori, G. A causal role for E-cadherin in the transition from adenoma to carcinoma. *Nature* **392**, 190-3 (1998).

299. Trolice, M. P., Pappalardo, A. & Peluso, J. J. Basic fibroblast growth factor and N-cadherin maintain rat granulosa cell and ovarian surface epithelial cell viability by stimulating the tyrosine phosphorylation of the fibroblast growth factor receptors. *Endocrinology* **138**, 107-13 (1997).

300. Davies, B. R., Worsley, S. D. & Ponder, B. A. Expression of E-cadherin, alpha-catenin and beta-catenin in normal ovarian surface epithelium and epithelial ovarian cancers. *Histopathology* **32**, 69-80 (1998).

301. Masuda, M. et al. The tumor suppressor protein TSLC1 is involved in cell-cell adhesion. *J Biol Chem* **277**, 31014-9 (2002).

302. Roman-Gomez, J. et al. Cadherin-13, a mediator of calcium-dependent cell-cell adhesion, is silenced by methylation in chronic myeloid leukemia and correlates with pretreatment risk profile and cytogenetic response to interferon alfa. *J Clin Oncol* **21**, 1472-9 (2003).

303. Faux, M. C. et al. Restoration of full-length adenomatous polyposis coli (APC) protein in a colon cancer cell line enhances cell adhesion. *J Cell Sci* **117**, 427-39 (2004).

304. Reddy, P. et al. Formation of E-cadherin-mediated cell-cell adhesion activates AKT and mitogen activated protein kinase via phosphatidylinositol 3 kinase and ligand-independent activation of epidermal growth factor receptor in ovarian cancer cells. *Mol Endocrinol* **19**, 2564-78 (2005).

305. Pizzolato, J. F. & Saltz, L. B. The camptothecins. *Lancet* **361**, 2235-42 (2003).

306. Sharom, F. J. & Lehto, M. T. Glycosylphosphatidylinositol-anchored proteins: structure, function, and cleavage by phosphatidylinositol-specific phospholipase C. *Biochem Cell Biol* **80**, 535-49 (2002).

307. Varma, R. & Mayor, S. GPI-anchored proteins are organized in submicron domains at the cell surface. *Nature* **394**, 798-801 (1998).

308. Wang, Y. The role and regulation of urokinase-type plasminogen activator receptor gene expression in cancer invasion and metastasis. *Med Res Rev* **21**, 146-70 (2001).

309. Kimura, Y. et al. GML sensitizes cancer cells to Taxol by induction of apoptosis. *Oncogene* **15**, 1369-74 (1997).

310. Rai, S. K. et al. Candidate tumor suppressor HYAL2 is a glycosylphosphatidylinositol (GPI)-anchored cell-surface receptor for jaagsiekte sheep retrovirus, the envelope protein of which mediates oncogenic transformation. *Proc Natl Acad Sci U S A* **98**, 4443-8 (2001).

311. Suzuki, K. et al. A novel glycosylphosphatidyl inositol-anchored protein on human leukocytes: a possible role for regulation of neutrophil adherence and migration. *J Immunol* **162**, 4277-84 (1999).

312. Stefanova, I., Horejsi, V., Ansotegui, I. J., Knapp, W. & Stockinger, H. GPI-anchored cell-surface molecules complexed to protein tyrosine kinases. *Science* **254**, 1016-9 (1991).

313. Conese, M. & Blasi, F. The urokinase/urokinase-receptor system and cancer invasion. *Baillieres Clin Haematol* **8**, 365-89 (1995).

314. Tansey, M. G., Baloh, R. H., Milbrandt, J. & Johnson, E. M., Jr. GFRalpha-mediated localization of RET to lipid rafts is required for effective downstream signaling, differentiation, and neuronal survival. *Neuron* **25**, 611-23 (2000).

315. Malhotra, J. D., Tsiotra, P., Karagogeos, D. & Hortsch, M. Cis-activation of L1-mediated ankyrin recruitment by TAG-1 homophilic cell adhesion. *J Biol Chem* **273**, 33354-9 (1998).

316. Cavallaro, U. & Christofori, G. Cell adhesion and signalling by cadherins and Ig-CAMs in cancer. *Nat Rev Cancer* **4**, 118-32 (2004).

317. Cavallaro, U., Niedermeyer, J., Fuxa, M. & Christofori, G. N-CAM modulates tumour-cell adhesion to matrix by inducing FGF-receptor signalling. *Nat Cell Biol* **3**, 650-7 (2001).

318. Fearon, E. R. DCC: is there a connection between tumorigenesis and cell guidance molecules? *Biochim Biophys Acta* **1288**, M17-23 (1996).

319. Plunkett, T. A. & Ellis, P. A. CEACAM1: a marker with a difference or more of the same? *J Clin Oncol* **20**, 4273-5 (2002).

320. Wu, H. et al. Hypomethylation-linked activation of PAX2 mediates tamoxifen-stimulated endometrial carcinogenesis. *Nature* **438**, 981-7 (2005).

321. Mei, F. C., Young, T. W., Liu, J. & Cheng, X. RAS-Mediated epigenetic inactivation of OPCML in oncogenic transformation of human ovarian surface epithelial cells. *Faseb J* (2005).

Appendix A

Solutions

Blocking solution (freshly-made & filter-sterilised)

15% (v/v) sheep serum, heat inactivated

2% (w/v) BSA

50 mM Tris-Cl, pH 7.5

150 mM NaCl

0.1% (v/v) Tween-20

in ultra-pure water

3x Denaturing sample buffer (stored at –20°C in aliquots)

25 mM trizma base

0.1 M SDS

15% (v/v) beta-mercaptoethanol

30% (v/v) glycerol

1% (w/v) bromophenol blue

in deionised water

10x Gel loading dye

0.25% (w/v) bromophenol blue

0.25% (w/v) xylene cyanol FF

30% (v/v) glycerol

in deionised water

Gel running buffer (protein)

25 mM trizma base

0.2 M glycine

0.1% (w/v) SDS

in deionised water

Maleic acid buffer (autoclaved)

100 mM maleic acid

150 mM sodium chloride

NTM(T) buffer (freshly-made)

100 mM NaCl

0.1% Tween-20

50 mM $MgCl_2$

(100 mM Tris-HCl, pH 9.5)

PBS

Purchased as tablets from Oxoid. Dissolved as per the manufacturer's instructions. Autoclaved. Optionally, DEPC-treated and re-autoclaved (for WISH).

PBT (DEPC-treated & autoclaved)

PBS containing 0.1% (v/v) Tween-20

Post-hybridisation solution (filter-sterilised)

50% (v/v) deionised formamide

5x SSC, pH 4.5 (from a DEPC-treated & autoclaved 20x stock solution; Sigma)

0.1% (v/v) Tween-20

0.5% CHAPS (from a 2% stock solution; Sigma)

Pre-hybridisation solution (filter-sterilised and stored at –20°C in aliquots)

50% (v/v) deionised formamide

5x SSC, pH 4.5 (from a DEPC-treated & autoclaved 20x stock solution; Sigma)

2% (w/v) Blocking Reagent (Roche; heated to 65°C to dissolve)

0.1% (v/v) Tween-20

0.5% (w/v) CHAPS (from a 2% stock solution; Sigma)

50 µg/ml yeast tRNA (Sigma)

5 mM EDTA

50 µg/ml heparin (Sigma)

Protein extraction buffer (freshly-made)

50 mM Tris, pH 7.5

5 mM EDTA, pH 8.5

150 mM sodium chloride

1% (v/v) Triton X-100

1 Complete Mini protease inhibitor cocktail tablet (Roche) per 10 ml buffer

in deionised water

Scott's tap water

42 mM sodium bicarbonate

81 mM magnesium sulphate

in water

SOC medium

2% (w/v) Bacto-tryptone

0.5% (w/v) Bacto-yeast extract

0.1 M sodium chloride

2.5 mM potassium chloride

in deionised water

autoclaved

added 0.2 M Mg^{2+} and 0.2 M glucose prior to use and filter-sterilised

20x TAE

0.8 M trizma base

0.2 M EDTA

5.7% (v/v) glacial acetic acid

in deionised water

TBS

50 mM trizma base

150 mM sodium chloride

in deionised water

TE buffer (DEPC-treated & autoclaved)

10 mM Tris

1 mM EDTA pH 8.0

in deionised water

TNT (freshly-made)

0.1% (v/v) Tween-20

150 mM NaCl

50 mM Tris-HCl, pH 7.5

in deionised water

Transfer buffer

25 mM trizma base

0.2 M glycine

in deionised water

Appendix B

Primer sequences

PRIMER	SEQUENCE (5' TO 3')
Human *OPCML* F1	TACCATAGATGACCGGGTAA
Human *OPCML* R	CTATTAGGTGAACCCGGGAC
Human *OPCML* F2	CCACTGGTCTGGATGGAATG
pTRE2hyg R1	CCATTCTAAACAACACCCTG
Human *OPCML* F3	GCCCACTTCTTCATCAAGTT
pTRE2hyg R2	AAGGGACATCTTTCCCATTCT
pTRE-Tight R	GGAGGTGTGGGAGGTTTT
Human *HNT* F	TCTAGGGTCCACCTCATTGT
Human *HNT* R	GGGAGAGATGTGTCTCCAAG
Human *LSAMP* F	CGACAAGCTTCACTCAAATG
Human *LSAMP* R	GTAGTTGCCGTAGTGCTCCT
Human *NEGR1* F	TGTTACCAACGTGACACAGG
Human *NEGR1* R	GCTCCCGGTAATTCCATACT
Human *ACTB* F	CTACGTCGCCCTGGACTTCGAGC
Human *ACTB* R	GATGGAGCCGCCGATCCACACGG
Human *ACTG1* F	ATGGCATCGTCACCAACTGG
Human *ACTG1* R	ATGACAATGCCAGTGGTGCG
Mouse *Opcml* F	CCTCGAGTGATGATTTTGGTG
Mouse *Opcml* R	CTGGTCAGTTTGATGTCTGA
Mouse *Hnt* F	TCGTGTGGTCCTCCTGAGT
Mouse *Hnt* R	TCCCGAGTGATGCCCTG
Mouse *Lsamp* F	GACAACATCACCGTGAGACA
Mouse *Lsamp* R	TGCAGACCAGGGTTACATTG
Mouse *Negr1* F	GGTGAGGAAAGGTGACACAG
Mouse *Negr1* R	CCAGTGGCCAAACAAGTAAG
Mouse *Actb* F	CTATGTTGCCCTGGATTTTG
Mouse *Actb* R	GGGGGAGCAATGATCTTAAT

NB F = forward primer

R = reverse primer

Appendix C

Vector maps

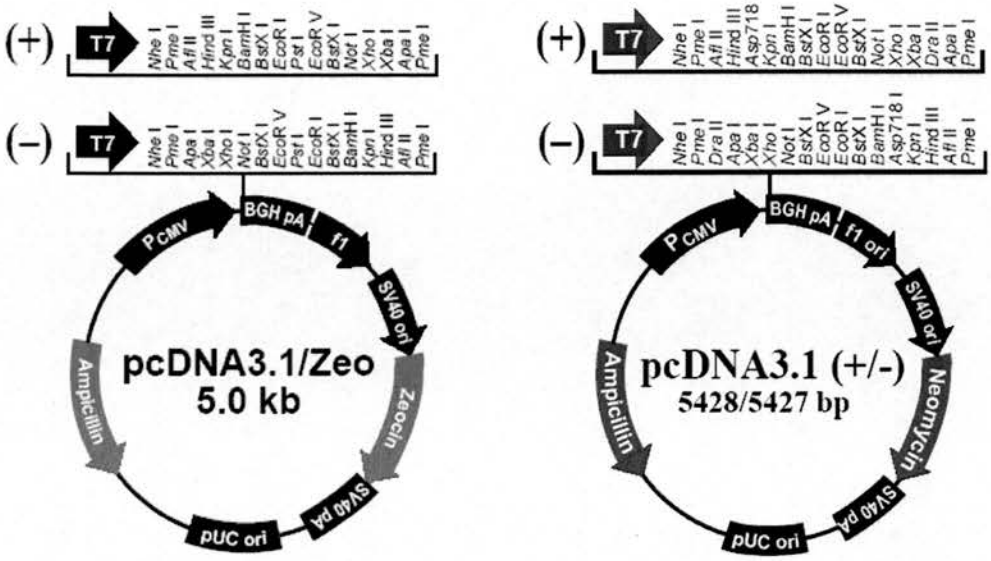
(+) T7 Nhe I Pme I Afl II Hind III Kpn I BamH I BstX I EcoR I Pst I EcoR V BstX I Not I Xho I Xba I Apa I Pme I
(–) T7 Nhe I Pme I Apa I Xba I Xho I Not I BstX I EcoR V Pst I EcoR I BstX I BamH I Kpn I Hind III Afl II Pme I
P CMV
BGH pA
f1
SV40 ori
Zeocin
SV40 pA
pUC ori
Ampicillin
pcDNA3.1/Zeo
5.0 kb
(+) T7 Nhe I Pme I Afl II Hind III Asp718 I Kpn I BamH I BstX I EcoR I EcoR V BstX I Not I Xho I Xba I Dra II Apa I Pme I
(–) T7 Nhe I Pme I Dra II Apa I Xba I Xho I Not I BstX I EcoR V EcoR I BstX I BamH I Asp718 I Kpn I Hind III Afl II Pme I
P CMV
BGH pA
f1 ori
SV40 ori
Neomycin
SV40 pA
pUC ori
Ampicillin
pcDNA3.1 (+/-)
5428/5427 bp

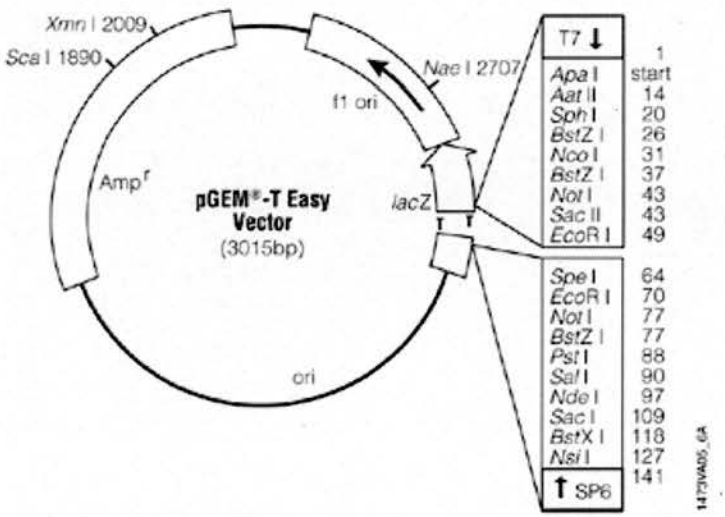
Xmn I 2009
Sca I 1890
Nae I 2707
f1 ori
Amp r
pGEM®-T Easy
Vector
(3015bp)
lacZ
ori
T7 ↓ 1
Apa I start
Aat II 14
Soh I 20
BstZ I 26
Nco I 31
BstZ I 37
Not I 43
Sac II 43
EcoR I 49
Spe I 64
EcoR I 70
Not I 77
BstZ I 77
Pst I 88
Sal I 90
Nde I 97
Sac I 109
BstX I 118
Nsi I 127
↑ SP6 141

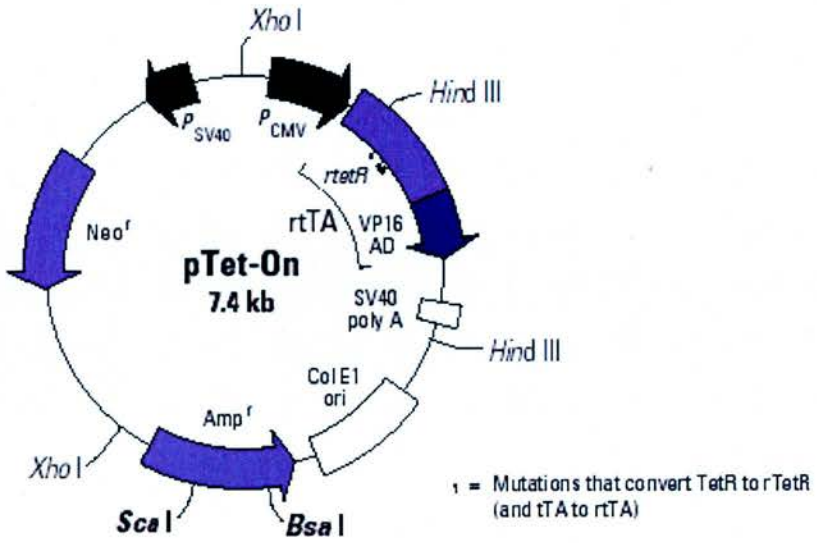
Xho I
Hind III
P SV40
P CMV
rtetR*
rtTA
VP16 AD
Neo r
pTet-On
7.4 kb
SV40 poly A
Hind III
Col E1 ori
Amp r
Xho I
Sca I
Bsa I
* = Mutations that convert TetR to rTetR (and tTA to rtTA)

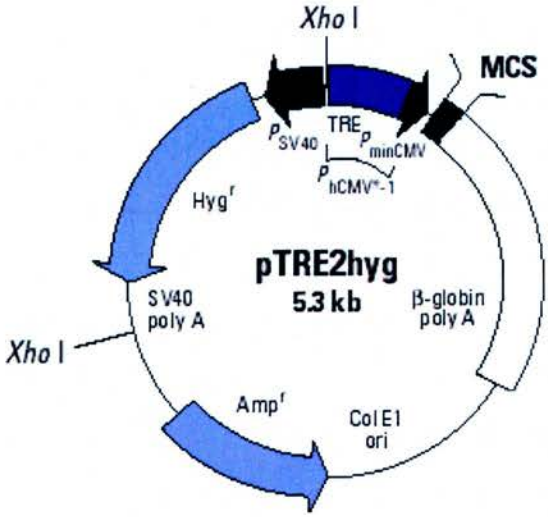
Xho I
MCS
P SV40
TRE
P minCMV
P hCMV*-1
Hyg r
pTRE2hyg
5.3 kb
SV40 poly A
β-globin poly A
Xho I
Amp r
Col E1 ori

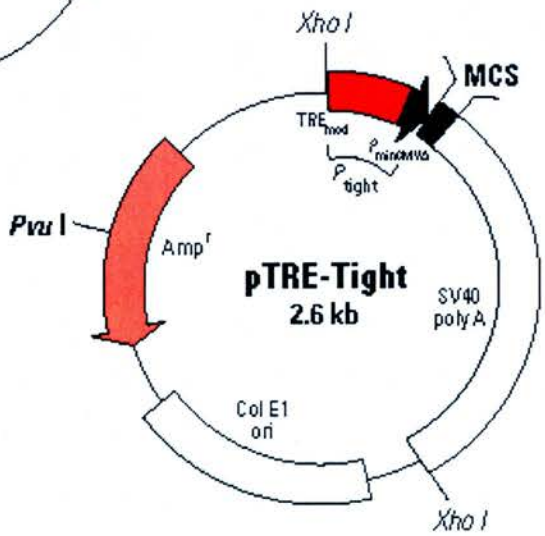
Xho I
MCS
TRE tight
P minCMVtet
P tight
Pvu I
Amp r
pTRE-Tight
2.6 kb
SV40 poly A
Col E1 ori
Xho I

Appendix D

Publications

The IgLON Family in Epithelial Ovarian Cancer: Expression Profiles and Clinicopathologic Correlates

Evangelos Ntougkos,[1] Robert Rush,[1] Diane Scott,[1] Tobias Frankenberg,[1] Hani Gabra,[2] John F. Smyth,[1] and Grant C. Sellar[1]

Abstract **Purpose:** The IgLON family of cell adhesion molecules, comprising OPCML, HNT, LSAMP, and NEGR1, has recently been linked to cancer, through two of its members being proposed as tumor suppressors. We examined the expression profile of the family in human sporadic epithelial ovarian cancer and the normal ovary.

Experimental Design: We determined the expression level of each IgLON in a panel comprising 57 tumor and 11 normal ovarian samples by quantitative real-time reverse transcription-PCR. The results were statistically tested for associations with clinicopathologic variables.

Results: *OPCML*, *LSAMP* and *NEGR1* exhibited reduced expression in the tumor samples relative to the normal samples, whereas *HNT* expression was elevated. Statistically significant changes were specific to histologic type. The expression levels of individual IgLONs were correlated, the most significant finding being a positive correlation between *LSAMP* and *NEGR1*. *LSAMP* expression was also negatively correlated with overall survival and was found to be a negative predictor of outcome.

Conclusions: The expression of the IgLON family is altered in sporadic epithelial ovarian tumors in comparison to the normal ovary. In our small but representative cohort of patients, we have found significant correlations and associations in expression and clinicopathology that suggest a wider role of the family in ovarian cancer.

Ovarian cancer is the leading cause of gynecologic death in both the U.S. and the U.K., in fact, it ranks fourth as a cause of death from any cancer in women (Cancer Research UK statistics; ref. 1).[3] The incidence of the disease increases with age, peaking in around the seventh to eighth decade (2). Approximately 90% of ovarian cancers are epithelial ovarian cancers (EOC), with 5% to 10% being familial in origin (3, 4). Although, if diagnosed early, it has a very good prognosis, with a 92% 5-year survival rate, most cases (75%) are diagnosed at a late stage of disseminated disease when the prognosis is much less favorable, with only a 25% 5-year survival rate (5). Treatment of ovarian cancer is usually based on surgical cytoreduction and platinum-based chemotherapy (6). Although primarily a chemoresponsive disease, chemoresistance develops in most cases, resulting in the high aforementioned mortality rate.

The IgLONs are an immunoglobulin subfamily of glycosylphosphatidylinositol-anchored cell adhesion molecules comprising opioid binding protein/cell adhesion molecule–like (OPCML/OBCAM; ref. 7), limbic system–associated membrane protein (LSAMP/LAMP; ref. 8), neurotrimin (HNT; ref. 9), and neuronal growth regulator 1 (NEGR1/Kilon; ref. 10). Our knowledge of the functions of these proteins is limited and mainly derives from studies of chick and rat brain, the tissue where they are primarily expressed. Their patterns of expression in the brain are overlapping but also distinct, with *OPCML* being mainly expressed in the gray matter (11), *HNT* in the sensorimotor cortex and the cerebellum (9), *LSAMP* in cortical and subcortical neurons of the limbic system (8), and *NEGR1* in the cerebrum and brain stem (10). In these studies, it is suggested that the IgLONs could have an important role in cell adhesion and cell-cell recognition, mediated by both homo- and heterophilic interactions in *cis* and *trans* that are likely to be stabilized by clustering of the proteins on the cell surface (12). It has been recently suggested that IgLONs function mainly as heterodimers termed Diglons (13).

OPCML has been shown to exhibit functional characteristics of a tumor suppressor gene in an ovarian cancer cell line *in vitro* and also *in vivo* when xenografted into nude mice (14). Abrogated expression was found in 83% of sporadic EOC samples examined. The mechanism underlying *OPCML* silencing was shown to be CpG island hypermethylation. This first report of an IgLON involvement in cancer was followed by a further one, where the *LSAMP* promoter was shown to be

Authors' Affiliations: [1]Cancer Research UK Centre, University of Edinburgh, Edinburgh and [2]Department of Cancer Medicine, Imperial College, London, United Kingdom

Received 11/22/04; revised 5/16/05; accepted 5/26/05.

Grant support: Cancer Research UK.

The costs of publication of this article were defrayed in part by the payment of page charges. This article must therefore be hereby marked *advertisement* in accordance with 18 U.S.C. Section 1734 solely to indicate this fact.

Requests for reprints: Grant C. Sellar, Cancer Research UK Centre, The University of Edinburgh, Crewe Road South, Edinburgh EH4 2XR, United Kingdom. Phone: 44-131-777-3541; Fax: 44-131-777-3520; E-mail: grant.sellar@cancer.org.uk.

doi:10.1158/1078-0432.CCR-04-2388

[3] http://cancerresearchuk.org/aboutcancer/statistics/mortality.

methylated in 26% of a panel of sporadic clear cell renal cell carcinomas (15). Moreover, expression of *LSAMP* in clear cell renal cell carcinoma lines inhibited cell proliferation.

We have investigated the expression of the four members of the IgLON family in a panel of 11 normal human ovaries and 57 tumor samples from patients with EOC. Our primary objective has been to observe each gene separately, as well as to attempt to draw conclusions from the interrelationships of data that emerge. In this extensive study, we report significant associations between the expression levels of the IgLONs and various clinicopathologic variables.

Materials and Methods

Patient samples. Primary human ovarian tumor material and nonmalignant tissues were obtained from patients having undergone gynecologic surgery in the Lothian University Hospitals National Health Service Trust. Institutional ethical approval was granted for this work by the Lothian University National Health Service Trust, Medicine/Clinical Oncology Research Ethics Subcommittee. Tissue samples were excised and stored in liquid nitrogen. Nonmalignant tissue samples were derived from patients that underwent bilateral oophorectomies for suspected malignancy, but were found to have benign histologies; samples were collected from apparently normal contralateral ovaries.

In this study, a panel comprising 57 sporadic ovarian tumors and 11 normal ovaries was used. The features of the panel are shown in Table 1. Overall, our unselected cohort is very representative of the presentation of 1,400 women from the Scottish community over 20 years to a single center in a completely unselected fashion from primary care (16). Our present cohort is exactly as expected for stage distribution in a Scottish population; although it is skewed slightly towards a more adverse grade distribution. The overrepresentation of grade 3 tumors may account for a slightly shorter median survival of 2.25 years compared with 2.50 years.

Table 1. The panel of normal ovaries and EOC samples

Description	*n*
All samples	68
Normal	11
Tumors	57
Serous	29
Clear Cell	12
Mucinous	4
Endometrioid	8
Mixed	1
Unclassified	3
Median age at diagnosis (years)	64
FIGO stage	
I	8
II	4
III	37
IV	8
Grade	
1	2
2	11
3	41
Median survival (y)	2.25

Abbreviation: FIGO, Federation Internationale des Gynaecologistes et Obstetristes.

RNA preparation. Total RNA was prepared from the ovarian tissues and DNase I-treated using the Absolutely RNA reverse transcription-PCR Miniprep Kit (Stratagene, La Jolla, CA), as per the manufacturer's instructions.

Quantitative real-time reverse transcription-PCR. Quantitative reverse transcription-PCR was done using Rotorgene 2000 and 3000 real-time thermal cyclers (Corbett Research, Australia). Fifteen-microliter reactions were set up using 40 ng of DNase I-treated total RNA, 0.3 μmol/L each of forward and reverse primer and the Quantitect SYBR Green one-step reverse transcription-PCR kit (Qiagen, Crawley, United Kingdom), according to the manufacturer's guidelines. Primers were designed using Primer 3 v0.2. Primer sequences are available upon request. All reactions were carried out in triplicate for the standard curve samples and in quadruplicate for the experimental samples and the negative control (no template). Fluorescence was detected using the FAM channel (source 470 mm, detector 510 nm). Analysis and quantification was done using Rotorgene v4.6 and v5 software. The relative quantification method was employed by extrapolation from a standard curve and calculation of expression levels as ratios to β-actin.

Cycling conditions were set as follows: reverse transcription at 50°C for 30 minutes, followed by a 15-minute polymerase activation at 95°C, and 40 cycles of denaturation at 94°C for 15 seconds, annealing at 57°C for 30 seconds and extension at 72°C for 30 seconds; after a final extension at 72°C for 1 minute, product melting was set across a 72°C to 99°C temperature ramp, with 5-second steps of 1°C. Data were corrected for inter-run variation using a "normalizer" sample that was included in all runs.

Statistical analysis. All statistical analyses were conducted in SPSS v12 (SPSS Inc., Chicago, IL). Nonparametric comparisons between unmatched samples were made using the Mann-Whitney (U) test for two samples or the Kruskal-Wallis (χ^2) test for more than two samples. Nonparametric correlations were tested using the Spearman rank (r_s) test. Regression models were made using linear regression analysis. Survival curves were produced using the Kaplan-Meier method and tested with the log-rank test. Survival models were estimated using Cox proportional hazards regression analysis.

Results

IgLON expression levels differ between normal ovaries and EOC. In order to evaluate the RNA expression levels of the four IgLON family members in the panel that comprised 11 normal human ovaries and 57 ovarian tumor samples, a real-time quantitative reverse transcription-PCR approach was followed. The results are shown in Fig. 1. For *OPCML*, *LSAMP*, and *NEGR1*, the majority of tumors exhibit reduced expression as compared with the normal ovary samples. In contrast, tumor samples have increased *HNT* expression in relation to nonmalignant ones. The distribution of values in all four genes is not normal, hence, nonparametric approaches were chosen for statistical analysis.

Associations of IgLON expression with EOC histologic types. The expression data prompted us to take a closer look at each gene separately in the different histologic types and make comparisons to expression in the normal ovaries. In all four IgLONs, there are statistically significant differences between normal ovaries and tumor subgroups (Fig. 2). More specifically, *OPCML* expression is reduced in clear cell carcinomas ($U = 19$, $P = 0.039$); *LSAMP* expression is reduced in endometrioid tumors ($U = 28$, $P = 0.012$); and *NEGR1* expression is reduced in serous ($U = 59$, $P = 0.014$), clear cell ($U = 9$, $P = 0.009$), and endometrioid ($U = 7$, $P = 0.001$) tumors. In contrast, *HNT* expression is elevated in serous carcinomas as compared with normal ovaries ($U = 113$, $P = 0.008$).

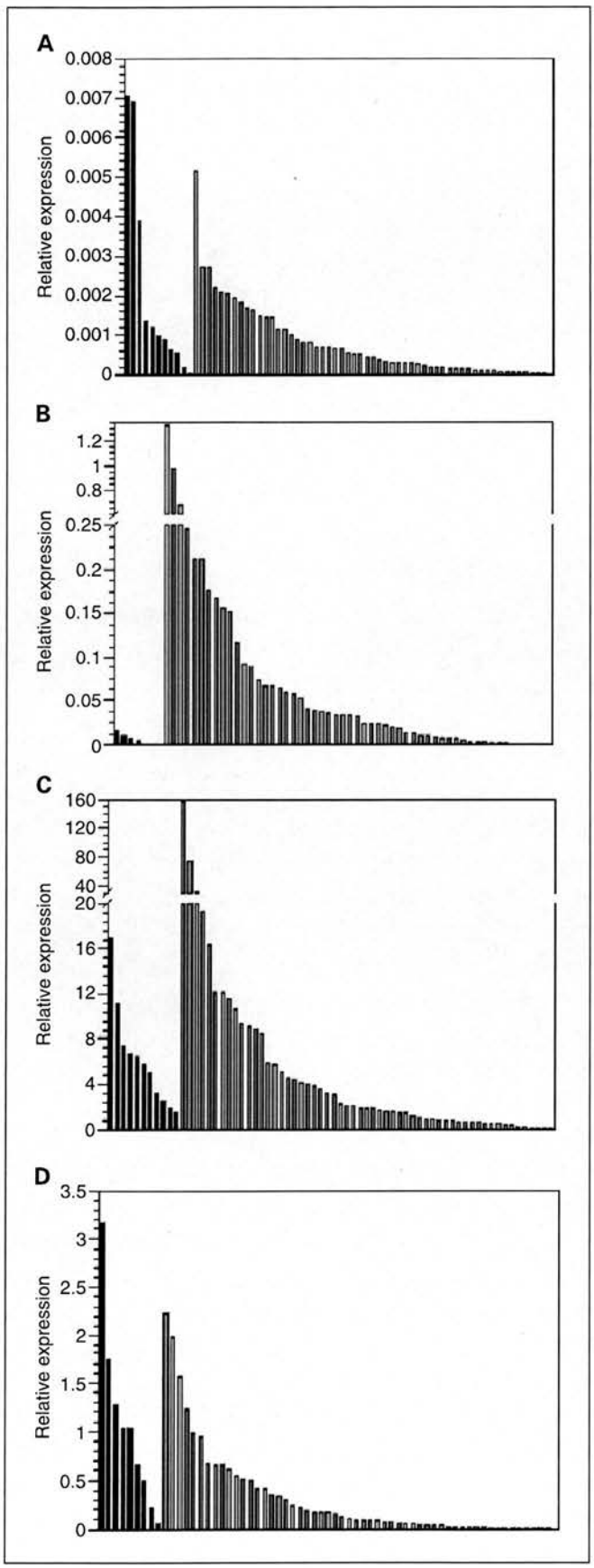

Correlations in expression between IgLONs. As all the four genes that constitute the focus of this study are structurally and functionally related, a question that arises is whether their individual expression levels are interlinked. The following statistically significant correlations of expression between IgLONs were found: *LSAMP* and *NEGR1* (r_s = 0.553, P < 0.001); *OPCML* and *NEGR1* (r_s = 0.389, P = 0.001); *OPCML* and *LSAMP* (r_s = 0.356, P = 0.003). In all these cases, the correlations are positive.

Associations between IgLON expression and clinicopathologic variables. In an attempt to establish whether expression of IgLON family members could be a function of age as a continuous variable, the expression of each gene was tested against age. However, evidence to support associations was not found, either by correlation testing or by regression analysis.

Neither was stage found to differentiate IgLON expression; nonetheless, there is a statistically significant difference in *LSAMP* expression among tumors of different grades (χ^2 = 6.73, P = 0.035). In fact, as can be seen in Fig. 3, this difference is even more significant when comparing grade 3 tumors with grades 1 and 2 tumors: undifferentiated carcinomas have lower levels of *LSAMP* than moderately or well-differentiated ones (U = 148, P = 0.017). In comparison to the large study of Clark et al. (16), grade 1 tumors are underrepresented in our relatively small sample cohort. The low number of grade 1 cases in our cohort has prevented us from comparing expression in these samples against grades 2 or 3, which is a more customary comparison.

IgLON expression and survival. The impact of IgLON expression levels on the survival of the patients was tested at two levels. Firstly, correlation between expression of each gene and overall survival was investigated. This highlighted *LSAMP* as having a negative correlation (r_s = −0.296, P = 0.025).

Patients were then divided into high and low expressers for each gene, using the median values of the normal samples as cutoff points. Survival curves were plotted and high expressers were compared with low expressers (data not shown). However, we were not able to show statistical significance for any of the four genes on this division.

To address whether the expression level of an *IgLON* gene can predict clinical outcome, we tested the expression variables, as well as the clinicopathologic ones, for prognostic value by Cox regression analysis. As can be seen in Table 2, in univariate analyses, log-transformed *LSAMP* expression, as well as stage, were found to be negative predictors of overall survival. Both variables were still found to be significant predictors of overall survival when tested together by multivariate analysis.

Discussion

When the link between a member of the IgLON family, *OPCML*, and EOC was put forward (14), questions were raised regarding the role of this gene in ovarian physiology and ovarian cancer pathology. The realization that the family as a whole might be associated with ovarian or other types of cancer also

Fig. 1. IgLON expression in EOC and normal ovaries. The relative expression levels of the four IgLON genes, *OPCML* (*A*), *HNT* (*B*), *LSAMP* (*C*), and *NEGR1* (*D*) were investigated in a panel of EOC samples and normal human ovaries using a quantitative reverse transcription-PCR approach. *Black,* normal samples; *gray,* tumor samples.

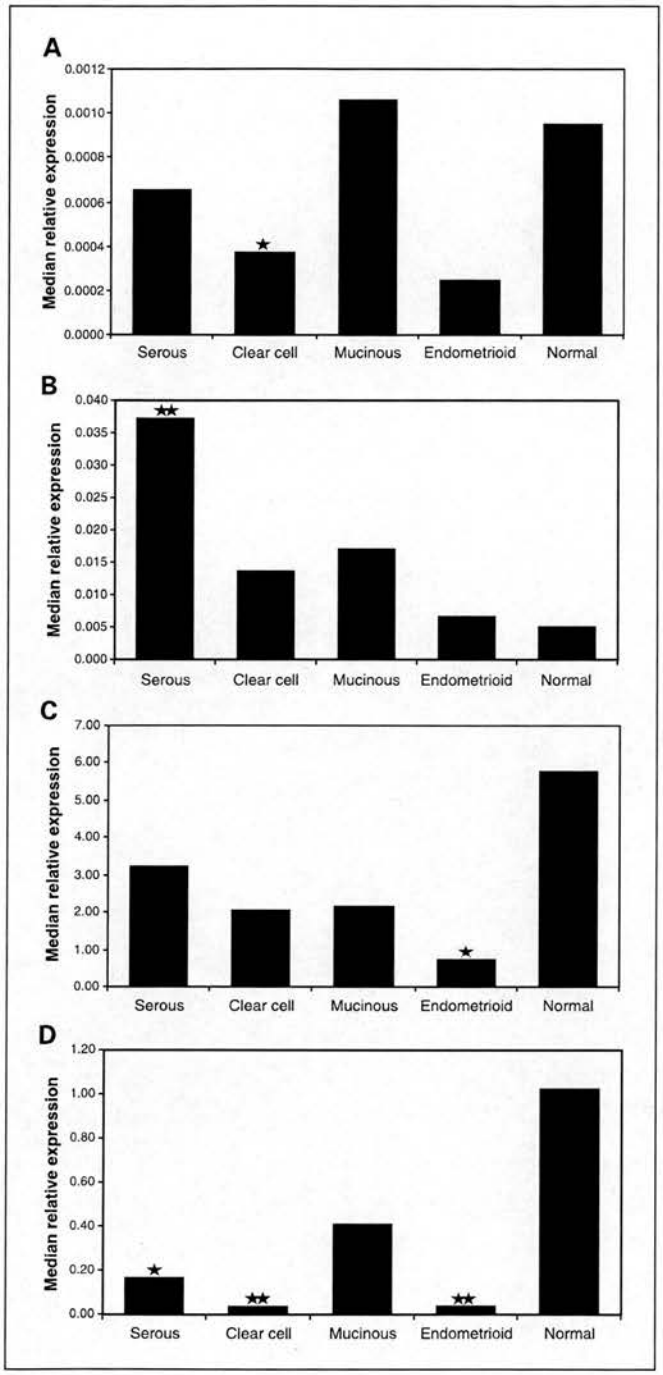

Fig. 2. IgLON expression according to histologic type. The EOC sample panel was categorized by histologic type, i.e., into serous, clear cell, mucinous, and endometrioid tumors. The median relative expression levels of *OPCML* (*A*), *HNT* (*B*), *LSAMP* (*C*), and *NEGR1* (*D*) are shown for these subgroups as compared with normal ovary samples. *, $P < 0.05$; **, $P < 0.01$.

emerged. This probability was subsequently strengthened by the finding of another IgLON, *LSAMP*, being associated with clear cell renal cell carcinomas as a putative tumor-suppressor gene (15). Could there be a case for the IgLON family being of importance in cancer?

To answer this question, one needs a powerful global approach that examines the family as a whole. This study has been based on a well-characterized panel of ovarian tumors and normal ovaries, which has come under scrutiny for the expression of each IgLON separately, but also for expression patterns and associations deduced in a statistically sound manner.

Here we present evidence that, at least with respect to EOC, it is not just *OPCML*, but the other members as well, which may be of relevance. We have shown that the expression of all the IgLONs differs significantly between normal ovaries and EOC at the RNA level. The expression levels of *OPCML*, *LSAMP*, and *NEGR1* are all reduced in EOC, whereas that of *HNT* is increased. Confirmation of these trends at the protein level will merit investigating whether, apart from OPCML, there could be a case for LSAMP and NEGR1 acting as tumor suppressors in sporadic EOC. It has been shown that the cause of the reduction in expression in the case of *OPCML* in EOC is mainly epigenetic (14), and there is evidence that the same applies for *LSAMP* in clear cell renal cell carcinomas (15). Thus, it seems likely that the reduction in *LSAMP* and *NEGR1* expression in EOC may be attributed to epigenetic mechanisms. In addition, we have found a significant positive correlation, the strongest in this study, between the expression of *LSAMP* and that of *NEGR1*. Consequently, it could be hypothesized that both genes need not be genetically or epigenetically silenced in EOC; the reduction in expression of the one could result in a reduction in expression of the other, potentially through a mechanism of coordinated transcriptional regulation. Although epigenetic modification is an age-related variable which affects gene expression, we have not found an association between altered IgLON expression and age in this study.

We have shown that in EOC, the importance of each IgLON might be specific to histologic type. *OPCML* expression is significantly reduced in clear cell carcinomas, *LSAMP* in endometrioid, and *NEGR1*, exhibiting the most striking reduction in expression, in serous, clear cell, and endometrioid tumors. In contrast, *HNT* is significantly elevated in serous carcinomas. With regard to mucinous carcinomas, it should be noted that the lack of statistical significance could be accounted for by the under-representation of this type of tumor in the panel.

Malignant transformation in ovarian cancer is characterized by a differentiation process, in contrast with most other tumor

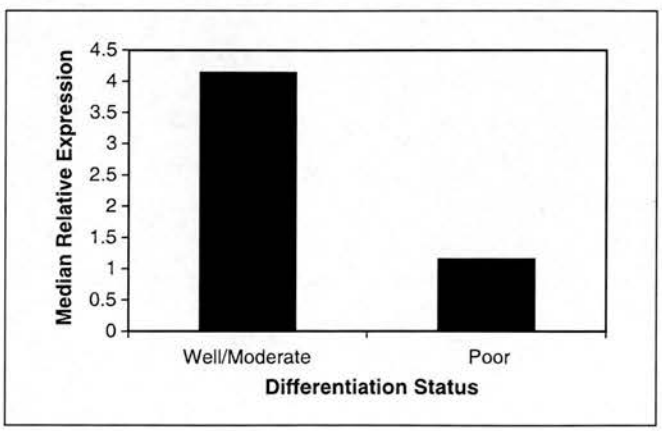

Fig. 3. *LSAMP* expression according to differentiation status. The EOC sample panel was divided into tumors of poor differentiation, i.e., of grade 3 histology, and tumors that are moderately or well-differentiated, i.e., of grades 1 or 2 histology. *Columns,* median relative expression of *LSAMP* in each of these tumor subgroups.

Table 2. Survival models

	Variable	Odds ratio	95% Confidence interval		Significance
			Lower	Upper	
Univariate	*OPCML**	0.84	0.50	1.41	0.506
	*HNT**	1.15	0.84	1.57	0.376
	*LSAMP**	1.63	1.10	2.41	0.015
	*NEGR1**	1.30	0.86	1.96	0.221
	stage†	8.86	2.10	37.32	0.003
	grade‡	22.06	0.04	13126	0.343
	age at diagnosis	1.03	1.00	1.06	0.020
	age last recorded	1.01	0.98	1.04	0.400
Multivariate	*LSAMP**	1.85	1.14	3.02	0.013
	stage†	10.21	2.40	43.77	0.002

NOTE: The expression and clinical variables were tested by univariate regression analysis. The two variables that were found to be statistically significant were further tested by multivariate analysis.

*Log-transformed.

†Early (i.e., stages I and II) versus late (i.e., stages III and IV).

‡High (i.e., grade 3) versus rest (i.e., grades 1 and 2).

types, where the converse occurs (17). Normal ovarian epithelium is not fully differentiated, retaining certain mesenchymal characteristics; upon transformation, differentiation drives the epithelium toward certain histologic morphologies, depending on the type of the tumor. Because IgLONs have partially distinct patterns of histologic subtype expression, they could be part of a different pathway that guides this differentiation process.

Interestingly, *LSAMP* expression is significantly higher in moderately and well-differentiated tumors. This indicates that the level of *LSAMP* expression is likely to be a biological function of differentiation. It could be speculated that the significance of reduction of *LSAMP* expression in the process of malignant transformation of the ovarian surface epithelium could lie in the cells acquiring a less differentiated phenotype, which is considered to be of higher malignant potential.

Furthermore, *LSAMP* was found to be a negative prognostic factor in both univariate and multivariate models of EOC in addition to being negatively correlated with overall survival. In both cases, the impact of *LSAMP* on survival is not high. This link may seem paradoxical, given that its overall tumor levels are significantly lower than in normal ovaries. However, the role of residual *LSAMP* in the tumors might be antithetical to its original functions in the normal ovary. In terms of the multifactorial output described as survival, ovarian tumors could be disadvantaged by not expressing *LSAMP* and losing its novel functions. The true reason behind this paradoxical finding remains as yet undetermined.

The analysis of the present study, albeit deriving from a relatively small cohort and requiring confirmation in a larger study, has pointed to a very interesting and novel association of the IgLON family with ovarian cancer. In order to integrate *OPCML* and its relatives into models of ovarian carcinogenesis, we need to establish their functions in the normal ovary, their localization within the ovarian environment and the pathway that links them to ovarian cancer. In addition, the functional importance of homo- and heterodimers needs to be addressed. Finally, profiling the expression of the IgLONs in other types of neoplasia might reveal that this hitherto mysterious family has a wider importance in cancer.

References

1. Jemal A, Clegg LX, Ward E, et al. Annual report to the nation on the status of cancer, 1975–2001, with a special feature regarding survival. Cancer 2004;101:3–27.
2. Runnebaum IB, Stickeler E. Epidemiological and molecular aspects of ovarian cancer risk. J Cancer Res Clin Oncol 2001;127:73–9.
3. Stratton JF, Gayther SA, Russell P, et al. Contribution of BRCA1 mutations to ovarian cancer. N Engl J Med 1997;336:1125–30.
4. Wenham RM, Lancaster JM, Berchuck A. Molecular aspects of ovarian cancer. Best Pract Res Clin Obstet Gynaecol 2002;16:483–97.
5. Holschneider CH, Berek JS. Ovarian cancer: epidemiology, biology, and prognostic factors. Semin Surg Oncol 2000;19:3–10.
6. Ozols RF. Update on the management of ovarian cancer. Cancer J 2002;8 Suppl 1:S22–30.
7. Schofield PR, McFarland KC, Hayflick JS, et al. Molecular characterization of a new immunoglobulin superfamily protein with potential roles in opioid binding and cell contact. EMBO J 1989;8:489–95.
8. Levitt P. A monoclonal antibody to limbic system neurons. Science 1984;223:299–301.
9. Struyk AF, Canoll PD, Wolfgang MJ, Rosen CL, D'Eustachio P, Salzer JL. Cloning of neurotrimin defines a new subfamily of differentially expressed neural cell adhesion molecules. J Neurosci 1995;15:2141–56.
10. Funatsu N, Miyata S, Kumanogoh H, et al. Characterization of a novel rat brain glycosylphosphatidylinositol-anchored protein (Kilon), a member of the IgLON cell adhesion molecule family. J Biol Chem 1999;274:8224–30.
11. Hachisuka A, Nakajima O, Yamazaki T, Sawada J. Localization of opioid-binding cell adhesion molecule (OBCAM) in adult rat brain. Brain Res 1999;842:482–6.
12. McNamee CJ, Reed JE, Howard MR, Lodge AP, Moss DJ. Promotion of neuronal cell adhesion by members of the IgLON family occurs in the absence of either support or modification of neurite outgrowth. J Neurochem 2002;80:941–8.
13. Reed J, McNamee C, Rackstraw S, Jenkins J, Moss D. Diglons are heterodimeric proteins composed of IgLON subunits, and Diglon-CO inhibits neurite outgrowth from cerebellar granule cells. J Cell Sci 2004;117:3961–73.
14. Sellar GC, Watt KP, Rabiasz GJ, et al. OPCML at 11q25 is epigenetically inactivated and has tumor-suppressor function in epithelial ovarian cancer. Nat Genet 2003;34:337–43.
15. Chen J, Lui WO, Vos MD, et al. The t(1;3) breakpoint-spanning genes LSAMP and NORE1 are involved in clear cell renal cell carcinomas. Cancer Cell 2003;4:405–13.
16. Clark TG, Stewart ME, Altman DG, Gabra H, Smyth JF. A prognostic model for ovarian cancer. Br J Cancer 2001;85:944–52.
17. Auersperg N, Wong AS, Choi KC, Kang SK, Leung PC. Ovarian surface epithelium: biology, endocrinology, and pathology. Endocr Rev 2001;22:255–88.